Technische Universität München

Max-Planck-Institut für Physik
(Werner-Heisenberg-Institut)

Electroweak contributions to SUSY particle production processes at the LHC

Edoardo Mirabella

Vollständiger Abdruck der von der Fakultät für Physik
der Technischen Universität München
zur Erlangung des akademischen Grades eines
Doktors der Naturwissenschaften (Dr. rer. nat.)
genehmigten Dissertation.

Vorsitzender:		Univ.-Prof. Dr. L. Oberauer
Prüfer der Dissertation:	1.	Hon.-Prof. Dr. W. F. L. Hollik
	2.	Univ.-Prof. Dr. A. J. Buras

Die Dissertation wurde am 25. Juni 2009
bei der Technischen Universität München eingereicht und
durch die Fakultät für Physik am 22. Juli 2009 angenommen.

Contents

Chapter 1

Introduction

The attempt to explain the complexity of the world in terms of a small number of fundamental building blocks has been an usual procedure of mankind during the centuries. According to Aristotle, the first philosopher using such reductionist approach was Thales. Thales taught can be stated as: "*Water constituted the principle of all things*" (Diogenes Laertius). Many steps forward in the understanding of the world were done during the centuries. Currently it is believed that matter is constituted by a relatively small number of point-like particles. According to this picture, particles interact, and these interactions allow the formation of complex structures. These interaction are described by a (spontaneously broken) Yang-Mills Quantum Field Theory, the Standard Model (SM) [1, 2]. Almost all the particles entering the SM have been observed. The only particle missing is the scalar Higgs boson. The predictions obtained within the SM agree well with the experimental data. In this sense this model is one of the best-tested theories of physics.

In spite of its success, the SM is not the ultimate theory. Indeed, this model does not describe gravity and does not provide a candidate for the observed amount of cold dark matter in the universe. These deficiencies suggest the existence of a a more fundamental theory including the SM. Some "aesthetic" problems, such as the non-existence of a Grand Unification scale and the hierarchy problem, reinforce this idea and can be used as a guideline in the hunting for the new theory.

Among the others, the extensions of the Standard Model fulfilling supersymmetry (SUSY) [3] are an appealing option, since they can both solve the hierarchy problem and provide the unification of the three gauge couplings. The Minimal Supersymmetric extension of the Standard Model (MSSM) [4], is achieved by extending the Poincaré group in a non-trivial way. Supersymmetry relates particles with different spin and is realized introducing for each

bosonic (fermionic) SM degree of freedom a fermionic (bosonic) supersymmetric degree of freedom.

The huge number of unknown parameters entering the MSSM can be lowered performing some assumption on the SUSY breaking mechanism, making the predictive power of the MSSM comparable to that of the SM. Unlike the SM, in the MSSM the electroweak (EW) symmetry breaking is realized radiatively. Moreover, if an extra symmetry, R-parity, is imposed, the lightest SUSY particle (LSP) becomes stable. Since phenomenology requires the LSP to be weakly interacting, LSP is a natural cold dark matter candidate. This model is consistent with experimental data. As far as TeV-scale SUSY is concerned, the indirect access through virtual effects in electroweak precision data [5] provides an overall fit in the MSSM [6, 7] at least as good as in the SM, even better in specific observables such as $g-2$ of the muon [8, 9].

If, as suggested by electroweak precision data, SUSY is realized at the TeV scale or below, it will be accessible to direct experimental measurements at the Large Hadron Collider (LHC) through the production of SUSY particles. In particular, colored particles like the SUSY partners of quarks and gluons, *i.e.* squarks and gluinos, will be copiously produced. The cross section of these processes is in the range from 0.5 to 10 pb for masses of squarks and gluinos below 1 TeV. The decay chains of squarks and gluinos terminate when the LSP is produced and lead to clear signatures constituted by missing E_T plus jets and possibly leptons, which allow an early discovery of TeV-scale SUSY, *i.e.* within the first inverse fb of integrated luminosity.

An accurate knowledge of the processes leading to the production of SUSY colored particles is mandatory. The first prediction of the cross section for hadronic production of squark pairs was done in the early 1980's at lowest order $\mathcal{O}(\alpha_s^2)$ in supersymmetric QCD [10–14]. QCD contributions at the next-to-leading order (NLO), $\mathcal{O}(\alpha_s^3)$, were calculated more than ten years later [15–20]. They increase the cross section by typically 20 to 40 %, and they substantially reduce the dependence on the factorization and renormalization scale. More recent is the estimation of the logarithmically enhanced next-to-next-to-leading order (NNLO) QCD contributions to squark hadroproduction [21], the resummation of the QCD Sudakov logarithms at the next-to-leading-logarithmic (NLL) accuracy [22, 23], and the resummation of the leading Coulomb corrections [23]. Their inclusion stabilizes the prediction against scale variation. The NNLO QCD contributions amounts up to 9%, while the NLL contributions are of the order of $2-8\%$ of the NLO QCD predictions, provided the squark and gluino masses are $\mathcal{O}(1$ TeV). In this mass range the contribution of the Coulomb corrections amounts up to 5%.

Besides the QCD-based production mechanisms, there are also contributions of electroweak origin. In particular, there are tree-level contributions of $\mathcal{O}(\alpha^2)$ and $\mathcal{O}(\alpha_s\alpha)$ and NLO EW contributions, of $\mathcal{O}(\alpha_s^2\alpha)$. The tree-level EW contributions can also become sizable, reaching values up to 20% [24, 25] of the LO QCD predictions.
In this thesis we consider the NLO EW contributions of three classes of processes leading to the production of SUSY colored particles. The computation of the NLO EW corrections completes the investigation of the one loop contributions. Although the NLO EW corrections are expected to be smaller than the NLO corrections of QCD origin, they deserve to be analysed. Indeed:

1. The structure of the NLO EW corrections is rather involved. Beside the flavour dependence present in the case of the QCD contributions as well, the EW contributions depend on the chirality and on the charge of the produced squark. The whole set of the MSSM parameters enter the NLO EW contributions, therefore the importance of these contributions can depend strongly on the scenario. A systematic investigation of the impact of the EW contribution on the different production processes and in different scenarios is the only way one can decide in which scenarios the EW contributions can be safely neglected.

2. The NLO EW contributions can be important in the proper definition of the distributions since in the high-energy limit EW corrections can be enhanced by Sudakov-type logarithms.

3. The NLO EW contributions are of the same size as the NNLO QCD contributions. Even if in practice the latter contributions are expected to be bigger than the former, the impact of these contributions can be altered in the sum and have to be investigated. Similar effects can occur between LO and NLO EW contributions since the relative yield of the tree-level EW contributions is of the order of several percent which is the expected size of the NLO EW corrections.

4. In the SUSY scenarios where the NLO EW corrections turns out to be below the expected experimental accuracy, their size is a reliable estimate of the theoretical uncertainty arising from missing higher order terms.

The outline of the thesis is the following. In chapter 2, we introduce the framework in which the computations of this thesis are performed. We start describing the structure of the SM and some of the problems this model leaves unexplained. Then, we introduce the concept of SUSY as the only

possibility to evade the Coleman-Mandula theorem [26]. We define the supersymmetry algebra, superspace and superfields and we use them to obtain the general structure of a Supersymmetric Yang-Mills theory. The Minimal Supersymmetric extension of the SM is obtained as a particular Super Yang-Mills theory with the same gauge group as the SM and conserving R-parity. The description of the spectrum of the MSSM completes this chapter.

In chapter. 3, we give a brief overview of the SUSY searches at colliders. We present the main results of SUSY searches at the different experiments collecting data at LEP, HERA, and Tevatron. We present the expected discovery reach of ATLAS and CMS, the two multi-purpose experiments at the LHC.

In chapter 4 we present the processes considered in this thesis. We describe the general structure of the different contributions to these processes and we give some details about the computation of their NLO EW corrections. In particular, we tackle the problem of the UV divergences. In order to obtain UV finite results, the MSSM has to be renormalized at next-to-leading order, properly taking care of different regularization schemes in presence of supersymmetry. The soft and collinear divergences are cancelled by real photon and real gluon emission. The cancellation of the mass singularities of photonic and gluonic origin in suitable observables is explicitly shown. Moreover, we describe the two methods we use to regularize and isolate these divergences.

In the subsequent three chapters we present the numerical impact of the EW contributions to three different processes leading to the production of SUSY colored particles at the LHC. In chapter 5, we consider gluino pair production. Such process is the most important process leading to the production of SUSY colored particles when the gluino is lighter than the squarks. We describe the partonic processes entering the $\mathcal{O}(\alpha_s^2)$ and the $\mathcal{O}(\alpha_s^2\alpha)$ contributions to this process. The NLO EW corrections arising from photon-induced partonic processes are considered as well. After studying the reliability of the different renormalization schemes in the considered SUSY scenarios, we present the numerical impact of the EW contributions at the LHC. We consider the total hadronic cross sections and different distributions. Several scans over the parameters of the MSSM are performed as well. Finally, we briefly discuss the impact of the EW contributions to gluino pair production at the Tevatron.

Chapter 6 is devoted to the diagonal squark–anti-squark production processes at the LHC, *i.e.* to the production of a given squark together with its own anti-particle in proton-proton collisions at 14 TeV. We describe the LO

contribution, $\mathcal{O}(\alpha_s)$, and the NLO EW corrections of $\mathcal{O}(\alpha_s^2\alpha)$. The tree-level EW contribution $\mathcal{O}(\alpha^2)$ and $\mathcal{O}(\alpha_s\alpha)$, are introduced as well. The numerical effect of the LO and NLO EW contributions are investigated in different SUSY scenarios. Different distributions are considered and the dependence of the total cross section on the mass of the produced squarks is investigated as well.

In chapter 7, we discuss the gluino–squark associated production at the LHC. This process is the main production channel of SUSY colored particles when squarks and gluinos have comparable masses. The general structure of the chapter is similar to that of the previous one. We describe the tree-level contributions and the NLO EW corrections. Finally, the EW contributions to various distributions and to the total cross section are investigated in different SUSY scenarios.

Several appendices complete the thesis. In appendix A we define the signature of the Minkowski space and the Pauli matrices. In appendix B a brief overview of the spinorial representation of the Poincaré group is given, while in appendix C, we set some definitions concerning Grassmann variables. The parametrization of the two- and three- particle phase space is described in appendix D, while in appendix E, we collect some quantities entering the treatment of the mass singularities within the dipole subtraction method. Appendix F, G, and H collect the Feynman diagrams entering the processes of gluino pair production, squark–anti-squark pair production and squark–gluino production respectively.

Chapter 2

The Standard Model and the MSSM

2.1 The Standard Model

The Standard Model (SM) [1, 2] is the relativistic quantum field theory which gives the best description of the electroweak and strong phenomena at the currently experimentally accessible energies. The SM is a theoretically consistent and well tested theory [27], but, besides its success, there are many open questions that can be addressed only by going beyond this model. In the following subsection we will briefly describe the Lagrangian of the SM and the issues indicating the incompleteness of the model.

2.1.1 Lagrangian of the SM

The Standard model (SM) is a Yang-Mills theory with gauge group

$$SU(3)_C \times SU(2)_L \times U(1)_Y. \tag{2.1}$$

This group is spontaneously broken to $SU(3)_C \times U(1)_Q$ via the Higgs mechanism [28]. The generators of the three components of the group (2.1), the corresponding couplings and gauge fields are collected in Table 2.1. According to Ref. [29], leptons and quarks can be described by left-handed Weyl spinors. These (matter) fields can be grouped into three (reducible) multiplets of the gauge groups

$$(\Psi_i)_\alpha = \left[\ (q_i)_\alpha;\ (\ell_i)_\alpha;\ (u_i^c)_\alpha;\ (d_i^c)_\alpha;\ (e_i^c)_\alpha \ \right] \quad (i = 1, 2, 3), \tag{2.2}$$

where $q_i = (q_{i1}, q_{2i}) = (u_i, d_i)$ and $\ell_i = (\ell_{1i}, \ell_{2i}) = (\nu_i, e_i)$. Under the gauge group the different components of Ψ_i transform according to the following

group	generators	coupling	gauge bosons
$SU(3)_C$	$T_{A=1,..,8}$	g_s	g_A^μ
$SU(2)_L$	$I_{i=1,2,3}$	g	W_i^μ
$U(1)_Y$	Y	g'	B^μ

Table 2.1: Standard Model, gauge group. For each component of this group we show the notation describing the generators, the couplings, and the gauge fields.

representations

$$\left[\ (\mathbf{3},\mathbf{2},1/6);\ (\mathbf{1},\mathbf{2},-1/2);\ (\bar{\mathbf{3}},\mathbf{1},-2/3);\ (\bar{\mathbf{3}},\mathbf{1},1/3);\ (\mathbf{1},\mathbf{1},1)\ \right] \tag{2.3}$$

This unusual notation is introduced for later convenience, when the supersymmetric extension of the SM will be described. The most common description of the matter content of the SM uses Dirac spinors ψ_{f_i}. These spinors can be related to ours via

$$\psi_{f_i} = \begin{pmatrix} (f_i)_\alpha \\ (\overline{f_i^c})^{\dot\alpha} \end{pmatrix}, \tag{2.4}$$

where the right-handed spinors $(\overline{f^c})^{\dot\alpha}$ are defined in appendix B.

The spontaneous breaking of the gauge group into $SU(3)_C \times U(1)_Q$ is guaranteed by introducing a complex scalar doublet

$$\phi = \begin{pmatrix} \phi^+ \\ \phi^0 \end{pmatrix} = \begin{pmatrix} \phi^1 + i\phi^2 \\ \phi^3 + i\phi^4 \end{pmatrix},$$

that transforms under the gauge group according to $(\mathbf{1},\mathbf{2},1/2)$.

Renormalizability, hermiticity, and gauge invariance uniquely fix the structure of the SM Lagrangian that can be divided into two pieces,

$$\mathcal{L}_{\rm SM} = \mathcal{L}_{\rm G} + \mathcal{L}_{\rm H}. \tag{2.5}$$

$\mathcal{L}_{\rm G}$ is the minimal Lagrangian for a Yang-Mills theory with gauge group (2.1) including the multiplets Ψ_i. Since the SM is a chiral theory mass terms for the fermions are not allowed. $\mathcal{L}_{\rm H}$ describes the doublet ϕ and its interaction with gauge and matter fields

$$\begin{aligned} \mathcal{L}_{\rm H} &= (\mathcal{D}^\mu\phi)^\dagger(\mathcal{D}_\mu\phi) - \mu^2(\phi^\dagger\phi) + \lambda(\phi^\dagger\phi)^2 \\ &- \left(\lambda^U_{ij}\phi^0 q_{1i}u^c_j - \lambda^D_{ij}\phi^+ q_{2i}d^c_j - \lambda^E_{ij}\phi^+\ell_{2i}e^c_j + \text{ h.c. }\right), \end{aligned} \tag{2.6}$$

where a summation over repeated indices is understood and $\mathcal{D}_\mu$ is the covariant derivative.

Assuming $\mu^2 > 0$, the Higgs potential has a minimum at a non-zero value of $\phi^\dagger\phi$ given by

$$\phi^\dagger\phi = \frac{\mu^2}{2\lambda} = v^2.$$

According to the Goldstone criterion, this ensures the spontaneous breaking of the gauge symmetry. The vacuum configuration is chosen to be $\langle\phi\rangle = (0, v)^T$, the nine unbroken generators are the $SU(3)_C$ generators and the linear combination $Q = I_3 + Y$. Due to the definition of the hyper-charge Y, Q is nothing but the generator of $U(1)_Q$. The physical degrees of freedom can be obtained by fixing the gauge to the unitary gauge and expanding around the chosen minimum $\langle\phi\rangle$. After this expansion, $\mathcal{L}_{\text{H}}$ contains the kinetic term and the mass term of a scalar particle

$$h = \sqrt{2}\,\left(\mathfrak{Re}\{\phi^0\} - v\right). \tag{2.7}$$

This particle is the Higgs boson and its mass is $m_h = \sqrt{2}\mu$. Moreover, $\mathcal{L}_{\text{H}}$ exhibits bi-linear terms proportional to the vacuum expectation value v that will give rise to the mass terms. In particular we have the gauge bosons mass eigenstates,

$$W^\pm_\mu = \frac{1}{\sqrt{2}}\left(W_{1\mu} \mp iW_{2\mu}\right), \qquad \begin{pmatrix} A_\mu \\ Z_\mu \end{pmatrix} = \begin{pmatrix} c_{\theta_W} & s_{\theta_W} \\ -s_{\theta_W} & c_{\theta_W} \end{pmatrix} \begin{pmatrix} B_\mu \\ W_{3\mu} \end{pmatrix}, \tag{2.8}$$

where $\theta_W = \arctan g'/g$ is the electroweak mixing angle, $c_{\theta_W} = \cos\theta_W$, and $s_{\theta_W} = \sin\theta_W$. The respective tree-level masses are

$$M_W = \frac{gv}{\sqrt{2}}, \qquad M_Z = \frac{\sqrt{g^2 + g'^2}}{\sqrt{2}}v, \qquad M_A = 0. \tag{2.9}$$

As expected, there is a massless gauge boson associated to the unbroken generator Q. Similarly, mass eigenstates for quarks and leptons can be obtained after diagonalization. Neutrinos stay massless, owing to the absence of a term like $\lambda^N_{ij}\phi^0\ell_{1i}\nu^c_j$ in (2.6). After diagonalization, quarks belonging to different multiplets (2.2) can interact via charged currents, with the strength of such an interaction being proportional to a 3×3 unitary matrix, the Cabibbo-Kobayashi-Maskawa (CKM) matrix [30].

2.1.2 Problems of the SM

Despite of its success, there are several indications the Standard Model is not the ultimate theory.

Strong indications for the existence of physics beyond the Standard Model (BSM) come from cosmology and astrophysics. First of all, the SM does not include gravity, whose relativistic quantum mechanical description in terms of a Yang-Mills theory leads to a non-renormalizable theory. Moreover, the SM can not provide the amount of cold dark matter necessary to explain the large structure formation in the early universe [31, 32], since its dark matter candidates, the neutrinos, are relativistic particles. Another problem is related to the baryon asymmetry in the universe. Even if the SM fulfills the Sacharov [33] conditions, it cannot reproduce the value of the observed asymmetry [32]. Finally, neutrino masses and oscillations can be a breakdown of this model, provided the existence of Majorana mass terms[1].

Besides these phenomenological evidences, a theoretical argument in favour of the existence of BSM physics is related to the presence of a Landau pole in the running of the quartic coupling λ appearing in the Higgs potential. New physics should enters to regularize this singularity.

Once the existence of BSM physics is established, the SM has to be considered a low energy effective theory of a larger theory involving also energy scales $\Lambda_{\rm NP}$, higher than the electroweak scale $v \sim 170$ GeV. New physics is expected to enter at the Planck scale $M_{\rm P} = 10^{19}$ GeV, but one expects the existence of other relevant scales $\Lambda_{\rm NP}$. A possible guideline in the hunting for such a theory is *naturalness*, namely the requirement of the existence of some mechanism that keeps the electroweak scale light relative to the new physics scale. Such a mechanism guarantees the decoupling of the new physics from the SM.

It is worth to stress that this naturalness requirement is not fulfilled without making special assumptions. If the SM is an effective theory, the Higgs mass m_h is an effective mass that can be perturbatively evaluated. At $\mathcal{O}(\alpha)$ this mass reads

$$m_h^2 = \tilde{m}_h^2 + \delta\tilde{m}_h^2, \tag{2.10}$$

where $\tilde{m}_h^2$ is the square of the Higgs mass in the underlying theory while $\delta\tilde{m}_h^2$ is the contribution from the heavy modes of the underlying theory. It turns out that $\delta\tilde{m}_h^2$ is proportional to the square of the mass of the particles the Higgs couples to. Since these masses are $\mathcal{O}(\Lambda_{\rm NP})$ and $\Lambda_{\rm NP} >> m_h$, $\tilde{m}_h^2$ has to be fine tuned in order to cancel with sufficient accuracy the big contributions from $\delta\tilde{m}_h^2$. This is the so called *hierarchy problem* [34].

Such unnatural fine-tuning can be solved making some assumption on the underlying theory. One possibility to is to introduce a new symmetry

[1]Current experimental results are consistent with Dirac neutrino masses, which fits naturally in the SM structure

that protects the effective Higgs mass against such big corrections. This is the option that leads to supersymmetric models [3] and that will be discussed at length in the following sections. Needless to say, this is not the only possibility. For instance, one could reject the hypothesis that the Higgs is a fundamental particle or suppose that new physics enters only at a scale comparable to the electroweak scale. The first option leads to (certain class of) technicolor models [34, 35], while the latter possibility is the solution of the hierarchy problem proposed in the context of large Universal Extra Dimensions models [36].

2.2 Supersymmetry

In this section we will present one possible solution of the hierarchy problem, supersymmetry (SUSY). The following subsections will introduce this symmetry, describe the general structure of a theory invariant under SUSY and then present the minimal supersymmetric extension of the SM.

In order to have a first contact with SUSY, it is worth to have a closer look on the form of the corrections to the Higgs mass, namely to the possible contributions to $\delta\tilde{m}_h^2$. A fermion field F which couples to the Higgs via a term like $\frac{\lambda_F}{\sqrt{2}}\bar{F}FH$ contributes to $\delta\tilde{m}_h^2$ as [37],

$$-\frac{\lambda_F^2}{16\pi^2}\left\{2m_F^2\left[1-\ln\left(\frac{m_F^2}{\mu^2}\right)\right]-4m_F^2\ln\left(\frac{m_F^2}{\mu^2}\right)\right\}+\ldots, \tag{2.11}$$

where terms not quadratically dependent on m_F are dropped. Let us suppose the existence of a scalar particle S coupling to the Higgs via an interaction term

$$\frac{\lambda_S}{2}H^2|S|^2+\lambda'_S H|S|^2.$$

The contribution of this scalar field can be obtained from the diagrams in Fig. 2.1 and reads

$$-\frac{\lambda_S}{16\pi^2}m_S^2\left[1-\ln\left(\frac{m_S^2}{\mu^2}\right)\right]-\frac{(\lambda'_S)^2}{16\pi^2}\ln\left(\frac{m_S^2}{\mu^2}\right)+\ldots, \tag{2.12}$$

where terms that do not depend quadratically on m_S are omitted.

SUSY accommodates in each multiplet a fermion and two scalars forcing their couplings to the Higgs bosons to be correlated, in particular $\lambda_S=-\lambda_F^2$ and $\lambda'_S=\sqrt{2}m_F\lambda_F$. Directly from Eq. (2.11) and (2.12) one can infer the quadratically enhanced contributions to $\delta\tilde{m}_h^2$ are cancelled. Such a symmetry guarantees the cancellation of these dangerous quadratic contributions beyond one-loop as well.

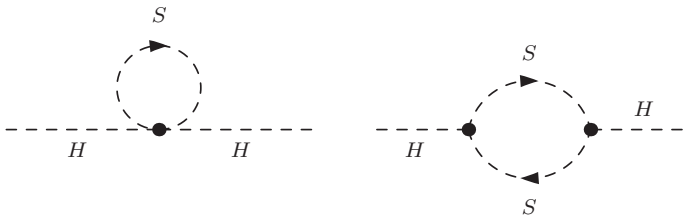

Figure 2.1: Contributions to the Higgs self energy arising from a scalar particle S

2.2.1 Superalgebra and Supergroup

Since SUSY relates fermions and bosons, its generators have non-trivial transformations properties under space rotations. This implies that supersymmetry is a space-time symmetry, in the sense that it has to contain the Poincaré group as a subgroup. Moreover, according to the Coleman-Mandula theorem [26], such a symmetry can not be described by a Lie group and, consequently, their generators cannot constitute a Lie algebra. This is somehow expected, since the generators turning bosons into fermions and vice-versa should satisfy anticommutation relations. Therefore the generators of SUSY have to form a graded Lie algebra.

A rigorous definition of what a graded Lie algebra is beyond the scope of this section and can be found in the literature [38]. An interesting feature is that a basis of a graded Lie algebra divides into two families. The odd operators F_j and the even operators B_i satisfying the following relations

$$[B_i; B_j] = if_{ijk}B_k, \quad [B_i; F_j] = ig_{ijk}F_k, \quad \{B_i; B_j\} = is_{ijk}B_k. \tag{2.13}$$

Even operators of SUSY are the generators of the Poincaré group, and f_{ijk} are its structure constants. The properties of the odd operators and the structure constants g_{ijk} and s_{ijk} in an interacting relativistic quantum field theory are fixed by the Haag-Łopuszanski-Sohnius (HLS) [39] theorem.

This theorem states that the set of the odd generators is constituted by N pairs of generators transforming under the left-handed spinorial representation of the Lorentz group

$$Q^A_\alpha = (Q^A_1, Q^A_2) \quad (A = 1, \ldots, N),$$

together with their hermitian conjugates $(Q^A_\alpha)^\dagger = \bar{Q}^A_{\dot{\alpha}}$, which transform under the right-handed spinorial representation of the Lorentz group. Chiral

theories arise only if $N = 1$. In this case HLS theorem uniquely defines the structure of the graded Lie algebra (also called superalgebra)

$$\begin{aligned}
[M_{\mu\nu}, M_{\rho\sigma}] &= i(g_{\nu\rho}M_{\mu\sigma} + g_{\mu\sigma}M_{\nu\rho} - g_{\nu\sigma}M_{\mu\rho} - g_{\mu\rho}M_{\nu\sigma}),\\
[P_\mu, P_\nu] &= 0, \qquad [M_{\mu\nu}, P_\rho] = -i(g_{\rho\mu}P_\nu - g_{\rho\nu}P_\mu),\\
[Q_\alpha, P_\mu] &= 0, \qquad [Q_\alpha, M_{\mu\nu}] = -\frac{1}{2}(\sigma_{\mu\nu})_\alpha^{\ \beta} Q_\beta,\\
[\bar{Q}_{\dot\alpha}, P_\mu] &= 0, \qquad [\bar{Q}_{\dot\alpha}, M_{\mu\nu}] = -\frac{1}{2}(\bar\sigma_{\mu\nu})_{\dot\alpha}^{\ \dot\beta} \bar{Q}_{\dot\beta},\\
\{Q_\alpha, Q_\beta\} &= 0, \qquad \{\bar{Q}_{\dot\alpha}, \bar{Q}_{\dot\beta}\} = 0,\\
\{Q_\alpha, \bar{Q}_{\dot\beta}\} &= 2(\sigma_\mu)_{\alpha\dot\beta}P^\mu.
\end{aligned} \tag{2.14}$$

$M_{\mu\nu}$ and P_μ are the generators of the Lorentz and translation algebra respectively while $\sigma_{\mu\nu}$ and $\bar\sigma_{\mu\nu}$ are defined in appendix B.

In analogy with the (connected) Lie groups, the elements of the supergroup can be obtained by exponentiating the superalgebra. The parameters related to the spinorial generators have to be Grassmann variables satisfying the anticommuting algebra introduced in appendix C and anticommuting with the spinorial generators Q_α and $\bar{Q}_{\dot\alpha}$. Such positions allow to express the graded Lie algebra in terms of a Lie algebra and to obtain finite transformation starting from the infinitesimal ones via exponentiation. The generic element of the supergroup reads

$$G(\tau^\mu, \omega^{\nu\sigma}, \xi_\alpha, \bar\xi_{\dot\alpha}) = \exp\left[i\left(\tau^\mu P_\mu + \frac{1}{2}\omega^{\nu\sigma}M_{\nu\sigma} + \xi Q + \bar\xi\bar{Q}\right)\right],$$

where $\xi Q = \xi^\alpha Q_\alpha$ and $\bar\xi\bar{Q} = \bar\xi_{\dot\alpha}\bar{Q}^{\dot\alpha}$.

2.2.2 Superspace and Superfields

SUSY field theories can be built starting from fields in a space in which it is possible to define a representation of the supergroup. Moreover, these fields have to transform according to a representation of the supergroup. In this subsection we will introduce such fields (the superfields) and the space where they are defined (the Minkowski superspace) [40].

The Poincaré superalgebra is a semidirect product of the Lorentz group and the superalgebra generated by P_μ, Q_α and $\bar{Q}_{\dot\alpha}$. Therefore, in analogy with the Minkowski space, we can define the Minkowski superspace as the space of the right coset of the Lorentz group. Points in the superspace are

then in one-to-one correspondence with the parameters of the elements of the superalgebra of the type

$$G(x_\mu, 0, \theta_\alpha, \bar{\theta}_{\dot{\alpha}}) = \exp\left[i\left(x^\mu P_\mu + \theta Q + \bar{\theta}\bar{Q}\right)\right]. \tag{2.15}$$

The generic point of the superspace is then $(x_\mu, \theta_\alpha, \bar{\theta}_{\dot{\alpha}})$. This point transforms according to the superalgebra (2.14), provided that the operators P, Q, $\overline{Q}$ entering Eq. (2.15) fulfill the opposite superalgebra[2]. In particular the spinorial generators are

$$\mathcal{P}_\mu = -i\partial_\mu, \quad \mathcal{Q}_\alpha = -i\partial_\alpha - (\sigma^\mu)_{\alpha\dot{\beta}}\bar{\theta}^{\dot{\beta}}\partial_\mu, \quad \bar{\mathcal{Q}}_{\dot{\alpha}} = i\bar{\partial}_{\dot{\alpha}} + \theta^\beta(\sigma^\mu)_{\beta\dot{\alpha}}\partial_\mu, \tag{2.16}$$

where ∂_α and $\bar{\partial}_{\dot{\alpha}}$ are anti-commuting operators defined in appendix C.

Fields defined on the Minkowski superspace are called superfields. They can be Taylor-expanded in terms of the Grassmann variables. Owing to the anticommuting algebra, Eq. (C.1) in appendix C, a generic superfield $F(x, \theta, \bar{\theta})$ can be expanded as follows,

$$\begin{aligned} F(x,\theta,\bar{\theta}) &= \phi(x) + \theta\psi(x) + \bar{\theta}\bar{\chi}(x) + (\theta\theta)m(x) + (\bar{\theta}\bar{\theta})n(x) \\ &+ \theta\sigma^\mu\bar{\theta}v_\mu(x) + (\theta\theta)\bar{\theta}\bar{\lambda}(x) + (\bar{\theta}\bar{\theta})\theta\eta(x) + (\theta\theta)(\bar{\theta}\bar{\theta})d(x). \end{aligned} \tag{2.17}$$

The coefficient multiplying the Grassmann variables are ordinary fields defined in the Minkowski space, and they are the components of the superfield.

We will construct SUSY theories using Superfields transforming as scalars under the supergroup. Under a transformation such that $(x, \theta, \bar{\theta}) \to (x', \theta', \bar{\theta}')$, a scalar superfield will transform according to

$$F(x, \theta, \bar{\theta}) \to F'(x', \theta', \bar{\theta}') = F(x, \theta, \bar{\theta}).$$

This transformation rule fixes the transformation properties of the components of the superfield. Using the notation of Eq. (2.18) ϕ, m,n and d are scalar fields, ψ and η are left-handed Weyl Spinors while $\bar{\chi}$ and $\bar{\lambda}$ are right-handed Weyl Spinors. v_μ is a vector field.

Scalar superfields give rise to a realization of SUSY, but not an irreducible one. Indeed, there are two subsets of the scalar Superfields that are invariant under SUSY. The first set is the subset of the scalar superfields $V(x, \theta, \bar{\theta})$

[2]The opposite superalgebra is obtained multiplying the brackets in Eq. (2.14) by -1.

such that $V = V^\dagger$. The expansion of such superfields reads

$$\begin{aligned} V(x,\theta,\bar\theta) &= c(x) + i\theta\chi(x) - i\bar\theta\bar\chi(x) + \frac{i}{2}(\theta\theta)m(x) \\ &- \frac{i}{2}(\bar\theta\bar\theta)m^*(x) + \theta\sigma^\mu\bar\theta v_\mu(x) + i(\theta\theta)\bar\theta\bar\lambda(x) \\ &- i(\bar\theta\bar\theta)\theta\lambda(x) + \frac{1}{2}(\theta\theta)(\bar\theta\bar\theta)d(x). \end{aligned} \tag{2.18}$$

Since v_μ is a real vector field these superfields are called *vector superfields*. The sum and the product of vector superfields is a vector superfield as well. Others subsets of the scalar superfields that are invariant under SUSY can be obtained with the help of the following spinorial operators

$$D_\alpha = \partial_\alpha + i(\sigma^\mu)_{\alpha\dot\beta}\bar\theta^{\dot\beta}\partial_\mu, \quad \bar D_{\dot\alpha} = -\bar\partial_{\dot\alpha} - i\theta^\beta(\sigma^\mu)_{\beta\dot\alpha}\partial_\mu, \tag{2.19}$$

obeying to the following algebra:

$$\begin{aligned} \{D_\alpha, \mathcal{Q}_\beta\} &= \{\bar D_{\dot\alpha}, \mathcal{Q}_\beta\} = \{D_\alpha, \bar{\mathcal{Q}}_{\dot\beta}\} = \{\bar D_{\dot\alpha}, \bar{\mathcal{Q}}_{\dot\beta}\} = 0, \\ \{D_\alpha, D_\beta\} &= \{\bar D_{\dot\alpha}, \bar{\mathcal{Q}}_{\dot\beta}\} = [P_\mu, D_\alpha] = [P_\mu, \bar D_{\dot\beta}] = 0, \\ \{D_\alpha, \bar D_{\dot\beta}\} &= -2i(\sigma^\mu)_{\alpha\dot\beta}P_\mu. \end{aligned} \tag{2.20}$$

The subset of *chiral* (*anti-chiral*) *superfields*, fulfilling the condition $\bar D_{\dot\alpha}\Phi = 0$ ($D_\alpha\bar\Phi = 0$), is closed under the action of the supergroup. The generic chiral superfield can be written as

$$\begin{aligned} \Phi(x,\theta,\bar\theta) &= A(x) + \sqrt{2}\theta\psi(x) - \frac{1}{4}(\theta\theta)(\bar\theta\bar\theta)\partial^\mu\partial_\mu A(x) \\ &+ i(\theta\sigma^\mu\bar\theta)\partial_\mu A(x) - \frac{i}{\sqrt{2}}(\theta\theta)(\partial_\mu\psi\sigma^\mu\bar\theta) + \theta\theta F(x), \end{aligned} \tag{2.21}$$

while the decomposition of a anti-chiral superfield reads

$$\begin{aligned} \bar\Phi(x,\theta,\bar\theta) &= B(x) + \sqrt{2}\bar\theta\bar\xi(x) - \frac{1}{4}(\theta\theta)(\bar\theta\bar\theta)\partial^\mu\partial_\mu B(x) \\ &- i(\theta\sigma^\mu\bar\theta)\partial_\mu B(x) + \frac{i}{\sqrt{2}}(\bar\theta\bar\theta)(\theta\sigma^\mu\partial_\mu\bar\xi(x)) + \bar\theta\bar\theta G(x). \end{aligned} \tag{2.22}$$

It is worth to mention that the set of (anti-)chiral superfields is closed under sum and multiplication and that the product of a chiral and an anti-chiral superfield is a vector superfield. Moreover the complex conjugate of a chiral superfield is anti-chiral.

2.2.3 Supersymmetric gauge theories

We are now ready to write the Lagrangian of a SUSY theory involving chiral fields. We will start with the most general SUSY Lagrangian involving chiral superfields and then we will modify it in order to implement gauge symmetry.

Under a SUSY transformation the F term in Eq. (2.22) and the G field in Eq. (2.23) transform as a four-divergence. Similarly the d term of Eq. (2.18) transforms as a total derivative under SUSY transformation. Therefore SUSY invariant terms are

$$\begin{aligned} \int d^4x\ F(x) &= \int d^4x \int d^2\theta\ \Phi(x,\theta,\bar\theta), \\ \int d^4x\ G(x) &= \int d^4x \int d^2\bar\theta\ \bar\Phi(x,\theta,\bar\theta), \\ \frac{1}{2}\int d^4x\ d(x) &= \int d^4x \int d^4\theta\ V(x,\theta,\bar\theta), \end{aligned} \tag{2.23}$$

where the integration over Grassmann variables is defined in the appendix C. The most general renormalizable SUSY Lagrangian involving chiral superfields is

$$\mathcal{L}_{\rm wz} = \int d^4\theta\ \overline{\mathbf{\Phi}}\mathbf{\Phi} + \left[\int d^2\theta\ \left(\lambda_i\Phi_i + \frac{m_{ij}}{2}\Phi_i\Phi_j + \frac{g_{ijk}}{3}\Phi_i\Phi_j\Phi_k\right) + \text{h.c.}\right], \tag{2.24}$$

where $\mathbf{\Phi} = (\Phi_1, \ldots, \Phi_n)^T$ and $\overline{\mathbf{\Phi}} = \mathbf{\Phi}^\dagger$. This is the so called Wess-Zumino model [41].

Before implementing gauge symmetry into the aforementioned Lagrangian some definition is in order. Given a group $\mathfrak{g}$ of dimension N and an n-dimensional representation of $\mathfrak{g}$ generated by the matrices $\mathbf{t}^a$, we define the set of extended gauge transformations acting on $\mathbf{\Phi}$ according to

$$\mathbf{\Phi} \to \mathbf{\Phi}' = \exp\left[i2g\Psi_a\mathbf{t}^a\right]\mathbf{\Phi}, \qquad \overline{\mathbf{\Phi}} \to \overline{\mathbf{\Phi}'} = \overline{\mathbf{\Phi}}\exp\left[-i2g\bar\Psi_a\mathbf{t}^a\right], \tag{2.25}$$

where Ψ_a is a set of chiral superfields, while $\bar\Psi_a = \Psi_a^\dagger$. This class of transformations extend the ordinary gauge transformations. The latter arise when the only non-zero component of each Ψ_a is $A(x)$. In order to build a theory invariant under the transformations (2.25), we have to modify the Lagrangian (2.24). Indeed the term $\overline{\mathbf{\Phi}}\mathbf{\Phi}$ is not invariant,

$$\overline{\mathbf{\Phi}}\mathbf{\Phi} \to \overline{\mathbf{\Phi}}\exp\left[-i2g\bar\Psi_a\mathbf{t}^a\right]\exp\left[i2g\Psi_a\mathbf{t}^a\right]\mathbf{\Phi} \neq \overline{\mathbf{\Phi}}\mathbf{\Phi}.$$

Gauge invariance is restored introducing a connection matrix $\mathbf{\Gamma}(x,\theta,\bar{\theta})$ with the transformation property

$$\mathbf{\Gamma}(x,\theta,\bar{\theta}) \to \exp\left[i2g\Psi_a \mathbf{t}^a\right] \mathbf{\Gamma}(x,\theta,\bar{\theta}) \exp\left[-i2g\bar{\Psi}_a \mathbf{t}^a\right]. \tag{2.26}$$

An hermitian connection involving fields whose transformation properties are independent of the particular representation of $\mathfrak{g}$ under which $\mathbf{\Phi}$ transforms is

$$\mathbf{\Gamma}(x,\theta,\bar{\theta}) = \exp\left[2gV_a \mathbf{t}^a\right], \tag{2.27}$$

where $(V_1,\ldots,V_N)$ is a set of vector superfields whose transformation rule can be obtained from (2.26) using the Baker-Campbell-Hausdorff formula. Such a transformation rule allows to put the vector superfields in a convenient form. One can always choose the *Wess-Zumino gauge* where the vector superfields read

$$V_a(x,\theta,\bar{\theta}) = \theta\sigma^\mu\bar{\theta}(v_a)_\mu(x) + i(\theta\theta)\bar{\theta}\bar{\lambda_a}(x) - i(\bar{\theta}\bar{\theta})\theta\lambda_a(x) + \frac{1}{2}(\theta\theta)(\bar{\theta}\bar{\theta})d_a(x).$$

Ordinary gauge transformations preserve the Wess-Zumino gauge. They transform $(v_a)_\mu$ as a Yang-Mills gauge field, and λ_a and d_a as matter field in the adjoint representation.

The last step for writing a SUSY gauge theory is to find a superfield generalizing the gauge invariant Field strength tensor. This superfield turns out to be

$$\mathbf{W}_\alpha = -\frac{1}{8g}\bar{D}\bar{D}\exp\left[-2gV_a\mathbf{T}^a\right] D_\alpha \exp\left[2gV_a\mathbf{T}^a\right],$$

which, owing to the anticommutativity of the $\bar{D}'s$, is a chiral superfield, *i.e.* $\bar{D}_{\dot{\beta}}\mathbf{W}_\alpha = 0$. $\mathbf{W}_\alpha$ transforms according to the left-handed spinorial representation Poincaré group. The hermitian conjugate of $\mathbf{W}_\alpha$,

$$\overline{\mathbf{W}}_{\dot{\alpha}} = \frac{1}{8g}DD\exp\left[2gV_a\mathbf{T}^a\right]\bar{D}_{\dot{\alpha}}\exp\left[-2gV_a\mathbf{T}^a\right],$$

is an anti-chiral superfield in the right-handed spinorial representation of the Lorentz group.

We now have all the ingredients to write the most general Lagrangian describing a SUSY gauge theory [42],

$$\begin{aligned}\mathcal{L} &= \frac{1}{4}\left[\int d^2\theta\ \mathbf{W}^\alpha\mathbf{W}_\alpha + \int d^2\bar{\theta}\ \overline{\mathbf{W}}_{\dot{\alpha}}\overline{\mathbf{W}}^{\dot{\alpha}}\right] + \int d^4\theta\ \overline{\mathbf{\Phi}}\exp\left[2gV_a\mathbf{t^a}\right]\mathbf{\Phi} \\ &+ \left[\int d^2\theta\ \mathcal{W}(\mathbf{\Phi}) + \int d^2\bar{\theta}\ \left(\mathcal{W}(\mathbf{\Phi})\right)^\dagger\right],\end{aligned} \tag{2.28}$$

where $\mathcal{W}$ is the so-called superpotential,

$$\mathcal{W}(\mathbf{\Phi}) = \frac{m_{ij}}{2}\Phi_i\Phi_j + \frac{g_{ijk}}{3}\Phi_i\Phi_j\Phi_k.$$

The coefficients multiplying m_{ij} and g_{ijk} have to be singlets under the gauge group. Notice that, once the Wess-Zumino gauge is imposed, the theory is no longer invariant under supersymmetry but it is invariant under ordinary gauge transformations. The d (F) component of each vector (chiral) superfield in Eq. (2.28) is an auxiliary field that can be eliminated with the help of the Euler-Lagrange equations. Therefore, in the Wess-Zumino gauge, each superfield has two components. In the case of a chiral superfield, these components are a complex scalar and a left-handed spinor, while in the vector superfield case, they are a spin one boson and a left-handed spinor.

2.3 The Minimal Supersymmetric Standard Model

The previous section enables us to write a SUSY Yang-Mills theory. This section will be devoted to the description of the minimal supersymmetric extension of the SM, the Minimal Supersymmetric Standard Model (MSSM) [4].

2.3.1 MSSM Lagrangian

Before writing the Lagrangian, the gauge group of the MSSM, its (super)field content and the transformation rules of the superfields have to be fixed. A natural choice for the gauge group is $SU(3)_C \times SU(2)_L \times U(1)_Y$, while the field content of the MSSM is obtained substituting each left-handed Weyl spinor and each Higgs field of the SM with a chiral superfield and each gauge boson with a vector superfield. The representation of the gauge group under which the superfield transforms is inherited from the corresponding SM field. Anomaly cancellation and the existence of Yukawa couplings involving right-handed down-type quarks force us to enlarge the Higgs sector. The minimal way to accomplish it is to introduce an extra gauge doublet. The superfield content of the MSSM is summarized in the Table 2.2. As a notational aside, the SUSY partner of a fermion (gauge boson) is called sfermion (gaugino), while that of an Higgs boson is called Higgsino.

Once the field content of the theory is set, the Lagrangian can be obtained specifying the superpotential $\mathcal{W}$ in Eq. (2.28). In the case of the MSSM the

	Superfield	bosonic field	fermionic field	$SU(3) \times SU(2) \times U(1)$
quarks	$Q_i = (U_i, D_i)^T$	$\tilde{q}_i = (\tilde{u}_i, \tilde{d}_i)^T$	$q_i = (u_i, d_i)^T$	$(\mathbf{3}, \mathbf{2}, \frac{1}{6})$
	U_i^c	$\tilde{u}_i^c$	u_i^c	$(\bar{\mathbf{3}}, \mathbf{1}, -\frac{2}{3})$
	D_i^c	$\tilde{d}_i^c$	d_i^c	$(\bar{\mathbf{3}}, \mathbf{1}, \frac{1}{3})$
leptons	$L_i = (N_i, E_i)^T$	$\tilde{\ell}_i = (\tilde{\nu}_i, \tilde{e}_i)^T$	$\ell_i = (\nu_i, e_i)^T$	$(\mathbf{1}, \mathbf{2}, -\frac{1}{2})$
	E_i^c	$\tilde{e}_i^c$	e_i^c	$(\mathbf{1}, \mathbf{1}, 1)$
gauge	W_i^μ	W_i^μ	$\tilde{W}_i$	$(\mathbf{1}, \mathbf{3}, 0)$
bosons	B^μ	B^μ	$\tilde{B}$	$(\mathbf{1}, \mathbf{1}, 0)$
	G_A^μ	g_A^μ	$\tilde{g}_A$	$(\mathbf{8}, \mathbf{1}, 0)$
Higgs	$H_u = (H_{u1}, H_{u2})^T$	$h_u = (h_u^+, h_u^0)^T$	$\tilde{h}_u = (\tilde{h}_u^+, \tilde{h}_u^0)^T$	$(\mathbf{1}, \mathbf{2}, \frac{1}{2})$
bosons	$H_d = (H_{d1}, H_{d2})^T$	$h_d = (h_d^0, h_d^-)^T$	$\tilde{h}_d = (\tilde{h}_d^0, \tilde{h}_d^-)^T$	$(\mathbf{1}, \mathbf{2}, -\frac{1}{2})$

Table 2.2: Superfield content of the MSSM. The physical fields in the supermultiplets are shown as well. In the last column we show the quantum numbers of the supermultiplets.

superpotential reads as follows,

$$\begin{aligned} \mathcal{W}_{\text{MSSM}} &= \lambda_{ij}^U U_i^c \left[U_j H_{u2} - D_j H_{u1}\right] - \lambda_{ij}^D D_i^c \left[U_j H_{d2} - D_j H_{d1}\right] \\ &- \lambda_{ij}^E E_i^c \left[D_j H_{d2} - E_j H_{d1}\right] - \mu \left[H_{u1} H_{d2} - H_{u2} H_{d1}\right], \end{aligned} \tag{2.29}$$

where, in order to shorten our notation, color indices have been dropped.

Renormalizability and invariance under the Poincaré supergroup do not forbid the presence of baryon and lepton violating terms in the superpotential

$$\begin{aligned} \mathcal{W}_{\Delta B, \Delta L \neq 0} &= \frac{1}{2} \lambda_{ijk} E_k^c \left[N_i E_j - E_i N_j\right] + \lambda'_{ijk} D_k^c \left[N_i D_j - E_i U_j\right] \\ &+ \mu'_i \left[N_i H_{u2} - E_i H_{u1}\right] + \frac{1}{2} \lambda''_{ijk} D_i^c U_j^c D_k^c, \end{aligned} \tag{2.30}$$

which should be suppressed to avoid unobserved processes such as proton decay. In the SM, lepton and baryon conservation is an accidental symmetry arising from Lorentz invariance and can be violated by non-perturbative EW effects. This retains from imposing lepton and baryon number conservation as a fundamental symmetry. Instead, one postulates the conservation of the matter-parity, $P_M = (-1)^{3(B-L)}$, a multiplicatively discrete symmetry that forbids terms like (2.30) and whose exact conservation can be explained in

different theoretically satisfactory ways[3]. Since angular momentum is conserved, conservation of P_M implies the conservation of the R-parity, defined as

$$P_R = (-1)^{3(B-L)+2s},$$

where s is the spin of the particles. R-parity conservation forces the lightest supersymmetric particle to be stable and weakly interacting, hence a suitable candidate for non-baryonic dark matter.

Since degenerate SUSY multiplets are not observed, in any phenomenologically consistent model SUSY has to be broken. Spontaneous breaking of supersymmetry via a non zero vacuum expectation value (VEV) of some field is not viable. Indeed, in order to prevent the breakdown of Lorentz invariance, spontaneous SUSY breaking has to be triggered by a non-zero VEV of the F component of a chiral multiplet (O'Raifeartaigh mechanism [44]) or of the d component of a vector superfield (Fayet-Iliopoulos mechanism [45]). In the MSSM case both mechanism fails, the former would violate gauge invariance while the latter would lead to color or charge breaking.
In the MSSM SUSY is broken explicitly, supposing the breakdown arises spontaneously in an hidden sector of the theory and is mediated to the visible sector (*i.e.* the MSSM) by some interaction shared between the two sectors. The effect of the breakdown is encoded in extra terms entering the MSSM Lagrangian. To ensure the solution of the hierarchy problem, these terms have to break SUSY softly, *i.e.* they do not have to introduce extra quadratic divergences. Terms fulfilling this requirement are mass terms for gauginos, sfermions and Higgs bosons, and couplings involving three scalar particles [46]. These terms have to be added to the MSSM Lagrangian

$$\begin{aligned}
\mathcal{L}_{\text{soft}} &= -\left[\frac{M_3}{2}\tilde{g}^\alpha\tilde{g}_\alpha + \frac{M_2}{2}(\tilde{W}_i)^\alpha(\tilde{W}_i)_\alpha + \frac{M_1}{2}\tilde{B}^\alpha\tilde{B}_\alpha + \text{h.c.} \right] \\
&- \Bigg[(m_Q^2)_{ij}\left(\tilde{u}_i^*\tilde{u}_j + \tilde{d}_i^*\tilde{d}_j\right) + (m_L^2)_{ij}\left(\tilde{\nu}_i^*\tilde{\nu}_j + \tilde{e}_i^*\tilde{e}_j\right) + (m_U^2)_{ij}\tilde{u}_i^{c*}\tilde{u}_j^c \\
&\quad + (m_D^2)_{ij}\tilde{d}_i^{c*}\tilde{d}_j^c + (m_E^2)_{ij}\tilde{e}_i^{c*}\tilde{e}_j^c \Bigg] \\
&- \Bigg[(a^U)_{ij}\tilde{u}_i^c\left(\tilde{u}_j h_{u2} - \tilde{d}_j h_{u1}\right) + (a^D)_{ij}\tilde{d}_i^c\left(\tilde{u}_j h_{d2} - \tilde{d}_j h_{d1}\right)
\end{aligned}$$

[3]For instance, such conservation arises as a remnant of a spontaneously broken $U(1)$ theory fulfilling certain anomaly cancellation conditions [43].

$$
\begin{aligned}
&+ (a^E)_{ij}\tilde{e}^c_i\,(\tilde{\nu}_j h_{d2} - \tilde{e}_j h_{d1}) + \text{h.c.} \Big] \\
- &\left[m^2_{H_u} h^\dagger_u h_u + m^2_{H_d} h^\dagger_d h_d + (b h_{u1} h_{d2} - b h_{u2} h_{d1} + \text{h.c.}) \right]. \quad (2.31)
\end{aligned}
$$

The classical MSSM Lagrangian can be obtained from Eq. (2.28) inserting the superpotential (2.29) and adding the soft breaking terms (2.31). Quantisation of the MSSM requires to add two extra terms to the Lagrangian. The first one fixes the gauge, while the second one describes the dynamics of the Fadeev-Popov ghosts . Their explicit expression can be found in the literature [47] and will not be given here.

2.3.2 MSSM parameters

The SUSY-preserving part of the MSSM Lagrangian has the same number of parameters appearing in the SM, while the SUSY-breaking part of the Lagrangian introduces 105 new parameters, lowering the predictive power of the MSSM.

Nevertheless, these new parameters are tightly constrained since they lead to flavor mixing and CP violation. For instance, the suppression of flavor-changing neutral currents (FCNC) puts limits on the non-diagonal entries of $m^2_{Q,L,U,D,E}$ and $a^{U,D,E}$. Complex phases of the gaugino mass terms and of the trilinear couplings $a^{U,D,E}$ have to be suppressed in order to avoid large CP-violating effects [48]. According to these experimental facts, we neglect family mixing. In particular we set the Yukawa couplings as real and diagonal,

$$
\begin{aligned}
\lambda^U &= \text{diag}(y_{u_1}, y_{u_2}, y_{u_3}), \quad \lambda^D = \text{diag}(y_{d_1}, y_{d_2}, y_{d_3}), \\
\lambda^E &= \text{diag}(y_{e_1}, y_{e_2}, y_{e_3}). \quad (2.32)
\end{aligned}
$$

As a consequence, the CKM matrix is taken as the unity matrix. The trilinear couplings are taken as real and diagonal as well,

$$
\begin{aligned}
a^U &= \text{diag}(A_{u_1} y_{u_1}, A_{u_2} y_{u_2}, A_{u_3} y_{u_3}), \quad a^D = \text{diag}(A_{d_1} y_{d_1}, A_{d_2} y_{d_2}, A_{d_3} y_{d_3}), \\
a^E &= \text{diag}(A_{e_1} y_{e_1}, A_{e_2} y_{e_2}, A_{e_3} y_{e_3}). \quad (2.33)
\end{aligned}
$$

Moreover we set

$$
m^2_X = \text{diag}(M^2_{X,1}, M^2_{X,2}, M^2_{X,3}), \quad \text{with } X = Q, L, U, D, E. \quad (2.34)
$$

These assumptions are the only ones we made throughout our computations. They resemble the assumptions defining the phenomenological MSSM

(pMSSM) [49], although we do not assume the universality of the first two sfermion generations. It is worth to notice that the mass of quarks and leptons of the first two generations are neglected. As will be discussed in chapter 4, these masses are kept as regulators of the mass singularities.

The constraints from FCNC and CP-violations can be evaded supposing that symmetry breaking is "universal", *i.e.* mass matrices at the SUSY breaking scale are flavor blind and can be written as

$$(m_X^2)_{ij} = M_X^2 \delta_{ij}, \qquad \text{with } X = Q, L, U, D, E. \tag{2.35}$$

Further suppression of the FCNC can be achieved supposing that at the SUSY-breaking scale $a_{U,D,E}$ is proportional to the couplings $\lambda^{U,D,E}$ appearing in the superpotential (2.29),

$$(a^X)_{ij} = A_X (\lambda^X)_{ij}, \qquad \text{with } X = U, D, E. \tag{2.36}$$

Undesired CP-violating phases are avoided assuming

$$\arg(M_i), \quad \arg(A_X) \in \{0, \pi\}, \qquad \text{with } i = 1, \ldots, 3 \text{ and } X = U, D, E. \tag{2.37}$$

Conditions (2.35-2.37) ensure that at the EW scale the flavor-mixing couplings and CP-violating phases not belonging to the CKM matrix are suppressed. Under these assumptions all the soft breaking parameters are real.

Universality of the SUSY breaking mechanism reduces substantially the number of parameters; the picture can be further simplified making some assumption on the SUSY breaking mechanism. We will briefly describe the one we will consider in (part of the) numerical analyses performed in this thesis. A more comprehensive discussion on this topic can be found in the literature [50–52].

We will assume that the interaction responsible of the mediation of the SUSY breaking from the hidden to the visible sector is gravity. The connection between the two sectors is therefore described by a non-renormalizable Lagrangian of the type [50]

$$\begin{aligned} \mathcal{L}_{\text{NR}} &= -\frac{1}{M_{\text{P}}} \left(\frac{F_X}{2} \sum_a f_a (\xi_a)^\alpha (\xi_a)_\alpha + \text{h.c.} \right) - \frac{1}{M_{\text{P}}^2} F_X^* F_X k_{ij} \phi_i \phi_j \\ &- \frac{1}{M_{\text{P}}} \left[F_X \left(\frac{1}{6} \lambda'_{ijk} \phi_i \phi_j \phi_k \frac{1}{2} \mu'_{ij} \phi_i \phi_j \right) + \text{h.c.} \right]. \end{aligned} \tag{2.38}$$

ϕ_i (ξ_a) are the scalar (gaugino) fields of the MSSM, while F_X is the F component of a chiral multiplet Φ_X responsible for the SUSY breaking. Soft terms

at the SUSY breaking scale arise expanding the theory around the VEV of F_X and can read from Eq. (2.38) substituting F_X with $\langle F_X \rangle$. The structure of the soft terms is drastically simplified assuming gravity is described by the minimal supergravity (mSUGRA) effective Lagrangian. Indeed under this assumption $f_a = f$, $k_{ij} = k\delta_{ij}$ while μ'_{ij} and λ'_{ijk} can be related to μ and $\lambda^{U,D,E}$ appearing in the superpotential (2.29). Therefore, $m^2_{H_u}$, $m^2_{H_d}$, b, and the parameters in Eqs. (2.35-2.37), can be written in terms of five quantities

$$\begin{aligned} M_3 &= M_2 = M_2 = m_{1/2} \\ M_L^2 &= M_Q^2 = M_U^2 = M_D^2 = M_E^2 = m^2_{H_u} = m^2_{H_d} = m_0^2 \\ A_U &= A_D = A_E = A_0 \\ b &= B_0\mu. \end{aligned} \tag{2.39}$$

The five parameters that fix uniquely the MSSM Lagrangian are usually chosen to be

$$m_0, \quad m_{1/2}, \quad A_0, \quad t_\beta, \quad \text{sign}(\mu), \tag{2.40}$$

where t_β will be defined in section 2.3.3.

2.3.3 MSSM spectrum

This section is devoted to the description of the MSSM spectrum and the masses of the physical fields. As in the SM, in the MSSM electroweak symmetry is spontaneously broken and such breakdown accounts for the masses of quarks, leptons and gauge bosons.

In analogy with the SM case, the $SU(2)_L \times U(1)_Y$ group is spontaneously broken to $U(1)_Q$ via a non-zero VEV of the components of the Higgs doublets. Defining

$$h_u = \begin{pmatrix} h_{u1} \\ h_{u2} \end{pmatrix} = \begin{pmatrix} h_u^+ \\ h_u^0 \end{pmatrix}, \qquad h_d = \begin{pmatrix} h_{d1} \\ h_{d2} \end{pmatrix} = \begin{pmatrix} h_d^0 \\ h_d^- \end{pmatrix},$$

the Higgs potential reads

$$\begin{aligned} V_{\text{Higgs}} &= (|\mu|^2 + m^2_{H_u})(|h_u^0|^2 + |h_u^+|^2) + (|\mu|^2 + m^2_{H_d})(|h_d^0|^2 + |h_d^-|^2) \\ &+ \frac{g^2 + g'^2}{8}\left(|h_u^0|^2 + |h_u^+|^2 - |h_d^0|^2 - |h_d^0|^2\right) \\ &+ \left[b(h_u^+ h_d^- - h_u^0 h_d^0) + \text{h.c.}\right] + \frac{g^2}{2}\left|h_u^+ h_d^{0*} - h_u^0 h_d^{-*}\right|^2. \end{aligned} \tag{2.41}$$

Thanks to $SU(2)_L \times U(1)_Y$ invariance it is always possible to fix an $U(1)_Q$-invariant minimum of the type

$$h_u = \begin{pmatrix} 0 \\ v_u \end{pmatrix}, \quad h_d = \begin{pmatrix} v_d \\ 0 \end{pmatrix}, \tag{2.42}$$

with $v_{u,d}$ non-negative numbers. If the origin is not a stable minimum and if the potential is bounded, the configuration (2.42) is a minimum. The aforementioned requirements lead to the conditions

$$2|\mu|^2 + m_{H_u}^2 + m_{H_d}^2 - 2b > 0, \qquad (|\mu|^2 + m_{H_u}^2)(|\mu|^2 + m_{H_d}^2) < b^2. \tag{2.43}$$

If conditions (2.43) are fulfilled the value of the two VEV's is obtained solving

$$\begin{aligned} (|\mu|^2 + m_{H_u}^2)v_u &= bv_d + \frac{1}{4}\left(g^2 + g'^2\right)(v_d^2 - v_u^2), \\ (|\mu|^2 + m_{H_d}^2)v_d &= bv_u - \frac{1}{4}\left(g^2 + g'^2\right)(v_d^2 - v_u^2). \end{aligned} \tag{2.44}$$

The masses of the different particles can be obtained by expanding Eq. (2.41) around the VEV, using the decomposition

$$h_u = \begin{pmatrix} \phi_u^+ \\ v_u + \frac{1}{\sqrt{2}}(\phi_u^0 + i\chi_u^0) \end{pmatrix}, \quad h_d = \begin{pmatrix} v_d + \frac{1}{\sqrt{2}}(\phi_d^0 - i\chi_d^0) \\ -\phi_d^- \end{pmatrix}, \tag{2.45}$$

and diagonalizing the mass matrices. In the following, we give a brief discussion on the spectrum of the MSSM.

Higgs bosons

The mass terms of the Higgs bosons can be obtained plugging (2.45) into the potential (2.41) and evaluating the second derivative with respect to ϕ's and χ's at the vacuum configuration. The mass eigenstates read

$$\begin{aligned} \begin{pmatrix} H^0 \\ h^0 \end{pmatrix} &= \begin{pmatrix} c_\alpha & s_\alpha \\ -s_\alpha & c_\alpha \end{pmatrix} \begin{pmatrix} \phi_d^0 \\ \phi_u^0 \end{pmatrix}, \\ \begin{pmatrix} G^0 \\ A^0 \end{pmatrix} &= \begin{pmatrix} c_\beta & s_\beta \\ -s_\beta & c_\beta \end{pmatrix} \begin{pmatrix} \chi_d^0 \\ \chi_u^0 \end{pmatrix}, \\ \begin{pmatrix} G^\pm \\ H^\pm \end{pmatrix} &= \begin{pmatrix} c_\beta & s_\beta \\ -s_\beta & c_\beta \end{pmatrix} \begin{pmatrix} \phi_d^\pm \\ \phi_u^\pm \end{pmatrix}, \end{aligned} \tag{2.46}$$

where c_α and s_α are abbreviations for $\cos\alpha$ and $\sin\alpha$ respectively. Physical fields are the CP-even Higgs h^0 and H^0, the CP-odd boson A^0 and the charged Higgs $H^\pm$. G^0 and $G^\pm$ are the unphysical would-be Goldstone bosons related to spontaneous symmetry breaking. The mixing angles β and α are given by

$$\begin{aligned} t_\beta &= \frac{v_u}{v_d}, \text{ with } 0 < \beta < \frac{\pi}{2}, \\ t_{2\alpha} &= t_{2\beta}\,\frac{b^2(t_\beta + 1/t_\beta)^2 + M_Z^2}{b^2(t_\beta + 1/t_\beta)^2 - M_Z^2}, \text{ with } -\frac{\pi}{2} < \alpha < 0. \end{aligned} \tag{2.47}$$

t_γ, is the abbreviation of $\tan\gamma$. The masses of the Higgs particles read as follows,

$$\begin{aligned} M_{A^0} &= b(t_\beta + 1/t_\beta), \\ M_{H^0,h^0} &= \frac{1}{\sqrt{2}}\sqrt{M_A^2 + M_Z^2 \pm \sqrt{(M_{A^0}^2 + M_Z^2)^2 - 4M_Z^2 M_{A^0}^2 c_{2\beta}^2}}, \\ M_{H^\pm} &= \sqrt{M_{A^0}^2 + M_W^2}. \end{aligned} \tag{2.48}$$

The previous relations set an upper bound on the mass of the lightest Higgs h^0, $M_{h^0} < M_Z$. Such a light Higgs should have been already discovered at LEP [53] and Tevatron [54]. The non observation of h^0 can be explained including higher order corrections to the Higgs mass [5] that increase the tree-level value of the Higgs mass up to $50 - 100$ % [55]. Nevertheless, the MSSM predicts a rather light Higgs particle h^0, whose mass has to be below 135 GeV [56].

SM fermions and gauge bosons

As in the SM case, the mass eigenstates of the gauge bosons are given by Eq. (2.8), while the corresponding masses can be obtained from Eq. (2.9) performing the substitution $v \to \sqrt{v_u^2 + v_d^2}$.

The mass terms of quark and leptons are obtained from the Yukawa interaction terms

$$\mathcal{L}_{\rm SM,f} = -\left[v_u \lambda_{ij}^U (u_i)^\alpha (u_j^c)_\alpha + v_d \lambda_{ij}^D (d_i)^\alpha (d_j^c)_\alpha + v_d \lambda_{ij}^E (e_i)^\alpha (e_j^c)_\alpha + \text{h.c.}\right].$$

Mass eigenstates can be obtained by means of a bi-unitary transformation,

$$f_i' = U_{ij}^f f_j, \qquad f_i'^c = (V^f)_{ij} f_j^c \qquad (f = u, d, e).$$

The physical masses read (no sum over i):

$$\begin{aligned} m_{u_i} &= v_u (U^{u*})_{ij} \lambda_{jk}^U (V^{u\dagger})_{ki}, \quad m_{d_i} = v_d (U^{d*})_{ij} \lambda_{jk}^D (V^{d\dagger})_{ki}, \\ m_{e_i} &= v_d (U^{e*})_{ij} \lambda_{jk}^E (V^{e\dagger})_{ki}. \end{aligned} \tag{2.49}$$

Notice that the mass eigenstates can be arranged into Dirac spinors

$$\psi_{u_i} = \begin{pmatrix} (u_i)_\alpha \\ \overline{u_i^c}^{\dot\alpha} \end{pmatrix}, \quad \psi_{d_i} = \begin{pmatrix} (d_i)_\alpha \\ \overline{d_i^c}^{\dot\alpha} \end{pmatrix}, \quad \psi_{e_i} = \begin{pmatrix} (e_i)_\alpha \\ \overline{e_i^c}^{\dot\alpha} \end{pmatrix}.$$

In terms of these Dirac spinors, the mass term can be written as follows,

$$-\left[m_{u_i} \bar\psi_{u_i} \psi_{u_i} + m_{d_i} \bar\psi_{d_i} \psi_{d_i} + m_{e_i} \bar\psi_{e_i} \psi_{e_i}\right].$$

Assuming diagonal Yukawa couplings, Eqs. (2.32), we have $V_{ij}^x = U_{ij}^x = \delta_{ij}$. In this case the CKM matrix is the identity matrix.

Neutralinos, charginos and gluinos

Having the same quantum numbers, neutral higgsinos and neutral gauginos mix to give rise to four mass eigenstates, called neutralinos. The mass terms are described by

$$\mathcal{L}_{\text{Neut.}} = -\frac{1}{2}\left[(\psi_i)^\alpha Y_{ij}(\psi_j)_\alpha + \text{h.c.}\right], \tag{2.50}$$

where $\psi = (\tilde{B}, \tilde{W}^0, \tilde{h}_d^0, \tilde{h}_u^0)^T$, while the matrix Y is given by

$$Y = \begin{pmatrix} M_1 & 0 & -M_Z s_W c_\beta & M_Z s_W s_\beta \\ 0 & M_2 & M_Z c_W c_\beta & -M_Z c_W s_\beta \\ -M_Z s_W c_\beta & M_Z c_W c_\beta & 0 & -\mu \\ M_Z s_W s_\beta & -M_Z c_W s_\beta & -\mu & 0 \end{pmatrix}. \tag{2.51}$$

In the real MSSM this is a real symmetric matrix that can be diagonalized by a unitary matrix N. The mass eigenstates and the corresponding masses are given by

$$\psi_i' = N_{ij}\psi_i, \qquad m_{\tilde{\chi}_i^0} = (N^*)_{ij} Y_{jk} (N^\dagger)_{ki}. \tag{2.52}$$

Neutralinos are usually described by means of four-dimensional Majorana spinors,

$$\tilde{\chi}_i^0 = \begin{pmatrix} (\psi_i')_\alpha \\ (\overline{\psi'}_i)^{\dot{\alpha}} \end{pmatrix}. \tag{2.53}$$

Similarly, charged higgsinos and gauginos can mix giving mass eigenstates, the charginos. They are obtained diagonalizing the following mass term,

$$\mathcal{L}_{\text{Charg.}} = -\frac{1}{2}\left[(\psi_i^-)^\alpha X_{ij}(\psi_j^+)_\alpha + (\psi_i^+)^\alpha X_{ji}(\psi_j^-)_\alpha + \text{h.c.}\right], \tag{2.54}$$

where $\psi^\pm$ are defined as

$$\psi^- = \begin{pmatrix} \tilde{W}^- \\ \tilde{h}_d^- \end{pmatrix}, \quad \psi^+ = \begin{pmatrix} \tilde{W}^+ \\ \tilde{h}_u^+ \end{pmatrix}, \quad \text{with } \tilde{W}^\pm = \frac{1}{\sqrt{2}}\left(\tilde{W}^1 \mp i\tilde{W}^2\right). \tag{2.55}$$

The matrix X,

$$X = \begin{pmatrix} M_2 & \sqrt{2}s_\beta M_W \\ \sqrt{2}c_\beta M_W & \mu \end{pmatrix}, \tag{2.56}$$

can be diagonalized by a bi-unitary transformation, yielding mass eigenstates and corresponding masses as follows,

$$\psi_i'^- = U_{ij}\psi_j^-, \quad \psi_i'^+ = V_{ij}\psi_j^+, \quad m_{\tilde{\chi}_i^\pm} = (U^*)_{ij} X_{jk} (V^\dagger)_{ki}. \tag{2.57}$$

These left-handed spinors can be combined into a four-dimensional Dirac spinor,

$$\tilde{\chi}_i^{\pm} = \begin{pmatrix} (\psi_i'^{\pm})_\alpha \\ (\overline{\psi'^{\mp}}_i)^{\dot{\alpha}} \end{pmatrix}. \tag{2.58}$$

Being the only fermionic octet of $SU(3)_C$, gluinos do not mix with any other particle. Therefore gauge eigenstates ($\tilde{g}$) are mass eigenstates and, in the case of the real MSSM, the mass eigenvalue is M_3. Usually the left-handed Weyl spinors describing gluinos are arranged in a four-dimensional Majorana spinor,

$$\psi_{\tilde{g}} = \begin{pmatrix} \tilde{g}_\alpha \\ \overline{\tilde{g}}^{\dot{\alpha}} \end{pmatrix}.$$

Sfermions

Neglecting flavor mixing (*i.e.* assuming that $(m^2_{Q,L})_{ij}$ and $(m^2_{U,D,E})_{ij}$ are diagonal) the sfermion mass terms read

$$\mathcal{L}_{\text{Sfer.}} = -\sum_{i=1}^{3} \left\{ \sum_{f=u,d,e} \left[(\tilde{f}^*_{Li}, \tilde{f}^*_{Ri}) M^2_{\tilde{f}_i} \begin{pmatrix} \tilde{f}_{Li} \\ \tilde{f}_{Ri} \end{pmatrix} \right] + \left(M^2_{Li} - \frac{1}{2} M_Z^2 c_{2\beta} \right) \tilde{\nu}^*_{Li} \tilde{\nu_{Li}} \right\},$$

where $(\tilde{f}_{Li}, \tilde{f}_{Ri}) = (\tilde{f}_i, \tilde{f}_i^c)$ and $\tilde{\nu}_{Li} = \tilde{\nu}_i$. The matrix $M^2_{\tilde{f}_i}$ is defined as

$$M^2_{\tilde{f}_i} = \begin{pmatrix} M^2_{Fi} + M_Z^2 c_{2\beta}(I_3^f - Q_f s_W^2) + m^2_{f_i} & m_{f_i}(A_{f_i} - \mu\kappa) \\ m_{f_i}(A_{f_i} - \mu\kappa) & M^2_{F'i} + M_Z^2 c_{2\beta} Q_f s_W^2) + m^2_{f_i} \end{pmatrix}, \tag{2.59}$$

with $(\tilde{f}, F, F') \in \{(\tilde{u}, Q, U), (\tilde{d}, Q, D), (\tilde{e}, L, E)\}$, while $\kappa = 1/t_\beta$ if $f = u$ and $\kappa = t_\beta$ otherwise. $\tilde{\nu}_{Li}$ is a mass eigenstate and its mass reads

$$m^2_{\tilde{\nu}_{Li}} = M_L^2 - \frac{1}{2} M_Z^2 c_{2\beta}. \tag{2.60}$$

The others mass eigenstates can be obtained diagonalizing $M^2_{\tilde{f}_i}$,

$$\begin{pmatrix} \tilde{f}_{1i} \\ \tilde{f}_{2i} \end{pmatrix} = \begin{pmatrix} c_{\theta_{\tilde{f}_i}} & s_{\theta_{\tilde{f}_i}} \\ -s_{\theta_{\tilde{f}_i}} & c_{\theta_{\tilde{f}_i}} \end{pmatrix} \begin{pmatrix} \tilde{f}_{Li} \\ \tilde{f}_{Ri} \end{pmatrix}. \tag{2.61}$$

The corresponding mass eigenvalues are

$$\begin{aligned} m^2_{\tilde{f}_{1i,2i}} &= m^2_{f_i} + \frac{1}{2}\left[M^2_{Fi} + M^2_{F'i} + M_Z^2 c_{2\beta} I_3^f \mp \sqrt{\Delta_{f_i}} \right], \qquad (2.62) \\ \Delta_{f_i} &= \left[M^2_{Fi} - M^2_{F'i} + M_Z^2 c_{2\beta}(I_f^3 - 2Q_f s_W^2) \right]^2 + 4 m^2_{fi} \left(A_{fi} - \mu\kappa \right)^2. \end{aligned}$$

From Eq. (2.59) one can infer that, if the mass m_{f_i} of the fermion f_i can be neglected, mass eigenstates coincide with gauge eigenstates.

For later reference we will express the matrix (2.59) in terms of the mass eigenstates $m_{\tilde{f}_{1,2i}}$ and the mixing angle $\theta_{\tilde{f}_i}$,

$$M^2_{\tilde{f}_i} = \begin{pmatrix} c^2_{\theta_{\tilde{f}_i}} m^2_{\tilde{f}_{i1}} + s^2_{\theta_{\tilde{f}_i}} m^2_{\tilde{f}_{i2}} & c_{\theta_{\tilde{f}_i}} s_{\theta_{\tilde{f}_i}} (m^2_{\tilde{f}_{i1}} - m^2_{\tilde{f}_{i2}}) \\ c_{\theta_{\tilde{f}_i}} s_{\theta_{\tilde{f}_i}} (m^2_{\tilde{f}_{i1}} - m^2_{\tilde{f}_{i2}}) & c^2_{\theta_{\tilde{f}_i}} m^2_{\tilde{f}_{i2}} + s^2_{\theta_{\tilde{f}_i}} m^2_{\tilde{f}_{i1}} \end{pmatrix}. \tag{2.63}$$

Comparing Eq. (2.59) and Eq. (2.63) one gets

$$\sin 2\theta_{\tilde{f}_i} = \frac{2 m_{f_i} (A_{f_i} - \mu\kappa)}{m^2_{\tilde{f}_{i1}} - m^2_{\tilde{f}_{i2}}}. \tag{2.64}$$

Notice that from $SU(2)$ invariance, the entries of the mass matrices $M^2_{\tilde{u}_i}$ and $M^2_{\tilde{d}_i}$ are no longer independent since

$$c^2_{\theta_{\tilde{d}_i}} m^2_{\tilde{d}_{i1}} + s^2_{\theta_{\tilde{d}_i}} m^2_{\tilde{d}_{i2}} - m^2_{d_i} = c^2_{\theta_{\tilde{u}_i}} m^2_{\tilde{u}_{i1}} + s^2_{\theta_{\tilde{u}_i}} m^2_{\tilde{u}_{i2}} - m^2_{u_i} - M^2_W c_{2\beta}. \tag{2.65}$$

Therefore, the squark sector is described by five distinct parameters, since μ and t_β are usually fixed in other sectors of the MSSM.

Chapter 3

Supersymmetry at colliders

In this chapter we give a short review of the status of the SUSY searches at colliders. The first three sections are devoted to the description of the various strategies used at LEP (section 3.1), Tevatron (section 3.2) and HERA, (section 3.3). Section 3.4 describes the searches which are foreseen at the Large Hadron Collider and their discovery potential.

3.1 Direct searches at LEP

The large electron positron collider at CERN operated from 1989. Four different experiments (ALEPH [57], DELPHI [58], L3 [59] and OPAL [60]) collected data during the eleven years of running. After a first run at the Z-boson resonance peak ($\sqrt{s} \sim 91$ GeV), from 1995 the center-of-mass energy was constantly increased reaching 209 GeV. Each experiment collected ~ 1 fb^{-1} of data, of which 235 pb^{-1} above 204 GeV. This set of data is the most relevant for new physics searches.
Being an e^+e^- collider, all SUSY particles except the gluino can be produced at LEP. Accordingly, each experiment performed many searches for the production of different type of SUSY particles.

Higgs Bosons

In the scenarios accessible at LEP, The main search channel for neutral Higgs Bosons are the Higgsstrahlung processes

$$e^+e^- \to \mathcal{H}Z \quad (\mathcal{H} = h^0, H^0), \tag{3.1}$$

with s-channel Z-exchange. Four different final states topologies have been considered, according to the different decay channels of the particles. The

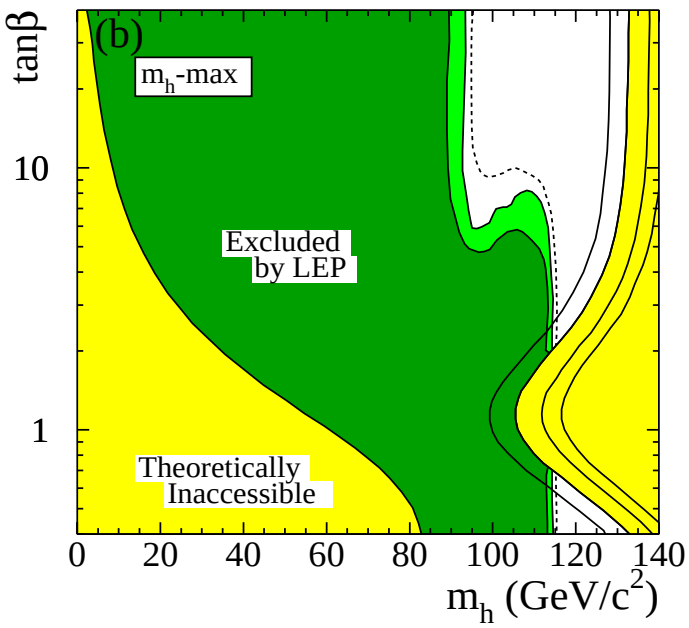

Figure 3.1: 95% CL (light green) and 99.7% CL (dark green) exclusion limit in the (m_{h^0}, t_β) plane [53]. The dashed line is the expected 95% CL exclusion limit in absence of signal. The upper boundaries correspond to four different top masses (from left to right 169.3, 174.3, 179.3 and 183 GeV)

first topology considered is the four jets topology, $(\mathcal{H} \to b\bar{b})(Z \to q\bar{q})$, in which the invariant mass of two jets is close to the mass of the Z boson, while the other two jets are tagged as b-jets. The other topologies are the two b-jets and two leptons topology, $(\mathcal{H} \to b\bar{b})(Z \to \ell^+\ell^-)$, the missing energy topology, $(\mathcal{H} \to b\bar{b}, \tau^+\tau^-)(Z \to \nu\bar{\nu})$, and the tau-leptons topology $(\mathcal{H} \to \tau^+\tau^-)(Z \to q\bar{q})$ and $(\mathcal{H} \to b\bar{b}, \tau^+\tau^-)(Z \to \tau^+\tau^-)$. Background comes mainly from fermion pair production and from di-boson production possibly accompanied by photon and gluon radiation.

Another important process is the associated production

$$e^+e^- \to \mathcal{H}A^0, \tag{3.2}$$

which has a sensitivity in the MSSM parameter space complementary to that of the process (3.1). The signal topologies are mainly three: four b-jets from $(\mathcal{H} \to b\bar{b})(A^0 \to b\bar{b})$, four τ leptons from $(\mathcal{H} \to \tau^+\tau^-)(A^0 \to \tau^+\tau^-)$ and the mixed final states $(\mathcal{H} \to \tau^+\tau^-)(A^0 \to b\bar{b})$ and $(\mathcal{H} \to b\bar{b})(A^0 \to \tau^+\tau^-)$. The SM background has the same origin as that of Higgsstrahlung.
No significant excess over the SM background has been found, and the outcome of the Neutral Higgs searches is the exclusion of regions of the MSSM

parameter space. The combined result of the four experiments is available in Ref. [53] while the singular analyses of the different experiments are available in Ref. [61]. As an example, in Fig. 3.1 we show the exclusion limit in the (m_{h^0}, t_β) plane set by the combined analysis. The scenario considered is the most conservative one, namely the $m_h^{\max}$. At 95% confidence level the regions $m_{h^0} \leq 92.8$ GeV and $0.7 \leq t_\beta \leq 2$ are excluded.
Particular studies have been devoted to the possibility of Higgs decay into SUSY particles, in particular to scenarios in which $h^0 \to \tilde{\chi}_1^0\tilde{\chi}_1^0$ is allowed [62]. If the Higgs production cross section is the SM one[1], such possibility do not alter the SM bounds on the Higgs mass.

Concerning the charged Higgs boson, the main production channel at LEP is

$$e^+e^- \to H^+H^-. \tag{3.3}$$

Under the assumption $BR(H^+ \to \tau^+\bar{\nu}_\tau) + BR(H^+ \to c\bar{s}) = 1$, the signal topologies are three: four jets from $(H^+ \to c\bar{s})(H^- \to \bar{c}s)$, two jets, a τ and missing energy from $(H^+ \to c\bar{s})(H^- \to \tau^-\bar{\nu}_\tau)$ and two a-complanar τ lepton arising from $(H^+ \to \tau^+\nu_\tau)(H^- \to \tau^-\bar{\nu}_\tau)$. The main SM background is the W^+W^- production. Each of the four collaboration performed this analysis [63], the combined results of the four experiments [64] lead to a lower bound of 78.6 GeV on $m_{H^\pm}$. This bound holds for every value of $BR(H^+ \to \tau^+\bar{\nu}_\tau)$.

3.1.1 Charginos and neutralinos

At LEP, there were dedicated searches for the production of a pair of lightest charginos,

$$e^+e^- \to \tilde{\chi}_1^+\tilde{\chi}_1^-. \tag{3.4}$$

If kinematically allowed, the main decay channel of the chargino is a two body decay $\tilde{\chi}_1^\pm \to \ell^\pm\tilde{\nu}$. Otherwise the three-body chargino decay chain $\tilde{\chi}_1^\pm \to f\bar{f}'\tilde{\chi}_1^0$ is dominant.
When sfermions are heavier than $\tilde{\chi}_1^0$ and $M_2 \leq 1$ TeV, the topologies of the signal are three: the all hadronic topology, $(\tilde{\chi}_1^+ \to q\bar{q}'\tilde{\chi}_1^0)(\tilde{\chi}_1^- \to q''\bar{q}'''\tilde{\chi}_1^0)$, the fully leptonic one, $(\tilde{\chi}_1^+ \to \ell\nu\tilde{\chi}_1^0)(\tilde{\chi}_1^- \to \ell'\nu'\tilde{\chi}_1^0)$, and the mixed topologies $(\tilde{\chi}_1^+ \to \ell\nu\tilde{\chi}_1^0)(\tilde{\chi}_1^- \to q''\bar{q}'''\tilde{\chi}_1^0)$ and $(\tilde{\chi}_1^+ \to q\bar{q}'\tilde{\chi}_1^0)(\tilde{\chi}_1^- \to \ell'\nu'\tilde{\chi}_1^0)$. No excess over the SM background was observed and a lower limit of the order of 203 GeV has been set for $m_{\tilde{\chi}^\pm,1}$, provided that $m_{\tilde{\nu}} \geq 200$ GeV [65].
When $M_2 \geq 1$ TeV, the difference $m_{\tilde{\chi}^\pm,1} - m_{\tilde{\chi}^0,1}$ is so small that the selection efficiency of the signal decreases. In these scenarios a hard photon from the

[1] This is the case in the low t_β regime.

initial state can be used to tag the produced chargino pair $e^+e^- \to \tilde{\chi}_1^+\tilde{\chi}_1^-\gamma$. The combination of these two strategies allow to set a lower bound on $m_{\tilde{\chi}^\pm,1}$. This lower bound equals 92 GeV [66] and it is independent of the mass difference $m_{\tilde{\chi}_1^\pm} - m_{\tilde{\chi}_1^0}$.

When the 2-body decay is kinematically allowed, *i.e.* when the sfermion masses are lower, the sensitivity of the previous analysis become so bad that the process (3.4) become almost invisible. In this case, constraints on the chargino mass can be set assuming gaugino and sfermions mass unification and looking at slepton production and neutralino pair production processes. However, the mass limit set in the case of heavy slepton mass is practically unchanged.

In the scenario considered at LEP the lightest neutralino is the LSP. In principle, direct searches for the LSP can be performed using the process

$$e^+e^- \to \tilde{\chi}_1^0\tilde{\chi}_1^0\gamma, \tag{3.5}$$

where the photon tags the invisible final state. In practice, this process is completely hidden in the irreducible background related to the process $e^+e^- \to \nu\bar{\nu}\gamma$ which, above the Z production threshold, becomes important. Therefore, limits on the mass of the lightest neutralino can be constrained from chargino, leptons and Higgs searches, provided that some assumptions on the model are done. Assuming gaugino and sfermion mass unification, the lower limit on the $m_{\tilde{\chi}_1^0}$ is 47 GeV [67]. In a more constrained MSSM, in which μ is obtained from the other parameters, $m_{\tilde{\chi}_1^0} \geq 50$ GeV [68].

3.1.2 Sleptons

The most model-independent channel in slepton searches is the production of a pair of right-handed muon sleptons,

$$e^+e^- \to \tilde{\mu}_R\tilde{\mu}_R^*, \tag{3.6}$$

via s-channel Z or γ exchange. Since the mixing in the smuon sector is negligible, besides the smuon mass only SM parameters enter at tree level. The main decay mode is $\tilde{\mu}_R \to \tilde{\chi}_1^0\mu$ leading to a signal topology of two acomplanar muons and missing energy. The smuon decay is model-dependent and in particular depends on the difference $m_{\tilde{\mu},R} - m_{\tilde{\chi}_1^0}$. The leading SM background depends on this difference as well[2]. Therefore, the results depend

[2]If $m_{\tilde{\mu},R} - m_{\tilde{\chi}_1^0}$ is big the main background comes from WW production. If $\tilde{\mu}_R$ and $\tilde{\chi}_1^0$ become degenerate, the selection efficiency decrease and the main background is the process $e^+e^- \to e^+e^-\mu^+\mu^-$ with two virtual photon interacting and the electrons escaping in the beam pipe.

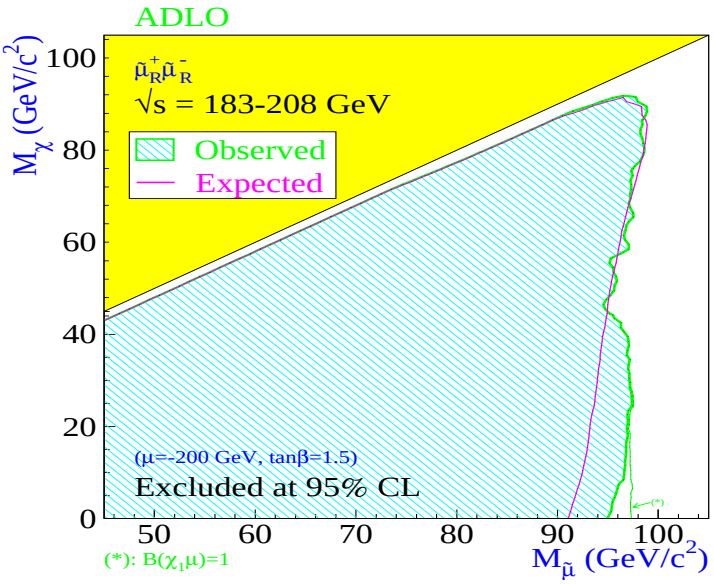

Figure 3.2: 95% CL exclusion limit in the $(m_{\tilde{\mu},R}, m_{\tilde{\chi}^0,1})$ plane [69]. The dotted green line is the expected 95% CL exclusion assuming $\mathrm{BR}(\tilde{\mu}_R \to \tilde{\chi}^0_1\mu) = 1$

either on the smuon mass and on the mass of the LSP. Exclusion limits in the $(m_{\tilde{\mu},R}; m_{\tilde{\chi}^0_1})$ plane set by the combination of the four experiments [69] are shown in Fig. 3.2. If $m_{\tilde{\mu},R} - m_{\tilde{\chi}^0_1} \geq 5$ GeV, smuon masses below 99 GeV are excluded.

A similar analysis can be applied to the process of pair production of the lightest stau $\tilde{\tau}_1$. The limit on the lightest stau turns out to be lower than the limit on the smuon mass, *i.e.* $m_{\tilde{\tau},1} \geq 86 - 95$ GeV, depending on $m_{\tilde{\chi}^0_1}$ and provided that $m_{\tilde{\tau},1} - m_{\tilde{\chi}^0_1} \geq 7$ GeV [69]. The main difficulties related to stau production is the non-negligible mixing between $\tilde{\tau}_R$ and $\tilde{\tau}_L$, which can reduce the Z–$\tilde{\tau}_1$–$\tilde{\tau}^*_1$ coupling. Moreover, the selection efficiency of the signal is reduced by the presence of at least one neutrino arising from the τ decay.

The previous technique applies to right-handed selectron as well. In this case the production process is

$$e^+e^- \to \tilde{e}_R\tilde{e}^*_R, \tag{3.7}$$

and the signal is identified as two a-complanar electrons and missing energy. Constraints on the selectron masses can be obtained only making some assumption on the model. Indeed, the process (3.7) depends on the particular

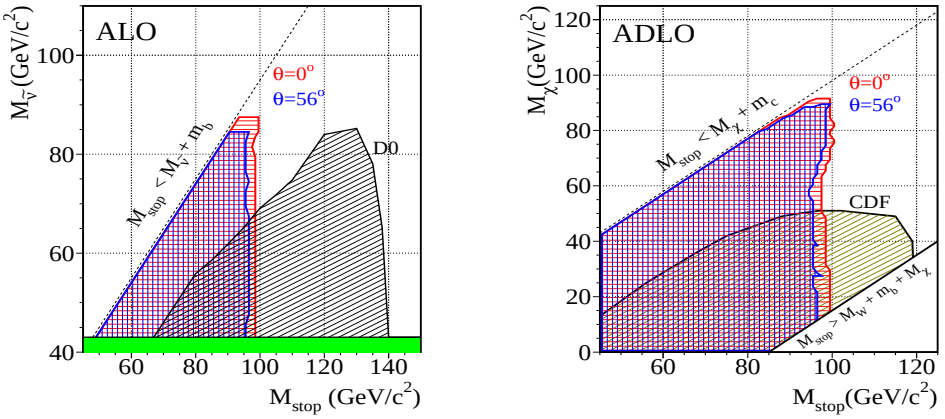

Figure 3.3: Left panel: 95% CL exclusion limit from $\tilde{t}_1 \to b\ell\tilde{\nu}$ [72]. Excluded region are given for two different values of the mixing angle $\theta_{\tilde{t}}$. The D0 experiment results quoted in Ref. [73] are shown as well. Right panel: 95% CL exclusion limit from $\tilde{t}_1 \to c\tilde{\chi}_1^0$ [72]. Again, the excluded regions are shown for two values of $\theta_{\tilde{t}}$. CDF experiments limits available in Ref. [74] are quoted.

scenario owing to the presence of diagrams with t-channel neutralino exchange. In the case of selectron production, associated $\tilde{e}_L\tilde{e}_R$ production is helpful in the hunting for $\tilde{e}_R$ when $m_{\tilde{e},R} - m_{\tilde{\chi}_1^0}$ is small[3]. Assuming gaugino and slepton mass unification, a lower bound of 73 GeV on $m_{\tilde{e},R}$ is set, independently on $m_{\tilde{e},R} - m_{\tilde{\chi}_1^0}$ [70].

Finally, constraints on the sneutrino mass can be set measuring the invisible width of the Z boson. In the case of sneutrino LSP or NLSP (next to lightest SUSY particle) $m_{\tilde{\nu}} \geq 45$ GeV [71].

3.1.3 Squarks

At LEP, the searches for squarks were focused on the search for the squarks of the third generations, *i.e.* top and bottom squarks. This is because in many SUSY scenarios, the lightest stop and sbottom, $\tilde{t}_1$ and $\tilde{b}_1$, are the lightest among the squarks.

[3]Indeed, a single electron final state from the decay $\tilde{e}_L \to e\tilde{\chi}_1^0$ tags the associated production.

The main production channel of top squarks is

$$e^+e^- \to \tilde{t}_1\tilde{t}_1^*, \tag{3.8}$$

via s-channel Z and γ exchange. If kinematically allowed, the main decay channel is $\tilde{t}_1 \to b\ell\tilde{\nu}$. Otherwise the leading decay is $\tilde{t}_1 \to c\tilde{\chi}_1^0$, since at the energy range accessible at LEP $\tilde{t} \to b\tilde{\chi}_1^+$ is kinematically forbidden. In both cases, the main SM background is constituted by di-bosons, $We\nu$, and $q\bar{q}\gamma$ production, and depends on the value of the difference $m_{\tilde{t},1} - m_{\tilde{\nu}}$.
If the decay into sneutrino is kinematically allowed, the signal topology is constituted by two a-complanar b-jets, two isolated leptons and missing energy. The combined analysis of the four experiments for $\tilde{t}_1$ searches do not observe any excess from the SM background, and allows to exclude regions of the $(m_{\tilde{t},1}, m_{\tilde{\nu}})$ plane [72]. In the left panel of Fig. 3.3 we show the exclusion limit in the $(m_{\tilde{t},1}, m_{\tilde{\nu}})$ plane for two values of the mixing angle of the stop sector $\theta_{\tilde{t}}$. In particular the value $\theta_{\tilde{t}} = 0°$ corresponds to a left-handed $\tilde{t}_1$ and $\theta_{\tilde{t}} = 56°$, corresponds to vanishing Z–$\tilde{t}_1$–$\tilde{t}_1^*$ coupling. The latter is the worst-case scenario and leads to the most conservative bounds on the stop mass. This bound is 96 GeV, provided $m_{\tilde{\nu}} \leq 86$ GeV.
When the dominant stop decay channel is $\tilde{t}_1 \to c\tilde{\chi}_1^0$, the signal topology is two a-complanar jets and missing energy. In the right panel of Fig. 3.3 we show the 95% CL exclusion limit in the $(m_{\tilde{t},1}, m_{\tilde{\chi}_1^0})$ plane arising from the combined analysis of the four collaborations [72]. In the worst-case scenario the region $m_{\tilde{t}_1} \leq 96$ GeV is excluded, provided $m_{\tilde{t},1} - m_{\tilde{\chi}_1^0} - m_c \geq 5$ GeV. It is worth to mention that when $m_{\tilde{t},1} - m_{\tilde{\chi}_1^0}$ is small (*i.e.* ≤ 6 GeV) the stop lifetime is sizable and the possibility of long lived R-hadrons has to be taken into account. A dedicated analysis [75] set a limit of 63 GeV on the stop mass, independently on the difference $m_{\tilde{t},1} - m_{\tilde{\chi}_1^0}$.

The lightest sbottom $\tilde{b}_1$, is mainly produced in pairs via the process

$$e^+e^- \to \tilde{b}_1\tilde{b}_1^*. \tag{3.9}$$

Sbottom searches are simpler than the stop ones, since the (tree-level) dominant decay mode is $\tilde{b}_1 \to b\tilde{\chi}_1^0$. The signal topology is two a-complanar b-jets and the combined results of the four LEP experiments do not observe any significant deviation from the SM background. Lower bounds on $m_{\tilde{b},1}$ depend on the mixing angle $\tilde{\theta}_{\tilde{b}}$. In the worst-case scenario, corresponding to vanishing Z–$\tilde{b}_1$–$\tilde{b}_1^*$ coupling ($\theta_{\tilde{b}} = 68°$), the lower bound is 95 GeV [72].

3.2 Direct searches at the Tevatron

Tevatron is a proton-anti–proton ($p\bar{p}$) collider at Fermilab. At the time of writing (2009), this collider is running, likely it will run the next year while the running in 2011 is under evaluation. Two experiments are collecting data at this collider: CDF [76] and D0 [77]. The first phase of running (Run I) was characterized by a center-of-mass energy of 1.8 TeV and lead to the discovery of the top quark (1995). The second phase (Run II) began in 2001, the center-of-mass energy was increased to 1.96 TeV, and the instantaneous luminosity was increased as well. At the end of 2008, 5 fb^{-1} of data were delivered by Tevatron and others 1.5 fb^{-1} are foreseen for this year.

The center-of-mass energy available at Tevatron is bigger than that available at LEP and allows a wider energy range for new particles searches. Nevertheless, Tevatron is an hadron collider, therefore the background is larger than the background at LEP. Both CDF and D0 performed many searches for SUSY particle production processes. In the following a small overview of such processes is given.

3.2.1 Higgs bosons

At the Tevatron, the dominant production mechanism for the SM Higgs boson H is gluon fusion with subsequent $b\bar{b}$ decay,

$$gg \to H \to b\bar{b}. \tag{3.10}$$

Because of the huge QCD background, this channel is not feasible and the associated production process,

$$q\bar{q}' \to HW, HZ, \tag{3.11}$$

is used instead. These searches apply as well in the MSSM scenarios characterized by low values of t_β. Their sensitivity, however, is not yet sufficient to provide constraints.
More favourable are the MSSM scenarios characterized by high t_β. In these scenarios neutral Higgs bosons are produced by gluon fusion,

$$gg \to \mathcal{H} \quad (\mathcal{H} = h^0, A^0, H^0). \tag{3.12}$$

In the MSSM, the decay channels $\mathcal{H} \to b\bar{b}$ and $\mathcal{H} \to \tau^+\tau^-$ are enhanced by a factor t_β. Such enhancement is not sufficient to render the $\mathcal{H} \to b\bar{b}$ channel feasible but makes the $\mathcal{H} \to \tau^+\tau^-$ channel viable. The signal topologies are

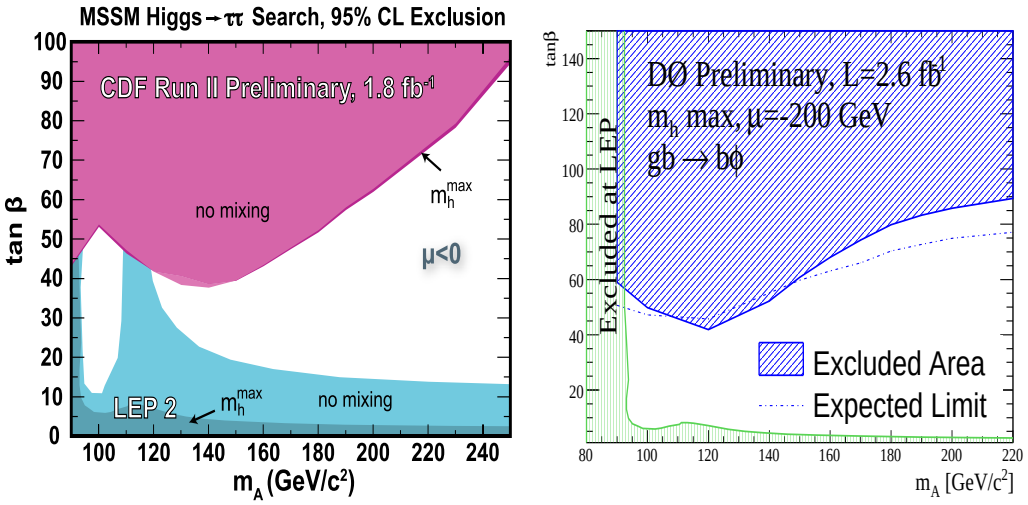

Figure 3.4: Left panel: 95% CL exclusion limit in the (m_{A^0}, t_β) plane by CDF [78]. The production process is gluon fusion and the scenario is $m_h^{\max}$. Right panel: 95% CL exclusion limit in the (m_{A^0}, t_β) plane set by the D0 [80], considering $b\mathcal{H}$ associated production. The scenario is $m_h^{\max}$

$e\tau_{had}$, $\mu\tau_{had}$, $e\mu$[4]. The leptonic decay ensures proper triggering. The main background is $Z \to \tau^+\tau^-$ and W+jets. The outcome of the searches performed by CDF [78] and D0 [79] are translated into exclusion limits in the (m_{A^0}, t_β) plane within benchmark scenarios. In Fig. 3.4 we show such limit in the $m_h^{\max}$ scenario.
In the high t_β regime, an interesting production channel is the associated $b\mathcal{H}$ production

$$bg \to b\mathcal{H}. \tag{3.13}$$

In spite of the huge QCD background, the $\mathcal{H} \to b\bar{b}$ decay mode is feasible. No signal has been observed [80, 81], and both experiments set limit in the (m_{A^0}, t_β) plane. In the right panel of Fig. 3.4, we show the limits set by D0 collaboration in the $m_h^{\max}$ scenario. It is worth to mention an interesting possibility explored by D0 [82]. They looked for the production (3.13) and the $\mathcal{H} \to \tau^+\tau^-$ decay channel. The leptonic decay of the τ allows a better disentanglement of the signal from the background. Owing to the small amount of integrated luminosity used in the analysis (1.2 fb^{-1}), the constraints in the (m_{A^0}, t_β) plane are not competitive with those shown in Fig. 3.4.

The strategies used when searching for charged Higgs at the Tevatron depend on the Higgs mass and in particular whether $m_{H^+} \geq m_t$ or $m_{H^+} \leq$

[4] τ_{had} denotes the hadronic decay of the τ, into hadrons and a ν_τ.

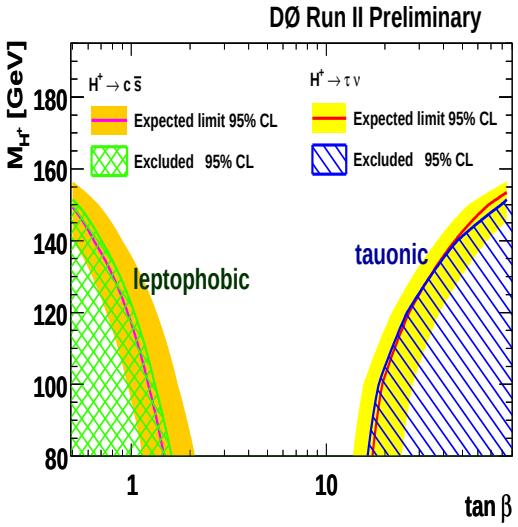

Figure 3.5: 95% CL exclusion limit on m_{H^+} as a function of t_β, according to the analysis of the top decay performed by the D0 collaboration [84]. The excluded region comprises leptophobic models, characterized by $t_\beta \leq 1.5$ and $\mathrm{BR}(H^+ \to c\bar{s}) \sim 1$, and tauonic scenarios, in which $t_\beta \geq 1.5$ and $\mathrm{BR}(H^+ \to \tau^+\tau^-) \sim 1$.

m_t.
If $m_{H^+} \leq m_t$, the top decay channel

$$t \to H^+ b, \tag{3.14}$$

is kinematically allowed. Therefore the channel (3.14) will change the relative fraction of the different signal topologies related to $t\bar{t}$ production. Searches looking for deviations from SM in the $t\bar{t}$ decay topologies [83, 84] do not show any significant deviations from SM predictions and allow to set limits in the (m_{H^+}, t_β) plane. The limits of the D0 analysis are shown in Fig. 3.5, leptophobic models and tauonic scenarios are excluded at 95% CL.
If $m_{H^+} \geq m_t$, resonant charged Higgs can be produced via a process similar to s-channel single top production,

$$q\bar{q}' \to H^+ \to t\bar{b}. \tag{3.15}$$

Therefore, the analysis developed for single top searches can be applied to charged Higgs searches. The analysis performed by D0 [85] has shown no excess over the SM background and has set limits on the production cross section in type I, II and III two doublets Higgs model (2HDM). A region in the (m_{H^+}, t_β) plane has been excluded in type I 2HDM.

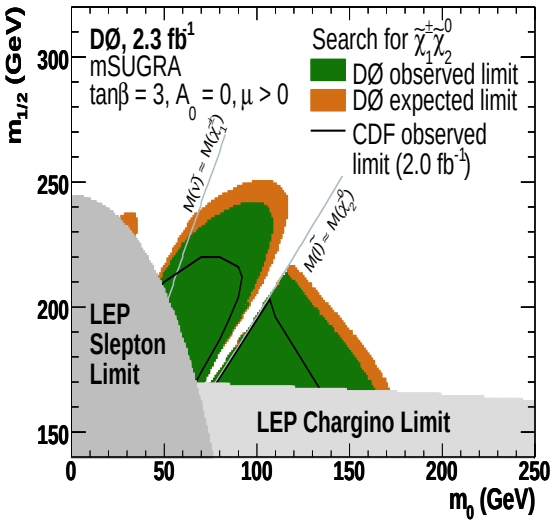

Figure 3.6: 95% CL exclusion limit in the $(m_0, m_{1/2})$ plane arising from the trilepton signal. This plot is provided by the D0 collaboration [86], but the CDF observed limits [87] are shown as well.

3.2.2 Charginos and neutralinos

At the Tevatron chargino and neutralino are searched looking for the associated production

$$p\bar{p} \to \tilde{\chi}^{\pm}\tilde{\chi}^{0}_{2}, \tag{3.16}$$

followed by the decays $(\tilde{\chi}^{\pm} \to \ell\nu\tilde{\chi}^{0}_{1})(\tilde{\chi}^{0}_{2} \to \ell^{+}\ell^{-}\tilde{\chi}^{0}_{1})$. Such decays proceed via W or Z exchange and by slepton exchange. If the slepton mass is light enough, signal topologies constituted by three leptons ad missing energy are enhanced enough to be viable. The main background is the associated WZ production. Such analysis has been performed by D0 [86] and CDF [87], resulting in exclusion limits on the $(m_0, m_{1/2})$ plane, as shown in Fig. 3.6. The gap in the exclusion limit in the $(m_0, m_{1/2})$ plane is related to the loss of acceptance of the trilepton signal. Indeed in this region the mass difference $m_{\tilde{\chi}^{0}_{2}} - m_{\tilde{\ell}}$ is so small that one among the three leptons is too soft to be detected. It is worth to mention that D0 has shown the possibility to fill this gap requiring two same-sign leptons as signal topology [88].

3.2.3 Squarks and gluinos

All the possible production channels of squarks and gluinos read as follows,

$$p\bar{p} \to \tilde{g}\tilde{g},\ \tilde{q}\tilde{g},\ \tilde{q}^{*}\tilde{g},\ \tilde{q}\tilde{q}',\ \tilde{q}^{*}\tilde{q}'^{*},\ \tilde{q}\tilde{q}'^{*}, \tag{3.17}$$

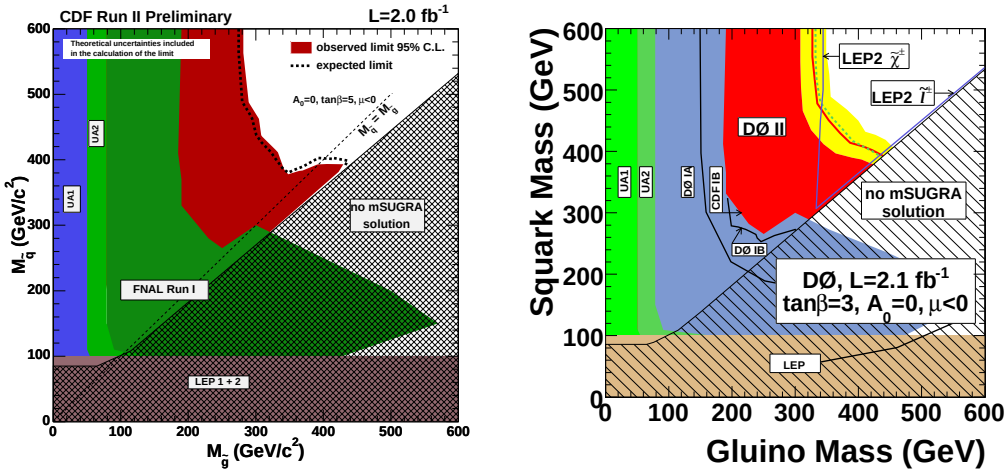

Figure 3.7: 95% CL exclusion limit in the $(m_{\tilde{g}}, m_{\tilde{q}})$ plane by CDF [90] (left panel) and D0 [89] (right panel), assuming mSUGRA scenarios with fixed values of A_0, sign(μ) and t_β. In the right panel, the red line is the observed limit and the yellow band is the uncertainty of this limit. Blue curves are limits from lepton and chargino searches at LEP.

their relative yield depending on the $\tilde{g}$ and $\tilde{q}$ mass hierarchy. The signal topology is constituted by at least two, three, or four jets and missing energy. The SM background is constituted by $W/Z+$ jets, di-boson, $t\bar{t}$ and single top production. Another source of background, of QCD origin, is related to multijet production whit jet energy mis-measurements or with τ decay of the heavy quark flavors. Inclusive searches for gluino and squarks production were performed by D0 [89] and CDF [90]. The top squarks are not included in the analysis and, in the case of CDF, bottom squarks are excluded as well. No significant excess over the SM background was observed and limits on the $(m_{\tilde{q}}, m_{\tilde{g}})$ plane were set, $m_{\tilde{q}}$ being the average mass of the squark considered in the analysis. In Fig. 3.7 we show the limits set by CDF (left panel) and D0 (right panel). Each point in the plane is obtained from the spectrum of a mSUGRA sample varying the value of m_0 and $m_{1/2}$ for fixed value of A_0, sign(μ) and t_β. As can be inferred from Fig. 3.7, CDF set a lower limit of 280 GeV (390 GeV) for the gluino (squark) mass in the slope of the mSUGRA MSSM characterized by $A_0 = 0$, $t_\beta = 5$, $\mu < 0$. Similar results are obtained by D0 that excludes gluino (squarks) masses lower than 308 GeV (379 GeV) in the benchmark slope $A_0 = 0$, $t_\beta = 3$, $\mu < 0$.

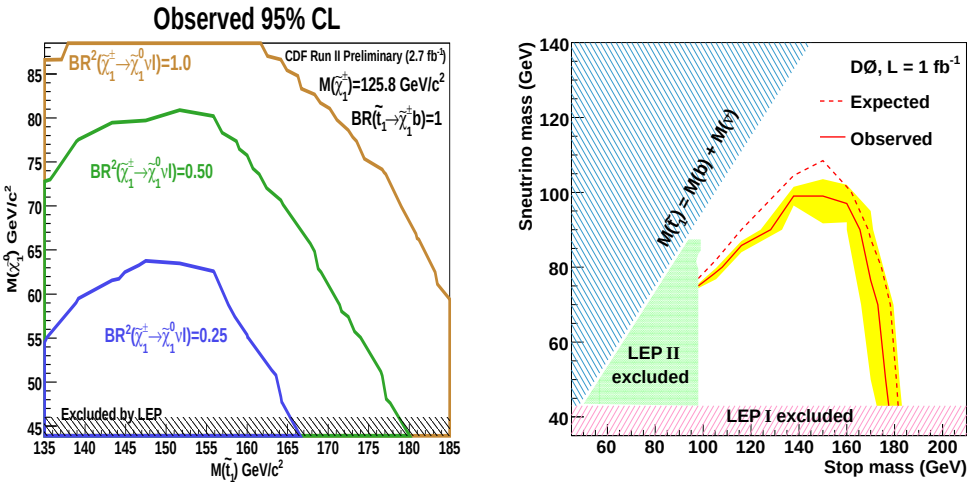

Figure 3.8: Left panel: 95% CL exclusion limit in the $(m_{\tilde{t},1}, m_{\tilde{\chi}_1^0})$ plane by CDF [91] for $m_{\tilde{\chi}_1^\pm} = 105.8$ GeV and different values of BR$(\tilde{\chi}_1^+ \to \tilde{\chi}_1^0 \ell\nu)$. Right panel: 95% CL exclusion in the sneutrino mass versus $\tilde{t}_1$ mass plane as obtained by D0 [92]. The yellow band is the effect of the uncertainty on the cross section.

3.2.4 Top and bottom squarks

Dedicated searches for the lightest squarks belonging to the third generation, *i.e.* $\tilde{t}_1$ and $\tilde{b}_1$, have been performed at the Tevatron. Indeed, the tagging of heavy flavor jets allows to distinguish top and bottom squarks from the squarks of the first two generations.

Top squarks are produced in pairs, at the Tevatron the main partonic process is

$$q\bar{q} \to \tilde{t}_1 \tilde{t}_1^*. \tag{3.18}$$

Similarly to the searches at LEP, searches for stop depend on the mass hierarchy of the particular SUSY scenario. Indeed, this hierarchy determines the branching ratio of the stop decay. In particular, when kinematically allowed, the main decay channel is $\tilde{t}_1 \to b\tilde{\chi}^+$. Otherwise, stop undergoes the 3-body decay $\tilde{t}_1 \to b\ell\tilde{\nu}$. Finally if $\tilde{t}_1$ is the NLSP the only decay channel is the loop induced flavor changing process $\tilde{t}_1 \to c\tilde{\chi}_1^0$.

If the stop decay into chargino and bottom is kinematically allowed, the signal topology is given by two leptons (e or μ), two b-jets, and missing energy. The main background is top pair production[5]. No excess over SM

[5]Actually, the signal itself mimics top events signatures.

events were found by CDF [91], but limits in the $(m_{\tilde{t},1}, m_{\tilde{\chi}_1^0}, m_{\tilde{\chi}_1^\pm})$ space were set. In Fig. 3.8, we show these exclusion limits in the $(m_{\tilde{t},1}, m_{\tilde{\chi}_1^0})$ plane for a given chargino mass and for different values of $\mathrm{BR}(\tilde{\chi}_1^+ \to \tilde{\chi}_1^0 \ell\nu)$. The region excluded by LEP is sizably enlarged.

If the $b\tilde{\chi}_1^+$ channel is forbidden, the dominant decay channel is $\tilde{t}_1 \to b\ell\tilde{\nu}$. This is an attractive channel, if both the produced top squarks decay through this channel, beside missing energy, the final state exhibits two b-jets and two high transverse momentum leptons, leading to a rather clear experimental signature. D0 performed a search [92] using this channel, supposing $\mathrm{BR}(\tilde{t}_1 \to b\ell\tilde{\nu}) = 1$ and equal sharing among the three lepton flavor final states. The signal topology is $(\tilde{t}_1 \to b\ell\nu)(\tilde{t}_1^* \to \bar{b}\ell'\nu')$ with $\ell\ell' = e^+\mu^-, \mu^+e^-, e^+e^-$. The main SM background of this searches are di-boson, and $t\bar{t}$ production. QCD background enters as well. In the right panel of Fig. 3.8 we show the limits in the $(m_{\tilde{t},1}, m_{\tilde{\nu}})$ plane arising from the D0 analyses. The exclusion regions set by LEP is enlarged even if the LEP results are still the most constraining in the region $m_{\tilde{t},1} - m_{\tilde{\nu}} \leq 40$ GeV. For $m_{\tilde{t},1} - m_{\tilde{\nu}}$ bigger than 100 GeV, values of the stop mass lower than 170 GeV are excluded. Such lower bound decreases with the difference $m_{\tilde{t},1} - m_{\tilde{\nu}}$. For instance, $m_{\tilde{t}_1} \leq 150$ GeV when $m_{\tilde{t},1} - m_{\tilde{\nu}} = 60$ GeV. The largest stop mass excluded is $m_{\tilde{t}_1} = 175$ GeV for a sneutrino mass of 45 GeV, while the largest sneutrino mass excluded is 96 GeV for a stop mass of 140 GeV.

Both D0 [93] and CDF [94] performed an analysis on stop production, supposing the stop is the NLSP. As already explained, the dominant decay is $\tilde{t}_1 \to c\tilde{\chi}_0^1$ and then the signal topology is two a-complanar charm jets and missing energy. Both analyses did not observe an excess over the SM background, constituted by di-boson, $W/Z+$ jets, $t\bar{t}$, and single top production. The exclusion limits in the $(m_{\tilde{t},1}, m_{\tilde{\chi}_1^0})$ plane derived by D0 are shown in the left panel of Fig. 3.9, assuming $\mathrm{BR}(\tilde{t}_1 \to c\tilde{\chi}_0^1) = 1$. At the 95% CL the largest limit on $m_{\tilde{t},1}$ is 155 GeV, provided that $m_{\tilde{\chi}_1^0} = 70$ GeV.

Concerning the bottom squark, if $m_{\tilde{b},1} < m_{\tilde{\chi}_2^0} + m_b$ and $m_{\tilde{b},1} > m_{\tilde{\chi}_1^0} + m_b$, its relevant decay is $\tilde{b}_1 \to b\tilde{\chi}_1^0$. Searches for $\tilde{b}_1$ in scenarios characterized by $\tilde{\chi}_1^0$ LSP and the aforementioned mass relations were performed by CDF [94] and D0 [95]. The signal topology is two b-jets and missing energy, while the background is multijet, $W/Z+$ jets, $t\bar{t}$, single top and di-boson production. Instrumental background enters as well. No evidence for sbottom production was observed and this result can be interpreted as 95% CL limit in the $(m_{\tilde{b},1}, m_{\tilde{\chi}_1^0})$ plane. As can be inferred from the right panel of Fig. 3.9, the mass of the lightest sbottom is excluded up to 193 GeV, limit reached when $m_{\tilde{\chi}_1^0} = 40$ GeV. The gap between the kinematic limit $m_{\tilde{b},1} = m_{\tilde{\chi}_1^0} + m_b$ and

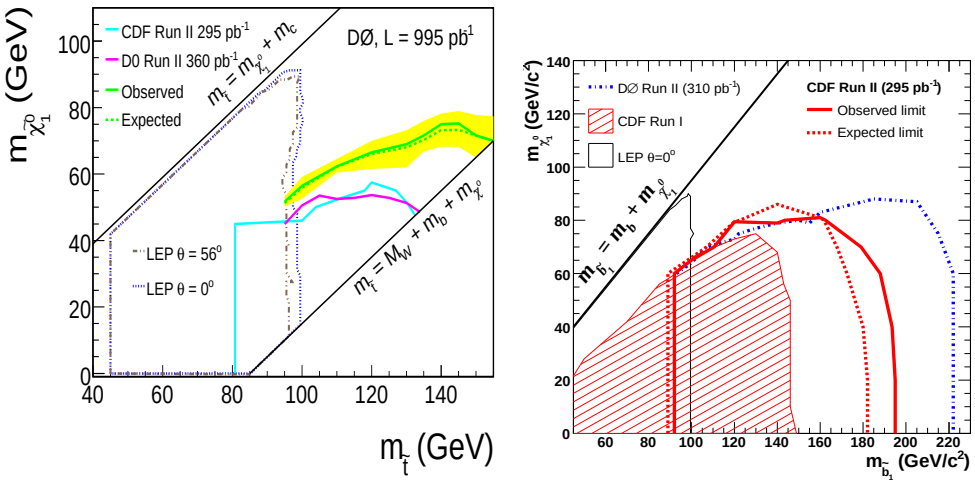

Figure 3.9: Left panel: 95% CL exclusion limit in the $(m_{\tilde{t},1}, m_{\tilde{\chi}_1^0})$ plane arising from the searches of two a-complanar charm jets performed by D0 [93]. The yellow band is the uncertainty related to the uncertainty on the cross section. Right panel: 95% CL exclusion in the plane $(m_{\tilde{b}_1}, m_{\tilde{\chi}_1^0})$ provided by CDF [94].

the excluded region is related to the loss of efficiency of the signal owing to the missing energy requirement in the signal.
More stringent bounds on the sbottom mass are obtained considering a scenario in which $\tilde{b}_1$ is the only squark lighter than the gluino, *i.e.* BR$(\tilde{g} \rightarrow \tilde{b}_1 b) \sim 1$. Assuming BR$(\tilde{b}_1 \rightarrow \tilde{\chi}_1^0 b) = 1$, the search for a signal constituted by four b-jets and missing energy allows to exclude sbottom masses lower than 325 GeV for $m_{\tilde{g}} = 340$ GeV and $m_{\tilde{\chi}_1^0} = 60$ GeV [96].

3.3 Direct searches at HERA

The HERA experiment at DESY terminated its operations in June 2007. HERA was a ep collider with center of mass energy of 320 GeV. HERA operations were divided in two phases with an upgrade in 2001. Thanks to this upgrade higher luminosities were reached and the possibility to use polarized $e^{\pm}$ beams was allowed. During the two phases the experiments H1 [98], HERA-B [99], HERMES [100], and ZEUS [101] collected data. SUSY searches at HERA were performed by H1 and ZEUS and they were dedicated to single squark resonant production within R-parity violating SUSY scenarios. Even if this is beyond the scope of this discussion, which is focused on R-parity conserving scenarios, it is worth to mention the main results obtained by H1 and ZEUS.

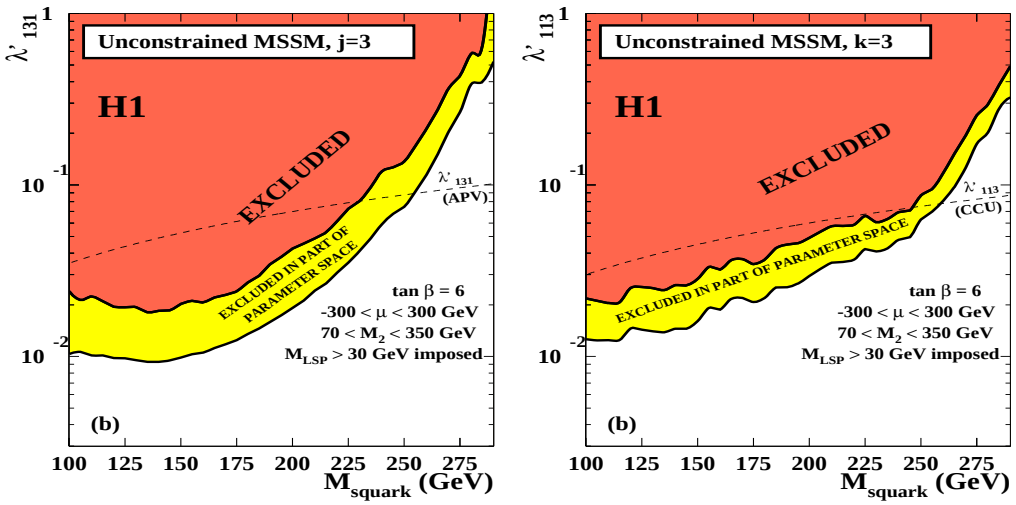

Figure 3.10: Left panel: 95% CL exclusion limit in the $(\lambda'_{131}, m_{\tilde{q}})$ plane from the H1 search [97]. The limits are set performing a two-dimensional scan over the parameters (μ, M_2) of the phenomenological MSSM. M_1 and M_3 are obtained from M_2 using the well known $\overline{\text{DR}}$ relations [50], while $t_\beta = 6$. Sleptons and squarks are assumed to be degenerate with diagonal mixing matrices. The common mass of the sleptons is 90 GeV. In the plots are also shown limits from neutrinoless double beta decay ($\beta\beta0\nu$). Right panel: As the left panel, but considering the 95% CL confidence level in the $(\lambda'_{113}, m_{\tilde{q}})$ plane. The right panel shows limits from tests of charged current universality (CCU).

At HERA, resonant squarks are produced via the processes

$$e^- u \to \tilde{d}_{Rk}, \quad e^+ d \to \tilde{u}_{Lk}, \tag{3.19}$$

with corrections proportional to λ'_{11k} and λ'_{1k1}, respectively. λ'_{ijk} is defined in section 2.3.1. The produced squarks can decay via R-parity violating channels $\tilde{q} \to q'\ell, q''\nu$ leading to either a high p_T electron and one jet or missing energy and a jet. Alternatively, a squark can undergo an R-parity conserving decay $\tilde{q} \to q\tilde{\chi}^0, q\tilde{g}, q'\tilde{\chi}^\pm$. Depending on the subsequent decay of the gaugino, signal topologies are characterized by jets, up to two leptons and possibly missing energy. The background for these searches are neutral and charged current deep inelastic scattering, direct and resolved photon production, the processes $ep \to eWX$, $ep \to eZX$ and QCD multijets production. Direct searches performed by ZEUS [102] and H1 [97, 103] found no excess over the SM expectations and they allow to set limit in the MSSM parameter space. As an example, in Fig. 3.10, we show the exclusion limits obtained by the H1 analysis [97]. In the left [right] panel the projection of the 95%

CL limits in the $(\lambda'_{131}, m_{\tilde{q}})$ $[(\lambda'_{113}, m_{\tilde{q}})]$ plane from a two-dimensional scan over the phenomenological MSSM is shown. $m_{\tilde{q}}$ is the mass of the squarks, assumed to be degenerate. The limits are independent on μ and M_2. In case of $\lambda' \sim \sqrt{4\pi\alpha} \sim 0.3$ squark masses below 275 GeV are excluded.

3.4 Direct searches at the LHC

The Large Hadron Collider (LHC) is a proton-proton (pp) collider built at CERN. The first beam circulated on 10$^{\text{th}}$ September 2008. A fault occurring on 19$^{\text{th}}$ September damaged some of the magnets which, at the time of writing, are under repair. Currently, the beam is expected to run again in fall 2009. The LHC is designed to collide two proton beams at a center of mass energy of 14 TeV. Heavy ions collisions are scheduled as well. Four experiments will collect data at LHC. Beside the multi-purpose experiments ATLAS [104] and CMS [105], there are two other experiments, ALICE [106] and LHCb [107]. In particular, one of the major goal of the two multi-purpose experiments is the hunting for SUSY. In the following we will briefly describe the 5σ discovery reach of SUSY realized via mSUGRA MSSM at ATLAS and CMS, according to the latest technical design reports (TDR) of these two collaborations [105, 108].

3.4.1 Inclusive searches

At the time of writing, the SUSY searches of both ATLAS and CMS are mainly focused on strategies for early discovery at the LHC. In these searches the direct production of squarks and gluino plays a fundamental role. Indeed if squarks and gluino are light enough (*i.e.* lower than $1 - 1.5$ TeV) they will be copiously produced at the LHC. Depending on the mass hierarchy among squarks and gluinos, these SUSY colored particles undergo two and/or three body decays and they cascade down to the LSP that, if R-parity is conserved, is stable. For instance, typical decay chains are

$$\begin{aligned}
\tilde{g} \to \tilde{q}\bar{q},\ \tilde{q} \to q\tilde{\chi}, \quad & \text{if} \quad \tilde{g} \text{ is the heaviest SUSY colored particle,} \\
\tilde{q} \to \tilde{g}q,\ \tilde{g} \to q\bar{q}\tilde{\chi}, \quad & \text{if} \quad \tilde{g} \text{ if the lightest SUSY colored particle,} \\
\tilde{q} \to \tilde{g}q,\ \tilde{g} \to \tilde{q}'\bar{q}',\ \tilde{q}' \to q'\chi, \quad & \text{if} \quad m_{\tilde{q}'} < m_{\tilde{g}} < m_{\tilde{q}}.
\end{aligned}$$

In mSUGRA scenarios $\tilde{\chi}_1^0$ ($\tilde{\chi}_2^0$) is almost $\tilde{B}$- ($\tilde{W}$-) like, therefore $\tilde{q}_R$ decays almost exclusively to $\tilde{\chi}_1^0$ while $\tilde{q}_L$ decays mainly in $\tilde{\chi}_1^0$ even if the branching ratios for $\tilde{q}_L \to q'\tilde{\chi}_1^\pm$ and $\tilde{q}_L \to q\tilde{\chi}_2^0$ are not negligible. Therefore, the decay modes of $\tilde{\chi}_2^0$ and $\tilde{\chi}_1^\pm$ trigger SUSY production events and can give signatures

for this events. In order of importance the decay modes of $\tilde{\chi}_2^0$ and $\tilde{\chi}_1^\pm$ are

$$\tilde{\chi}_2^0 \to \tilde{\ell}\ell,\ \tilde{\nu}\nu,\ h^0\tilde{\chi}_1^0,\ Z^0\tilde{\chi}_1^0,\ \ell^+\ell^-\tilde{\chi}_1^0,$$
$$\tilde{\chi}_1^\pm \to \tilde{\ell}\nu,\ \tilde{\nu}\ell,\ W^\pm\tilde{\chi}_1^0,\ H^\pm\tilde{\chi}_1^0,\ \ell^\pm\nu\tilde{\chi}_1^0.$$

Therefore, typical SUSY signatures at the LHC are events characterized by (two or more) jets, missing transverse energy, $\not{E}_T$, and eventually leptons. The SM background comes from $t\bar{t}$, W/Z+jet, di-boson, single top production, and background of QCD origin. In order to cope with this background, SUSY searches will be performed imposing selection cuts. Such cuts depend on the particular analysis considered and a detailed discussion is beyond our scope. Nevertheless, it can be interesting to briefly describe and motivate the selection criteria adopted by the two collaborations.

ATLAS will select events having high missing transverse energy $\not{E}_T$, typically more than 100 GeV, and at least bigger than 20% of the effective mass M_{eff}. The effective mass,

$$M_{\text{eff}} = \sum_j p_T^{(j)} + \sum_\ell p_T^{(\ell)} + \not{E}_T, \tag{3.20}$$

is an estimate of the total activity of the event. $p_T^{(j)}$ ($p_T^{(\ell)}$) is the transverse momentum of the jet j (lepton ℓ). A lower cut bigger than 800 GeV on M_{eff} is set as well. The number of jets is required to be bigger than three and $p_T^{(j)} \geq 50$ GeV (with the leading one being ≥ 100 GeV). Since fake missing energy tend to be close to the jets, a cut on the azimuthal angle φ of the jets and $\not{E}_T$ will reduce the QCD background. SUSY particles are produced almost at rest so their decay products are expected to be isotropically distributed. A reduction of the QCD background can be obtained imposing a lower cut on the transverse sphericity S_T of the events[6].

Similar cuts are implemented in the CMS inclusive studies. Events are selected requiring high missing transverse energy. The lower cut on $\not{E}_T$ depends on the particular analysis and is of the order of $150 - 200$ GeV. Depending on the particular analysis, CMS requires at least two, three or four jets with $E_T \geq 50$ GeV. In many analyses further cuts on the energy of the leading jet is required. A cut on the pseudo-rapidity of the jets forces them to be in the central region of the detector, *i.e.* $|\eta^{(j)}| \leq 2.5$. A cut on the azimuthal angle between the jets and $\not{E}_T$ is implemented as well.

In the remaining part of this subsection we will briefly describe the expected results of the inclusive searches ATLAS and CMS will perform in

[6]The sphericity S_T is a variable describing the shape of the event. Spherical events exhibit $S_T \sim 1$ while in the case of back to back events $S_T = 0$.

the early stages of the LHC run. Such studies have been performed at different benchmark points chosen by the collaborations. ATLAS considered seven mSUGRA MSSM scenarios (SU1 - SU4, SU6, SU8.1, SU9) in different regions of the parameters space. CMS, instead, choosed eight low mass mSUGRA scenarios (LM1-LM6, LM8, LM9), four scenarios characterized by heavier particles (HM1-HM4), and two scenarios in between (LM7, LM10). LM7 is characterized by heavy squarks ($m_{\tilde{q}} \sim 3000$ GeV) and a light gluino ($m_{\tilde{g}} \sim 680$ GeV), while LM10 exhibits heavy squarks and gluino ($m_{\tilde{q}} \sim 3100$ GeV and $m_{\tilde{g}} \sim 1300$ GeV).

Analyses with jets and $\not{E}_T$

The least model dependent SUSY signature is multiple jets and missing transverse energy. Traditionally high multiplicity is required in order to reduce the background from QCD and W/Z+jets.

ATLAS requires final states characterized by at least four jets, $\not{E}_T$ and no leptons. Such selection criteria allows for an early discovery (*i.e.* integrated luminosity of 1 fb^{-1}) in all the ATLAS benchmark points different from SU2. Such point is characterized by heavy squarks and gluinos, therefore the production rate of such particles is small.
ATLAS has considered events with fewer jets, *i.e.* two or three jets. These events are favored in certain SUSY models and have a simpler topology, easier to reconstruct. Two different selection criteria have been used for these searches. The first one mimic the selections described previously while the other selection criterion relies on the properties of the transverse mass m_{T2} [109][7]. In this channel early discovery is likely in all the scenarios but the SU2. Significance is lower than in the four jets analysis owing to the increasing importance of the QCD background.

Missing transverse energy plus multiple jets (*i.e.* ≥ 3) final states have been studied by CMS as well. Once the systematic uncertainties are included, the 5σ discovery of the light mass benchmark scenarios LM1 - LM6, LM8, and LM9, can be reached already with 1 fb^{-1}.

Analyses with jets, $\not{E}_T$, and a lepton

The sensitivity on the QCD background, can be reduced requiring one lepton in the final state. Inclusive SUSY searches using multiple jets (*i.e* ≥ 3), $\not{E}_T$

[7]Indeed, a lower cut on this variable discards either jets with low p_T and events characterized by low or non-isolated missing energy. In case of semi-invisible decay, m_{T2} grows as the difference among the mass of the decaying particle and the masses of the products, therefore m_{T2} is higher in SUSY events than in top or W events.

and exactly (at least) one lepton have been performed by ATLAS (CMS).

Concerning ATLAS, a cut on the transverse mass of the missing energy and the lepton is set in order to exclude events in which the missing energy comes from the leptonic W decay. In the ATLAS benchmark scenarios the significance is ≥ 5, already at 1 fb^{-1} *i.e.* 5σ discovery is possible already at 1 fb^{-1}. Again, the exception is the point SU2, the reasons being explained previously.

CMS will perform inclusive searches requiring at least one isolated μ with $p_T \geq 30$ GeV. Assuming 10 fb^{-1} and including the systematic uncertainty, the significance in the light mass benchmark points is well above 5, *i.e.* 5σ discovery should be possible below 10 fb^{-1}.

Analyses with dileptons

If final states including two leptons, multiple jets, and missing transverse energy are considered, particular features of neutralinos and gluinos can be exploited to perform inclusive SUSY searches.

Final states with two opposite-sign-same flavor (OSSF) leptons arise from the three body neutralino decay $\tilde{\chi}_2^0 \rightarrow \ell^+\ell^-\tilde{\chi}_1^0$. OSSF leptons can therefore trigger events with a neutralino in the decay chain. In SM events, OSSF leptons and opposite-sign-different-flavor (OSDF) leptons arise with equal probability. Therefore, a non-resonant excess of OSSF leptons over OSDF leptons in the final states would be a clear indication of new physics, possibly SUSY. It is worth to mention that the dilepton invariant mass has a triangular shape that can be related to the masses of the SUSY particles entering the decay. The masses of the particle in the decay chain can be obtained finding the endpoints of invariant mass distributions involving the two leptons and the jets in the final states.
ATLAS requires two isolated OSSF leptons with $p_T \geq 10$ GeV and $|\eta| < 2.5$. The benchmark points SU3 and SU4 have an high discovery potential at 1 fb^{-1}. The point SU2 is, as usual, difficult to search for. The point SU1 is problematic as well, since its degenerate spectrum makes the produced leptons soft. The significance depends on the value of the cut, in general harder cuts have to be preferred.
CMS requires at least two OSSF leptons with $p_T > 10$ GeV. At a luminosity of 10 fb^{-1} all the low mass test points will be in the 5σ discovery reach region.

SM allows a low rate of same-sign di-leptons in the final state that nevertheless are common in the decay chains of the gluino, which is insensitive

on the lepton charge.
ATLAS will perform searches looking for final states with exactly two same-sign leptons with $p_T > 20$ GeV. ATLAS collaboration claims that likely 5σ discovery of the SU1, SU3, and SU4 would be possible already at 1 fb^{-1}.
CMS will search for same sign di-muons final states that have the advantage of an efficient and well understood di-muon trigger immediately after the LHC start-up. Therefore, they require at least two same-sign isolated muons with $p_T > 10$ GeV. LM7 and all the light mass benchmark scenarios considered by CMS have a statistical significance bigger than 16σ at 10 fb^{-1}. This channel is therefore a good candidate for low mass SUSY discovery during the early running of the LHC.

Analyses with ditaus

In SUSY models τ decays can become important, even dominant over e and μ decays (especially if $t_\beta \gg 1$). The ditau final state can be used to infer the value of the masses of the particles in the decay chain. However, owing to the neutrino arising from the tau decay, the $\tau^+\tau^-$ invariant mass do not show a sharp endpoint and the endpoint itself has to be obtained from the inflection point after fitting the $\tau^+\tau^-$ invariant mass distribution.

ATLAS will look for signatures with τ decaying hadronically. At least a τ is required with $p_T > 40$ GeV and $|\eta| < 2.5$. The transverse mass calculated using the missing transverse energy and the visible momentum of the τ has to be bigger than 100 GeV. This cut eliminates τ leptons originated from W decay. ATLAS studies showed the possibility of the 5σ discovery of the benchmark points SU3 and SU6 with 1 fb^{-1}.

The CMS collaboration will search for signal constituted by at least two τ candidates. These candidates are required to be close in the (η, φ) plane, to select τ leptons coming from the decay $\tilde{\chi}_2^0 \rightarrow \tau^\pm\tilde{\tau}^\mp \rightarrow \tau^\pm\tau^\mp\tilde{\chi}_1^0$, and to reject both SM background and SUSY events with two independent τ leptons produced. The light mass scenarios (LM1 - LM6, LM8,LM9) will be discovered with 5σ significance already at 1 fb^{-1}.

Analyses with b-jets

In many SUSY scenarios, top and bottom squarks are lighter than the squarks of the first two generations and therefore SUSY signal are typically rich of b quarks. Moreover, heavy flavor production is enhanced by the Higgsino components of charginos and neutralinos. Requiring b-jets in the final states can therefore enhance the signal over background ratio and can suppress the QCD background.

The cuts used in the ATLAS study require at least four jets and at least two of them have to be b-jets. This analysis has been performed in five benchmark points SU1, SU2, SU3, SU4 and SU6. All points except SU2 will be discovered at 1 fb^{-1}. This analysis can be important in the SU6 point, somehow problematic if other channels are considered.
ATLAS considered the possibility that the two b-jets arise from the decay of the lightest Higgs h^0 produced by the decay $\tilde{\chi}_2^0 \to \tilde{\chi}_1^0 h^0$. This channel is the dominant decay process if $m_{\tilde{\ell}}, m_{\tilde{\nu}} \geq m_{\tilde{\chi}^0,2}$. Such mass hierarchy is realized in the SU9 point, the point considered in the analysis. The signal topology is two light-jets, two b-jets, missing energy, and no leptons. Besides the usual SM background, SUSY events can pollute the signal as well. ATLAS has shown the possibility to see the h^0 peak in the bb invariant mass distribution with 10 fb^{-1}.

In the case of the CMS analysis at least four jets are required, two of them being b-jets. The two b-jets are selected to be decay products of the lightest Higgs h^0. Since m_{h^0} is large, b-jets are expected to have a small distance in the (η, φ) plane. Therefore a lower cut on this distance selects such $b\bar{b}$ pairs. A scan in the $(m_0, m_{1/2})$ plane was performed showing the possibility of a 5σ discovery with 10 fb^{-1} in a sizable region, up to 1100 GeV in m_0 and 600 GeV in $m_{1/2}$.

Analyses with particular particles in the decay chains

CMS has performed two more inclusive searches trying to isolate events with a particular particle in the squark and gluino decay chains.

The first study considers final states with a Z^0 originated from the decay $\tilde{\chi}_2^0 \to Z^0 \tilde{\chi}_1^0 \to \ell^+\ell^-\tilde{\chi}_1^0$. Signal events are selected requiring two OSSF electrons (muons) with $p_T > 17$ GeV ($p_T > 7$ GeV) and $|\eta| < 2.4$. Their invariant mass has to be consistent with the Z^0 mass and their azimuthal angle less than 2.65 rad. A scan in the $(m_0, m_{1/2})$ plane has shown the possibility of 5σ discovery of SUSY scenarios in the range 240 GeV $< m_{1/2} <$ 340 GeV, 150 GeV $< m_0 <$ 2000 GeV with 10 fb^{-1} of integrated luminosity.

In most SUSY scenarios, the first stop is the lightest squark and it will be copiously produced. Moreover, in a big part of the $(m_0, m_{1/2})$ plane the stop decays to a top and a neutralino. Signal topologies are characterized by at least four jets (at least one of them being a b-jet), $\not{E}_T$ and at least an isolated lepton. In order to suppress semi-leptonic top decays, the azimuthal distance between the $\not{E}_T$ and the reconstructed top has to be less than 2.6 rad. A scan in the $(m_0, m_{1/2})$ plane has shown that a large region can be discovered at the LHC already with integrated luminosities below 30 fb^{-1}. In particular

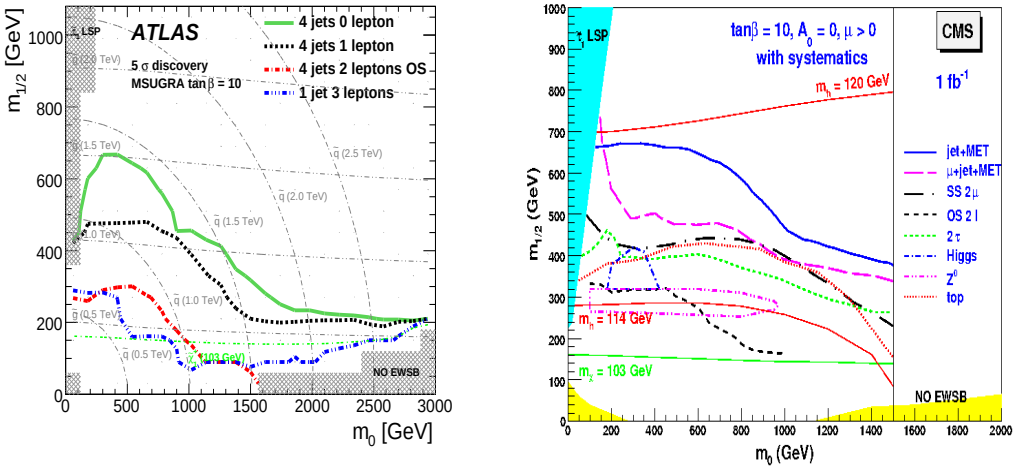

Figure 3.11: Left panel: 5σ discovery reach of ATLAS in the $(m_0, m_{1/2})$ plane using inclusive channels at 1 fb^{-1}. In this plot $A_0 = 0$, sign(μ)> 1 and $t_\beta = 10$. Right panel: Same as the left panel but considering the inclusive searches performed by CMS.

the region 100 GeV $< m_0 <$ 1600 GeV, $m_{1/2} <$ 400 GeV will be probed at the LHC with 10 fb^{-1}.
The presence of a top in a decay chain can be exploited by ATLAS as well. A preliminary study in the SU4 scenario, characterized by light stop $\tilde{t}_1$ and BR$(\tilde{t}_1 \to \tilde{\chi}_1^{\pm} b) = 1$, has shown the possibility to reconstruct the kinematical endpoint of the invariant mass of the top-bottom pair arising from the decay chain $\tilde{g} \to \tilde{t}_1 t \to \tilde{\chi}_1^{\pm} bt$. This endpoint depends on the mass of the particles involved in the aforementioned decay chain.

Summary on the inclusive analyses

The analyses described in this section have been performed in different SUSY scenarios scanning the $(m_0, m_{1/2})$ plane for fixed values of A_0, sign(μ), and t_β.

The results of the ATLAS collaboration are summarized in the left panel of Fig. 3.11. In this plot is shown the 5σ discovery contours of different channels characterized by jets, $\not{E}_T$ and eventually leptons at 1 fb^{-1}. The channel excluding leptons in the final states (zero-lepton mode) is the most effective. The one-lepton mode, that exhibits exactly one lepton in the final state, has a lower discovery reach with respect to the zero-lepton mode but it is less sensitive of the QCD background that can arise from detector problems.
The discovery reach of the different analyses performed by CMS are summa-

rized in the right panel of Fig. 3.11. In this plot is shown the 5σ discovery reach in the $(m_0, m_{1/2})$ plane at 1 fb^{-1}, the different inclusive searches shown separately. The most promising channels are the $\not{E}_T$+jets and the μ+$\not{E}_T$+jets.

As can be inferred from Fig. 3.11, both ATLAS and CMS should be able to discover SUSY scenarios with squark and gluino masses up to $1.5-2$ TeV, already at 1 fb^{-1}. Interestingly, SUSY signals can be seen in different search channels improving the confidence on eventual new physics evidence. Searches which are promising for SUSY mass reconstruction, such as ditau searches or inclusive searches including Z^0 and h^0, will be feasible at the LHC.

It is worth to mention that the region that ATLAS and CMS will probe is favored by experimental constraints from electroweak precision data, B-physics observables and the amount of cold dark matter in the universe. Indeed, such constraints can be used to find the preferred values of the mSUGRA MSSM parameters performing an overall fit of the aforementioned observables within the mSUGRA MSSM. Many studies were performed in this direction (*e.g.* see Ref. [7] and references therein). A recent analysis was performed in Ref. [110] using Markov chain Monte Carlo techniques to find the probability with which the MSSM describes experimental data. As can be inferred from Fig. 3.12, the 95% likelihood contour from the fit performed in Ref. [110] is almost entirely included in the 5σ discovery contour of ATLAS and CMS. Therefore, if mSUGRA MSSM is realized in nature, with 95% confidence LHC will discover it with 1 fb^{-1} of data. Interestingly, (big part) of the 68% likelihood region is included inside the 5σ discovery reach of channels such as the same-sign di-lepton channels, which are well suited for quantitative studies such as sparticle-mass reconstruction.

3.4.2 Higgs bosons

Concerning neutral MSSM Higgs bosons, the production mechanisms are similar to those of the Tevatron. In particular, we have direct production,

$$gg \to \mathcal{H} \quad (\mathcal{H} = h^0, A^0, H^0), \tag{3.21}$$

and the production in association of a bottom quarks,

$$gg \to b\bar{b}\mathcal{H}. \tag{3.22}$$

If both (one of the two) bottoms are treated inclusively, large collinear logarithms can be absorbed introducing the bottom parton distribution function and substituting the process (3.22) with $b\bar{b} \to \mathcal{H}$ ($bg \to b\mathcal{H}$ and $\bar{b}g \to \bar{b}\mathcal{H}$).

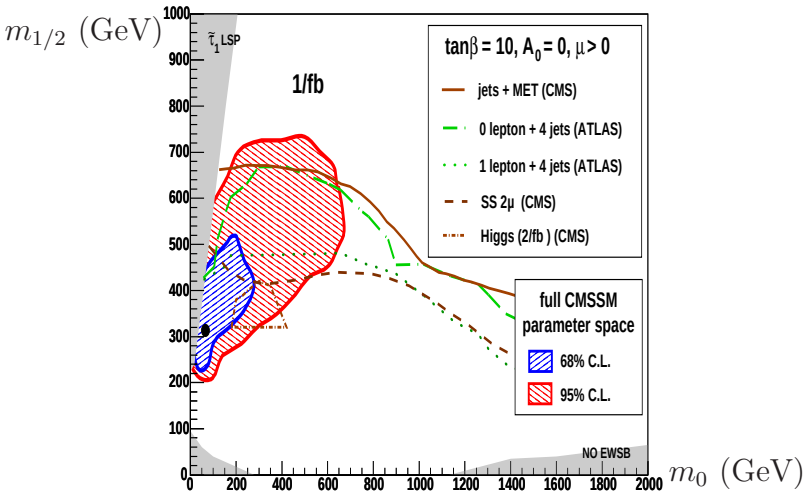

Figure 3.12: 5σ discovery reach in the $(m_0, m_{1/2})$ plane for different inclusive searches performed by ATLAS and CMS at 1 fb^{-1}. The filled circle is the results of the best fit of electroweak precision data, B-physics observables, and cold dark matter constraints within the mSUGRA MSSM as performed in [110]. The blue (red) area is the 68% (95%) CL likelihood region.

A comparison among these different approaches can be found in Ref. [111] and references therein.

In case of MSSM Higgs bosons, an important signature comes from the decay $\mathcal{H} \to \tau^+\tau^- \to \ell\ell' 4\nu$. ATLAS looks for two leptons, $\not{E}_T$, and at least one b-jet. CMS searches for opposite-sign-different-flavor (OSDF) leptons, $\not{E}_T$ and at least one b-jet. The main backgrounds are instead Drell-Yan production of a Z, $t\bar{t}$ and W+jets production. The 5σ reach of the study of ATLAS is plotted in the left panel of Fig. 3.13 in the $m_h^{\max}$ scenario. Similar results are obtained by CMS.
Studies focusing on the Higgs decay $\mathcal{H} \to \mu^+\mu^-$ have been performed by both collaborations. The muonic decay is suppressed with respect to the tauonic one, but it has a clear signature owing to the presence of two muons in the final state. Discovery reach and 95% CL exclusion limits are worse but comparable with those obtained from the τ decay of the Higgs and the subsequent leptonic decay of the τ leptons.

CMS has performed a study considering the SUSY decay of the heavy neutral Higgs $H^0/A^0 \to \chi_2^0\chi_2^0 \to 4\ell + \not{E}_T$. This channel is interesting in low and intermediate regions of t_β, regions in which the decay $\mathcal{H} \to \tau^+\tau^-$ is not sufficiently enhanced. Besides the SM background constituted by ZZ^*/γ^*

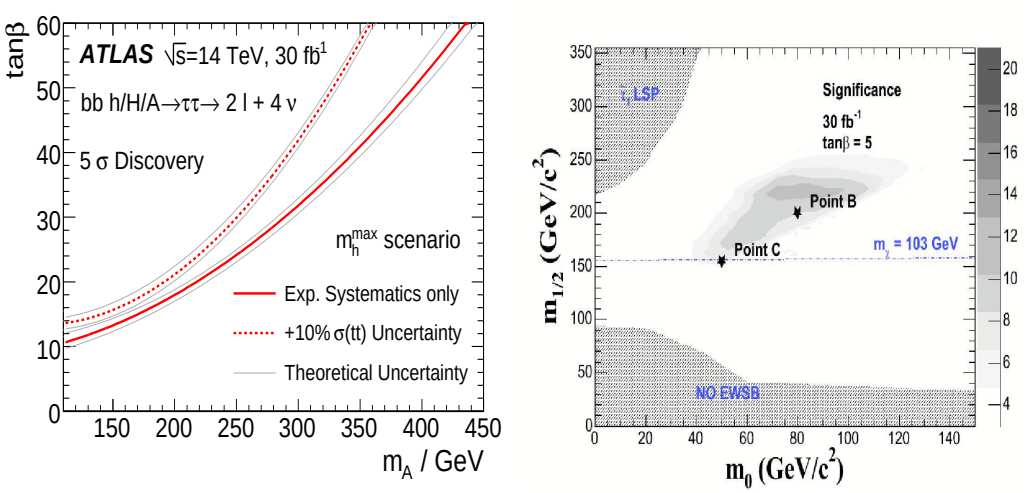

Figure 3.13: Left panel: 5σ discovery reach in the (m_{A^0}, t_β) plane for ATLAS using the tauonic decay channel of the neutral Higgs bosons. The continuous line is the main result while the dashed line is the result including 10% uncertainty on the $t\bar{t}$ cross section. The grey lines represent the effect of the theoretical systematic uncertainty on the signal. Right panel: 5σ discovery reach of CMS in the $(m_0, m_{1/2})$ plane using the $A^0/H^0 \to \tilde{\chi}_2^0\tilde{\chi}_2^0$ channel. In this plot $A_0 = 0$, sign$(\mu) = 1$, and $t_\beta = 5$

$Zb\bar{b}$ and $t\bar{t}$ production, one has to cope with SUSY background as well. Such background is mainly due to the squark and gluinos production and the production of sleptons and gauginos. In the right panel of Fig 3.13 we show the 5σ discovery reach of this channel in the $(m_0, m_{1/2})$ plane for $A_0 = 0$, sign$(\mu) = 1$ and $t_\beta = 5$. As can be inferred from the plot, A^0 and H^0 can be discovered by means of this channel in the range $30 < m_0 < 120$ GeV, $150 < m_{1/2} < 250$ GeV.

Another interesting channel for the observation of the pseudo-scalar A^0 is the decay chain $A^0 \to Zh^0 \to \ell^+\ell^- b\bar{b}$. This is a promising channel in the low t_β region and if $m_Z + m_{h^0} < m_{A^0} < 2m_t$. Moreover, large values of μ and M_2 make this channel dominating on the aforementioned $A^0 \to \chi\chi$ channel. A dedicated study performed by CMS has shown the possibility of A^0 discovery via this channel in the range $0 < t_\beta < 1$, 170 GeV$< m_{A^0} <$ 350 GeV with 30 fb^{-1} of integrated luminosity.

ATLAS performed a study looking at the invisible decay modes of the neutral Higgs, *i.e.* Higgs boson decaying into two LSP. The two production processes considered are vector boson fusion (VBF),

$$qq' \to q''q'''\phi \quad (\phi = h^0, H^0), \tag{3.23}$$

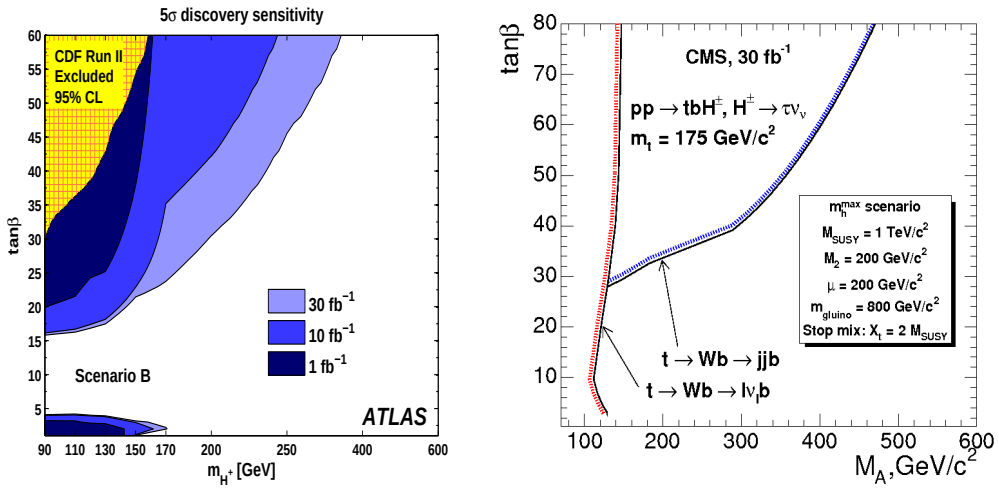

Figure 3.14: Left panel: 5σ discovery reach of ATLAS in the (m_{H^+}, t_β) plane using the tauonic decay of H^+. The scenario considered is the $m_h^{\max}$ scenario. Right panel: 5σ discovery reach of CMS in the (m_{A^0}, t_β) plane using the same channel as the left panel. The red (blue) shadowed line refers to the light (heavy) charged Higgs studies. The colored bands describe the effect of theoretical uncertainties

and associated $Z\phi$ production,

$$q\bar{q} \to Z^0\phi. \tag{3.24}$$

In the case of VBF the signal is $\not{E}_T$ and two jets with high separation in η and correlated in the azimuthal angle. The main backgrounds are multijet and W/Z+jets production. The signature for the associated $Z\phi$ production is two OSSF leptons and $\not{E}_T$, while the main background is $ZZ \to \ell^+\ell^-\nu\bar{\nu}$. With 30 fb^{-1}, ATLAS is sensitive to the Higgs production in the VBF (associated $Z\phi$) channel and the subsequent invisible Higgs decay. The BSM cross section has to be 90% (80%) of the SM Higgs boson production and the Higgs mass has to be lower than 250 GeV (150 GeV).

The discussion on charged Higgs searches, is pretty similar to that of the Tevatron. In particular, the search strategies depend on the hierarchy between the mass of the charged Higgs and the mass of the top.
In the case of light charged Higgs, *i.e.* $m_{H^+} < m_t + m_b$, charged Higgs are mainly produced as a decay product of the top via the process $t \to bH^+$. Detection channels are therefore $t\bar{t}$ process with the subsequent top decay into charged Higgs. Both CMS and ATLAS consider the channel

$$t\ \bar{t} \to bH^+\ \bar{b}W^- \to b\tau^+_{\rm had}\nu_\tau\ \bar{b}\ell\nu_\ell. \tag{3.25}$$

ATLAS investigates two other channels characterized by hadronic decay of the W,

$$t\,\bar{t} \to bH^+\,\bar{b}W^- \to b\tau^+_{\rm had}\nu_\tau\bar{b}\;qq',$$
$$t\,\bar{t} \to bH^+\,\bar{b}W^- \to b\tau^+_{\rm lep}\nu_\tau\;\bar{b}qq'.$$

Besides the QCD background, in all these three channels the background is given by $t\bar{t}$, single top, and $W+$ jets production.
In the case of heavy Higgs boson, $m_{H^+} > m_t + m_b$, the main production channel is associated $tH^+(b)$ production. The signal topologies considered by both CMS and ATLAS are

$$t\;H^+\;(b) \to bqq'\;\tau_{\rm had}\nu\;(b),$$
$$t\;H^+\;(b) \to t\;tb\;(b) \to bW\;bWb\;(b) \to b\ell\nu\;bqq'b\;(b), \qquad (3.26)$$

while the background is similar to that of the light charged Higgs boson studies.

The outcome of these studies are the 5σ discovery reach of ATLAS and CMS, shown in Fig. 3.14. As can be inferred from the plots, a discovery sensitivity is reached by ATLAS [CMS] in a large part of the (m_{H^+}, t_β) $[(m_{A^0}, t_\beta)]$ plane. The discovery reach of the two experiments differs if the charged Higgs is light: in particular ATLAS does not cover the region $5 < t_\beta < 15$, where the H^+ cross section exhibits a minimum. Nevertheless, according to ATLAS TDR [108], this region can be covered if the uncertainty arising from Montecarlo can be neglected.

3.4.3 Charginos and neutralinos

SUSY searches looking at the direct production of charginos and neutralinos can play an important role in SUSY scenarios in which the SUSY colored particles are heavy and they are produced at a low rate.

The main production channel of charginos and neutralinos is the associated production

$$qq' \to \tilde{\chi}^0_i\tilde{\chi}^\pm_j, \qquad (3.27)$$

the process of $\tilde{\chi}^0_2\tilde{\chi}^\pm_1$ production being the dominant. $\tilde{\chi}^+_i\tilde{\chi}^-_j$ and $\tilde{\chi}^0_i\tilde{\chi}^0_j$, present as well, have smaller cross section. The decay channel

$$\tilde{\chi}^0_i\;\tilde{\chi}^\pm_j \to \tilde{\chi}^0_1\ell^+\ell^-\;\tilde{\chi}^0_1\ell'\nu \quad (\ell, \ell' = e, \mu), \qquad (3.28)$$

gives the signal topology characterized by two OSSF leptons, one more lepton and $\not{E}_T$. The SM background is $t\bar{t}$, di-boson, $W+$jets, $WW+$jets and $Wt+$jets

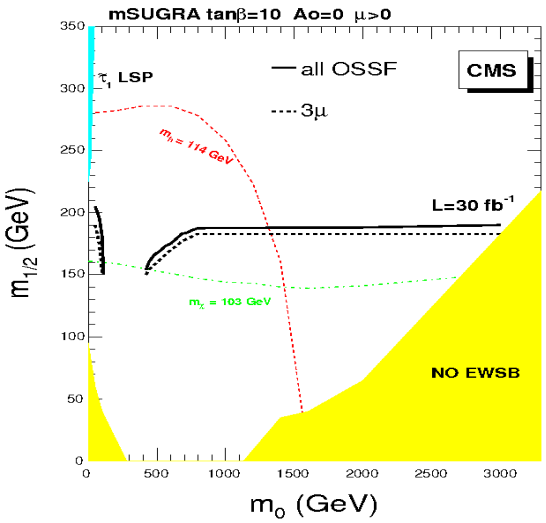

Figure 3.15: 5σ discovery reach of CMS in the $(m_0; m_{1/2})$ plane from the trilepton signal. Shown are the discovery reach of all the OSSF combinations (continuous line) and of the tri-muon channel (dashed line). Systematic uncertainties are included.

production. Processes leading to the production of charginos and neutralinos in cascade decays of squarks, sleptons, and gluinos give the same signature. CMS treats these events as background, while ATLAS keeps the possibility to include them in the background imposing a veto on the jets with $p_T >$ 20 GeV.

The 5σ SUSY discovery reach of CMS in the $(m_0, m_{1/2})$ plane using this three-lepton channel is shown in Fig. 3.15. In the plot the discovery reach of the tri-muon final states and that of all the OSSF pairs combination are shown. In the large m_0 region, *i.e* $m_0 > 1000$ GeV, SUSY scenarios characterized by $m_{1/2} < 180$ GeV can be discovered. ATLAS has simulated this analysis in the benchmark mSUGRA points set by ATLAS collaboration. If only direct production of charginos and neutralinos is considered, discovery is expected with several tens of fb^{-1}. If the jet veto is not imposed, discovery can occur earlier, with several fb^{-1}.

Chapter 4

Computational techniques and methods

In this chapter, we present the processes leading to the production of colored SUSY particles at hadron colliders. In particular, we discuss some technical aspects needed for the computation of the electroweak contributions to these processes.

The structure of the chapter is as follows. In section 4.1, we describe the general structure of the EW contributions. Section 4.2 is devoted to the description of the renormalization procedure leading to UV-finite predictions. In section 4.3 we explicitly show the cancellation of mass singularities of photonic origin at one-loop and we describe the methods we use for the extraction and these singularities. In section 4.4 we extend the discussion given in section 4.3 to the case of gluonic mass singularities.

4.1 Structure of the tree-level and one-loop contributions

We compute contributions of the order $\mathcal{O}(\alpha_s\alpha)$, $\mathcal{O}(\alpha^2)$, and $\mathcal{O}(\alpha_s^2\alpha)$ to the processes of hadronic production of colored SUSY particles. We will consider the production of a pair of gluinos, the production of a squark and an anti-squark, the associated production of a (anti-)squark and a gluino, and the production of a (anti-)quark–(anti-)quark pair, *i.e.*,

$$P\ P \to F, \quad \text{with} \quad F = \tilde{g}\ \tilde{g};\ \tilde{q}_{iA}\ \tilde{q}^*_{jB};\ \tilde{q}_{iA}\ \tilde{g};\ \tilde{q}^*_{iA}\ \tilde{g};\ \tilde{q}_{iA}\ \tilde{q}_{jB};\ \tilde{q}^*_{iA}\ \tilde{q}^*_{jB}, \tag{4.1}$$

where $q = u, d$, and $i, j = 1, 2$. $A, B = 1, 2$ denote the mass eigenstates. We do not consider here the production of top and bottom squarks. Indeed, owing to

b-tagging, bottom and top squarks can be experimentally distinguished from the squarks of the first two generations [112–117]. In the subsequent chapters we will focus on three classes of the processes presented in Eq. (4.1). In particular we will concentrate on gluino pair production, on diagonal squark–anti-squark production, $P\ P \to \tilde{q}_{iA}\ \tilde{q}^*_{iA}$, and on the associated production of a (anti-)squark and a gluino. Nevertheless, the discussions presented in this chapter are completely general and apply to all the processes appearing Eq. (4.1).

4.1.1 LO and NLO QCD contributions

First of all, we briefly review the structure of the leading order (LO) contribution and of the next-to-leading order (NLO) QCD corrections, which are already known.

The LO contribution to the process (4.1) is of $\mathcal{O}(\alpha_s^2)$ and reads [10, 11, 13, 14, 118]

$$\begin{aligned} d\sigma^{\rm LO}_{PP\to F}(S) &= \int_0^1 dx_1 \int_0^1 dx_2\ \delta(\tau - x_1 x_2) \\ &\quad \sum_{ij}\ f_{i|P_1}(x_1) f_{j|P_2}(x_2) d\sigma^{2,0}_{ij\to F}(\tau S). \end{aligned} \tag{4.2}$$

The sum over i, j runs over the five light quarks and the gluons. $f_{i|H}(x)$ is the momentum distribution (PDF) of the parton i in the hadron H. Here and in the following we will use the convention $d\sigma^{a,b}_X$ to denote the cross section for a partonic process X at a given order $\mathcal{O}(\alpha_s^a \alpha^b)$ in the strong and electroweak coupling constants. Identical notation is used in the description of the amplitudes[1]. The differential cross section reads

$$d\sigma^{2,0}_{ij\to F}(s) = \frac{1}{4N_i N_j} \frac{dt}{16\pi s^2} \sum\ \left|\mathcal{M}^{1,0}_{ij\to F}\right|^2. \tag{4.3}$$

$\sum$ means sum over the color and the spin of the external particles. The 2-particle phase space integration measure is defined in appendix D, while N_i is the color average factor of the parton i. In particular, $N_i = 3$ ($N_i = 8$) if i is a quark (gluon). The factor 1/4 arises from the average over the helicities (polarizations) of the initial quarks (gluons).

In Fig. 4.1, we show the total cross section and the relative weights of the different processes in Eq. (4.1) as a function of the gluino mass and of $m_{\tilde{q}}$, $m_{\tilde{q}}$ being the mass of the squarks of the first two generations, assumed

to be mass degenerate. We consider four different classes of processes, final states related by charge conjugation are collected together and the chiralities and flavors of the squarks are treated inclusively. The four classes are gluino pair production ($PP \to \tilde{g}\tilde{g}$), associated (anti-)squark gluino production ($PP \to \tilde{q}\tilde{g} + \tilde{q}^*\tilde{g}$), squark–anti-squark production ($PP \to \tilde{q}\tilde{q}^*$) , and (anti-)squark–(anti-)squark production ($PP \to \tilde{q}\tilde{q}+\tilde{q}^*\tilde{q}^*$). As already pointed out in Ref. [15], at the LHC the relative yields of the final states strongly depend on the hierarchy between $m_{\tilde{g}}$ and $m_{\tilde{q}}$. If squarks are light and the gluino is heavy, *i.e.* $m_{\tilde{q}} \leq 800$ GeV and $m_{\tilde{g}} \geq 1000$ GeV, the dominant production channel is squark–anti-squark production. In scenarios characterized by light gluino, *i.e.* $m_{\tilde{g}} \leq 600$ GeV, the dominant channel is gluino pair production, its relative yield approaching one if $m_{\tilde{q}} \geq 1000$ GeV. The process of (anti-)squark gluino associated production is important in the region $m_{\tilde{q}} \sim m_{\tilde{g}}$, while (anti-)squark–(anti-)squark production leads when both gluino and squarks are heavy, $m_{\tilde{g}} \geq 1300$ GeV, $m_{\tilde{q}} \geq 1000$ GeV. It is worth to notice that the total cross section for the production of colored SUSY particles, *i.e.* the sum of the total cross section of the four classes of processes shown in Fig. 4.1, is bigger than 5 pb in a wide region of the ($m_{\tilde{g}}$, $m_{\tilde{q}}$) plane, namely the region $m_{\tilde{q}}, m_{\tilde{g}} \leq 700$ GeV. The total cross section increases as the mass of the gluino decreases, becoming bigger than 50 pb if $m_{\tilde{g}} \leq 500$ GeV.

The most important corrections are of QCD origin, of $\mathcal{O}(\alpha_s^3)$. An extensive discussion on the computation of such contributions and on their numerical importance at the LHC andat the Tevatron can be found in the literature [15–19]. Here we briefly describe the general structure of such contributions that can be written as

$$\begin{aligned} d\sigma^{\text{NLO QCD}}_{PP\to FX} &= \int_0^1 dx_1 \int_0^1 dx_2\, \delta(\tau - x_1x_2)\Bigg\{ \\ &\sum_{ij} f_{i|P_1}(x_1) f_{j|P_2}(x_2) \left(d\sigma^{3,0}_{ij\to F}(\tau S) + d\sigma^{3,0}_{ij\to Fg}(\tau S)\right) \\ &+ \sum_{q_i}\sum_{kl} f_{k|P_1}(x_1) f_{l|P_2}(x_2) \left(d\sigma^{3,0}_{kl\to Fq_i}(\tau S) + d\sigma^{3,0}_{kl\to F\bar{q}_i}(\tau S)\right) \\ &+ \mathcal{T}(x_1, x_2, s)\Bigg\}. \end{aligned} \tag{4.4}$$

There are three different contributions. The first one is given by the virtual QCD corrections to the partonic processes entering at LO, Eq. (4.2). Tree-level contributions to the aforementioned partonic processes but with an

[1] When amplitudes are concerned, a and b can assume fractional values.

extra gluon in the final state have to be included as well. These processes have to be considered since the final states F and Fg become degenerate when the gluon becomes soft (*i.e.* its momentum approaches zero) or collinear to a massless external particle (*i.e.* the scalar product of the four-momenta of the two particles vanishes). Therefore, in these two limits any possible measurement has to deal with a final state which is a statistical mixture of F and Fg final states. The last class of contributions arises from reactions involving an extra massless (anti-)quark in the final state.
The differential cross sections entering Eq. (4.4) are

$$\begin{aligned} d\sigma^{3,0}_{ij\to F}(s) &= \frac{1}{4N_iN_j}\frac{dt}{16\pi s^2}\sum\, 2\,\mathfrak{Re}\{(\mathcal{M}^{1,0}_{ij\to F})^*\mathcal{M}^{2,0}_{ij\to F}\}, \\ d\sigma^{3,0}_{ij\to Fx}(s) &= \frac{1}{4N_iN_j}\frac{d\Phi_3(s)}{2s}\sum\, \left|\mathcal{M}^{3/2,0}_{ij\to Fx}\right|^2 \quad (x=g,q,\bar{q}). \end{aligned} \tag{4.5}$$

$d\Phi_3$ is the three-particle phase space integration measure defined in appendix D. The last term entering Eq. (4.4) is $\mathcal{T}(x_1,x_2,s)$ and deserves some comment. This term is of $\mathcal{O}(\alpha_s^3)$ and it arises from the $\mathcal{O}(\alpha_s)$ factorization of the parton distribution functions (PDFs). Its actual form depends on the factorization scheme and on the regularization scheme used to handle the collinear singularities[2]. In the forthcoming discussion, we will not consider the contributions of $\mathcal{O}(\alpha_s^3)$. Therefore, $\mathcal{T}(x_1,x_2,s)$ does not enter our discussions and we will not give its explicit expression. Nevertheless, its actual form can be found in the literature [15][3]. The explicit expression of the contribution of $\mathcal{O}(\alpha_s^2\alpha)$ arising from the factorization of the PDFs will be introduced in section 4.1.2.

4.1.2 LO and NLO EW contributions

The tree-level $\mathcal{O}(\alpha_s\alpha)$ and $\mathcal{O}(\alpha^2)$ contributions to the processes (4.1) are

$$\begin{aligned} d\sigma^{\text{LO, EW}}_{PP\to F}(S) &= \int_0^1 dx_1 \int_0^1 dx_2\, \delta(\tau-x_1x_2)\Bigg\{ \\ &\qquad \sum_{ij} f_{i|P_1}(x_1)f_{j|P_2}(x_2)\left(d\sigma^{1,1}_{ij\to F}(\tau S)+d\sigma^{0,2}_{ij\to F}(\tau S)\right)\Bigg\}. \end{aligned} \tag{4.6}$$

The sum over i,j runs over all the partonic species inside the proton, namely the five light quarks, the gluons and the photons, that appear at $\mathcal{O}(\alpha)$. The

[2]More details are available in section 4.3 and in section 4.4.

[3]This reference quotes results within the $\overline{\text{MS}}$ factorization scheme. Collinear singularities are treated using dimensional regularization.

differential cross sections appearing Eq. (4.7) can be written in terms of the partonic amplitudes as follows,

$$\begin{aligned} d\sigma^{1,1}_{ij\to F}(s) &= \frac{1}{4N_iN_j}\frac{dt}{16\pi s^2}\sum\ \mathcal{S}^{1,1}_{ij\to F}, \\ d\sigma^{0,2}_{ij\to F}(s) &= \frac{1}{4N_iN_j}\frac{dt}{16\pi s^2}\sum\ |\mathcal{M}^{0,1}_{ij\to F}|^2. \end{aligned} \tag{4.7}$$

Since the photon is a color singlet, $N_\gamma = 1$. Depending on the particular partonic process, $\mathcal{S}^{1,1}_{ij\to F}$, can be either

$$\left|\mathcal{M}^{1/2,1/2}_{ij\to F}\right|^2, \quad \text{or} \quad 2\,\mathfrak{Re}\{(\mathcal{M}^{1,0}_{ij\to F})^*\mathcal{M}^{0,1}_{ij\to F}\}.$$

The tree-level EW contributions related to $q\bar{q}-$, $qq-$, and $\bar{q}\bar{q}-$ initiated processes, are available in the literature [24, 25]. Photon-induced partonic processes leading to contributions of $\mathcal{O}(\alpha_s\alpha)$ have been evaluated as well [120–122].

The $\mathcal{O}(\alpha_s^2\alpha)$ contributions to the processes (4.1) read

$$\begin{aligned} d\sigma^{\text{NLO EW}}_{PP\to FX} &= \int_0^1 dx_1 \int_0^1 dx_2\ \delta(\tau - x_1x_2)\Bigg\{ \\ &\quad \sum_{ij}\ f_{i|P_1}(x_1)f_{j|P_2}(x_2)\left(d\sigma^{2,1}_{ij\to F} + d\sigma^{2,1}_{ij\to F\gamma} + d\sigma^{2,1}_{ij\to Fg}\right) \\ &+ \sum_q\sum_{kl}\ f_{k|P_1}(x_1)f_{l|P_2}(x_2)\left(d\sigma^{2,1}_{kl\to Fq} + d\sigma^{2,1}_{kl\to F\bar{q}}\right) \\ &+ \mathcal{R}(x_1,x_2,s)\Bigg\}. \end{aligned} \tag{4.8}$$

Again, there are three different contributions. $d\sigma^{2,1}_{ij\to F}$ are the virtual $\mathcal{O}(\alpha_s^2\alpha)$ corrections to the partonic processes present already at $\mathcal{O}(\alpha_s^2)$. The correction arising from the same partonic processes but with an extra photon or gluon in the final state, $ij \to F\gamma$ and $ij \to Fg$, enters as well, owing to the already mentioned degeneracy of the final states F, $F\gamma$, and Fg in the soft and collinear limit. We will treat gluon (photon) fully inclusively without implementing cuts on the gluonic (photonic) phase space. The third type of contributions are related to the processes leading to the final states Fq and $F\bar{q}$. The observables we will present in this thesis are fully inclusive in the treatment of the final (anti-)quark.

The differential cross section appearing Eq. (4.8) can be expressed in terms of the partonic amplitudes

$$
\begin{aligned}
d\sigma^{2,1}_{ij\to F}(s) &= \frac{1}{4N_iN_j}\frac{dt}{16\pi s^2}\sum\; 2\mathfrak{Re}\{(\mathcal{M}^{1,0}_{ij\to F})^*\mathcal{M}^{1,1}_{ij\to F}+(\mathcal{M}^{0,1}_{ij\to F})^*\mathcal{M}^{2,0}_{ij\to F}\},\\
d\sigma^{2,1}_{ij\to F\gamma}(s) &= \frac{1}{4N_iN_j}\frac{d\Phi_3}{2s}\sum\; \left|\mathcal{M}^{1,1/2}_{ij\to F\gamma}\right|^2,\\
d\sigma^{2,1}_{ij\to Fg}(s) &= \frac{1}{4N_iN_j}\frac{d\Phi_3}{2s}\sum\; 2\,\mathfrak{Re}\{(\mathcal{M}^{1/2,1}_{ij\to Fg})^*\mathcal{M}^{3/2,0}_{ij\to Fg}\},\\
d\sigma^{2,1}_{ij\to Fq}(s) &= \frac{1}{4N_iN_j}\frac{d\Phi_3}{2s}\sum\; \mathcal{S}^{2,1}_{ij\to Fq}.
\end{aligned}
\tag{4.9}
$$

$d\Phi_3$ is the three-particle phase space integration measure defined in appendix D. $\mathcal{S}^{2,1}_{ij\to Fq}$ can be either

$$
\left|\mathcal{M}^{1,1/2}_{ij\to Fq}\right|^2,\quad \text{or}\quad 2\,\mathfrak{Re}\{(\mathcal{M}^{1/2,1}_{ij\to Fq})^*\mathcal{M}^{3/2,0}_{ij\to Fq}\}. \tag{4.10}
$$

The last term in Eq. (4.8), $\mathcal{R}(x_1,x_2,s)$, is a term that has to be inserted owing to the factorization of the quark PDFs at $\mathcal{O}(\alpha_s)$ and $\mathcal{O}(\alpha)$. This term is dependent on the factorization scheme used and on the regularization scheme employed to regularize the collinear divergences. We regularize the collinear singularities retaining the mass of the quarks (mass regularization). Within mass regularization, $\mathcal{R}(x_1,x_2,s)$ reads as follows,

$$
\begin{aligned}
\mathcal{R}(x_1,x_2,s) &= \int_{z_0}^1 dz\Bigg\{-\frac{\alpha_s}{2\pi}C_F\sum_{ij}\; f_{i|P_1}(x_1)f_{j|P_2}(x_2)\Bigg(\\
&\quad [\mathcal{H}^{(1)}_i(z)+\lambda^{(s)}h^{(1)}(z)]_+ + [\mathcal{H}^{(1)}_j+\lambda^{(s)}h^{(1)}]_+\Bigg)d\sigma^{1,1}_{ij\to F}(zs)\\
&- \frac{\alpha}{2\pi}\sum_{ij}\; f_{i|P_1}(x_1)f_{j|P_2}(x_2)\Bigg(e_i^2[\mathcal{H}^{(1)}_i+\lambda^{(e)}h^{(1)}]_+\\
&\quad +e_j^2[\mathcal{H}^{(1)}_j+\lambda^{(e)}h^{(1)}]_+\Bigg)d\sigma^{2,0}_{ij\to F}(zs)\\
&- \frac{\alpha_s}{2\pi}T_R\sum_{ij}\; \Bigg(f_{g|P_1}(x_1)f_{j|P_2}(x_2)(\mathcal{H}^{(2)}_i+\lambda^{(s)}h^{(2)})(\delta_{iq}+\delta_{i\bar{q}})\\
&\quad +f_{i|P_1}(x_1)f_{g|P_2}(x_2)(\mathcal{H}^{(2)}_j+\lambda^{(s)}h^{(2)})(\delta_{jq}+\delta_{j\bar{q}})\Bigg)d\sigma^{1,1}_{ij\to F}(zs)
\end{aligned}
$$

$$- \frac{3\alpha}{2\pi}\sum_{ij}\Bigg(f_{\gamma|P_1}(x_1)f_{j|P_2}(x_2)e_i^2(\mathcal{H}_i^{(2)}+\lambda^{(e)}h^{(2)})(\delta_{iq}+\delta_{i\bar{q}}) \\ +f_{i|P_1}(x_1)f_{\gamma|P_2}(x_2)e_j^2(\mathcal{H}_j^{(2)}+\lambda^{(s)}h^{(2)})(\delta_{jq}+\delta_{j\bar{q}})\Bigg)d\sigma^{2,0}_{ij\to F}(zs)\Bigg\}. \tag{4.11}$$

z_0 is defined as $z_0 = th.^2/s$, where $th.$ is the sum of the masses of the particles in the final state, *i.e.* $th.$ is the threshold for the production of the final state. $C_F = 4/3$ while $T_R = 1/2$. The $[\cdots]_+$ distribution is defined as

$$\int_a^1 dx\,[f(x)]_+ g(x) = \int_a^1 dx\, f(x)\big[g(x)-g(1)\big] - g(1)\int_0^a dx\, f(x). \tag{4.12}$$

The functions $\mathcal{H}$ and h read as follows,

$$\begin{aligned}
\mathcal{H}_i^{(1)} &= P_{qq}(z)\left[\ln\left(\frac{\mu^2}{m_i^2}\frac{1}{(1-z)^2}\right)-1\right], \\
\mathcal{H}_i^{(2)} &= P_{qg}(z)\ln\left(\frac{\mu^2}{m_i^2}\right), \\
h^{(1)} &= P_{qq}(z)\ln\left(\frac{1-z}{z}\right)-\frac{3}{2}\frac{1}{1-z}+2z+3, \\
h^{(2)} &= P_{qg}(z)\ln\left(\frac{1-z}{z}\right)-1+8z-8z^2.
\end{aligned} \tag{4.13}$$

The splitting functions are defined in the usual way,

$$P_{qq}(z) = \frac{1+z^2}{1-z}, \qquad P_{qg}(z) = z^2+(1-z)^2. \tag{4.14}$$

The dependence on the factorization scheme is encoded in $\lambda^{(s)}$ and $\lambda^{(e)}$. In particular $\lambda^{(s)} = 1$ ($\lambda^{(e)} = 1$) if the $\mathcal{O}(\alpha_s)$ ($\mathcal{O}(\alpha)$) contributions to the PDFs are factorized in the DIS scheme. If the scheme used to factorize the $\mathcal{O}(\alpha_s)$ ($\mathcal{O}(\alpha)$) contributions is the $\overline{\rm MS}$ scheme, one has $\lambda^{(s)} = 0$ ($\lambda^{(e)} = 0$).

4.2 UV divergences

At loop level, the computation of amplitudes implies dealing with divergent integrals. Since the MSSM is a renormalizable theory [123, 124], such divergences cancel once the parameters in the Lagrangian (which are unphysical)

are traded with observable quantities. This procedure can be summarized as follows.

Regularization.— A regulator Λ has to be introduced in order to control the divergences and to render the integral finite. The divergences are recovered in the limit $\Lambda \to \Lambda_0$. Cancellation of the UV divergences in physical observables is then achieved when such observables stay finite as $\Lambda \to \Lambda_0$.

Renormalization.— To achieve the cancellation of UV divergences we use multiplicative renormalization. Given a set of independent parameters of the MSSM Lagrangian, a generic element of this set, P_i^0, is written in terms of a renormalized parameter P_i and a renormalization constant Z_{P_i},

$$P_i^0 = Z_{P_i} P_i = (1 + \delta Z_{P_i})\, P_i \equiv P_i + \delta P_i. \tag{4.15}$$

The value of the renormalized parameters and of the renormalization constants are fixed once renormalization conditions are imposed. The renormalization constants are divergent quantities that cancel the divergences in any S-matrix element once the bare couplings are replaced by means of Eq. (4.15). Finite Green functions can be obtained renormalizing the fields φ_j^0 appearing in the Lagrangian,

$$\varphi_j^0 = \sqrt{Z_{\varphi_j}}\varphi_j = \left(1 + \frac{\delta Z_{\varphi_j}}{2}\right)\varphi_j.$$

Writing $Z = 1 + \delta Z$ we have that the (bare) Lagrangian $\mathcal{L}$, a function of P_i^0 and φ_j^0, can be written as

$$\mathcal{L}(P_i^0, \varphi_j^0) = \mathcal{L}(P_i, \varphi_j) + \delta\mathcal{L}(P_i, \varphi_j, \delta Z_{P_i}, \delta Z_{\varphi_j})$$

$\delta\mathcal{L}$ gives rise to the so called counter terms, extra Feynman rules that ensure the cancellation of the UV divergences in every physically meaningful observable.

In the following subsections we will describe the renormalization procedure in detail. In section 4.2.1 we present the regularization procedure while in section 4.2.2 the renormalization is shown. In the latter subsection, moreover, we describe the renormalization of the sector which is relevant in the computation of the EW contributions of the processes (4.1).

4.2.1 Regularization

There are many different methods to regularize the divergences we get from the loop integrals [125–133]. We will discuss the two we use in this thesis.

These methods use as regulator the dimension d of the spacetime. They respect Lorentz and gauge invariance. The general idea is to compute the divergent integrals in a number of dimensions small enough that they converge and then to consider d as a complex variable, UV divergences appear as poles on integer values of d.

Dimensional regularization

Given a divergent integral, the actual effect of dimensional regularization (DREG) [126–128] is to perform the substitution

$$\int d^4q \to (2\pi\mu)^{4-d} \int d^dq.$$

μ has dimension of a mass and is introduced to keep the dimension of the integral independent of the dimension d of the space-time.

The algebraic manipulations of d-dimensional integrals can be performed after a proper definition of this object. Such definition and a careful analysis about its uniqueness and its properties is available in Ref. [134][4]. One has also to define the d-dimensional extension to the Clifford algebra and to the trace operation. The d-dimensional γ^μ matrices satisfy the usual anti-commutation relations and hermiticity conditions. The trace is determined imposing the usual conditions of ciclicity and linearity and setting $\mathrm{tr}\{1\} = 4$.
More involved is the definition of γ_5 and $\varepsilon_{\mu\nu\rho\sigma}$ which are intrinsically four dimensional objects. Different generalizations are possible [128, 135–140], we use the approach defined in Ref. [139, 140], defining the d-dimensional γ_5 according to

$$\{\gamma_5, \gamma^\mu\} = 0, \quad (\gamma_5)^2 = 1, \quad \mathrm{Tr}\{\gamma_5\gamma^\mu\gamma^\nu\gamma^\rho\gamma^\sigma\} = 4i\varepsilon^{\mu\nu\rho\sigma}, \tag{4.16}$$

which is fine at one-loop in the case of anomaly-free theories.

After proper algebraic manipulations and standard decomposition techniques [141–146], d-dimensional integrals can be expressed in terms of scalar integrals

$$T_0^N(p_1, \ldots, p_{N-1}, m_0, \ldots, m_{N-1}) \equiv \frac{(2\pi\mu)^{4-d}}{i\pi^2} \int d^dq \, \frac{1}{D_0 \ldots D_N}, \tag{4.17}$$

where the propagators D_j are defined as

$$D_j = (q + p_j)^2(1 - \delta_{j0}) + q^2\delta_{j0} - m_j^2 + i\epsilon. \tag{4.18}$$

[4]The generalization of integration is linear, translation invariant and it has the correct scaling under rescaling of the integration variable.

These integrals can be manipulated introducing Feynman parameters and exploiting translation invariance of the d-dimensional integration. The outcome is

$$T_0^N = \frac{(2\pi\mu)^{4-d}}{i\pi^2} \int_0^1 dx_0 \dots dx_{N-1} \delta \left(1 - \sum_{i=0}^{N-1} x_i\right) \left[\int d^d q \frac{\Gamma(N)}{(q^2 - C)^N}\right], \tag{4.19}$$

where C is a function of p_i, x_i and m_i,

$$C = \left(\sum_{i=1}^{N-1} x_i p_i\right)^2 - \sum_{i=1}^{N-1} x_i (p_i^2 - m_i^2) + x_0 m_0^2. \tag{4.20}$$

The d-dimensional integral (4.19) can be computed using the general definition in Ref. [134]. Therefore T_0^N becomes

$$T_0^N = (4\pi\mu^2)^{\frac{4-d}{2}} (-1)^N \Gamma(N - d/2) \int_0^1 dx_0 \dots dx_{N-1} \delta \left(1 - \sum_{i=0}^{N-1} x_i\right) C^{(d/2-N)},$$

where Γ is the Euler's Gamma function. Potential divergences show up as poles in $\varepsilon = (4 - d)$.

DREG spoils SUSY. In the case of Super Yang-Mills theories regularized within DREG, SUSY Ward identities are violated at one-loop [130, 147, 148]. Violation of Slavnov-Taylor identities has been checked at one-loop in the case of softly broken SUSY QCD [149–151]. The main reason for such a violation is that the relative number of bosonic and fermionic degrees of freedom varies with the dimension d. Therefore, theories which are supersymmetric in four dimensions are not necessarily supersymmetric in d-dimensions [129, 130, 152].

Dimensional reduction

Dimensional reduction (DRED) [129] is an elegant way to modify DREG making it compatible with SUSY. The main idea is to compactify the space-time. Therefore, space-time is reduced from 4 to $d < 4$ dimensions while the number of the components of the fields is left unchanged.

As a consequence, space-time momenta live in a d-dimensional space with metrics $\hat{g}_{\mu\nu}$. $g_{\mu\nu}$, instead, is the metrics tensor of the 4-dimensional space. The complement of the d-dimensional space, with dimension $\varepsilon = 4 - d$, has a metric $\tilde{g}_{\mu\nu}$. Beside the relation $g_{\mu\nu} = \hat{g}_{\mu\nu} + \tilde{g}_{\mu\nu}$, these metric tensors fulfills

the following relations [153]:

$$\begin{aligned} \hat{g}_{\mu\nu}\hat{g}^{\mu\nu} &= d, & g^{\mu\nu}\hat{g}^{\sigma}_{\nu} &= \hat{g}^{\mu\sigma}, \\ \tilde{g}_{\mu\nu}\tilde{g}^{\mu\nu} &= \varepsilon, & g^{\mu\nu}\tilde{g}^{\sigma}_{\nu} &= \tilde{g}^{\mu\sigma}, \\ g_{\mu\nu}g^{\mu\nu} &= 4, & \hat{g}^{\mu\nu}\tilde{g}^{\sigma}_{\nu} &= 0. \end{aligned} \tag{4.21}$$

In its original formulation, DRED has been shown to be inconsistent [154]. Such inconsistency is harmless in many practical computations [148] and it drops out when DRED is formulated in a mathematically consistent way [153, 155, 156]. In particular, the four dimensional space has to be realized as a "quasi four dimensional space" that retains 4-dimensional features but, nevertheless, that is infinite dimensional. This implies that the Clifford algebra is exactly the same as in four dimension but Fierz identities do not hold and index counting is not possible.
Another problem is related to the mass factorization arising when DRED is used to regularize collinear singularities. Such problem does not affect us[5] and has been recently solved [157].

Concerning the compatibility between SUSY and DRED, SUSY Ward identities have been explicitly checked at one loop [130]. SUSY Ward identities involving self energies have been shown to hold up to three loops [155, 156]. Slavnov-Taylor identities have been checked at loop-level in the case of softly broken SUSY Yang-Mills theories [149–151]. Consistency checks arise from the internal consistency of DRED-results for β functions [158–161]. Moreover, the aforementioned results have been successfully compared with the non-perturbative ones [158–161].

4.2.2 Renormalization

In order to accomplish our renormalization program, renormalization conditions have to be imposed defining the renormalization scheme. Here we briefly review the renormalization schemes we use.

$\overline{\text{MS}}$ scheme.— Given a Green function regularized within DREG, the $\overline{\text{MS}}$ prescription fixes the renormalization constants requiring the cancellation of the terms proportional to

$$\Delta_{\text{UV}} = \frac{2}{\varepsilon} - \gamma_E + \ln 4\pi,$$

where γ_E is the Euler-Mascheroni constant. Therefore, the renormalization constants have no finite part and the overall (one-loop) result depends on

[5] We treat IR singularities within mass regularization, *cf.* section 4.3 and section 4.4.

the choice of the scale μ. μ has to be chosen to be of the order of the typical scale of the process, in order to minimize the contributions arising from the higher order terms in the perturbative expansion.

$\overline{\text{DR}}$ scheme.— This scheme is equal to the previous one, the only difference being the regularization scheme used to regularize the divergences. In the $\overline{\text{DR}}$ scheme divergent integrals are regularized within DRED.

On-shell (OS) scheme.— This scheme is used to define the renormalization constants of the mass and the wavefuntion of the particles. Given a particle p, the renormalization constant δm_p of its mass and the renormalization constant δZ_p of its wavefunction are defined requiring that the p–p inverse two point function has a pole at m_p^2 with unit residue. According to the Källen-Lehman decomposition of the two point function, m_p is therefore the physical mass of the particle. Moreover, the LSZ formula is simplified by the choice of unit residue when the particle p goes on shell.

In the following we will give an explicit description of the renormalization of the sectors of the MSSM that need to be renormalized in order to make the EW virtual corrections to the processes (4.1) UV finite.

Quark sector

The kinetic term of a quark f_i reads

$$\mathcal{L}_{f_i} = \bar{\psi}_{f_i} (i \not{\partial} - m_{f_i}) \psi_{f_i} \quad (f = u, d). \tag{4.22}$$

Since we approximate the CKM matrix by the identity, fermions belonging to different generations do not mix at one-loop and renormalization is achieved performing the following substitution into Eq. (4.22):

$$m_{f_i} \to m_{f_i} + \delta m_{f_i}, \qquad \psi_{f_i} \to \left[1 + \frac{1}{2} \begin{pmatrix} \delta Z_{f_i}^L & 0 \\ 0 & \delta Z_{f_i}^R \end{pmatrix}\right] \psi_{f_j}. \tag{4.23}$$

$\delta Z_{f_i}^{L,R}$, and δm_{f_i} are renormalized in the OS scheme. Such position gives

$$\begin{aligned} \delta m_{f_i} &= \frac{m_{f_i}}{2} \mathfrak{Re} \left\{ \Sigma_{f_i}^L(m_{f_i}^2) + \Sigma_{f_i}^R(m_{f_i}^2) + 2\Sigma_{f_i}^S(m_{f_i}^2) \right\}, \qquad (4.24) \\ \delta Z_{f_i}^{L,R} &= -\mathfrak{Re} \left\{ \Sigma_{f_i}^{L,R}(m_{f_i}^2) \right\} \\ &\quad -m_{f_i}^2 \mathfrak{Re} \left\{ \frac{\partial \Sigma_{f_i}^L(k^2)}{\partial k^2} + \frac{\partial \Sigma_{f_i}^R(k^2)}{\partial k^2} + 2\frac{\partial \Sigma_{f_i}^S(k^2)}{\partial k^2} \right\}_{\Big| k^2 = m_{f_i}^2} . \end{aligned}$$

The scalar coefficients are defined according to the following decomposition of the f_i–f_i self energy,

$$\Sigma_{f_i}(p) = \not{p}\,\omega_-\Sigma^L_{f_i}(p^2) + \not{p}\,\omega_+\Sigma^R_{f_i}(p^2) + m_{f_i}\Sigma^S_{f_i}(p^2),$$

where $\omega_\pm$ are the right- and left- handed chirality projectors respectively.

Squark sector

Due to $SU(2)$ invariance, squark families belonging to the same $SU(2)$ doublets have to be renormalized simultaneously. Therefore, one has to consider the kinetic terms of $\tilde{u}_i$ and $\tilde{d}_i$ simultaneously,

$$\mathcal{L}_{\tilde{u}_i,\tilde{d}_i} = \sum_{\tilde{f}=\tilde{u},\tilde{d}} \left[(\partial_\mu \tilde{f}^*_{Li}, \partial_\mu \tilde{f}^*_{Ri}) \begin{pmatrix} \partial^\mu \tilde{f}_{Li} \\ \partial^\mu \tilde{f}_{Ri} \end{pmatrix} - (\tilde{f}^*_{Li}, \tilde{f}^*_{Ri}) M^2_{\tilde{f}_i} \begin{pmatrix} \tilde{f}_{Li} \\ \tilde{f}_{Ri} \end{pmatrix} \right], \quad (4.25)$$

where $M^2_{\tilde{f}_i}$ is defined in Eqs. (2.59) and (2.63). According to our general procedure, the replacements

$$\begin{pmatrix} \tilde{f}_{Li} \\ \tilde{f}_{Ri} \end{pmatrix} \to R^T_{\tilde{f}_i} \left(\mathbf{1}_2 + \frac{1}{2}\delta Z_{\tilde{f}_i} \right) \begin{pmatrix} \tilde{f}_{1i} \\ \tilde{f}_{2i} \end{pmatrix}, \qquad M^2_{\tilde{f}_i} \to M^2_{\tilde{f}_i} + \delta M^2_{\tilde{f}_i},$$

are performed into the Lagrangian (4.25). $\delta Z_{\tilde{f}_i}$ is a 2×2 complex matrix with generic entry $(\delta Z_{\tilde{f}_i})_{j,k}$. $\delta M^2_{\tilde{f}_i}$ can be obtained expanding to the first order Eq. (2.59) or, equivalently, Eq. (2.63).

First renormalization scheme (Rs1).— This scheme is equivalent to that described in Ref. [162]. The idea is to use as independent parameters

$$m^2_{\tilde{u}_{i1}}, \quad m^2_{\tilde{u}_{i2}}, \quad m^2_{\tilde{d}_{i2}}, \quad \theta_{\tilde{u}_i}, \quad \theta_{\tilde{d}_i}. \quad (4.26)$$

Diagonal entries of $\delta Z_{\tilde{u}_i}$, $(\delta Z_{\tilde{d}_i})_{2,2}$, and the three squared masses are renormalized in the OS scheme,

$$\begin{aligned}
\delta\, m^2_{\tilde{u}_{i1}} &= \mathfrak{Re}\left\{\Sigma^{\tilde{u}_i}_{1,1}(m^2_{\tilde{u}_{i1}})\right\},\ (\delta Z_{\tilde{f}_i})_{1,1} = -\mathfrak{Re}\left\{ \frac{\partial \Sigma^{\tilde{u}_i}_{1,1}(k^2)}{\partial k^2} \right\}_{\Big| k^2 = m^2_{\tilde{u}_{i1}}}, \\
\delta\, m^2_{\tilde{u}_{i2}} &= \mathfrak{Re}\left\{\Sigma^{\tilde{u}_i}_{2,2}(m^2_{\tilde{u}_{i2}})\right\},\ (\delta Z_{\tilde{f}_i})_{2,2} = -\mathfrak{Re}\left\{ \frac{\partial \Sigma^{\tilde{u}_i}_{2,2}(k^2)}{\partial k^2} \right\}_{\Big| k^2 = m^2_{\tilde{u}_{i2}}}, \\
\delta\, m^2_{\tilde{d}_{i2}} &= \mathfrak{Re}\left\{\Sigma^{\tilde{d}_i}_{2,2}(m^2_{\tilde{d}_{i2}})\right\},\ (\delta Z_{\tilde{d}_i})_{2,2} = -\mathfrak{Re}\left\{ \frac{\partial \Sigma^{\tilde{d}_i}_{2,2}(k^2)}{\partial k^2} \right\}_{\Big| k^2 = m^2_{\tilde{d}_{i2}}}.
\end{aligned} \quad (4.27)$$

$\Sigma^{\tilde{f}_i}_{A,B}$ is the $\tilde{f}_{iA}$–$\tilde{f}_{iB}$ self energy. $\delta(Z_{\tilde{d}_i})_{1,1}$ is defined similarly,

$$(\delta Z_{\tilde{d}_i})_{1,1} = -\mathfrak{Re}\left\{\frac{\partial \Sigma^{\tilde{d}_i}_{1,1}(k^2)}{\partial k^2}\right\}_{\Big| k^2=m^2_{\tilde{d}_{i1}}}. \tag{4.28}$$

The non-diagonal entries of $\delta Z_{\tilde{f}_i}$ and the renormalization constant of the mixing angle $\theta_{\tilde{f}_i}$ are renormalized according to Ref. [163],

$$\begin{aligned}
\delta\theta_{\tilde{f}_i} &= \frac{\mathfrak{Re}\{\overline{\Sigma}^{\tilde{f}_i}_{1,2}(m^2_{\tilde{f}_{i1}})\} + \mathfrak{Re}\{\overline{\Sigma}^{\tilde{f}_i}_{1,2}(m^2_{\tilde{f}_{i2}})\}}{2(m^2_{\tilde{f}_{i1}} - m^2_{\tilde{f}_{i2}})}, \qquad (4.29)\\
(\delta Z_{\tilde{f}_i})_{1,2} = (\delta Z_{\tilde{f}_i})_{2,1} &= -\frac{\mathfrak{Re}\{\Sigma^{\tilde{f}_i}_{1,2}(m^2_{\tilde{f}_{i1}})\} - \mathfrak{Re}\{\Sigma^{\tilde{f}_i}_{1,2}(m^2_{\tilde{f}_{i2}})\}}{m^2_{\tilde{f}_{i1}} - m^2_{\tilde{f}_{i2}}}.
\end{aligned}$$

$\overline{\Sigma}^{\tilde{f}_i}_{A,B}$ is the gauge invariant part of the $\tilde{f}_{iA}$–$\tilde{f}_{iB}$ self energy. According to Ref. [163], the splitting between gauge dependent and gauge independent part of the self energy can be performed in a such a way that the latter vanishes in the 't Hooft-Feynman gauge. In this gauge

$$\overline{\Sigma}^{\tilde{f}_i}_{1,2}(k^2) = \Sigma^{\tilde{f}_i}_{1,2}(k^2),$$

and the $\tilde{f}_1$–$\tilde{f}_2$ mixing vanishes when one of the two sfermions goes on-shell. The mass of $\tilde{d}_{i1}$ is a dependent quantity whose renormalization constant can be obtained expanding to first order Eq. (2.65). This renormalization constant reads as follows,

$$\begin{aligned}
\delta m^2_{\tilde{d}_{i1}} &= \frac{1}{c^2_{\theta_{\tilde{d}}}}\Bigg[c^2_{\theta_{\tilde{u}}}\delta m^2_{\tilde{u}_{i1}} + s^2_{\theta_{\tilde{u}}}\delta m^2_{\tilde{u}_{i2}} - s^2_{\theta_{\tilde{d}}}\delta m^2_{\tilde{d}_{i2}} - s_{2\theta_{\tilde{u}}}\left(m^2_{\tilde{u}_{i1}} - m^2_{\tilde{u}_{i2}}\right)\delta\theta_{\tilde{u}_i}\\
&- 2m_{u_i}\delta m_{u_i} + s_{2\theta_{\tilde{d}}}\left(m^2_{\tilde{d}_{i1}} - m^2_{\tilde{d}_{i2}}\right)\delta\theta_{\tilde{d}_i} + 2m_{d_i}\delta m_{d_i} - \delta\left(\frac{1-t^2_\beta}{1+t^2_\beta}M^2_W\right)\Bigg].
\end{aligned}$$

The renormalization constant of the W mass is determined in the OS scheme,

$$\delta M^2_W = \mathfrak{Re}\left\{\Sigma^T_W(M^2_W)\right\},$$

with Σ^T_W the transverse part of the W self energy. the renormalization constant of t_β, δt_β, is defined in the $\overline{\rm DR}$ scheme [164–166] and is equivalent to

$$\delta t_\beta = \frac{1}{2M_Z c^2_\beta}\mathfrak{Re}\{\Sigma^{\rm div}_{A^0,Z}(M^2_{A^0})\}.$$

$\Sigma_{A^0,Z}$ is the A^0–Z self energy while the superscript "div." means retaining the terms proportional to $\Delta_{\rm UV}$ only. As pointed out in Ref. [166], this process-independent condition is also gauge-independent at one-loop[6].
In this scheme A_{d_i} is a dependent quantity. As pointed out in Ref. [167], the renormalization constant of A_{d_i} can give rise to a large correction to the value of A_{d_i} itself, spoiling the reliability of the perturbative expansion and the applicability of this renormalization scheme.

Second renormalization scheme (Rs2).—In this scheme, instead of using the mixing angle of the down-type squarks as input parameter, we use the value of A_{d_i} obtaining $\delta\theta_{\tilde{d}_i}$ as a dependent quantity.
$\delta m^2_{\tilde{u}_{i1,2}}$, $\delta m^2_{\tilde{d}_{i2}}$, $\delta\theta_{\tilde{u}_i}$ and the entries of $\delta Z_{\tilde{f}_i}$ are defined according to the previous scheme.
The $\overline{\rm DR}$ prescription is also used to define the parameter μ, which enters the relation between $\theta_{\tilde{d}_i}$ and A_{d_i}, *cf.* Eq. (2.64). $\delta\mu$ can be obtained retaining the divergent part of $\delta\mu$ as defined in the renormalization scheme proposed in Refs. [168, 169]. In this scheme

$$\begin{aligned}
\delta\mu = \frac{1}{M_2^2-\mu^2} \quad & \Big[\quad (m_{\chi_2^\pm} M_2 - m_{\chi_1^\pm}\mu)\delta m_{\chi_1^\pm} \\
& + \quad (m_{\chi_1^\pm} M_2 - m_{\chi_2^\pm}\mu)\delta m_{\chi_2^\pm} + \mu\delta M_W^2 + M_2\delta(M_W^2 s_{2\beta})\Big], \\
\delta m_{\chi_i^\pm} \quad & = \quad \frac{m_{\chi_i^\pm}}{2}\mathfrak{Re}\left\{\Sigma^L_{\chi_i^\pm}(m^2_{\chi_i^\pm}) + \Sigma^R_{\chi_i^\pm}(m^2_{\chi_i^\pm}) + 2\Sigma^S_{\chi_i^\pm}(m^2_{\chi_i^\pm})\right\}.
\end{aligned} \tag{4.30}$$

The mass of d_i is renormalized in the $\overline{\rm DR}$ scheme as well. The structure of δm_{d_i} can be read from Eq. (4.25), regularizing the self energies within DRED, and retaining only the contribution proportional to $\Delta_{\rm UV}$.
The trilinear coupling $A_{\tilde{d}_i}$ is fixed renormalizing the A^0–$\tilde{d}_{i1}$–$\tilde{d}_{i2}$ vertex in the $\overline{\rm DR}$ scheme. The value of δA_{d_i} reads as follows,

$$\begin{aligned}
\delta A_{d_i} \quad = \quad & \frac{\mathfrak{Re}\{\overline{\Sigma}^{\tilde{d}_i,\rm div}_{1,2}(m^2_{\tilde{d}_{i1}})\} + \mathfrak{Re}\{\overline{\Sigma}^{\tilde{d}_i,\rm div}_{1,2}(m^2_{\tilde{d}_{i2}})\}}{2m_{d_i}} + \delta\mu^{\rm div} t_\beta + \mu\delta t_\beta^{\rm div} + \frac{1}{m_{d_i}}\Bigg[\\
& t_{\theta_{\tilde{d}_i}}\Big(c^2_{\theta_{\tilde{u}_i}}\delta m^{2,\ \rm div}_{\tilde{u}_{i1}} + s^2_{\theta_{\tilde{u}_i}}\delta m^{2,\ \rm div}_{\tilde{u}_{i2}} - s_{2\theta_{\tilde{u}_i}}(m^2_{\tilde{u}_{i1}} - m^2_{\tilde{u}_{i2}})\delta\theta^{\rm div}_{\tilde{u}_i} - 2m_{u_i}\delta m^{\rm div}_{u_i} \\
- \quad & \delta(M_W^2 c_{2\beta})^{\rm div}\Big) - t_{\theta_{\tilde{d}_i}}\delta m^{2,\ \rm div}_{\tilde{d}_{i2}} + \left(2t_{\theta_{\tilde{d}_i}} m_{d_i} - \frac{s_{2\theta_{\tilde{d}_i}}}{2m_{d_i}}(m^2_{\tilde{d}_{i1}} - m^2_{\tilde{d}_{i2}})\right)\delta m^{\rm div}_{d_i}\Bigg],
\end{aligned}$$

[6] At least when the R_ξ gauges are considered

while $\delta\theta_{\tilde{d}_i}$ can be written as follows,

$$\begin{aligned}\delta\theta_{\tilde{d}_i} &= \frac{\mathfrak{Re}\{\Sigma_{1,2}^{\tilde{d}_i\ \mathrm{div}}(m^2_{\tilde{d}_{i1}})\} + \mathfrak{Re}\{\Sigma_{1,2}^{\tilde{d}_i\ \mathrm{div}}(m^2_{\tilde{d}_{i2}})\}}{2(m^2_{\tilde{d}_{i1}} - m^2_{\tilde{d}_{i2}})} + \frac{t_{\theta_{\tilde{d}_i}}}{m^2_{\tilde{d}_{i1}} - m^2_{\tilde{d}_{i2}}}\Bigg[\delta m^{2\ \mathrm{fin}}_{\tilde{d}_{i2}} \\ &- c^2_{\theta_{\tilde{u}_i}}\delta m^{2\ \mathrm{fin}}_{\tilde{u}_{i1}} - s^2_{\theta_{\tilde{u}_i}}\delta m^{2\ \mathrm{fin}}_{\tilde{u}_{i2}} + s_{2\theta_{\tilde{u}_i}}(m^2_{\tilde{u}_{i1}} - m^2_{\tilde{u}_{i2}})\delta\theta^{\mathrm{fin}}_{\tilde{u}_i} + 2m_{u_i}\delta m^{\mathrm{fin}}_{u_i} \\ &+ c_{2\beta}\delta M^{2\ \mathrm{fin}}_W\Bigg]. \end{aligned} \tag{4.31}$$

The superscript "fin" means retaining the finite part of the renormalization constant only. This scheme is equivalent to the "$\overline{\mathrm{DR}}$ bottom-quark mass" scheme of Ref. [167].

Third renormalization scheme (Rs3).— This scheme is similar to the previous one, the only difference is the definition of $\delta\theta_{\tilde{u}_i}$,

$$\delta\theta_{\tilde{u}_i} = \frac{\mathfrak{Re}\{\Sigma_{1,2}^{\tilde{u}_i,\ \mathrm{div}}(m^2_{\tilde{u}_{i1}})\} + \mathfrak{Re}\{\Sigma_{1,2}^{\tilde{u}_i,\ \mathrm{div}}(m^2_{\tilde{u}_{i2}})\}}{2(m^2_{\tilde{u}_{i1}} - m^2_{\tilde{u}_{i2}})}. \tag{4.32}$$

In other words, $\theta_{\tilde{u}_i}$ is defined in the $\overline{\mathrm{DR}}$ scheme.

Fourth renormalization scheme (Rs4).— In this scheme, the $\tilde{u}_i$ and $\tilde{d}_i$ sectors are treated in a symmetric way. This scheme is similar to the Rs1 scheme, the only differences are the renormalization of the mixing angles,

$$\delta\theta_{\tilde{f}_i} = \frac{\mathfrak{Re}\{\Sigma_{1,2}^{\tilde{f}_i,\ \mathrm{div}}(m^2_{\tilde{f}_{i1}})\} + \mathfrak{Re}\{\Sigma_{1,2}^{\tilde{f}_i,\ \mathrm{div}}(m^2_{\tilde{f}_{i2}})\}}{2(m^2_{\tilde{f}_{i1}} - m^2_{\tilde{f}_{i2}})}, \tag{4.33}$$

and the renormalization of $m_{d,i}$, which is performed in the $\overline{\mathrm{DR}}$ scheme.

Since the mass of the quarks belonging to the first two generations has been neglected, the corresponding squarks do not mix and in all the renormalization schemes presented above one has

$$\delta\theta_{\tilde{u}_i} = 0, \qquad \delta\theta_{\tilde{d}_i} = 0, \qquad \delta m_{d_i} = 0.$$

Therefore, in the case of the squarks belonging to the first two generations, all the schemes are equivalent.

Gluino sector

The renormalization of the gluino sector is similar to the renormalization of the quarks sector. The kinetic term of the Lagrangian is

$$\mathcal{L}_{\tilde{g}} = \bar{\psi}_{\tilde{g}} \left(i \not{\partial} - m_{\tilde{g}} \right) \psi_{\tilde{g}}, \tag{4.34}$$

and the splitting of the bare quantities in terms of renormalized ones and renormalization constants reads

$$m_{\tilde{g}} \to m_{\tilde{g}} + \delta m_{\tilde{g}}, \qquad \psi_{\tilde{g}} \to \left(1 + \frac{\delta Z_{\tilde{g}}}{2} \right) \psi_{\tilde{g}}. \tag{4.35}$$

In this case, there is no distinction between δZ^L and δZ^R since $\psi_{\tilde{g}}$ is a Majorana spinor. The wavefunction and the mass of the gluino are renormalized in the OS scheme,

$$\begin{aligned} \delta m_{\tilde{g}} &= m_{\tilde{g}} \mathfrak{Re} \left\{ \Sigma^L_{\tilde{g}}(m^2_{\tilde{g}}) + \Sigma^S_{\tilde{g}}(m^2_{\tilde{g}}) \right\}, \qquad (4.36) \\ \delta Z_{\tilde{g}} &= -\mathfrak{Re} \left\{ \Sigma^L_{\tilde{g}}(m^2_{\tilde{g}}) \right\} - 2 m^2_{\tilde{g}} \mathfrak{Re} \left\{ \frac{\partial \Sigma^L_{\tilde{g}}(k^2)}{\partial k^2} + \frac{\partial \Sigma^S_{\tilde{g}}(k^2)}{\partial k^2} \right\}_{\Big| k^2 = m^2_{\tilde{g}}}. \end{aligned}$$

Strong coupling constant

The renormalization of the strong coupling g_s, is strictly connected with that of the gluon field G_μ. As usual, the bare parameters are expressed in terms of renormalization constants and the renormalized quantities as follows,

$$g_s \to (g_s + \delta g_s) = (1 + \delta Z_g)\, g_s, \qquad G^\mu \to \left(1 + \frac{\delta Z_G}{2} \right) G^\mu. \tag{4.37}$$

The actual structure of the renormalization constants is obtained applying the $\overline{\text{MS}}$ scheme to the gluonic self-energy $\Pi^{\mu\nu}$ and to the triple gluon vertex $\Lambda^{\mu\nu\rho}$. δZ_G and δZ_g read

$$\delta Z_g = -\frac{\alpha_s}{4\pi} \left(\frac{3}{2} \Delta_{\text{UV}} \right), \qquad \delta Z_G = -\frac{\alpha_s}{4\pi} \left(3 \Delta_{\text{UV}} \right). \tag{4.38}$$

The $\overline{\text{MS}}$ scheme allows to exploit the infrastructures developed for proton colliders. Nevertheless, it leads to some potential problem that has to be considered.

First of all, at energies above the bottom mass, the PDFs are obtained by using a running $\overline{\text{MS}}$ strong coupling with five massless flavors ($\alpha_s^{(5)}(\mu)$). Such

a choice is not appropriate at scales comparable with the mass of the heavy particles (top, squarks and gluino), since these particles are not decoupled any more. Nevertheless, at such scales, $\alpha_s(\mu)$ and $\alpha_s^{(5)}(\mu)$ can be related. At one-loop such relation reads

$$\alpha_s(\mu) = \alpha_s^{(5)}(\mu) - \frac{\alpha_s^2}{2\pi}\left[\frac{1}{12}\sum_{f=u,d}\sum_{i=1}^{2}\ln\left(\frac{m^2_{\tilde{f}_i}}{\mu^2}\right) + \ln\left(\frac{m^2_{\tilde{g}}}{\mu^2}\right) + \frac{1}{3}\ln\left(\frac{m_t^2}{\mu^2}\right)\right].$$

Equivalently, one can absorb the term in square brackets into the definition of the renormalization constants [15, 170], which become

$$\begin{aligned}
\delta Z_g &= -\frac{\alpha_s}{4\pi}\left(\frac{3}{2}\Delta_{\rm UV}\right) - \frac{\alpha_s}{4\pi}\left[\frac{1}{12}\sum_{f=u,d}\sum_{i=1}^{3}\sum_{A=1}^{2}\ln\left(\frac{m^2_{\tilde{f}_{Ai}}}{\mu^2}\right)\right. \\
&+ \left.\ln\left(\frac{m^2_{\tilde{g}}}{\mu^2}\right) + \frac{1}{3}\ln\left(\frac{m_t^2}{\mu^2}\right)\right], \\
\delta Z_G &= -\frac{\alpha_s}{4\pi}\left(3\Delta_{\rm UV}\right) + 2\frac{\alpha_s}{4\pi}\left[\frac{1}{12}\sum_{f=u,d}\sum_{i=1}^{3}\sum_{A=1}^{2}\ln\left(\frac{m^2_{\tilde{f}_{Ai}}}{\mu^2}\right)\right. \\
&+ \left.\ln\left(\frac{m^2_{\tilde{g}}}{\mu^2}\right) + \frac{1}{3}\ln\left(\frac{m_t^2}{\mu^2}\right)\right].
\end{aligned}$$

As a consequence, $\alpha_s(\mu) = \alpha_s^{(5)}(\mu)$ at all energies. The renormalization scheme defined by means of Eq. (4.39) is called "zero momentum subtraction scheme" since in this scheme the divergences associated with heavy particles in the loops are subtracted when all the external momenta in $\Pi^{\mu\nu}$ and $\Lambda^{\mu\nu\rho}$ vanish.

Another problem is the incompatibility between dimensional regularization and SUSY. SUSY-QCD Slavnov-Taylor identities involving the squark–quark–gluino vertices are no longer fulfilled at one loop [150]. At one-loop, such identities can be restored adding the term

$$\begin{aligned}
-\sqrt{2}\; g_s\; T\left(\frac{4}{3}\frac{\alpha_s}{4\pi}\right)\sum_{f=u,d}\sum_{i=1}^{3} \;\Big\{\;& \Big[\bar{\psi}_{\tilde{g}}(c_{\theta_{\tilde{f}_i}}\omega_- - s_{\theta_{\tilde{f}_i}}\omega_+)\psi_{\tilde{f}_i}\tilde{f}^*_{i1} + \text{h.c.}\Big] \\
&- \Big[\bar{\psi}_{\tilde{g}}(s_{\theta_{\tilde{f}_i}}\omega_- + c_{\theta_{\tilde{f}_i}}\omega_+)\psi_{\tilde{f}_i}\tilde{f}^*_{i2} + \text{h.c.}\Big]\Big\},
\end{aligned} \tag{4.39}$$

to the SUSY-QCD Lagrangian. T are the generators of the adjoint representation of $SU(3)_C$. As usual, color indices are dropped. Such a SUSY-restoring

counter term is fundamental to guarantee the quark-quark-gluon and squark-quark-gluino effective coupling to be identical in SUSY-QCD, regularized within the $\overline{\rm MS}$ scheme [15, 171].
In actual computations, this term is taken into account substituting the renormalization constant δZ_{g_s} appearing the quark–squark–gluino counter term by $\delta Z_{\hat{g}_s}$, defined as

$$\delta Z_{\hat{g}} = \delta Z_g + \frac{4}{3}\frac{\alpha_s}{4\pi}. \tag{4.40}$$

4.3 Photonic mass singularities

Besides UV divergences, one-loop amplitudes are affected by other divergences, appearing in the loop integrals when combinations of external momenta and internal masses become small. Such singularities are logarithmic, and at one-loop they arise in the following situations [172].

- An external massless on-shell particle is attached to two massless propagators. Such singularities are *collinear singularities* since they arise when the external momentum and the momentum on the internal lines become collinear.

- Two external on-shell particles exchange a massless particle. These are *soft singularities* since they arise when the momentum of the internal massless particle vanishes. These singularities are also called *IR singularities*.

Moreover, processes producing the final state F together with a massless particle (γ, g q or $\bar{q}$) are affected by similar divergences that enter in the phase space integration.

- *Collinear singularities* arise when a massless particle is emitted from another massless particle in the collinear region.

- *Soft singularities* appear when the momentum of a massless particle in the final state approaches zero.

The transition probabilities summed over degenerate initial and final states are free from mass singularities. This is a non-trivial check of the consistency of the theory and is guaranteed by the Kinoshita-Lee-Nauenberg (KLN) theorem [172, 173]. Such theorem does not apply in our case. Indeed, the sum over degenerate initial states is not possible owing to the difficulties in preparing a three particle initial state. Nevertheless, according to the

Bloch-Nordsieck (BN) theorem [174], soft singularities cancel when degenerate final states are summed over. Moreover, in the case of hadronic collisions, the collinear singularities can be removed by means of the mass factorization.

In the next subsections we will show how the photonic divergences cancel and discuss their handling in actual computations.

4.3.1 General features

In this section we explicitly verify the cancellation of the soft and collinear divergences of photonic origin for the processes we are considering. We regularize IR and collinear divergences using mass regularization, *i.e.* giving a small mass (m_γ) to the photon and retaining a small mass for the light quarks. Such regularization breaks QED gauge invariance. Nevertheless, one can show that massive QED is a BRS invariant and finite theory with gauge-independent S-matrix elements [134, 175]. Its renormalization requires the same counter terms as in massless QED.
Within this regularization scheme, soft and collinear divergences show up as linear or quadratic terms of the logarithms $\ln\left(m_\gamma^2\right)$, $\ln\left(m_{f_i}^2\right)$.

First of all we consider a generic partonic process $ij \to F$ together with the real photon emission processes $ij \to F\gamma$. The particles of such processes and their momenta can be labelled as follows,

$$1(p_1; m_1),\ 2(p_2; m_2) \to 3(p_3; m_3),\ 4(p_4; m_4),\ [\gamma(k_\gamma; m_\gamma)]. \tag{4.41}$$

The structure of the mass singularities of the one-loop corrections to the differential cross section of the process $1, 2 \to 3, 4$ reads [176],

$$d\sigma^{2,1}_{1,2\to3,4} = \frac{\alpha}{2\pi}\left(\sum_{i\neq j;\ i,j=1}^{4} e_i\sigma_i e_j\sigma_j \mathcal{V}^{(1)}_{ij} + \sum_{j=1}^{4}(e_j\sigma_j)^2\mathcal{V}^{(2)}_{j}\right) d\sigma^{2,0}_{1,2\to3,4}. \tag{4.42}$$

e_i is the charge of the particle i expressed in unities of the positron charge. $\sigma_i = 1$ in the case of an ingoing particle and an outgoing anti-particle while $\sigma_i = -1$ if i is an ingoing anti-particle or an outgoing particle. Defining

$s_{ij} = 2p_ip_j$ and $v_{ij} = \sqrt{1 - 4m_i^2m_j^2/s_{ij}^2}$ one has

$$\begin{aligned}
\mathcal{V}_{ij}^{(1)} &= \Big(1 - \delta_{i3}\delta_{j4} - \delta_{i4}\delta_{j3}\Big)\left[\frac{1}{2}\ln\left(\frac{m_i^2m_j^2}{s_{ij}^2}\right)\ln\left(\frac{m_\gamma^2}{s_{ij}}\right) - \frac{1}{4}\ln^2\left(\frac{m_i^2}{s_{ij}}\right)\right. \\
&\left. -\frac{1}{4}\ln^2\left(\frac{m_j^2}{s_{ij}}\right)\right] + \Big(\delta_{i3}\delta_{j4} + \delta_{i4}\delta_{j3}\Big)\left[\frac{1}{2v_{34}}\ln\left(\frac{1-v_{34}}{1+v_{34}}\right)\ln\left(\frac{m_\gamma^2}{s_{34}}\right)\right], \\
\mathcal{V}_j^{(2)} &= -\ln\left(\frac{m_\gamma^2}{\mu^2}\right) - \frac{1}{2}\ln\left(\frac{m_j^2}{\mu^2}\right). \qquad (4.43)
\end{aligned}$$

The singularity structure of the real emission processes $1,2 \to 3,4,\gamma$ is universal and can be obtained exploiting general features of the real emission amplitudes in the soft and/or collinear limit. In these limits, the differential cross section reads [142]

$$\begin{aligned}
\sigma_{1,2\to3,4,\gamma}^{2,1} &= -\frac{\alpha}{2\pi}\left\{\left(\sum_{i\neq j;\ i,j=1}^{4} e_i\sigma_i e_j\sigma_j\mathcal{V}_{ij}^{(1)} + \sum_{j=1}^{4}(e_j\sigma_j)^2\mathcal{V}_j^{(2)}\right)d\sigma_{1,2\to3,4}^{2,0}\right. \\
&+ \left.\sum_{i=1}^{2}(e_i\sigma_i)^2\int_{z_0}^{1}dz\ \left[P_{qq}(z)\right]_+\ln\left(\frac{m_i^2}{s_{12}}\right)d\sigma_{1,2\to3,4}^{2,0}(zs_{12})\right\}, \qquad (4.44)
\end{aligned}$$

where the $[\cdots]_+$ distribution is defined in Eq. (4.12) and z_0 is defined in section 4.1.2. If the particle 1 (2) is a quark or an anti-quark, further collinear singularities appear in the process obtained by crossing the particle 1 (2) with the photon. In other words, processes like

$$\begin{aligned}
\gamma(k_\gamma;m_\gamma),\ 2(p_2;m_2) &\to 3(p_3;m_3),\ 4(p_4;m_4),\ \bar{1}(p_1;m_1), \qquad (4.45)\\
1(p_1;m_1),\ \gamma(k_\gamma;m_\gamma) &\to 3(p_3;m_3),\ 4(p_4;m_4),\ \bar{2}(p_2;m_2), \qquad (4.46)
\end{aligned}$$

exhibit collinear singularities. For instance, the partonic process $\gamma q \to \tilde{g}\tilde{g}q$ belongs to this category. This process is obtained crossing the process $\bar{q}q \to \tilde{g}\tilde{g}\gamma$, and its $\mathcal{O}(\alpha_s^2\alpha)$ contributions can be computed squaring the diagrams in Fig. F.3 of appendix F. In the collinear region, the differential cross sections for the processes (4.45) and (4.46) are

$$\begin{aligned}
d\sigma_{\gamma,2\to3,4,\bar{1}}^{2,1} &= \frac{3\alpha}{2\pi}e_1^2\int_{z_0}^{1}dz\ P_{qg}(z)\ln\left(\frac{s_{\gamma2}}{m_1^2}\right)d\sigma_{1,2\to3,4}^{2,0}(zs_{\gamma2})(\delta_{1q}+\delta_{1\bar{q}}),\\
d\sigma_{1,\gamma\to3,4,\bar{2}}^{2,1} &= \frac{3\alpha}{2\pi}e_2^2\int_{z_0}^{1}dz\ P_{qg}(z)\ln\left(\frac{s_{1\gamma}}{m_2^2}\right)d\sigma_{1,2\to3,4}^{2,0}(zs_{1\gamma})(\delta_{2q}+\delta_{2\bar{q}}),
\end{aligned} \qquad (4.47)$$

respectively. $s_{\gamma 2}$ and $s_{1\gamma}$ are defined as $s_{\gamma 2} = (k_\gamma + p_2)^2$ and $s_{1\gamma} = (p_1 + k_\gamma)^2$. The singular part left over in the sum of the Eq. (4.42) and (4.44) cancels against the singular contribution arising from the contribution of $\mathcal{R}(x_1, x_2, s)$ proportional to $f_{1|P_1}(x_1) f_{2|P_2}(x_2)$, *c.f.* Eq. (4.11),

$$\frac{\alpha}{2\pi} \sum_{i=1}^{2} (e_i \sigma_i)^2 \left\{ \int_{z_0}^{1} dz \ \left[P_{qq}(z) \right]_+ \ln \left(\frac{m_i^2}{\mu^2} \right) d\sigma^{2,0}_{1,2\to 3,4}(z s_{12}) \right\}. \tag{4.48}$$

Concerning the singular terms of the process (4.45), they cancel when summed with the terms of $\mathcal{R}(x_1, x_2, s)$ proportional to $f_{\gamma|P_1}(x_1) f_{2|P_2}(x_2)$,

$$\frac{3\alpha}{2\pi} e_1^2 \int_{z_0}^{1} dz \ P_{qg}(z) \ln \left(\frac{m_1^2}{\mu} \right) d\sigma^{2,0}_{1,2\to 3,4}(z s_{\gamma 2}) (\delta_{1q} + \delta_{1\bar{q}}). \tag{4.49}$$

Similarly, the singularities in the differential cross section of the process (4.46) are cancelled by the term of $\mathcal{R}(x_1, x_2, s)$ proportional to $f_{1|P_1}(x_1) f_{\gamma|P_2}(x_2)$,

$$\frac{3\alpha}{2\pi} e_2^2 \int_{z_0}^{1} dz \ P_{qg}(z) \ln \left(\frac{m_2^2}{\mu^2} \right) d\sigma^{2,0}_{1,2\to 3,4}(z s_{1\gamma}) (\delta_{2q} + \delta_{2\bar{q}}). \tag{4.50}$$

The regularization of the mass singularities of the virtual corrections is implemented in the package `LoopTools` [177, 178], the library used for the computation of the scalar integrals. More involved is the treatment of the mass singularities from the real emission processes. Indeed, such singularities appear in the phase space integration and have to be extracted properly in order to deal with a well-behaved integrand. In the following, we will briefly describe the two methods we use.

4.3.2 Phase space slicing

The phase space slicing technique restricts the phase space integration of the real photon emission process to a region with a minimum photon energy $\Delta E = \delta_s \sqrt{s}_{12}/2$. The integration over this region is thus convergent and can be performed numerically. The complementary integral over the singular region can be done analytically in the eikonal approximation [179–181], which is a good approximation if the cut δ_s is sufficiently small since the error is $\mathcal{O}(\delta_s)$. In case of the presence of collinear singularities we have to introduce a further collinear cutoff δ_c on the angle between the photon and the radiating initial particle. For sufficiently small δ_c the integration over the singular region can be approximated with an analytical formula, the error being $\mathcal{O}(\delta_c)$.

In the case of the real photon emission process $ij \to F\gamma$ or, using the notation of the previous section, $1,2 \to 3,4,\gamma$, the differential cross section in the soft limit is

$$d\sigma^{2,1}_{1,2\to 3,4,\gamma} = -\frac{\alpha}{2\pi}\left\{\sum_{i<j;\ i,j=1}^{4} e_i\sigma_i e_j\sigma_j \mathcal{I}^{(1)}_{ij} + \sum_{j=1}^{4}(e_j\sigma_j)^2\mathcal{I}^{(2)}_j\right\} d\sigma^{2,0}_{1,2\to 3,4}. \quad (4.51)$$

We define

$$\begin{aligned}
\mathcal{I}^{(1)}_{12} &= \sum_{i=1}^{2}\ln\left(\frac{s_{12}}{m_i^2}\right)\ln\left(\frac{4\Delta E^2}{m_\gamma^2}\right) - \frac{\pi^2}{3} - \frac{1}{2}\ln^2\left(\frac{s_{12}}{m_i^2}\right),\\
\mathcal{I}^{(1)}_{34} &= \frac{1}{v_{34}}\sum_{i=3}^{4}\ln\left(\frac{1+\beta_i}{1-\beta_i}\right)\ln\left(\frac{4\Delta E^2}{m_\gamma^2}\right) - 2\mathrm{Li}_2\left(\frac{2\beta_i}{1+\beta_i}\right) - \frac{1}{2}\ln^2\left(\frac{1-\beta_i}{1+\beta_i}\right),\\
\mathcal{I}^{(1)}_{ij} &= \ln\left(\frac{s_{ij}^2}{m_i^2 m_j^2}\right)\ln\left(\frac{4\Delta E^2}{m_\gamma^2}\right) - \frac{1}{2}\ln^2\left(\frac{s_{12}}{m_i^2}\right) - \frac{\pi^2}{3}\\
&\quad -2\mathrm{Li}_2\left(1 - \frac{2p_i^0 p_j^0}{s_{ij}}(1-\beta_j)\right) - 2\mathrm{Li}_2\left(1 - \frac{2p_i^0 p_j^0}{s_{ij}}(1+\beta_j)\right)\\
&\quad -\frac{1}{2}\ln^2\left(\frac{1-\beta_j}{1+\beta_j}\right), \quad \text{for} \quad (i,j) = (1,3),(1,4),(2,3),(2,4)\\
\mathcal{I}^{(2)}_j &= \ln\left(\frac{4\Delta E^2}{m_\gamma^2}\right) + \ln\left(\frac{m_j^2}{s_{12}}\right)(\delta_{j1}+\delta_{j2}) + \frac{1}{\beta_j}\ln\left(\frac{1-\beta_j}{1+\beta_j}\right)(\delta_{j3}+\delta_{j4}).
\end{aligned} \quad (4.52)$$

β_i is defined as $\beta_i = |\mathbf{p}_i|/p_i^0$ while $\mathrm{Li}_2(x)$ is the dilogarithm. In the (non-soft) collinear region the differential cross section reads

$$d\sigma^{2,1}_{1,2\to 3,4,\gamma} = \frac{\alpha}{2\pi}\sum_{i=1}^{2} e_i^2 \int_{z_0}^{1-\delta_s} dz\, P_{qq}(z)\left[\ln\left(\frac{s_{12}\delta_c^2}{4m_i^2}\right) - \frac{2z}{1+z^2}\right] d\sigma^{2,0}_{1,2\to 3,4}(z s_{12}),$$

where $P_{qq}(z)$, is the quark-quark splitting function defined in Eq. (4.14).

In the case of real (anti-)quark emission processes of the type $ij \to Fq$ and $ij \to F\bar{q}$, the only singularities are the collinear ones. Using the notation of Eq. (4.46), in the collinear region their differential cross sections are

$$\begin{aligned}
d\sigma^{2,1}_{\gamma,2\to 3,4,\bar{1}} &= \frac{3\alpha}{2\pi}e_1^2\int_{z_0}^{1} dz\ \left[P_{gq}(z)\ln\left(\frac{\delta_c^2 s_{\gamma 2}}{4m_1^2}(1-z)^2\right) + 2z(1-z)\right]\\
&\quad\times\ d\sigma^{2,0}_{1,2\to 3,4}(z s_{\gamma 2})(\delta_{1q}+\delta_{1\bar{q}}),\\
d\sigma^{2,1}_{1,\gamma\to 3,4,\bar{2}} &= \frac{3\alpha}{2\pi}e_2^2\int_{z_0}^{1} dz\ \left[P_{gq}(z)\ln\left(\frac{\delta_c^2 s_{1\gamma}}{4m_2^2}(1-z)^2\right) + 2z(1-z)\right],\\
&\quad\times\ d\sigma^{2,0}_{1,2\to 3,4}(z s_{1\gamma})(\delta_{2q}+\delta_{2\bar{q}}).
\end{aligned}$$

where $P_{qg}(z)$ is given in Eq. (4.14).

4.3.3 Dipole subtraction formalism

Phase space slicing is a well established and intuitive method. The only drawback is that in order to minimize the error introduced by the analytical approximation, δ_s and δ_c have to be small enough. Since the numerical integration depends logarithmically on δ_s and δ_c, the convergence of the numerical integration worsens as δ_s and δ_c decrease. Therefore, in actual computations, the value of the cut-off has to be tuned and chosen in a region where both the approximation is valid and the numerical integrations are stable.

Such numerical instabilities do not enter in subtraction methods. According to these approaches, one has to add and subtract an auxiliary function to the differential cross section of the real emission processes,

$$\begin{aligned} d\sigma^{2,1}_{ij\to Fx} &= \frac{1}{4N_iN_j}\frac{1}{2s}\Bigg\{\int d\Phi_3\left[\sum|\mathcal{M}^{1,1/2}_{ij\to Fx}|^2-|\mathcal{M}^{\rm sub}_{ij\to Fx}|^2\right] \\ &+ \int d\Phi_3|\mathcal{M}^{\rm sub}_{ij\to Fx}|^2\Bigg\} \quad (x=\gamma,q,\bar{q}). \end{aligned} \tag{4.53}$$

$|\mathcal{M}^{\rm sub}_{ij\to Fx}|^2$ has to match pointwise the singularities of $\sum|\mathcal{M}^{1,1/2}_{ij\to Fx}|^2$ and has to be simple enough to be integrated analytically; the difference in the square brackets is then regular over the whole three-particle phase space and can be integrated numerically.

Various subtraction methods, based on different formalisms, have been described for NLO QCD corrections in case of massless [182–184] and massive [185, 186] particles. Methods valid at NNLO are currently under construction [187]. Such methods are valid when the mass singularities are regularized within dimensional regularization (or reduction). Moreover, the dipole subtraction formalism has been extended to photonic IR and collinear divergences regularized within mass regularization in the case of collinear-safe [188] and non-collinear-safe [189] observables. In particular, we use the results quoted in the last two references. Although these results apply to processes involving fermions only, they can be generalized to processes with charged bosons owing to the universal structure of the soft singularities.

According to the dipole formalism, a choice for the subtraction function in the case of the real photon emission processes of the type $1,2\to3,4,\gamma$ is

$$|\mathcal{M}^{\rm sub}_{1,2\to3,4,\gamma}|^2=-\frac{\alpha}{2\pi}\left\{\sum_{i\neq j;\ i,j=1}^{4}e_i\sigma_ie_j\sigma_jg^{\gamma}_{ij}\sum|\mathcal{M}^{1,0}_{1,2\to3,4}(\tilde{\Phi}^{\gamma}_{ij})|^2\right\}. \tag{4.54}$$

$\mathcal{M}^{1,0}_{1,2\to3,4}$ is the tree-level QCD amplitude while the functions g^{γ}_{ij} are defined in appendix E. $\tilde{\Phi}^{\gamma}_{ij}$ is the mapping from the momenta of the process $1,2 \to 3,4,\gamma$ to the momenta of the process $1,2 \to 3,4$. This mapping is defined in appendix E, together with the analytical integration of the subtracted function over the whole photon phase space. A more general treatment is available in Ref. [188, 189], where a detailed explanation on how implementing cuts and obtaining distributions is given.

In the case of real (anti-)quark emission processes like those in Eq. (4.46), the subtraction functions matching the singular behaviour in the collinear region read as follows [189, 190],

$$\begin{aligned} |\mathcal{M}^{\rm sub}_{\gamma,2\to3,4,\bar{1}}| &= -\frac{\alpha}{2\pi}(e_1\sigma_1)^2\, h_{\gamma 2} \sum |\mathcal{M}^{1,0}_{1,2\to3,4}(\tilde{\Phi}^{\gamma}_{\gamma 2})|^2, \\ |\mathcal{M}^{\rm sub}_{1,\gamma\to3,4,\bar{2}}| &= -\frac{\alpha}{2\pi}(e_2\sigma_2)^2\, h_{1\gamma} \sum |\mathcal{M}^{1,0}_{1,2\to3,4}(\tilde{\Phi}^{\gamma}_{1\gamma})|^2. \end{aligned} \tag{4.55}$$

The functions $h_{\gamma 2}$, $h_{1\gamma}$, $\tilde{\Phi}^{\gamma}_{\gamma 2}$, and $\tilde{\Phi}^{\gamma}_{1\gamma}$ are defined in appendix E together with the integral over the whole photonic phase space of the subtracted function.

4.4 Gluonic mass singularities

The treatment of the gluonic soft and collinear singularities can be obtained with a slight modification of that of the photonic singularities. We use mass regularization to regularize mass gluonic singularities. Such a scheme spoils QCD gauge invariance. QCD Ward identities can be restored adding proper counter terms whenever the three and four gluons vertices are involved into the mass singularities [171]. This is not the case for our processes. Indeed, they exhibit IR and collinear gluonic singularities only in partonic processes without gluons in the initial states. Therefore the gluon behaves basically like a photon and the insertion of a gluon mass does not pose any problem.

The structure of this section is similar to that of section 4.3. In section 4.4.1 we explicitly show the cancellation of the gluonic mass divergences at one-loop. In section 4.4.2 and 4.4.3, we extend the phase space slicing and the dipole subtraction method introduced previously to the case of real gluonic mass singularities.

4.4.1 General features

For later convenience, it is worth to make some definition and set specific algebra. Our conventions are based on those of Ref. [186]. Let us consider a

partonic process such as

$$1(p_1;m_1;c_1);\ 2(p_2;m_2;c_2)\to 3(p_3;m_3;c_3);\ 4(p_4;m_4;c_4), \tag{4.56}$$

where c_i is the color of the particle i. $(\mathcal{M}_{1,2\to3,4})^{c_1,c_2,c_3,c_4}$ is the colored amplitude. Introducing a color basis $|b_1,b_2,b_3,b_4>$, the colored amplitude reads

$$(\mathcal{M}_{1,2\to3,4})^{c_1,c_2,c_3,c_4} =< c_1,c_2,c_3,c_4|\mathcal{M}_{1,2\to3,4}>, \tag{4.57}$$

and the squared amplitude becomes

$$\sum|\mathcal{M}_{1,2\to3,4}|^2 =<\mathcal{M}_{1,2\to3,4}|\mathcal{M}_{1,2\to3,4}>. \tag{4.58}$$

It is worth to introduce a color charge $\mathbf{t}_i$ and to associate it to the emission of a gluon from the particle i. Its action is

$$< c_1,c_2,c_3,c_4|\mathbf{t}_i|b_1,b_2,b_3,b_4 >= \delta_{c_1b_1}\dots t^c_{c_ib_i}\dots\delta_{b_4c_4}, \tag{4.59}$$

where c is the color of the emitted gluon. $t^c_{ij}=T^c_{ij}$ if the emitting particle is an incoming anti-(s)quark or an outgoing (s)quark, while $t^c_{ij}=-T^c_{ji}$ if the gluon is emitted by an incoming (s)quark or by an outgoing anti-(s)quark. The color charge algebra is such that

$$\mathbf{t}_j\mathbf{t}_i=\mathbf{t}_i\mathbf{t}_j,\qquad \mathbf{t}_i^2=C_i,\qquad \sum_{i=1}^{4}\mathbf{t}_i|\mathcal{M}_{1,2\to3,4}>=0.$$

C_i is the Casimir operator of the representation under which the particle i transforms under $SU(3)_C$. In particular, $C_i=C_F=4/3$ if i is a (s)quark or an anti-(s)quark, while $C_i=C_A=3$ if i is either a gluon or a gluino.

We are now ready to discuss the cancellations of the gluonic mass divergences. They appear in the processes which exhibit electroweak tree-level contributions. According to the notation introduced in Eq. (4.56), the singular behaviour of the one-loop corrections reads [176]

$$d\sigma^{2,1}_{1,2\to3,4}=\frac{\alpha_s}{2\pi}\left(\sum_{i\neq j;\ i,j=1}^{4}\mathcal{V}^{(1)}_{ij}d\sigma^{1,1}_{1,2\to3,4;\ (i,j)}+\sum_{j=1}^{4}\mathcal{V}^{(2)}_{j}d\sigma^{1,1}_{1,2\to3,4;\ (j,j)}\right), \tag{4.60}$$

where $\mathcal{V}^{(1)}_{ij}$ and $\mathcal{V}^{(2)}_{j}$ are defined in Eq. (4.43). $d\sigma^{1,1}_{1,2\to3,4;\ (i,j)}$ is defined as follows,

$$d\sigma^{1,1}_{1,2\to3,4;\ (i,j)}\equiv\frac{1}{4N_1N_2}\frac{dt}{16\pi s^2}2\mathfrak{Re}\{<\mathcal{M}^{1,0}_{1,2\to3,4}|\mathbf{t}_i\mathbf{t}_j|\mathcal{M}^{0,1}_{1,2\to3,4}>\}, \tag{4.61}$$

and $\mathcal{M}^{0,1}_{1,2\to3,4}$ ($\mathcal{M}^{1,0}_{1,2\to3,4}$) is the tree-level EW (QCD) amplitude of the process (4.56).

Concerning the process of real gluon emission,

$$1(p_1;m_1;c_1);\ 2(p_2;m_2;c_2)\to 3(p_3;m_3;c_3);\ 4(p_4;m_4;c_4);\ g(k_g;m_g;c), \quad (4.62)$$

the IR and collinear structure of its differential cross section is

$$\begin{aligned} d\sigma^{2,1}_{1,2\to3,4,g} &= -\frac{\alpha_s}{2\pi}\Bigg\{\left(\sum_{i\neq j;\ i,j=1}^{4}\mathcal{V}^{(1)}_{ij}d\sigma^{1,1}_{1,2\to3,4;\ (i,j)}+\sum_{j=1}^{4}\mathcal{V}^{(2)}_{j}d\sigma^{1,1}_{1,2\to3,4;\ (i,i)}\right)\\ &+\sum_{i=1}^{2}\int_{z_0}^{1}dz\ \left[\frac{1+z^2}{1-z}\right]_+\ln\left(\frac{m_i^2}{s_{12}}\right)d\sigma^{1,1}_{1,2\to3,4;\ (i,i)}(zs_{12})\Bigg\}. \quad (4.63)\end{aligned}$$

If the particle 1 or the particle 2 is an (anti-)quark, further collinear singularities appear in the crossed processes

$$\begin{aligned} g(k_g;m_g;c),\ 2(p_2;m_2;c_2) &\to 3(p_3;m_3;c_3),\ 4(p_4;m_4;c_4),\ \bar{1}(p_1;m_1;c_1),\\ 1(p_1;m_1;c_1),\ g(k_g;m_g;c) &\to 3(p_3;m_3;c_3),\ 4(p_4;m_4;c_4),\ \bar{2}(p_2;m_2;c_2). \end{aligned} \quad (4.64)$$

Such collinear singularities read

$$\begin{aligned} d\sigma^{2,1}_{g,2\to3,4,\bar{1}} &= \frac{\alpha_s}{2\pi}T_R\int_{z_0}^{1}dz\ P_{qg}(z)\ln\left(\frac{s_{g2}}{m_1^2}\right)d\sigma^{1,1}_{1,2\to3,4}(zs_{g2})(\delta_{1q}+\delta_{1\bar{q}}),\\ d\sigma^{2,1}_{1,g\to3,4,\bar{2}} &= \frac{\alpha_s}{2\pi}T_R\int_{z_0}^{1}dz\ P_{qg}(z)\ln\left(\frac{s_{1g}}{m_2^2}\right)d\sigma^{1,1}_{1,2\to3,4}(zs_{1g})(\delta_{2q}+\delta_{2\bar{q}}), \end{aligned} \quad (4.65)$$

defining $s_{g2}=(k_g+p_2)^2$ and $s_{1g}=(p_1+k_g)^2$. T_R has been defined in section 4.1.2. The singularities in Eq. (4.63) and (4.60) cancel when summed together with those arising from the PDF factorization terms,

$$\frac{\alpha_s}{2\pi}\sum_{i=1}^{2}\left\{\int_{z_0}^{1}dz\ \left[\frac{1+z^2}{1-z}\right]_+\ln\left(\frac{m_i^2}{\mu^2}\right)d\sigma^{1,1}_{1,2\to3,4;\ (i,i)}(zs_{12})\right\}. \quad (4.66)$$

The collinear singularities related to the processes (4.65) cancel when summed to the contributions of $\mathcal{R}(x_1,x_2,s)$ proportional to $f_{g|P_1}(x_1)f_{2|P_2}(x_2)$ and $f_{1|P_1}(x_1)f_{g|P_2}(x_2)$. As can be inferred from Eq. (4.11), such contributions read

$$\begin{aligned} &-\frac{\alpha_s}{2\pi}T_R\int_{z_0}^{1}dz\ P_{qg}(z)\ln\left(\frac{\mu^2}{m_1^2}\right)(\delta_{1q}+\delta_{1\bar{q}})d\sigma^{1,1}_{1,2\to3,4}(zs_{g2}),\\ &-\frac{\alpha_s}{2\pi}T_R\int_{z_0}^{1}dz\ P_{qg}(z)\ln\left(\frac{\mu^2}{m_2^2}\right)(\delta_{2q}+\delta_{2\bar{q}})d\sigma^{1,1}_{1,2\to3,4}(zs_{1g}). \end{aligned} \quad (4.67)$$

We handle the gluonic singularities using both phase space slicing and dipole subtraction. The adaption of such methods to the case of gluonic singularities is described below.

4.4.2 Phase space slicing

The general ideas are the same as in the photonic case. The only difference is the form of the amplitude in the singular region. The formulae quoted in section 4.3.2 have to be modified in order to take into account color correlations after the emission of the soft gluon.

Concerning the process (4.62), in the soft region the differential cross section reads,

$$d\sigma^{2,1}_{1,2\to 3,4g} = -\frac{\alpha_s}{2\pi}\left\{\sum_{i<j;\ i,j=1}^{4} \mathcal{I}^{(1)}_{ij} d\sigma^{1,1}_{1,2\to 3,4;\ (i,j)} + \sum_{j=1}^{4} \mathcal{I}^{(2)}_{j} d\sigma^{1,1}_{1,2\to 3,4;\ (j,j)}\right\}, \tag{4.68}$$

where $\mathcal{I}^{(1)}_{ij}$ and $\mathcal{I}^{(2)}_{j}$ are defined in Eq. (4.52). In the collinear region, the differential cross section becomes

$$d\sigma^{2,1}_{1,2\to 3,4g} = \frac{\alpha_s}{2\pi}\sum_{i=1}^{2}\int_{z_0}^{1-\delta_s} dz\, P_{qq}(z)\left[\ln\left(\frac{s\delta_c^2}{4m_i^2}\right) - \frac{2z}{1+z^2}\right] d\sigma^{1,1}_{1,2\to 3,4;\ (i,i)}(zs_{12}).$$

The differential cross section is determined when the actual form of $d\sigma^{1,1}_{1,2\to 3,4;\ (i,j)}$ is set. According to Eq. (4.61), this is achieved once

$$[i,j] \equiv < \mathcal{M}^{1,0}_{1,2\to 3,4} | \mathbf{t}_i \mathbf{t}_j | \mathcal{M}^{0,1}_{1,2\to 3,4} >, \text{ with } i \neq j, \tag{4.69}$$

has been computed. According to Ref. [186], these scalar products can be written in terms of $[1,2]$ and $[1,3]$ as follows,

$$\begin{aligned}
[3,4] &= \frac{1}{2}(C_1 + C_2 - C_3 - C_4) < \mathcal{M}^{1,0}_{1,2\to 3,4} | \mathcal{M}^{0,1}_{1,2\to 3,4} > + [1,2], \\
[2,4] &= \frac{1}{2}(C_1 + C_3 - C_2 - C_4) < \mathcal{M}^{1,0}_{1,2\to 3,4} | \mathcal{M}^{0,1}_{1,2\to 3,4} > + [1,3], \\
[2,3] &= \frac{1}{2}(C_4 - C_1 - C_2 - C_3) < \mathcal{M}^{1,0}_{1,2\to 3,4} | \mathcal{M}^{0,1}_{1,2\to 3,4} > - [1,2] - [1,3], \\
[1,4] &= -C_1 < \mathcal{M}^{1,0}_{1,3\to 3,4} | \mathcal{M}^{0,1}_{1,2\to 3,4} > - [1,2] - [1,3].
\end{aligned}$$

The matrix elements of the operators $\mathbf{t}_1\mathbf{t}_2$ and $\mathbf{t}_1\mathbf{t}_3$ read

$$\begin{aligned}
[1,2] &= \left[(\mathcal{M}^{1,0}_{1,2\to 3,4})^{b_1,b_2,a_3,a_4}\right]^* t^c_{b_1a_1} t^c_{b_2a_2} (\mathcal{M}^{0,1}_{1,2\to 3,4})^{a_1,a_2,a_3,a_4}, \\
[1,3] &= \left[(\mathcal{M}^{1,0}_{1,2\to 3,4})^{b_1,a_2,b_3,a_4}\right]^* t^c_{b_1a_1} t^c_{b_3a_3} (\mathcal{M}^{0,1}_{1,2\to 3,4})^{a_1,a_2,a_3,a_4}.
\end{aligned}$$

In the case of the real (anti-)quark emission processes, the differential cross sections in the collinear region are

$$\begin{aligned} d\sigma^{2,1}_{g,2\to 3,4,\bar{1}} &= \frac{\alpha_s}{2\pi} T_R \int_{z_0}^1 dz \left[P_{gq}(z) \ln\left(\frac{\delta_c^2 s_{g2}}{4m_1^2}(1-z)^2 \right) + 2z(1-z) \right] \\ & \quad d\sigma^{1,1}_{1,2\to 3,4}(z s_{g2})(\delta_{1q} + \delta_{1\bar{q}}), \\ d\sigma^{2,1}_{1,g\to 3,4,\bar{2}} &= \frac{\alpha_s}{2\pi} T_R \int_{z_0}^1 dz \left[P_{gq}(z) \ln\left(\frac{\delta_c^2 s_{1g}}{4m_2^2}(1-z)^2 \right) + 2z(1-z) \right] \\ & \quad d\sigma^{1,1}_{1,2\to 3,4}(z s_{1g})(\delta_{2q} + \delta_{2\bar{q}}), \end{aligned}$$

where the notation in Eq. (4.65) has been used.

4.4.3 Dipole subtraction formalism

When using the dipole subtraction method within mass regularization, the formulae of Ref. [188, 189] have to be modified as well. Such modifications have been performed following the guidelines of Ref. [186].

In the case of real gluon emission processes of the type (4.62), the form of the subtraction function is

$$|\mathcal{M}^{\rm sub}_{1,2\to 3,4,g}|^2 = -\frac{\alpha_s}{2\pi} \left\{ \sum_{i\neq j;\ i,j=1}^{4} g^g_{ij}\ \mathcal{F}_{ij}(\tilde{\Phi}^g_{ij}) \right\}, \tag{4.70}$$

where $\mathcal{F}_{ij}$ is defined as

$$\mathcal{F}_{ij} = 2\mathfrak{Re}\{ < \mathcal{M}^{1,0}_{1,2\to 3,4} | \mathbf{t}_i \mathbf{t}_j | \mathcal{M}^{0,1}_{1,2\to 3,4} > \}. \tag{4.71}$$

The actual form of g^g_{ij} and $\tilde{\Phi}^g_{ij}$ is given in appendix E. The integral of the subtracted function over the whole gluonic phase space is available in appendix E as well.

The collinear singularities of the real (anti-)quark emission processes (4.65) are matched by

$$\begin{aligned} |\mathcal{M}^{\rm sub}_{g,2\to 3,4,1}| &= -\frac{\alpha_s}{2\pi} T_R h_{g2}\ \mathcal{F}(\tilde{\Phi}^g_{g2}), \\ |\mathcal{M}^{\rm sub}_{1,g\to 3,4,2}| &= -\frac{\alpha_s}{2\pi} T_R h_{1g}\ \mathcal{F}(\tilde{\Phi}^g_{1g}), \end{aligned} \tag{4.72}$$

with

$$\mathcal{F} = 2\mathfrak{Re}\{ < \mathcal{M}^{1,0}_{1,2\to 3,4} | \mathcal{M}^{0,1}_{1,2\to 3,4} > \}. \tag{4.73}$$

Again, h_{g2}, h_{1g}, $\tilde{\Phi}^g_{g2}$, $\tilde{\Phi^g_{1g}}$, and the integration of the subtraction functions are collected in appendix E.

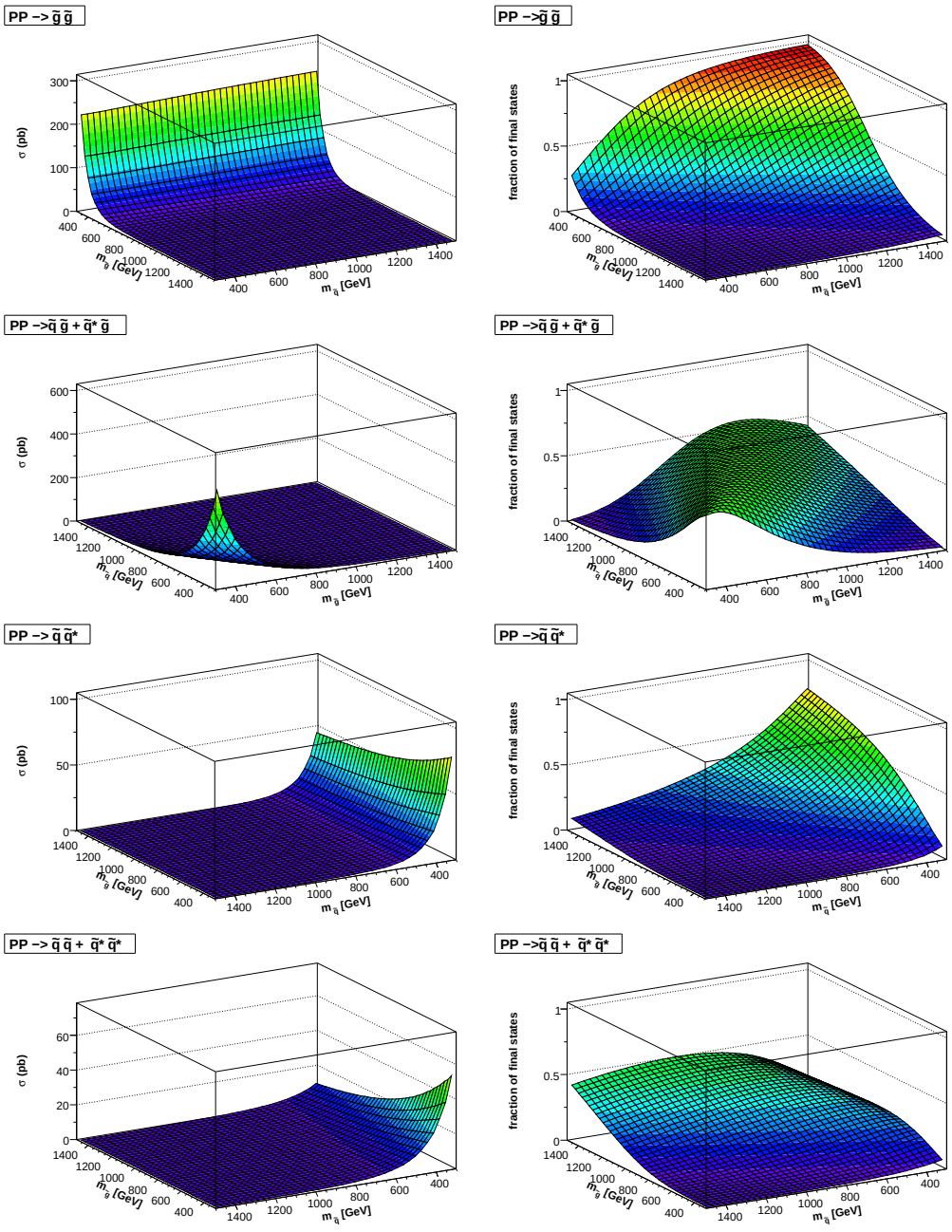

Figure 4.1: Total cross section and relative weights of $\tilde{g}\tilde{g}$, $\tilde{q}\tilde{g} + \tilde{q}^*\tilde{g}$, $\tilde{q}\tilde{q}^*$, and $\tilde{q}\tilde{q} + \tilde{q}^*\tilde{q}^*$ final states in the $(m_{\tilde{g}}, m_{\tilde{q}})$ plane. The notation used in denoting the final states is described in the text. $m_{\tilde{q}}$ is the mass of the squarks belonging to the first two generations, which are assumed to be degenerate. The PDF set used is the CTEQ6L one [119]. The factorization scale has been chosen as the average of the masses in the final states.

Chapter 5

Gluino pair production

In this chapter we consider the $\mathcal{O}(\alpha_s^2\alpha)$ contributions to the process of hadronic production of a pair of gluinos,

$$P\ P \to \tilde{g}\ \tilde{g}\ X. \tag{5.1}$$

At the LHC, this is one of the most important processes leading to the production of colored SUSY particles. Indeed, its cross section is big, $\mathcal{O}(10$ pb) for gluino masses of $\mathcal{O}(600$ GeV). Moreover, the gluino plays a key role in characterizing SUSY models. Indeed the measure of the spin of a (supposed to be) gluino [191] and the confirmation of its Majorana nature [115, 192, 193] allows not only to distinguish among different classes of BSM scenarios, but also among MSSM and other SUSY models involving Dirac gauginos, such as $N = 1/N = 2$ hybrid scheme [194].

The plan of the chapter is the following. In section 5.1 we briefly summarize the $\mathcal{O}(\alpha_s^2)$ contributions to the process we are interested in. In section 5.2 we describe the partonic processes that contributes at $\mathcal{O}(\alpha_s^2\alpha)$. Numerical results for the electroweak corrections to gluino pair production at LHC are presented in section 5.3, while section 5.4 is devoted to a brief discussion about the numerical value of the electroweak corrections at the Tevatron. Section 5.5 summarizes our results.

5.1 Gluino pair production in lowest order

The leading order contributions to the process (5.1) are of QCD origin and of $\mathcal{O}(\alpha_s^2)$. At lowest order in the perturbative expansion the differential cross

section reads:

$$\begin{aligned} d\sigma^{\rm LO}_{PP\to\tilde g\tilde g}(S) &= \int_0^1 dx_1 \int_0^1 dx_2 \delta(\tau - x_1x_2)\Big[f_{g|P_1}(x_1) f_{g|P_2}(x_2) d\sigma^{2,0}_{gg\to\tilde g\tilde g}(\tau S) \\ &+ \sum_q \Big(f_{q|P_1}(x_1) f_{\bar q|P_2}(x_2) d\sigma^{2,0}_{q\bar q\to\tilde g\tilde g}(\tau S) \\ &\qquad + f_{\bar q|P_1}(x_1) f_{q|P_2}(x_2) d\sigma^{2,0}_{\bar q q\to\tilde g\tilde g}(\tau S) \Big) \Big]. \end{aligned} \tag{5.2}$$

The sum runs over the quarks $q = u,\ d,\ c,\ s,\ b$. Equivalently, the differential cross section can be written as follows,

$$d\sigma^{\rm LO}_{PP\to\tilde g\tilde g}(S) = \sum_q \int_{\tau_0}^1 d\tau \frac{dL_{q\overline q}}{d\tau}(\tau) d\sigma^{2,0}_{q\overline q\to\tilde g\tilde g}(\tau S) + \int_{\tau_0}^1 d\tau \frac{dL_{gg}}{d\tau}(\tau) d\sigma^{2,0}_{gg\to\tilde g\tilde g}(\tau S), \tag{5.3}$$

with the help of the parton luminosities, defined according to

$$\frac{dL_{ij}}{d\tau}(\tau) = \frac{1}{1+\delta_{ij}} \int_\tau^1 \frac{dx}{x} f_{i|P_1}(x) f_{j|P_2}\left(\frac{\tau}{x}\right) + f_{j|P_1}(x) f_{i|P_2}\left(\frac{\tau}{x}\right). \tag{5.4}$$

The lower limit on the integral over τ, τ_0, is related to the threshold for the production of the gluino pair and reads

$$\tau_0 = \frac{4m^2_{\tilde g}}{S}.$$

$d\sigma^{2,0}_{q\bar q\to\tilde g\tilde g}$ and $d\sigma^{2,0}_{gg\to\tilde g\tilde g}$ are the lowest order differential cross sections for the parton processes

$$q(p_1)\ \overline q(p_2) \ \to\ \tilde g(k_1)\ \tilde g(k_2), \tag{5.5}$$
$$g(p_1)\ g(p_2) \ \to\ \tilde g(k_1)\ \tilde g(k_2), \tag{5.6}$$

respectively. These cross sections are summed over the spins and the colors of the external particles.

In lowest order, the partonic cross sections for the processes (5.5) and (5.6) can be obtained from the Feynman diagrams in Fig. F.1 of appendix F. These cross sections can be expressed in terms of the squared amplitudes,

$$\begin{aligned} d\sigma^{2,0}_{q\bar q\to\tilde g\tilde g} &= \frac{1}{72}\frac{dt}{16\pi s^2} \sum \left|\mathcal{M}^{1,0}_{q\bar q\to\tilde g\tilde g}\right|^2, \\ d\sigma^{2,0}_{gg\to\tilde g\tilde g} &= \frac{1}{512}\frac{dt}{16\pi s^2} \sum \left|\mathcal{M}^{1,0}_{gg\to\tilde g\tilde g}\right|^2, \end{aligned} \tag{5.7}$$

and the squared amplitudes summed over the spins and the colors of the external particles read [10–15]

$$\begin{aligned}
\sum \left|\mathcal{M}^{1,0}_{q\bar{q}\to\tilde{g}\tilde{g}}\right|^2 &= \frac{64}{3}\alpha_s^2\pi^2\Bigg\{\frac{72}{s^2}\left(2m_{\tilde{g}}^2 s + t_{\tilde{g}}^2 + u_{\tilde{g}}^2\right) \\
&+ \frac{36(m_{\tilde{g}}^2 s + t_{\tilde{g}}^2)}{s}\left(\frac{1}{t_{\tilde{q},1}} + \frac{1}{t_{\tilde{q},2}}\right) + 16t_{\tilde{g}}^2\left(\frac{1}{t_{\tilde{q},1}^2} + \frac{1}{t_{\tilde{q},2}^2}\right) \\
&+ \frac{36(m_{\tilde{g}}^2 s + u_{\tilde{g}}^2)}{s}\left(\frac{1}{u_{\tilde{q},1}} + \frac{1}{u_{\tilde{q},2}}\right) + 16u_{\tilde{g}}^2\left(\frac{1}{u_{\tilde{q},1}^2} + \frac{1}{u_{\tilde{q},2}^2}\right) \\
&+ 4m_{\tilde{g}}^2 s\left(\frac{1}{u_{\tilde{q},1}t_{\tilde{q},1}} + \frac{1}{u_{\tilde{q},2}t_{\tilde{q},2}}\right)\Bigg\}, \qquad (5.8)
\end{aligned}$$

$$\sum \left|\mathcal{M}^{1,0}_{gg\to\tilde{g}\tilde{g}}\right|^2 = 9216\,\alpha_s^2\,\pi^2\Bigg\{\left(1 - \frac{t_{\tilde{g}}u_{\tilde{g}}}{s^2}\right)\left[\frac{s^2}{t_{\tilde{g}}u_{\tilde{g}}} - 2 + 4\frac{m_{\tilde{g}}^2 s}{t_{\tilde{g}}u_{\tilde{g}}}\left(1 - \frac{m_{\tilde{g}}^2 s}{t_{\tilde{g}}u_{\tilde{g}}}\right)\right]\Bigg\}.$$

The Mandelstam variables are defined as

$$\begin{aligned}
s &= (p_1 + p_2)^2, \qquad (5.9)\\
t &= (p_2 - k_2)^2, \quad t_{\tilde{q},a} = t - m_{\tilde{q},a}^2, \quad t_{\tilde{g}} = t - m_{\tilde{g}}^2,\\
u &= (p_1 - k_2)^2, \quad u_{\tilde{q},a} = u - m_{\tilde{q},a}^2, \quad u_{\tilde{g}} = u - m_{\tilde{g}}^2,
\end{aligned}$$

and $u = 2m_{\tilde{g}}^2 - s - t$.

5.2 $\mathcal{O}(\alpha_s^2\alpha)$ corrections to the hadronic process

In this section we compute the $\mathcal{O}(\alpha_s^2\alpha)$ corrections to the process (5.1). The hadronic differential cross section reads, *c.f.* section 4.1.2,

$$\begin{aligned}
d\sigma^{\text{EW NLO}}_{PP\to\tilde{g}\tilde{g}X}(S) &= \sum_q \Bigg\{\int_{\tau_0}^1 d\tau\Bigg[\frac{dL_{q\bar{q}}}{d\tau}(\tau)\left(d\sigma^{2,1}_{q\bar{q}\to\tilde{g}\tilde{g}}(\tau S) + d\sigma^{2,1}_{q\bar{q}\to\tilde{g}\tilde{g}\gamma}(\tau S)\right) \\
&+ \frac{dL_{q\gamma}}{d\tau}(\tau)d\sigma^{2,1}_{q\gamma\to\tilde{g}\tilde{g}q}(\tau S) + \frac{dL_{\gamma\bar{q}}}{d\tau}(\tau)d\sigma^{2,1}_{\gamma\bar{q}\to\tilde{g}\tilde{g}\bar{q}}(\tau S)\Bigg]\Bigg\}. \qquad (5.10)
\end{aligned}$$

The $q\gamma$ and $\gamma\bar{q}$ luminosities entering (5.10) are built according to Eq. (5.4). Diagrams and amplitudes are generated with `FeynArts` [195, 196]. The reduction of the one-loop integrals is performed with the help of `FormCalc` [177, 178], while the scalar one-loop integrals are numerically evaluated using `LoopTools`. Infrared and Collinear singularities are treated using mass regularization, *i.e.* giving a small mass to the photon and to the five light quarks.

5.2.1 $q\bar{q}$ annihilation with electroweak loops

The first class of corrections entering Eq. (5.10) are the electroweak loop corrections to the unpolarized cross section of the processes (5.5),

$$d\sigma^{2,1}_{q\overline{q}\to\tilde{g}\tilde{g}} = \frac{1}{72}\frac{dt}{16\pi s^2}\sum 2\mathfrak{Re}\{\mathcal{M}^{1,0*}_{q\overline{q}\to\tilde{g}\tilde{g}}\mathcal{M}^{1,1}_{q\overline{q}\to\tilde{g}\tilde{g}}\}. \tag{5.11}$$

$\mathcal{M}^{1,0}_{q\overline{q}\to\tilde{g}\tilde{g}}$ is the tree-level contribution to the amplitude of the quark–anti-quark annihilation process while $\mathcal{M}^{1,1}_{q\overline{q}\to\tilde{g}\tilde{g}}$ is the one-loop electroweak contribution to the same amplitude. The diagrams responsible for the latter contribution are displayed in Fig. F.4 of appendix F. We treat UV divergences using dimensional reduction. In order to cure the UV divergences we have to renormalize the quark and the squark sector. The renormalization is performed according to the procedure described in chapter 4.

In the case of $b\bar{b}\to\tilde{g}\tilde{g}$ we keep the mass of the bottom that appears in the couplings, owing to the possible enhancement related to t_β. Therefore, in this case the last nine diagrams in Fig. F.4 of the appendix F have to be considered as well. It is well known [197–202] that, in the large t_β regime, the tree-level relation between the bottom mass m_b and the bottom Yukawa couplings y_{d_3} receives radiative corrections that can be strongly enhanced and have to be resummed. Power counting in $\alpha_s t_\beta$ shows that the leading t_β enhanced contributions, of $\mathcal{O}(\alpha_s^n t_\beta^n)$, can be accounted for by means of the substitution

$$m_b^{\mathrm{Rs}} \to \overline{m}_b^{\mathrm{Rs}} = \frac{m_b^{\mathrm{Rs}}}{1+\Delta_b} \tag{5.12}$$

in the relation between m_b and y_{d_3}. m_b^{Rs} is the bottom mass in a given renormalization scheme, Rs. Δ_b is defined as

$$\Delta_b = \frac{2\alpha_s}{3\pi} m_{\tilde{g}}\mu t_\beta G(m^2_{\tilde{b},1}, m^2_{\tilde{b},2}, m^2_{\tilde{g}}),$$
$$G(a,b,c) = \frac{1}{(a-b)(b-c)(a-c)}\left[ab\ln\left(\frac{a}{b}\right) + bc\ln\left(\frac{b}{c}\right) + ca\ln\left(\frac{c}{a}\right)\right].$$

Concerning the Higgs sector, the $b-\bar{b}-h_u^0$ coupling is dynamically generated at $\mathcal{O}(\alpha_s)$. Such coupling can be enhanced if t_β is large and it is worth to include such effects modifying the $b-\bar{b}-$Higgs Yukawa couplings. In particular, the effective Lagrangian that correctly takes into account these dynamically

generated extra-couplings is

$$\mathcal{L}^{\text{eff.}}_{\text{Higgs}} = \frac{\overline{m}_b^{\text{Rs}}}{v}\left[t_\beta\left(1-\frac{\Delta_b}{t_\beta^2}\right)A^0\bar{b}i\gamma^5 b + \frac{s_\alpha}{c_\beta}\left(1-\frac{\Delta_b}{t_\alpha t_\beta}\right)h^0\bar{b}b \right. \\ \left. -\frac{c_\alpha}{c_\beta}\left(1+\frac{\Delta_b t_\alpha}{t_\beta}\right)H^0\bar{b}b\right]. \tag{5.13}$$

5.2.2 $q\bar{q}$ annihilation with real photon emission

Another contribution of order $\mathcal{O}(\alpha_s^2\alpha)$ is the tree-level contribution of the partonic process of photon radiation,

$$q(p_1),\ \overline{q}(p_2) \rightarrow\ \tilde{g}(k_1)\ \tilde{g}(k_2)\ \gamma(k_3), \tag{5.14}$$

which can be computed using the Feynman diagrams depicted in Fig. F.2 of appendix F. The IR and collinear divergences appearing in the phase space integration are regularized using both the phase space slicing method and the dipole subtraction method, described in chapter 4. The comparison between the two methods for the partonic process $u\overline{u} \rightarrow \tilde{g}\tilde{g}\gamma$ is depicted in Fig. 5.1, as an example.

5.2.3 $q\gamma$ and $\gamma\bar{q}$ fusion

The last class of $\mathcal{O}(\alpha_s^2\alpha)$ contributions to the process (5.1) are the tree-level contributions of the partonic processes

$$q(\ p_1)\ \gamma(p_2) \ \rightarrow\ \tilde{g}(k_1)\ \tilde{g}(k_2)\ q(k_3), \tag{5.15}$$
$$\gamma(\ p_1)\ \overline{q}(p_2) \ \rightarrow\ \tilde{g}(k_1)\ \tilde{g}(k_2)\ \overline{q}(k_3). \tag{5.16}$$

These contributions can be computed from the Feynman diagrams depicted in Fig. F.3 of appendix F.

Note that, if $m_{\tilde{q}} > m_{\tilde{g}}$, the quark in the final state can be the decay product of an on-shell squark. If this is the case the last four diagrams depicted in Fig. F.3 become singular. The related poles have to be regularized inserting the width of the on-shell squarks into the corresponding propagator. Furthermore, the contribution obtained squaring the resonant diagrams has to be subtracted since it arises from the productions and the subsequent decay of an (anti-)squark through (anti-)quark–photon fusion,

$$q\ \gamma\ \rightarrow\ \tilde{g}\tilde{q} \qquad \text{and} \qquad \tilde{q}\ \rightarrow\ \tilde{g}\ q, \\ \gamma\ \bar{q}\ \rightarrow\ \tilde{g}\tilde{q}^* \qquad \text{and} \qquad \tilde{q}^*\ \rightarrow\ \tilde{g}\ \bar{q}. \tag{5.17}$$

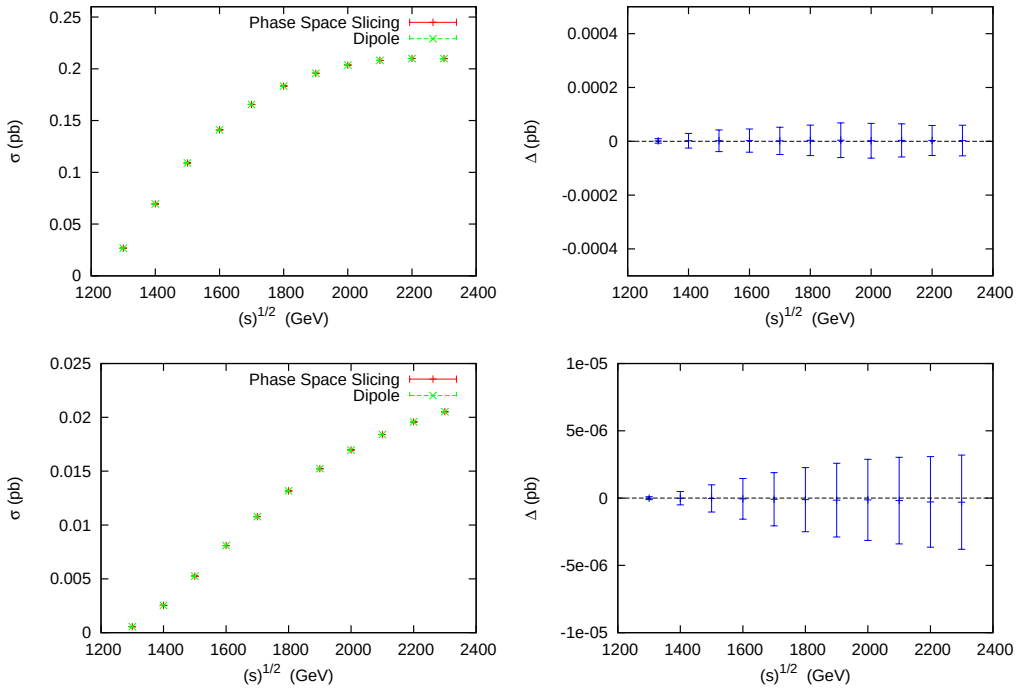

Figure 5.1: Lowest order partonic cross sections for the process $u\overline{u} \to \tilde{g}\tilde{g}\gamma$ (upper panels) and $u\gamma \to \tilde{g}\tilde{g}u$ (lower panels) computed with the two different methods. $\Delta = \sigma^{\text{Slicing}} - \sigma^{\text{Dipole}}$. The error bars represent the uncertainty sum under quadrature between the numerical uncertainties on σ^{Slicing} and σ^{Dipole}. The SUSY parameters are those of the SPS1a′ point [203].

According to Ref. [15], the extraction of the Breit-Wigner pole contribution has been performed in the narrow width approximation.

Collinear singularities arising from initial state emission are regularized using both the phase space slicing method and the dipole subtraction method described in section 4.3. As shown in Fig. 5.1, the two methods are in good numerical agreement.

The contribution of this channel is expected to be small owing to the suppression of the photon PDF inside the proton. Indeed, the photon PDF is intrinsically suppressed with respect to the valence quark PDF by a factor α, since this PDF is originated from the emission of a photon from a (anti-)quark. Therefore the actual order of the real (anti-)quark emission processes is $\mathcal{O}(\alpha_s^2\alpha^2)$. In the SUSY scenarios we consider the contribution of this partonic process amounts up to few percent of the whole $\mathcal{O}(\alpha_s^2\alpha)$ correction.

5.2.4 Factorization of initial collinear singularities

The term $\mathcal{R}(x_1, x_2, s)$ entering Eq. (4.8) is, in the case of gluino pair production, related to the $\mathcal{O}(\alpha)$ factorization of the (anti-)quark PDF. The integral of $\mathcal{R}(x_1, x_2, s)$ over x_1 and x_2 can be written as

$$\int_0^1 dx_1 \int_0^1 dx_2 \; \delta(\tau - x_1 x_2) \; \mathcal{R}(x_1, x_2, s) = \int_{\tau_0}^1 d\tau \; \overline{\mathcal{R}}(\tau, s), \tag{5.18}$$

and has to be added to Eq. (5.10). $\overline{\mathcal{R}}$ can be expressed in terms of the parton luminosities as follows,

$$\begin{aligned} \overline{\mathcal{R}}(\tau, s) &= \sum_q \Bigg\{ \Bigg[-\frac{\alpha}{\pi} e_q^2 \frac{dL_{q\overline{q}}}{d\tau}(\tau) \int_{z_0}^1 dz \left[\mathcal{H}_q^{(1)} + h^{(1)} \right]_+ d\sigma^{2,0}_{q\overline{q}\to\tilde{g}\tilde{g}}(zs) \\ &- \frac{3\alpha}{2\pi} e_q^2 \left(\frac{dL_{q\gamma}}{d\tau}(\tau) + \frac{dL_{\gamma\overline{q}}}{d\tau}(\tau) \right) \int_{z_0}^1 dz \; (\mathcal{H}_q^{(2)} + h^{(2)}) d\sigma^{2,0}_{q\overline{q}\to\tilde{g}\tilde{g}}(zs) \Bigg] \Bigg\}. \end{aligned}$$

The functions $\mathcal{H}$ and h are defined in Eq. (4.13). z_0 is defined as $z_0 = 4m_{\tilde{g}}/s$. We factorize the (anti-)quark PDFs at $\mathcal{O}(\alpha)$ in the DIS scheme. In the actual computation, we use the MRST2004qed parton distribution function at NLO QED and NLO QCD [204]. This fit takes into account the QED-effect into the DGLAP evolution equations and the parametrization of the PDF at the initial scale. The treatment of the heavy quarks is within the variable flavor number scheme (VFNS). The corresponding matching is performed according to the Roberts-Thorne procedure [205–207]. MRST2004qed PDFs are defined at NLO QCD within the $\overline{\text{MS}}$ mass factorization scheme. As discussed in Ref. [190], the DIS scheme is used for the factorization of the $\mathcal{O}(\alpha)$ corrections.

In our computation we set the renormalization scale, μ_R, equal to the factorization scale, μ_F, and to the gluino mass, *i.e.* $\mu_R = \mu_F = m_{\tilde{g}}$.

5.3 Numerical results, LHC

For our numerical discussion we use the set of Standard Model parameters quoted in Ref. [208]. The value of the bottom mass in the $\overline{\text{DR}}$ scheme is computed according to Ref. [167]. We choose two different SUSY scenarios. The first one, called SPS2, belongs to the set of Snowmass Points and Slopes,

introduced in Ref. [209]. The second scenario is the SPS1a′ suggested by the SUSY Parameters Analyses (SPA) [203] project for its studies. Both scenarios assume that SUSY breaking is realized within mSUGRA; therefore, they are uniquely defined once the value of m_0, $m_{1/2}$, A_0, and sign(μ) at the GUT scale are set, and t_β is specified. The parameter of the MSSM can be obtained from the renormalization group evolution from the GUT scale down to the desired low scale. Many publicly available codes tackle this task and compute the physical spectrum of the model [210–212]. We obtain the parameters of the two scenarios with the help of the program `SPheno` [210] and `SuSpect` [211] starting from the input parameters shown in Table 5.1.

parameter	SPS1a′	SPS2
$m_{1/2}$	250 GeV	300 GeV
m_0	70 GeV	1450 GeV
A_0	−300 GeV	0
sign(μ)	” + ”	” + ”
$t_\beta(M_Z)$	10.37	10

Table 5.1: MSSM input parameters for the computation of the spectrum of the two scenarios considered. $m_{1/2}$, m_0 and A_0 are defined at the GUT scale.

5.3.1 Dependence on the renormalization scheme

In the following we will study more systematically the reliability of the different schemes. Given a renormalization scheme Rs, its reliability is guaranteed once:

- the renormalization constants are much smaller than the value of the renormalized parameters. Typically this holds automatically in the case of the independent parameters while has to be checked in the case of dependent parameters.

- the value of the dependent parameters is stable, *i.e.* , given a dependent parameter $d = f(p_i)$ as a function of a set of independent parameter p_i, this relation has to hold up to term $\mathcal{O}(\alpha_s^2)$:

$$d^{\rm Rs} - d^{\overline{\rm DR}} = -\delta_F d^{\rm Rs} = -\sum_i \frac{\partial f}{\partial p_i}\Big|_{\,p_i^{\rm Rs}} \delta_F p_i^{\rm Rs}. \tag{5.19}$$

parameter	SPS1a′	SPS2
$m^{2\ \mathrm{Rs1}}_{\tilde{b},1}$	$243 \cdot 10^3 \mathrm{GeV}^2$	$167 \cdot 10^4\ \mathrm{GeV}^2$
$m^{2\ \mathrm{Rs1}}_{\tilde{b},1} - m^{2\ \overline{\mathrm{DR}}}_{\tilde{b},1}$	$35 \cdot 10^3\ \mathrm{GeV}^2$	$25 \cdot 10^3\ \mathrm{GeV}^2$
$\delta_F m^{2\ \mathrm{Rs1}}_{\tilde{b},1}$	$-38 \cdot 10^3\ \mathrm{GeV}^2$	$-26 \cdot 10^3\ \mathrm{GeV}^2$
A_t^{Rs1}	-527 GeV	-521 GeV
$A_t^{\mathrm{Rs1}} - A_t^{\overline{\mathrm{DR}}}$	54 GeV	21 GeV
$\delta_F A_t^{\mathrm{Rs1}}$	-43 GeV	-13 GeV
A_b^{Rs1}	425 GeV	781 GeV
$A_b^{\mathrm{Rs1}} - A_b^{\overline{\mathrm{DR}}}$	1372 GeV	1588 GeV
$\delta_F A_b^{\mathrm{Rs1}}$	-692 GeV	-981 GeV

Table 5.2: Dependent parameters in the Rs1 scheme. For each parameter we show its Rs1 value, the difference between this value and the value the parameter has in the $\overline{\mathrm{DR}}$ scheme, and the finite part of the renormalization constant in the Rs1 scheme.

where the abbreviation $\delta_F p^{\mathrm{Rs}} \equiv \delta p^{\overline{\mathrm{DR}}} - \delta p^{\mathrm{Rs}}$ has been used. δp^{X} is the renormalization constant of p in the renormalization scheme X. Therefore, the difference between right- and left-hand side of Eq. (5.19) has to be much smaller than the two sides themselves.

Rs1 scheme

In this case, the dependent parameters are A_b, A_t and $m^2_{\tilde{b}_1}$. In Table 5.2, we collect the numerical value of these parameters in the Rs1 scheme, the difference between this value and the value the parameters assume in the $\overline{\mathrm{DR}}$ scheme, and the finite part of their renormalization constant. This scheme is not reliable since the renormalization constant of A_b is neither small ($\delta_F A_b/A_b \sim 1$) nor stable. Looking at the expression of $\delta_F A_b$ it is easy to understand the size of this quantity. Indeed,

$$\delta_F A_b = (A_b - \mu t_\beta)\left[\frac{(\delta_F m^{2\ \mathrm{Rs1}}_{\tilde{b},1} - \delta_F m^{2\ \mathrm{Rs1}}_{\tilde{b},2})}{m^{2\ \mathrm{Rs1}}_{\tilde{b},1} - m^{2\ \mathrm{Rs1}}_{\tilde{b},2}} - \frac{\delta_F m_b^{\mathrm{Rs1}}}{m_b^{\mathrm{Rs1}}} + 2\cot\theta^{\mathrm{Rs1}}_{\tilde{b}}\delta_F\theta^{\mathrm{Rs1}}_{\tilde{b}}\right], \tag{5.20}$$

therefore, even if the terms inside the square brackets are typically below unity, the prefactor $(A_b - \mu t_\beta)$ can become bigger than A_b itself[1] enhancing

[1] In the SPS1a′ case, for instance, $A_b \simeq 500$ GeV while $(A_b - \mu t_\beta) \simeq 3500$ GeV.

parameter	SPS1a′	SPS2
$m^{2\ \mathrm{Rs2}}_{\tilde{b},1}$	$245 \cdot 10^3$ GeV^2	$167 \cdot 10^4$ GeV^2
$m^{2\ \mathrm{Rs2}}_{\tilde{b},1} - m^{2\ \overline{\mathrm{DR}}}_{\tilde{b},1}$	$26 \cdot 10^3$ GeV^2	$24 \cdot 10^3$ GeV^2
$\delta_F m^{2\ \mathrm{Rs2}}_{\tilde{b},1}$	$-28 \cdot 10^3$ GeV^2	$-25 \cdot 10^3$ GeV^2
A_t^{Rs2}	-527 GeV	-522 GeV
$A_t^{\mathrm{Rs2}} - A_t^{\overline{\mathrm{DR}}}$	54 GeV	21 GeV
$\delta_F A_t^{\mathrm{Rs2}}$	-43 GeV	-13 GeV
$\sin\theta_{\tilde{b}}^{\mathrm{Rs2}}$	0.35	$18.25 \cdot 10^{-3}$
$\sin\theta_{\tilde{b}}^{\mathrm{Rs2}} - \sin\theta_{\tilde{b}}^{\overline{\mathrm{DR}}}$	-0.10	$-0.54 \cdot 10^{-3}$
$\delta_F \sin\theta_{\tilde{b}}^{\mathrm{Rs2}}$	0.09	$0.56 \cdot 10^{-3}$

Table 5.3: Same as Table 5.2, but considering the Rs2 scheme

$\delta_F A_b$. The origin of the numerical instability can be understood from the analytic structure of the sum $A_b^{\mathrm{Rs1}} + \delta_F A_b^{\mathrm{Rs1}} - A_b^{\overline{\mathrm{DR}}}$,

$$\begin{aligned} A_b^{\mathrm{Rs1}} + \delta_F A_b^{\mathrm{Rs1}} - A_b^{\overline{\mathrm{DR}}} &= \frac{\sin\theta_{\tilde{b}}^{\overline{\mathrm{DR}}}}{m_b^{\overline{\mathrm{DR}}}} \left[2m_{\tilde{b},1}^{\overline{\mathrm{DR}}} \left(\sqrt{m^{2\ \mathrm{Rs1}}_{\tilde{b},1} + \delta_F m^{2\ \mathrm{Rs1}}_{\tilde{b},1}} - m_{\tilde{b},1}^{\overline{\mathrm{DR}}} \right) \right. \\ &- \left. 2m_{\tilde{b},2}^{\overline{\mathrm{DR}}} \left(\sqrt{m^{2\ \mathrm{Rs1}}_{\tilde{b},2} + \delta_F m^{2\ \mathrm{Rs1}}_{\tilde{b},2}} - m_{\tilde{b},2}^{\overline{\mathrm{DR}}} \right) \right] + \mathcal{E}. \end{aligned} \tag{5.21}$$

$\mathcal{E}$ is a term of $\mathcal{O}(\alpha_s^2)$ and is given by

$$\mathcal{E} = \left(\sin 2\theta_b \, \frac{\delta_F m_b^{\mathrm{Rs1}}}{2m_b} - \cos 2\theta_b \; \delta_F \theta_b^{\mathrm{Rs1}} \right) \left[\frac{\delta_F m^{2\ \mathrm{Rs1}}_{\tilde{b},1} - \delta_F m^{2\ \mathrm{Rs1}}_{\tilde{b},2}}{m_b} \right].$$

The first term of Eq. (5.21) is proportional to the differences

$$\sqrt{m^{2\ \mathrm{Rs1}}_{\tilde{b},1} + \delta_F m^{2\ \mathrm{Rs1}}_{\tilde{b},1}} - m_{\tilde{b},1}^{\overline{\mathrm{DR}}}, \quad \sqrt{m^{2\ \mathrm{Rs1}}_{\tilde{b},2} + \delta_F m^{2\ \mathrm{Rs1}}_{\tilde{b},2}} - m_{\tilde{b},2}^{\overline{\mathrm{DR}}}. \tag{5.22}$$

These differences are $\mathcal{O}(\alpha_s^2)$ but they are enhanced by the prefactor $2\ m_{\tilde{b},i}/m_b$. $\mathcal{E}$ is non-negligible as well owing to the enhancement of the term in square brackets.

parameter	SPS1a′	SPS2
$m^{2\ \mathrm{Rs3}}_{\tilde{b},1}$	$243 \cdot 10^3$ GeV^2	$168 \cdot 10^4$ GeV^2
$m^{2\ \mathrm{Rs3}}_{\tilde{b},1} - m^{2\ \overline{\mathrm{DR}}}_{\tilde{b},1}$	$24 \cdot 10^3$ GeV^2	$26 \cdot 10^3$ GeV^2
$\delta_F m^{2\ \mathrm{Rs3}}_{\tilde{b},1}$	$-26 \cdot 10^3$ GeV^2	$-28 \cdot 10^3$ GeV^2
A_t^{Rs3}	-534 GeV	-477 GeV
$A_t^{\mathrm{Rs3}} - A_t^{\overline{\mathrm{DR}}}$	47 GeV	66 GeV
$\delta_F A_t^{\mathrm{Rs3}}$	-38 GeV	-58 GeV
$\sin\theta_{\tilde{b}}^{\mathrm{Rs3}}$	0.32	$18.30 \cdot 10^{-3}$
$\sin\theta_{\tilde{b}}^{\mathrm{Rs3}} - \sin\theta_{\tilde{b}}^{\overline{\mathrm{DR}}}$	-0.12	$-0.49 \cdot 10^{-3}$
$\delta_F \sin\theta_{\tilde{b}}^{\mathrm{Rs3}}$	0.10	$0.50 \cdot 10^{-3}$

Table 5.4: Same as Table 5.2, but considering the Rs3 scheme

Rs2 and Rs3 scheme
In order to guarantee the reliability of these two schemes we have to check $\theta_{\tilde{b}}$, A_t and $m^2_{\tilde{b}_1}$. As can be inferred from Table 5.3 and Table 5.4, the schemes Rs2 and Rs3 are reliable.

Rs4 scheme
In this case the dependent parameters are A_b, A_t and $m^2_{\tilde{b}_1}$. As one can see from Table 5.5, this scheme is not reliable. This is due to the renormalization of A_b. Indeed $\delta_F A_b^{\mathrm{Rs4}}$ can be obtained from Eq. (5.20) setting Rs1 $\to$ Rs4 and, as in the Rs1 case, $\delta_F A_b^{\mathrm{Rs1}}$ can be enhanced. The origin of the numerical instability can be understood looking at $A_b^{\mathrm{Rs4}} - A_b^{\overline{\mathrm{DR}}} + \delta_F A_b^{\mathrm{Rs4}}$. Its analytical formula can be inferred from Eq. (5.21) setting Rs1 $\to$ Rs4 and $\mathcal{E} \to 0$. Therefore, the presence of the prefactors 2 $m_{\tilde{b},i}/m_b$ is the origin of the numerical instability.

Actual results
It is worth to analyse the numerical impact of the differences among the renormalization schemes. Therefore, we compute the $\mathcal{O}(\alpha_s^2)$ and $\mathcal{O}(\alpha_s^2\alpha)$ contributions to the total hadronic cross section related to the partonic process

$$b\,\bar{b} \;\to\; \tilde{g}\,\tilde{g}\,(\gamma). \tag{5.23}$$

The numerical results for the total hadronic cross section of the process (5.23) are displayed in Table 5.6. The number in parentheses is the uncertainty on the last digit. The main feature is that either at $\mathcal{O}(\alpha_s^2)$ and at $\mathcal{O}(\alpha_s^2\alpha)$

parameter	SPS1a′	SPS2
$m^{2\ \mathrm{Rs4}}_{\tilde{b},1}$	$237 \cdot 10^3$ GeV^2	$168 \cdot 10^4$ GeV^2
$m^{2\ \mathrm{Rs4}}_{\tilde{b},1} - m^{2\ \overline{\mathrm{DR}}}_{\tilde{b},1}$	$-18 \cdot 10^3$ GeV^2	$26 \cdot 10^3$ GeV^2
$\delta_F m^{2\ \mathrm{Rs4}}_{\tilde{b},1}$	$19 \cdot 10^3$ GeV^2	$-28 \cdot 10^3$ GeV^2
A_t^{Rs4}	-534 GeV	-477 GeV
$A_t^{\mathrm{Rs4}} - A_t^{\overline{\mathrm{DR}}}$	47 GeV	66 GeV
$\delta_F A_t^{\mathrm{Rs4}}$	-42 GeV	-58 GeV
A_b^{Rs4}	-3237 GeV	-921 GeV
$A_b^{\mathrm{Rs4}} - A_b^{\overline{\mathrm{DR}}}$	-2291 GeV	-114 GeV
$\delta_F A_b^{\mathrm{Rs4}}$	1794 GeV	119 GeV

Table 5.5: Same as Table 5.2, but considering the Rs4 scheme

the prediction can differ within 1%, even when we consider the non-reliable schemes (Rs1 and Rs4). The effect of the resummation in the relation between bottom mass and bottom Yukawa coupling is negligible as well, below 1% in the $\mathcal{O}(\alpha_s^2)$ and $\mathcal{O}(\alpha_s^2\alpha)$ contributions to the total cross section. This is expected since in the scenarios we are considering the value of t_β is moderate ($t_b \sim 10$). Therefore, in both scenarios, the difference between m_b and $\overline{m}_b$ is below 1% in every scheme considered.

5.3.2 Dependence on the SUSY scenario

We compute the total hadronic cross section using the Rs2 scheme, the results are collected in Table 5.7. The second column shows the lowest order results. The third column shows the sum of the lowest order and of the $\mathcal{O}(\alpha_s^2\alpha)$ contributions. In the fourth column the contribution of the $\mathcal{O}(\alpha_s^2\alpha)$ corrections relative to the total result is given, therefore δ is defined as

$$\delta \equiv \frac{\sigma^{\mathrm{NLO\ EW}}}{\sigma^{\mathrm{LO}} + \sigma^{\mathrm{NLO\ EW}}}.$$

In the last entry we give an estimate of the statistical error based on an integrated luminosity $L = 100$ fb^{-1} [213].
We do not distinguish the results in the different renormalization schemes since they agree within the integration error. This is expected since the main dependence on the renormalization schemes is in the $b\bar{b}$ annihilation channel. As shown in section 5.3.1, the difference among the renormalization schemes

point	scheme		$\mathcal{O}(\alpha_s^2)$ (fb)	$\mathcal{O}(\alpha_s^2+\alpha_s^2\alpha)$ (fb)
SPS1a′	Rs1		0.5543(2)	0.5434(2)
		(resum.)	0.5543(2)	0.5434(2)
	Rs2		0.5518(2)	0.5410(2)
		(resum.)	0.5507(2)	0.5400(2)
	Rs3		0.5559(2)	0.5357(2)
		(resum.)	0.5549(2)	0.5347(2)
	Rs4		0.5647(2)	0.5449(2)
		(resum.)	0.5647(2)	0.5408(2)
SPS2	Rs1		0.13709(5)	0.13234(5)
		(resum.)	0.13709(5)	0.13234(5)
	Rs2		0.13709(5)	0.13237(5)
		(resum.)	0.13709(5)	0.13237(5)
	Rs3		0.13717(5)	0.13246(5)
		(resum.)	0.13717(5)	0.13246(5)
	Rs4		0.13717(5)	0.13246(5)
		(resum.)	0.13717(5)	0.13246(5)

Table 5.6: Tree-level and NLO EW cross section of the process (5.23) in the four different renormalization schemes. We consider both the SPS1a′ and the SPS2 scenarios, and we show the results with and without resummation of the terms proportional to $\alpha_s^n t_\beta^n$ (*c.f.* section 5.2.1). The number in parentheses is the uncertainty on the last digit.

point	$\sigma^{\rm LO}$	$\sigma^{\rm LO}+\sigma^{\rm NLO\ EW}$	δ (%)	$\frac{1}{\sqrt{L\cdot\sigma^{\rm LO}}}$
SPS1a′	6.1865(6) pb	6.1822(6) pb	−0.07%	0.13%
SPS2	1.2127(1) pb	1.2089(1) pb	−0.31%	0.29%

Table 5.7: Total hadronic cross section. In the second (third) column we show the $\mathcal{O}(\alpha_s^2)$ ($\mathcal{O}(\alpha_s^2+\alpha_s^2\alpha)$) contribution for the points SPS1a′ and SPS2. In the fourth column the electroweak corrections in percent of the LO + NLO EW result are shown. The last column shows the statistical error for an integrated luminosity $L = 100$ fb^{-1}.

amounts up to few percents of the tree-level $b\bar{b}$ annihilation channel contributions. The latter contributions amount up to several fb, therefore the variation of the results in Table 5.7 is within the integration error.

As one can see, in the case of the point SPS1a′ the electroweak corrections

are much smaller than the statistical uncertainty and so they are not relevant. In the case of the point SPS2, the $\mathcal{O}(\alpha_s^2\alpha)$ corrections are of the same order of the statistical error but they are still much smaller than the theoretical systematic uncertainties such as the uncertainty on the PDF parametrization ($\sim 10\%$) [15] and the factorization scale dependence (from 3 to 5% if $m_{\tilde{g}} \leq$ 1 TeV) [22, 23].

The invariant mass distribution of the two gluinos is shown in Fig. 5.2. The EW corrections are small, their absolute value being at most of the order of 0.4% of the total contribution. Moreover, these corrections do not distort the shape of the distribution.

In Fig. 5.3 we consider the distribution of the largest transverse momentum of the two gluinos, for brevity we will refer to this observable as "transverse momentum distribution". The $\mathcal{O}(\alpha_s^2\alpha)$ corrections are rather small, the absolute value of their contribution relative to the total result is at most 1%, reaching this value in the high p_T region, *i.e.* $p_T \geq 1500$ GeV.

5.3.3 Dependence on the MSSM parameters

In this subsection we investigate the size of the $\mathcal{O}(\alpha_s^2\alpha)$ corrections to the process (5.1) in a more systematic way performing a scan over the parameter space of the MSSM. The parameters involved in the scan are the independent parameters in the second renormalization scheme. We suppose that all the sfermionic soft mass parameters are equal and we indicate its value in the third renormalization scheme as M_{Susy}. The physical masses of the sfermions can be obtained from M_{Susy} diagonalizing the mass matrices. Moreover, we consider the surfaces of the parameter space characterized by $A_t = A_\tau$. With these assumptions the parameters involved in the scan are eight, namely

$$M_{\text{Susy}}, \quad m_{\tilde{g}}, \quad \mu, \quad M_2, \quad A_t, \quad A_b, \quad t_\beta, \quad m_{A^0}.$$

The subregions of the parameter space involved in the scans are chosen imposing the exclusion limits arising from SUSY searches at LEP [53] and at the Tevatron [214], and the bound on the mass of the light Higgs. The physical mass of the light Higgs has been computed using `FeynHiggs 2.5.1` [56, 215, 216]. Moreover each point in the selected regions fulfills the condition $|\Delta\rho| \leq 0.025$, $\Delta\rho$ being the dominant SUSY corrections to the electroweak ρ parameter, corrections arising from top and bottom squarks contributions.

We perform four different scans. In each scan we select two parameters and we study the dependence of the quantity Δ,

$$\Delta \equiv \frac{\sigma^{\text{NLO EW}}}{\sigma^{\text{LO}} + \sigma^{\text{NLO EW}}} \cdot 100. \tag{5.24}$$

We repeat each of these scans for different values of another pair of parameters, while the remaining four are fixed to their SPS1a′ value. Here there is a brief discussion on the results of these scans.

1. **Scan over A_t and A_b.**
   The results of this scan are displayed in Fig. 5.4. As expected, Δ is quite independent on the parameter A_t which enters in the virtual correction of the process $b\overline{b} \to \tilde{g}\tilde{g}$ and in the definition of the mass of the top squarks. This feature is more evident for large t_β values. Δ varies only by an amount of the order of few percent for a variation of A_b and A_t over a quite broad range (from -1500 to 1500 GeV). Note that in the whole subregion considered the absolute value of Δ is of $\mathcal{O}(0.1)$.

2. **Scan over t_β and M_{A^0}.**
   As can be inferred from Fig. 5.5 the dependence of Δ on (t_β, m_{A^0}) strongly varies for different values of $m_{\tilde{g}}$ and M_{Susy}. As a general result the overall dependence is mild for each value of $(m_{\tilde{g}}, M_{\text{Susy}})$. In all cases the value of $|\Delta|$ is at most of the order of 0.7.

3. **Scan over μ and M_2.**
   As displayed in Fig. 5.6, Δ is almost independent on μ for each value of the pair $(m_{\tilde{g}}, M_{\text{Susy}})$ while the dependence on M_2 is more important and particularly pronounced when $m_{\tilde{g}} = 1250$ GeV and $M_{\text{Susy}} = 730$ GeV. In the case of the last three plots the value of Δ is of order -0.3 to -0.1, while in the first plot, characterized by $m_{\tilde{g}} \sim 2 \cdot M_{\text{Susy}}$, the value of Δ is enhanced for small values of M_2 reaching the value of -0.65.
   Notice that the mass of the lightest neutralino and chargino is almost independent on the value of μ but varies strongly as M_2 varies, growing as the value of this parameter grows. So this enhancement occurs when charginos/neutralinos are much lighter than the gluino.

4. **Scan over M_{Susy} and $m_{\tilde{g}}$.**
   In this scan we investigate the dependence of Δ on $m_{\tilde{g}}$ and M_{Susy}, which is expected to be the most important because of the dependence of the lowest order cross section on these parameters. We consider the variation of Δ as a function of $(m_{\tilde{g}}, M_{\text{Susy}})$ for different values of M_2 and t_β. In Fig. 5.7 we show some results of these scans. Note that we plot $\xi \equiv -\Delta$ instead of Δ. As a general feature ξ increases as $m_{\tilde{g}}$ increases and as M_{Susy} decreases. The behaviour of ξ as a function of M_{Susy} and $m_{\tilde{g}}$ is affected by the value of M_2 being enhanced for smaller values of this parameter. In particular $\xi \sim 3$ in the region $m_{\tilde{g}} \geq 1400$ GeV, $M_{\text{Susy}} \leq 500$ GeV.

Such enhancement is related to the increasing importance of the $q\bar{q}$ annihilation channel when the production threshold becomes higher. Indeed, the minimal value of the parton's momentum fraction rises as the gluino mass rises. Since the relative importance of the (anti-)quark PDF increases as the momentum fraction of the (anti-)quark increases, the EW corrections grow as the mass of the gluino grows.
Such enhancement is even more pronounced when $M_{\rm Susy}$ is small owing to the presence of tree-level diagrams with squarks exchanged in the t and u channel.

5.4 Numerical results, Tevatron

The analysis performed for the process (5.1) can be easily extended also for the Tevatron, *i.e.* for the process

$$P\ \overline{P} \to \tilde{g}\ \tilde{g}\ X. \tag{5.25}$$

Indeed, Eq. (5.3) and Eq. (5.10) remain valid: the only change to do is in the definition of the partonic luminosity. Instead of Eq. (5.4) in this case we have

$$\frac{dL_{i,j}}{d\tau}(\tau) = \frac{1}{1+\delta_{i,j}} \int_\tau^1 \frac{dx}{x} f_{i|P}(x) f_{j|\overline{P}}\left(\frac{\tau}{x}\right) + f_{j|P}(x) f_{i|\overline{P}}\left(\frac{\tau}{x}\right), \tag{5.26}$$

where $f_{i|H}(x)$ is the momentum distribution of the parton i into the hadron H.

For numerical evaluation, we focus on two different points of the MSSM parameter space, we will refer to these points as TP1 and TP2 respectively. These points belong to the region of the parameter space of the MSSM used in the data analysis made by CDF and D0 collaborations [217, 218]. We obtain the parameters in these scenarios with the help of `SPheno`, starting from the input parameters at the GUT scale described in Table 5.8. These points are compatible with the the experimental limits set by the analysis made by the D0 collaboration [214]. In particular, the first one corresponds to a scenario in which the gluino is heavier than the squarks ($m_{\tilde{g}} \sim 500$ GeV, $m_{\tilde{q}\neq\tilde{t}} \sim 460$ GeV), while the second one describes a scenario characterized by a light gluino ($m_{\tilde{g}} \sim 340$ GeV , and $m_{\tilde{q}\neq\tilde{t}} \sim 550$ GeV).

In Table 5.9 we show the total hadronic cross section in the two points considered. The second column shows the LO contribution to the cross section, the third column the sum of the LO and the NLO EW contributions to this observable. In the fourth column the $\mathcal{O}(\alpha_s^2\alpha)$ corrections in percent

parameter	TP1	TP2
$m_{1/2}$	200 GeV	500 GeV
m_0	130 GeV	120 GeV
A_0	0	0
sign(μ)	" $-$ "	" $-$ "
$t_\beta(M_Z)$	3	3

Table 5.8: MSSM input parameters for the computation of the spectrum of the scenarios TP1 and TP2.

point	$\sigma^{\rm LO}$	$\sigma^{\rm LO}+\sigma^{\rm NLO\ EW}$	δ (%)	$\frac{1}{\sqrt{L\cdot\sigma^{\rm LO}}}$
TP1	0.16714(1) fb	0.16691(1) fb	-0.14%	61%
TP2	0.048864(3) pb	0.048256(4) pb	-1.26%	3.6%

Table 5.9: Same as Table 5.7, but considering gluino pair production at the Tevatron, *i.e.* the process $P\overline{P}\to\tilde{g}\tilde{g}X$ at $\sqrt{S}=1.96$ TeV, and different SUSY scenarios.

of the total cross section are shown. In the case of the point TP1, the size of the electroweak corrections is so small that they will not be visible at the expected final luminosity 15 fb^{-1}. In the case of the point TP2 we obtain a relative statistical error of order 4% and so three times bigger than the size of the electroweak contributions. Moreover it is worth to notice that the systematic uncertainties are typically greater than 1%. For instance, Ref. [214] claims that the μ_F dependence of the total cross section gives an error from 15 to 20%.

The invariant mass distribution for the two points is shown in Fig. 5.8. In both cases the $\mathcal{O}(\alpha_s^2\alpha)$ corrections are small compared to the lowest order results and do not change the shape of the distribution. In particular, in the case of the point TP1 (TP2) the contribution of the EW corrections relative to the total contribution is of the order of -2% to 5% (-3% to -1%).

Similar considerations hold in the case of the transverse momentum distribution, shown in Fig. 5.9. The shape of the distribution is not affected by the insertion of the electroweak corrections in both points. The contribution of the electroweak corrections relative to the total contribution is of order of -2% to 4.5% in the case of the TP1 point and of the order of -2.5% to -1% in the other scenario considered.

5.5 Conclusions

In this chapter, we have computed the full $\mathcal{O}(\alpha_s^2\alpha)$ corrections to the gluino pair production at the LHC and Tevatron. As a cross check the different renormalization schemes introduced in section 4.2.2 were used. The numerical value of the $\mathcal{O}(\alpha_s^2\alpha)$ contribution is independent on the renormalization scheme, even when non-reliable schemes are used. The treatment of the IR and collinear singularities was performed within two different methods.

We have studied the numerical impact of the $\mathcal{O}(\alpha_s^2\alpha)$ contributions at the LHC in two different scenarios and we have performed scans over many regions of the parameter space. In these regions the EW corrections are negative and can be safely neglected.

We have provided numerical results for the one-loop electroweak corrections of the process of gluino pair production at the Tevatron selecting two points of the parameter space belonging to the region investigated by the D0 and CDF collaboration. $\mathcal{O}(\alpha_s^2\alpha)$ contribution are small and negligible in practice also at the Tevatron.

Finally, we would like to stress that the scan has shown an enhancement in some region of the parameter space of the MSSM. This fact motivates the study of the electroweak corrections to other processes of production of colored SUSY particles in which the EW contributions are expected to be more important, such as squark–anti-squark pair production or the associated production of a squark and a gluino.

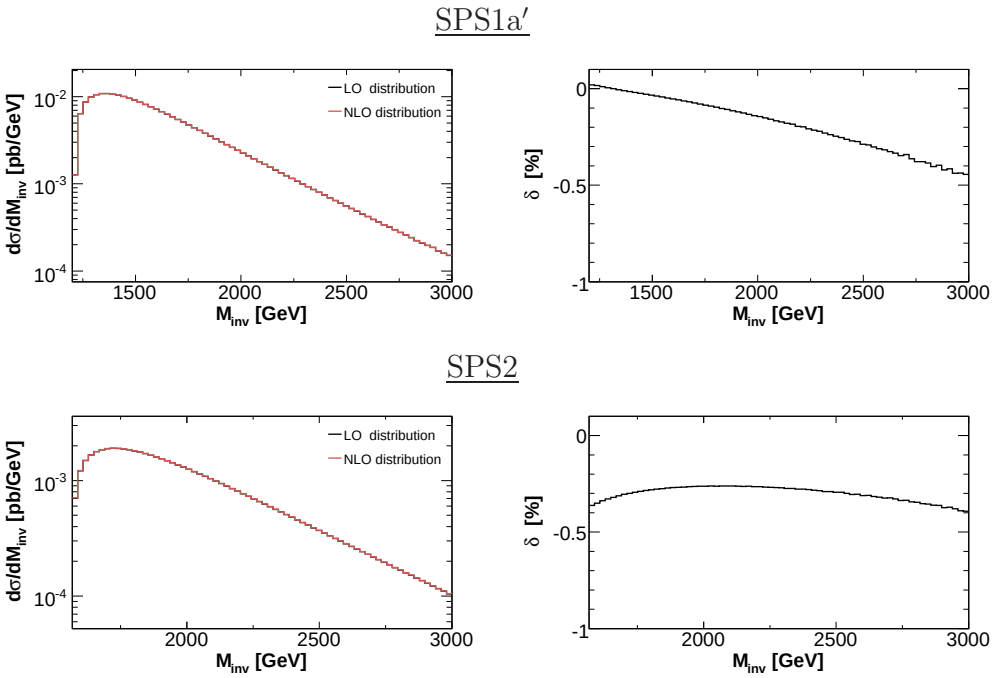

Figure 5.2: Invariant mass distribution for gluino pair production at the LHC. In the left panels we show the LO (black line) and the LO + NLO EW (line) contribution. The two lines are indistinguishable, owing to the smallness of the EW contributions. In the right panels the electroweak corrections in percent of the total result are shown.

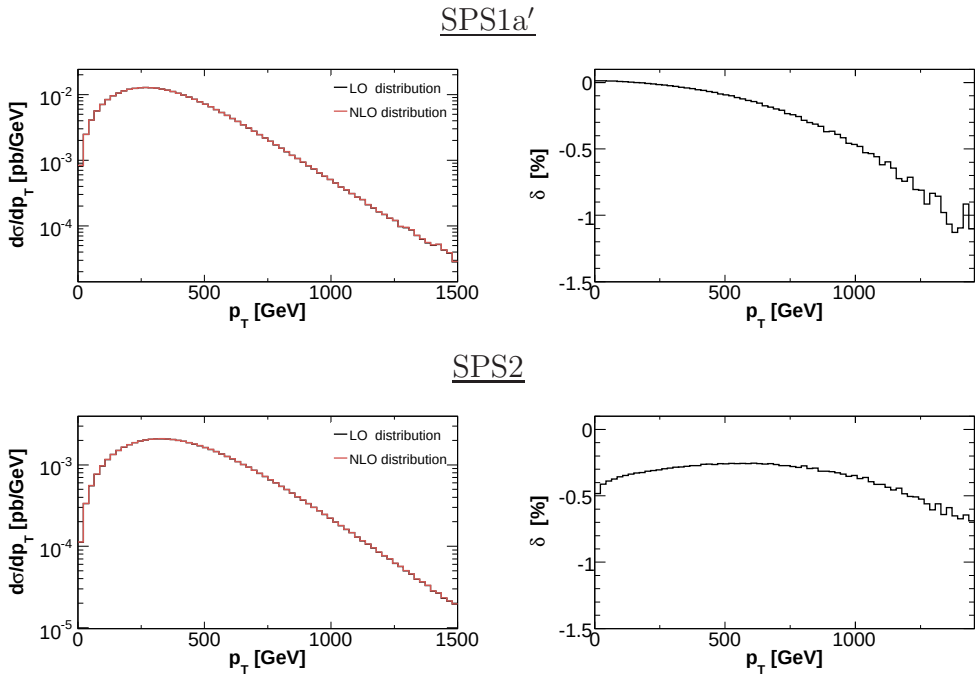

Figure 5.3: Transverse momentum distribution for gluino pair production at the LHC. The left panels show the LO and the LO + NLO EW contribution to this observable. In the right panels, the electroweak corrections in percent of the total result are shown.

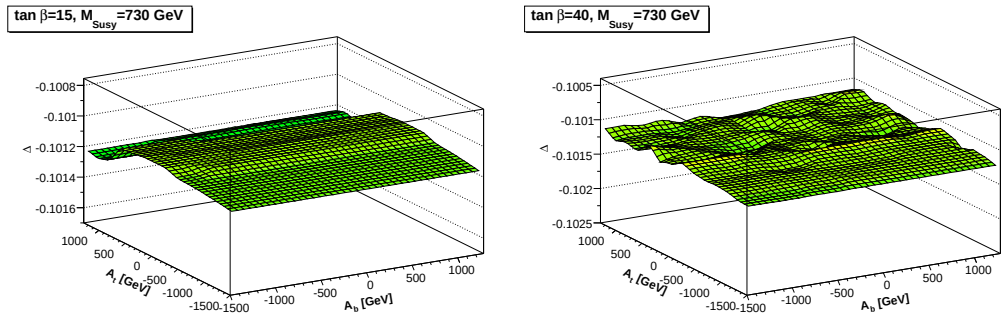

Figure 5.4: $\Delta = \sigma^{\text{NLO EW}}/(\sigma^{\text{LO}} + \sigma^{\text{NLO EW}}) \cdot 100$ as a function of A_t and A_b for different values of t_β and M_{Susy}. The other parameters are fixed to their SPS1a′ value.

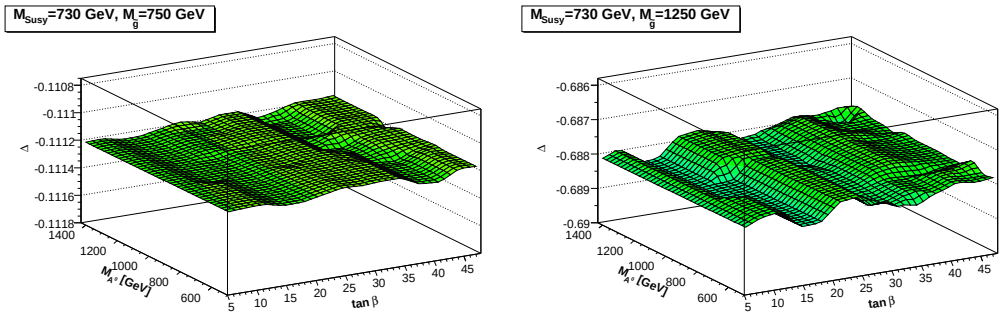

Figure 5.5: $\Delta = \sigma^{\text{NLO EW}}/(\sigma^{\text{LO}} + \sigma^{\text{NLO EW}}) \cdot 100$ as a function of t_β and m_{A^0} for different values of $m_{\tilde{g}}$ and M_{Susy}. The other parameters are fixed to their SPS1a′ value.

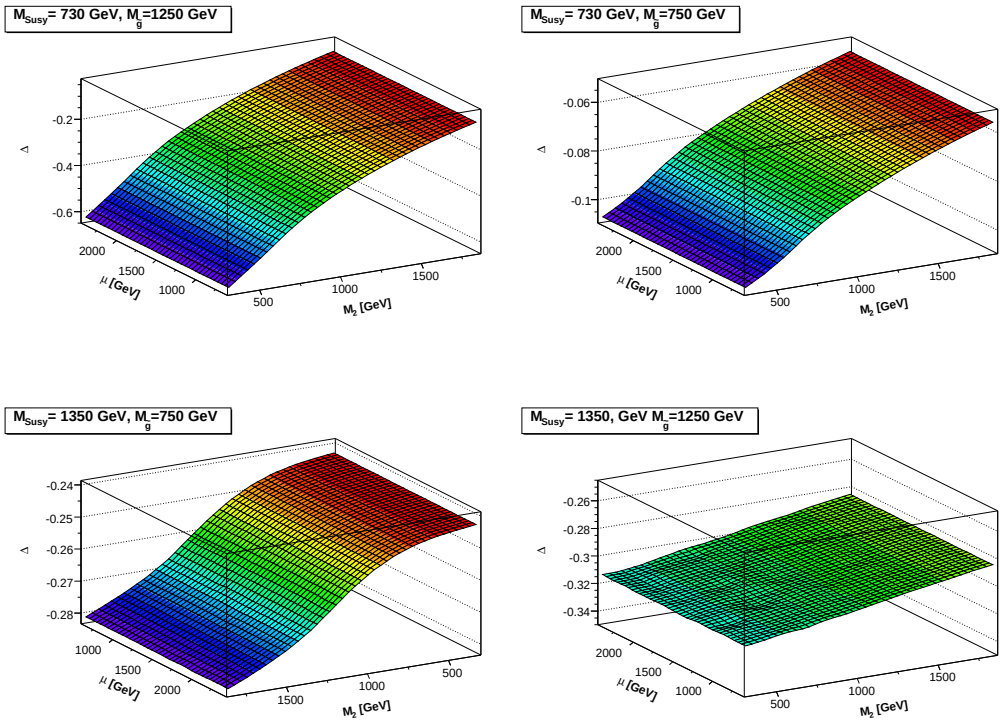

Figure 5.6: Variation of Δ, *c.f* Eq. (5.24), in the (μ, M_2) plane for different values of $m_{\tilde{g}}$ and M_{Susy}. The other parameters are fixed to their SPS1a′ value.

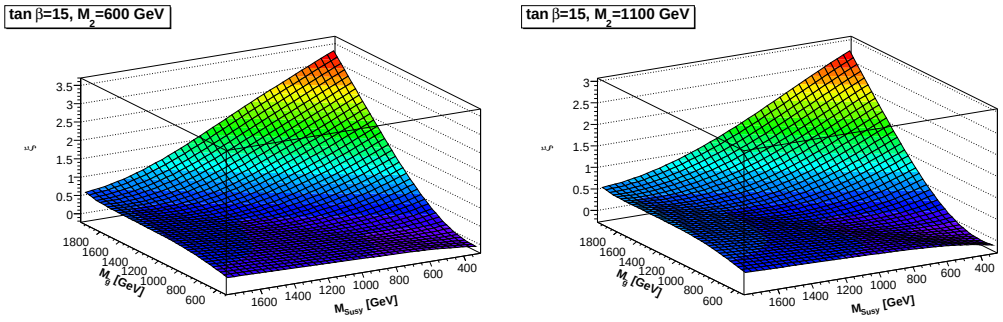

Figure 5.7: $\xi \equiv -\Delta = -\sigma^{\text{NLO EW}}/(\sigma^{\text{LO}} + \sigma^{\text{NLO EW}}) \cdot 100$ as a function of M_{Susy} and $m_{\tilde{g}}$ for different values of M_2 and t_β. The other parameters are fixed to their SPS1a′ value.

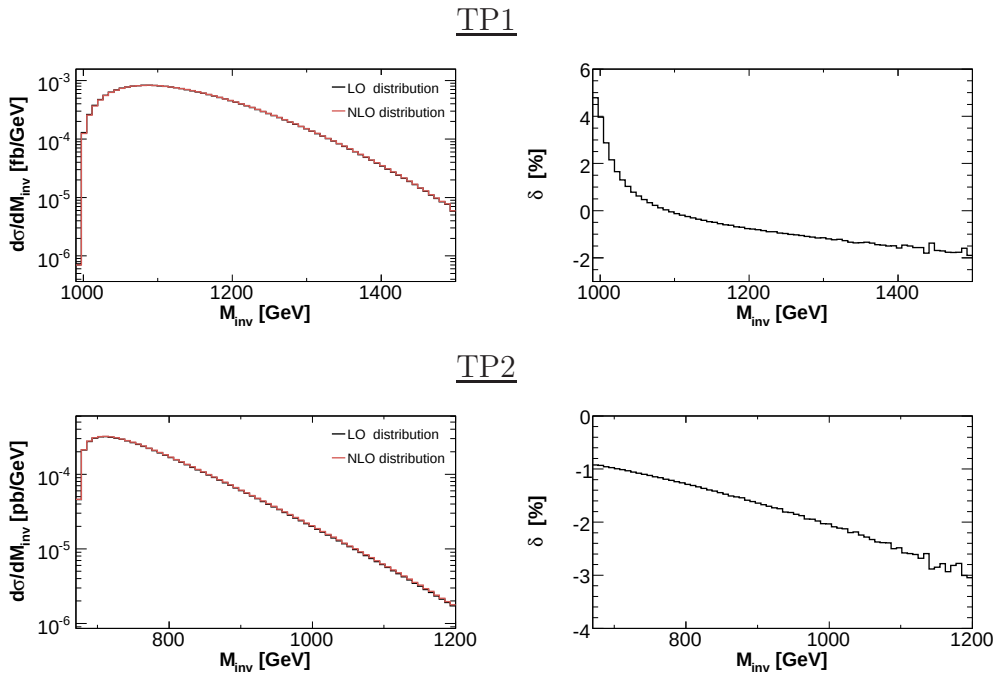

Figure 5.8: Invariant mass distribution of the two gluinos produced at the Tevatron via the process $P\overline{P} \to \tilde{g}\tilde{g}X$. In the left panels we show the LO and the LO + NLO EW contribution, while the electroweak corrections in percent of the total result are shown in the right panels.

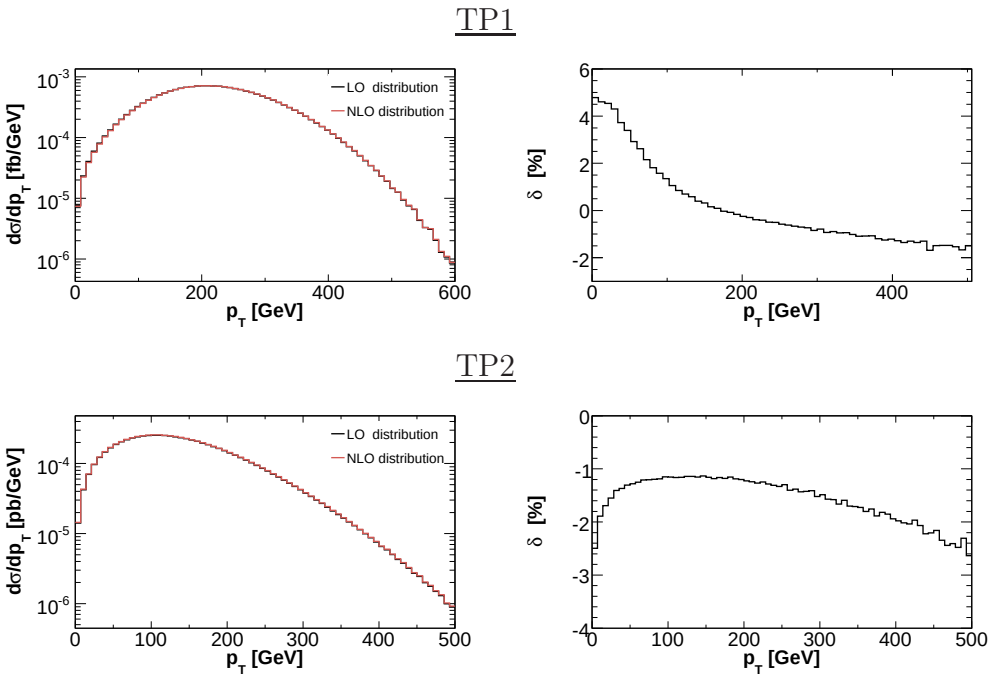

Figure 5.9: Transverse momentum distribution in case of gluino pair production at the Tevatron. The left panels show the LO and LO + NLO EW contribution. The relative contribution of the electroweak corrections is shown in the right panels.

Chapter 6

Diagonal squark-anti-squark production

In this chapter we present the LO and NLO electroweak contributions, of $\mathcal{O}(\alpha_s\alpha+\alpha^2)$ and $\mathcal{O}(\alpha_s^2\alpha)$ respectively, to the production of diagonal squark–anti-squark pairs different from top- and bottom-squarks,

$$P\ P \to \tilde{Q}_a\ \tilde{Q}_a^*\, X \quad (\tilde{Q} \neq \tilde{t}, \tilde{b})\,. \tag{6.1}$$

In the case of top-squark pair production [120, 121, 219], the NLO EW contributions were found to be significant, with effects up to 20%. In general, NLO EW contributions consist of loop contributions to the tree-level amplitudes for $q\bar{q}$ annihilation and gluon fusion, together with real photon and gluon bremsstrahlung processes, yielding an involved structure of interference terms in $q\bar{q}$ annihilation. The NLO EW corrections to the production of squarks of the first two generations show significant differences to top-squark production, based on the following peculiarities.

- In leading order, $\mathcal{O}(\alpha_s^2)$, the squark pair $\tilde{Q}_a\ \tilde{Q}_a^*$ can be produced via annihilation of a $Q\ \overline{Q}$ pair through amplitudes that involve also the exchange of a gluino in the t-channel, thus enhancing the relative weight of the annihilation channel in (6.1).

- Electroweak tree diagrams with t-channel neutralino and chargino exchange are part of the amplitudes for $Q\,\overline{Q} \to \tilde{Q}_a\tilde{Q}_a^*$ and $Q'\,\overline{Q'} \to \tilde{Q}_a\tilde{Q}_a^*$, where Q' is the isospin partner of Q in a quark doublet, yielding EW–QCD interference already at the tree-level.

- At $\mathcal{O}(\alpha_s^2\alpha)$ many types of interferences occur between amplitudes of $\mathcal{O}(\alpha_s\alpha)$ and $\mathcal{O}(\alpha_s)$ as well as between $\mathcal{O}(\alpha_s^2)$ and $\mathcal{O}(\alpha)$ amplitudes.

These features make the calculation of the EW contributions of $\mathcal{O}(\alpha_s^2\alpha)$ to the processes (6.1) more involved than in the case of $\tilde{t}\,\tilde{t}^*$ production where no t-channel diagrams occur at lowest order. Our analysis shows that the EW effects of NLO can reach the same size as the tree-level EW contributions of $\mathcal{O}(\alpha_s\alpha)$ and $\mathcal{O}(\alpha^2)$, which we will include in our discussion as well.

The outline of the chapter is as follows. In section 6.1 we briefly summarize the various tree-level contributions to the processes (6.1). Section 6.2 describes the structure of the NLO terms of EW origin that contribute at $\mathcal{O}(\alpha_s^2\alpha)$ and the strategy of the calculation. Evaluation of the EW effects and their analysis for the LHC are presented in section 6.3 and summarized in section 6.4.

6.1 Tree-level contributions to squark pair production

In this section we list the lowest-order cross sections for the process (6.1) arising from tree-level amplitudes at order $\mathcal{O}(\alpha_s^2)$, $\mathcal{O}(\alpha_s\alpha)$ and $\mathcal{O}(\alpha^2)$. The parton luminosities for getting to the hadronic cross section are given by the convolution in Eq. (5.4).

6.1.1 Squark pair production at leading order

The leading-order contribution to the process (6.1) is QCD based, of $\mathcal{O}(\alpha_s^2)$. The differential cross section reads as follows,

$$\begin{aligned} d\sigma^{\mathrm{LO}}_{PP\to\tilde{Q}_a\tilde{Q}_a^*}(S) &= \sum_q \int_{\tau_0}^1 d\tau\, \frac{dL_{q\overline{q}}}{d\tau}(\tau)\, d\sigma^{2,0}_{q\overline{q}\to\tilde{Q}_a\tilde{Q}_a^*}(s) \\ &\quad + \int_{\tau_0}^1 d\tau\, \frac{dL_{gg}}{d\tau}(\tau)\, d\sigma^{2,0}_{gg\to\tilde{Q}_a\tilde{Q}_a^*}(s). \end{aligned} \tag{6.2}$$

The sum runs over the quarks $q = u,\ d,\ c,\ s$. S and $s = \tau S$ are the squared CM energies of the hadronic process (6.1) and of the partonic sub-process, respectively. Moreover, with the squark mass $m_{\tilde{Q},a}$, the threshold value τ_0 is determined by $\tau_0 = 4m^2_{\tilde{Q},a}/S$.

$d\sigma^{2,0}_{q\overline{q}\to\tilde{Q}_a\tilde{Q}_a^*}$ and $d\sigma^{2,0}_{gg\to\tilde{Q}_a\tilde{Q}_a^*}$ denote the $\mathcal{O}(\alpha_s^2)$ differential cross sections for the partonic processes

$$q(p_1)\ \overline{q}(p_2) \ \to\ \tilde{Q}_a(k_1)\ \tilde{Q}_a^*(k_2), \tag{6.3}$$

$$g(p_1)\ g(p_2) \ \to\ \tilde{Q}_a(k_1)\ \tilde{Q}_a^*(k_2), \tag{6.4}$$

respectively, which are obtained from the Feynman diagrams in Fig. G.1 of appendix G. Explicit expressions for these leading-order cross sections are available in Ref. [11]. Owing to flavor conservation in SUSY QCD, the diagram with the exchange of a gluino in the t channel contributes only if $q = Q$.

6.1.2 Tree-level electroweak contributions of $\mathcal{O}(\alpha_s\alpha)$ and $\mathcal{O}(\alpha^2)$

The $\mathcal{O}(\alpha_s\alpha)$ and $\mathcal{O}(\alpha^2)$ contributions to the process (6.1), involving electroweak terms, can be written as follows,

$$d\sigma^{\text{EW LO}}_{PP\to\tilde{Q}_a\tilde{Q}_a^*X} = \sum_q \int_{\tau_0}^1 d\tau \left\{ \frac{dL_{q\overline{q}}}{d\tau}(\tau) \left(d\sigma^{1,1}_{q\overline{q}\to\tilde{Q}_a\tilde{Q}_a^*} + d\sigma^{0,2}_{q\overline{q}\to\tilde{Q}_a\tilde{Q}_a^*} \right) + \frac{dL_{\gamma g}}{d\tau}(\tau)\, d\sigma^{1,1}_{\gamma g\to\tilde{Q}_a\tilde{Q}_a^*} \right\}. \tag{6.5}$$

The partonic cross section $d\sigma^{0,2}_{q\overline{q}\to\tilde{Q}_a\tilde{Q}_a^*}$ is obtained squaring the tree-level electroweak diagrams depicted in Fig. G.2 of appendix G. The diagram with t-channel neutralino exchange contributes only if $q = Q$, and the diagram with chargino exchange appears only if $q' = Q$, q' being the SU(2) partner of the quark q, since we treat the CKM matrix as unity. $d\sigma^{1,1}_{q\overline{q}\to\tilde{Q}_a\tilde{Q}_a^*}$ originates from interference between the aforementioned tree-level electroweak diagrams and the tree-level QCD graphs of Fig. G.1 of appendix G. Analytical expressions for these cross sections can be found in Ref. [24].

As a new element at $\mathcal{O}(\alpha_s\alpha)$, photon–gluon fusion occurs as a further partonic process,

$$\gamma(p_1)\; g(p_2) \to\; \tilde{Q}_a(k_1)\; \tilde{Q}_a^*(k_2). \tag{6.6}$$

The corresponding cross section, with $t = (p_1 - k_1)^2$,

$$d\sigma^{1,1}_{\gamma g\to\tilde{Q}_a\tilde{Q}_a^*} = \frac{1}{32}\frac{dt}{16\pi s^2} \sum \left| \mathcal{M}^{1/2,1/2}_{\gamma g\to\tilde{Q}_a\tilde{Q}_a^*} \right|^2, \tag{6.7}$$

contains the spin- and color-summed squared tree-amplitudes from the diagrams in Fig. G.3,

$$\sum |\mathcal{M}^{1/2,1/2}_{\gamma g\to\tilde{Q}_a\tilde{Q}_a^*}|^2 = 512\pi^2\,\alpha\alpha_s e_{\tilde{Q}}\, \frac{m^4_{\tilde{Q},a}(m^4_{\tilde{Q},a} + s^2) + tu(tu - 2m^4_{\tilde{Q},a})}{(t - m^2_{\tilde{Q},a})^2\,(u - m^2_{\tilde{Q},a})^2},$$

with $u = (p_1 - k_2)^2$, and the electric charge $e_{\tilde{Q}}$ of the squark $\tilde{Q}$. The γg luminosity entering (6.5) is built according to Eq. (5.4).

6.2 Virtual and real $\mathcal{O}(\alpha_s^2\alpha)$ corrections

In this section we describe the computation of the $\mathcal{O}(\alpha_s^2\alpha)$ corrections to the process (6.1) arising from loops and from photon/gluon bremsstrahlung. The corresponding contributions to the hadronic cross section are expressed in obvious notation,

$$\begin{aligned} d\sigma^{\text{EW NLO}}_{PP\to\tilde{Q}_a\tilde{Q}_a^*X} &= \int_{\tau_0}^1 d\tau\, \frac{dL_{gg}}{d\tau}(\tau)\, \Big(d\sigma^{2,1}_{gg\to\tilde{Q}_a\tilde{Q}_a^*} + d\sigma^{2,1}_{gg\to\tilde{Q}_a\tilde{Q}_a^*\gamma}\Big) \\ &+ \sum_q \Bigg\{ \int_{\tau_0}^1 d\tau\, \frac{dL_{q\overline{q}}}{d\tau}(\tau)\Big(d\sigma^{2,1}_{q\overline{q}\to\tilde{Q}_a\tilde{Q}_a^*} + d\sigma^{2,1}_{q\overline{q}\to\tilde{Q}_a\tilde{Q}_a^*\gamma} \\ &+ d\sigma^{2,1}_{q\overline{q}\to\tilde{Q}_a\tilde{Q}_a^*}\Big) + \int_{\tau_0}^1 d\tau \left[\frac{dL_{qg}}{d\tau}(\tau) d\sigma^{2,1}_{qg\to\tilde{Q}_a\tilde{Q}_a^* q} \right. \\ &+ \left. \frac{dL_{\overline{q}g}}{d\tau}(\tau) d\sigma^{2,1}_{\overline{q}g\to\tilde{Q}_a\tilde{Q}_a^*\overline{q}}\right]\Bigg\}. \end{aligned} \tag{6.8}$$

Other bremsstrahlung contributions to the hadronic cross section are of the type

$$\gamma(p_1)\; q(p_2) \to\; \tilde{Q}_a(k_1)\; \tilde{Q}_a^*(k_2)\; q(k_3), \qquad \gamma(p_1)\; \overline{q}(p_2) \to\; \tilde{Q}_a(k_1)\; \tilde{Q}_a^*(k_2)\; \overline{q}(k_3).$$

We will not consider this class of processes here. Indeed, as in the case of the partonic processes described in section 5.2.3, they are suppressed because of the $\mathcal{O}(\alpha)$ suppression of the photon PDF inside the proton. Moreover, these processes are further suppressed by an additional factor α_s with respect to process (6.6), and thus negligible.

As in the case of gluino pair production, amplitudes are generated with the help of the publicly available code `FeynArts` [195, 196]. The algebraic treatment and numerical evaluation of loop integrals is performed with the support of `FormCalc` and `LoopTools` [177, 178].

6.2.1 Gluon fusion with electroweak loops

The first class of corrections entering Eq. (6.8) are the $\mathcal{O}(\alpha_s^2\alpha)$ electroweak virtual contributions to gg fusion (6.4), given by the partonic cross section

$$d\sigma^{2,1}_{gg\to\tilde{Q}_a\tilde{Q}_a^*} = \frac{1}{256}\frac{dt}{16\pi s^2} \sum 2\,\mathfrak{Re}\,\{\mathcal{M}^{1,0}_{gg\to\tilde{Q}_a\tilde{Q}_a^*}\,\mathcal{M}^{1,1}_{gg\to\tilde{Q}_a\tilde{Q}_a^*}\}. \tag{6.9}$$

$\mathcal{M}^{1,0}_{gg\to\tilde{Q}_a\tilde{Q}_a^*}$ is the tree level gg amplitude (Fig. G.1 of appendix G), and $\mathcal{M}^{1,0}_{gg\to\tilde{Q}_a\tilde{Q}_a^*}$ is the one-loop amplitude with EW insertions in the QCD-based gg tree diagrams. These loop diagrams are shown in Fig. G.8 of appendix G.

In order to get rid of the UV divergences we have to renormalize the squark sector only. We use the schemes described in section 4.2.2, which are equivalent since the mass of the quarks of the first two generations have been neglected.

Parts of the virtual corrections to squark pair production are loop diagrams for the gluon-gluon-H^0 vertex, with the heavy neutral MSSM Higgs boson H^0. These terms become resonant when $m_{H^0} \geq 2m_{\tilde{Q},a}$ and have to be considered a contribution to the process of H^0 production via gluon fusion with the subsequent decay $H^0 \to \tilde{Q}_a\tilde{Q}_a^*$, rather than an electroweak loop correction. We will not consider scenarios in which such resonances occur.

6.2.2 Gluon fusion with real photon emission

The IR singularities arising from virtual photons in (6.9) are cancelled by including bremsstrahlung of real photons at $\mathcal{O}(\alpha_s^2\alpha)$,

$$g(p_1)\; g(p_2) \to\; \tilde{Q}_a(k_1)\; \tilde{Q}_a^*(k_2)\; \gamma(k_3)\,, \tag{6.10}$$

according to the diagrams depicted in Fig. G.4 of appendix G. The integral over the photon phase space is IR divergent in the soft-photon region, *i.e.* for $k_3^0 \to 0$, and cancels the corresponding virtual singularities when added to the virtual contributions according to Eq. (6.8).

For the technical treatment of photon-momentum integration and isolation of divergences we apply the two different procedures described in section 4.3. Comparison between the two methods provides a non trivial check of the computation. As illustrated in Fig. 6.1, the two methods yield results which are in good numerical agreement.

6.2.3 $q\bar{q}$ annihilation with electroweak and QCD loops

The structure of the parton processes of $q\bar{q}$ annihilation at higher order is more involved and requires a simultaneous treatment of electroweak and QCD loops. The virtual contributions of one-loop order to the partonic cross section

is given by the interference of tree-level and loop amplitudes,

$$d\sigma^{2,1}_{qq\to\tilde{Q}_a\tilde{Q}_a^*} = \frac{1}{36}\frac{dt}{16\pi s^2}\sum\Big\{2\,\mathfrak{Re}\{\mathcal{M}^{1,0*}_{q\overline{q}\to\tilde{Q}_a\tilde{Q}_a^*}\mathcal{M}^{1,1}_{q\overline{q}\to\tilde{Q}_a\tilde{Q}_a^*}\} + 2\,\mathfrak{Re}\{\mathcal{M}^{0,1*}_{q\overline{q}\to\tilde{Q}_a\tilde{Q}_a^*}\mathcal{M}^{2,0}_{q\overline{q}\to\tilde{Q}_a\tilde{Q}_a^*}\}\Big\}, \tag{6.11}$$

where $\mathcal{M}^{1,0}_{q\overline{q}\to\tilde{Q}_a\tilde{Q}_a^*}$ ($\mathcal{M}^{0,1}_{q\overline{q}\to\tilde{Q}_a\tilde{Q}_a^*}$) is the amplitude related to the tree-level QCD (EW) diagrams depicted in Fig. G.1 (G.2) of appendix G. $\mathcal{M}^{1,1}_{q\overline{q}\to\tilde{Q}_a\tilde{Q}_a^*}$ is the one-loop amplitude arising from the EW corrections to the QCD tree-level diagrams and the QCD corrections to the EW tree-level diagrams. Finally, $\mathcal{M}^{2,0}_{q\overline{q}\to\tilde{Q}_a\tilde{Q}_a^*}$ is the one-loop amplitude corresponding to the QCD corrections to the QCD tree-level diagrams.
The diagrams entering $\mathcal{M}^{1,1}_{q\overline{q}\to\tilde{Q}_a\tilde{Q}_a^*}$ are displayed in Figs. G.6–G.9 of appendix G. They also contain the diagrams with counter term insertions required for renormalization and cancellation of UV divergences. Besides squark renormalization, also quark renormalization is needed.
$\mathcal{M}^{2,0}_{q\overline{q}\to\tilde{Q}_a\tilde{Q}_a^*}$ can be obtained from the Feynman diagrams in Fig. G.10, including the proper counter terms. Besides renormalization of the squark sector, we have to renormalize also the gluino mass, the strong coupling g_s and the quark–squark–gluino coupling $\hat{g}_s$, which is related to g_s via supersymmetry. We use the procedure described in section 4.2.2.

6.2.4 $q\bar{q}$ annihilation with real photon emission

The diagrams in Fig. G.5 of appendix G constitute the generic amplitude for photon bremsstrahlung at $\mathcal{O}(\alpha_s^2\alpha)$ in the $q\bar{q}$ annihilation channel,

$$q(p_1)\;\overline{q}(p_2)\to\;\tilde{Q}_a(k_1)\;\tilde{Q}_a^*(k_2)\;\gamma(k_3)\,. \tag{6.12}$$

The corresponding cross section is singular both in the IR soft-photon region and in the collinear region (*e.g.* whenever $k_3p_i\to 0$). The extraction of the singularities has been performed using the two different methods described in section 4.3. In Fig. 6.1 we visualize the comparison between the two methods in the specific case of the partonic process $u\overline{u}\to\tilde{u}_L\tilde{u}_L^*\gamma$ as an example.

6.2.5 $q\bar{q}$ annihilation with real gluon emission

Finally, we have to take into account the class of $q\bar{q}$ annihilation processes with real gluon bremsstrahlung,

$$q(p_1)\;\overline{q}(p_2)\to\;\tilde{Q}_a(k_1)\;\tilde{Q}_a^*(k_2)\;g(k_3)\,, \tag{6.13}$$

from either EW-based (appendix G, Fig. G.11a) or QCD-based Born diagrams (appendix G, Fig. G.11b). This class contributes to the cross section at $\mathcal{O}(\alpha_s^2\alpha)$ through interference between the graphs of Fig. G.11a and Fig. G.11b. The cross section exhibits singularities when the gluon becomes soft or collinear to the initial-state quark/anti-quark. The soft singularities cancel against those from the virtual photon/gluon contributions in $q\bar{q}$ annihilation, when added along Eq. (6.8), while remaining collinear singularities have to be absorbed in the PDFs by factorization. IR and collinear singularities can be treated by mass regularization within the two methods described in section 4.3. In Fig. 6.1 we illustrate the comparison between the two methods also for gluon radiation, with good numerical agreement.

6.2.6 $q(\bar{q})\,g$ fusion

A last class of partonic processes at the considered order is given by (anti-)quark-gluon fusion,

$$\begin{aligned} q(p_1)\; g(p_2) &\to\; \tilde{Q}_a(k_1)\; \tilde{Q}_a^*(k_2)\; q(k_3)\,, \\ \overline{q}(p_1)\; g(p_2) &\to\; \tilde{Q}_a(k_1)\; \tilde{Q}_a^*(k_2)\; \overline{q}(k_3)\,. \end{aligned} \tag{6.14}$$

This IR finite class contributes at $\mathcal{O}(\alpha_s^2\alpha)$ through the interference between the diagrams of Fig. G.12a and Fig. G.12b of appendix G. Mass singularities arise when the incoming gluon and outgoing (anti-)quark are collinear. These collinear divergences are again absorbed into the PDFs. Their extraction has been performed using the two methods mentioned in section 4.4. In Fig. 6.1 we show the agreement between the two methods for the example $ug \to \tilde{u}_L\tilde{u}_L^* u$.

In specific cases of SUSY parameters, when kinematically allowed, the internal-state gauginos can be on-shell. The poles are regularized by introducing the width of the corresponding gluino, neutralino, or chargino. Potential problems related to gauge invariance [220] do not occur here since the resonant diagrams are not affected by collinear singularities.

6.2.7 Factorization of initial collinear singularities

In the case of the process (6.1), the term $\mathcal{R}(x_1, x_2, s)$ in Eq. (4.8) is related to both $\mathcal{O}(\alpha_s)$ and $\mathcal{O}(\alpha)$ factorizations of the (anti-)quark PDF. The integral of $\mathcal{R}$ over x_1 and x_2 has to be added to Eq. (6.8), and can be expressed in terms of the integral over τ of a new function, $\overline{\mathcal{R}}(\tau, s)$. In others words, Eq. (5.18)

holds defining $\overline{\mathcal{R}}(\tau, s)$ as

$$\begin{aligned}
\overline{\mathcal{R}}(\tau,s) &= \sum_q \Bigg\{ -\frac{\alpha_s}{\pi} C_F \, \frac{dL_{q\overline{q}}}{d\tau}(\tau) \int_{z_0}^1 dz \, [\mathcal{H}_q^{(1)}]_+ \, d\sigma^{1,1}_{q\bar{q}\to\tilde{Q}_a\tilde{Q}_a^*}(zs) \\
&- \frac{\alpha}{\pi} e_q^2 \, \frac{dL_{q\overline{q}}}{d\tau}(\tau) \int_{x_0}^1 dz \, [\mathcal{H}_q^{(1)} + h^{(1)}]_+ \, d\sigma^{2,0}_{q\bar{q}\to\tilde{Q}_a\tilde{Q}_a^*}(zs) \\
&- \frac{\alpha_s}{2\pi} T_R \left(\frac{dL_{qg}}{d\tau}(\tau) + \frac{dL_{g\overline{q}}}{d\tau}(\tau) \right) \int_{x_0}^1 dz \, \mathcal{H}_q^{(2)} \, d\sigma^{1,1}_{q\bar{q}\to\tilde{Q}_a\tilde{Q}_a^*}(zs) \\
&- \frac{3\alpha}{2\pi} e_q^2 \left(\frac{dL_{q\gamma}}{d\tau}(\tau) + \frac{dL_{\gamma\overline{q}}}{d\tau}(\tau) \right) \int_{x_0}^1 dz \, (\mathcal{H}_q^{(2)} + h^{(2)}) \\
&\qquad \times d\sigma^{2,0}_{q\bar{q}\to\tilde{Q}_a\tilde{Q}_a^*}(zs) \Bigg\}, \qquad (6.15)
\end{aligned}$$

where $z_0 = (4m^2_{\tilde{Q},a})/s$. The functions $\mathcal{H}$ and h are defined in Eq. (4.13). For the calculation of hadronic observables we use the MRST2004qed parton distribution functions [204]. Accordingly, the factorization of $\mathcal{O}(\alpha_s)$ ($\mathcal{O}(\alpha)$) corrections is performed within the $\overline{\rm MS}$ (DIS) scheme. Factorization and renormalization scales are chosen as equal, $\mu_R = \mu_F = m_{\tilde{Q},a}$.

6.3 Numerical analysis

For the numerical evaluation and for illustration of the EW effects, we choose four different benchmark scenarios: the point SPS1a′ suggested by the SPA convention [203], the Snowmass point SPS5 [209] characterized by light stops, and two of the points chosen for detector simulation in the ATLAS "Computing System Commissioning" exercise [221]: the point SU1 in the co-annihilation region, and the point SU4 characterized by light SUSY particles. The input parameters $m_{1/2}$, m_0, A_0, defined at the GUT scale, and t_β are collected together in Table 6.1. The MSSM input for the actual calculation is obtained with the help of the program `SPheno` [210], together with the program `SuSpect` [211] as a cross check. The pole masses are collected in Table 6.2. Since the quarks of the first two generations are treated as massless, same-chirality and same-isospin squarks are degenerate, therefore we do not show the masses of the squarks belonging to the second generation. The difference between the masses provided by the two codes is below 1%. The different inputs given by the two codes give rise to a differences in the total cross section of the order of $2-3\%$. The standard model parameters are taken from Ref. [208].
We introduce the following conventions:

parameter	SPS1a′	SPS5	SU1	SU4
$m_{1/2}$	250 GeV	300 GeV	350 GeV	160 GeV
m_0	70 GeV	150 GeV	70 GeV	200 GeV
A_0	−300 GeV	−1000 GeV	0	−400 GeV
sign(μ)	+	+	+	+
$t_\beta(M_Z)$	10.37	5	10	10

Table 6.1: Input parameters in the four benchmark scenarios.

	SPS1a′	SPS5	SU1	SU4
$m_{\tilde{u},R}$	548.1	660.3	739.7	412.6
	(545.6)	(657.4)	(736.3)	(411.2)
$m_{\tilde{u},L}$	565.3	681.5	765.6	420.3
	(562.0)	(677.5)	(760.7)	(418.6)
$m_{\tilde{d},R}$	547.9	659.2	738.0	413.9
	(545.4)	(656.9)	(734.6)	(412.5)
$m_{\tilde{d},L}$	570.7	685.5	769.6	427.5
	(567.5)	(681.8)	(764.7)	(425.8)

Table 6.2: Pole masses (in GeV) of the squarks of the first generation in the various SUSY scenarios. They are obtained using `SPheno` [210]; those computed with `SuSpect` [211] are quoted inside the brackets for comparison.

- We will refer to the sum of $\mathcal{O}(\alpha_s\alpha)$, $\mathcal{O}(\alpha^2)$ and $\mathcal{O}(\alpha_s^2\alpha)$ contributions as "the EW contribution".
- We will use the quantity δ to denote the relative EW contribution, defined as $\delta = (\mathcal{O}_{\rm NLO} - \mathcal{O}_{\rm LO})/\mathcal{O}_{\rm LO}$, where $\mathcal{O}$ is a generic observable and $\mathcal{O}_{\rm NLO}$ is the sum of the LO in Eq. (6.2) and the EW contribution.

6.3.1 Different squark species

Electroweak interactions depend on the hypercharge of the squarks, hence the production cross sections are flavor and chirality dependent. In this subsection we will study the production of four squark species, focusing on the SPS1a′ point. Since the masses of the light quarks can be neglected, the weak eigenstates of the squarks are also the mass eigenstates; thus, in the following, the two squarks of a given flavor are distinguished by means of their chiralities, $\tilde{Q}_a = \tilde{Q}_L, \tilde{Q}_R$.

	$\tilde{u}_R\tilde{u}_R^*$	$\tilde{u}_L\tilde{u}_L^*$	$\tilde{d}_L\tilde{d}_L^*$	$\tilde{c}_L\tilde{c}_L^*$
$\mathcal{O}(\alpha_s^2)$	$36.83(3)\cdot 10^{-2}$	$31.31(1)\cdot 10^{-2}$	$25.89(1)\cdot 10^{-2}$	$22.65(1)\cdot 10^{-2}$
$\mathcal{O}(\alpha_s\alpha)$	$-9.00(1)\cdot 10^{-3}$	$-3.54(1)\cdot 10^{-2}$	$-3.83(1)\cdot 10^{-2}$	$2.82(1)\cdot 10^{-3}$
$\mathcal{O}(\alpha^2)$	$2.42(1)\cdot 10^{-3}$	$2.39(1)\cdot 10^{-2}$	$3.20(1)\cdot 10^{-2}$	$2.11(1)\cdot 10^{-3}$
$\mathcal{O}(\alpha_s^2\alpha)$	$-3.09(5)\cdot 10^{-3}$	$-1.05(1)\cdot 10^{-2}$	$-7.82(7)\cdot 10^{-2}$	$5.89(1)\cdot 10^{-3}$
$\delta(\%)$	-2.6	-7.0	-5.5	4.8

Table 6.3: Total cross section for the diagonal pair production of different squark species in the SPS1a′ scenario. Beside the LO contribution, of $\mathcal{O}(\alpha_s^2)$, we show the yields of the different orders contributing to the NLO EW corrections. Cross sections are given in pb. δ is defined according to section 6.3.

Dependence on squark flavor and chirality

In Table 6.3, we show the integrated hadronic cross section for the diagonal pair production of $\tilde{u}_L$, $\tilde{u}_R$, $\tilde{d}_L$ and $\tilde{c}_L$ in the SPS1a′ scenario. In the case of the production of the squarks of the first generation there is a cancellation between $\mathcal{O}(\alpha_s\alpha)$ and $\mathcal{O}(\alpha^2)$ contributions. The overall $\mathcal{O}(\alpha_s\alpha+\alpha^2)$ contribution is negative and of the same order of magnitude as the $\mathcal{O}(\alpha_s^2\alpha)$ one. Since they have the same sign their effect is enhanced. In the case of $\tilde{c}_L$ production the situation is different: $\mathcal{O}(\alpha_s\alpha)$, $\mathcal{O}(\alpha^2)$, and $\mathcal{O}(\alpha_s^2\alpha)$ corrections are positive, $\mathcal{O}(\alpha_s^2\alpha)$ contribution being the most important one (see also the discussion below).

As a general remark, the EW effects are always larger for left-handed squarks. For a given chirality and generation, the EW contributions are more important in the case of up-type squarks. For comparison we also estimate the corresponding NLO QCD corrections using the code `PROSPINO` [20]; they are positive, weakly dependent on the flavor of the produced squarks, and of the order of $47-48\%$.

Fig. 6.2 shows the relative EW contribution (right part) in the "cumulative invariant mass distribution" $\sigma(M_{\rm inv})$, that is the cross section integrated up to the value $M_{\rm inv}$ of the squark–anti-squark invariant mass,

$$\sigma(M_{\rm inv}) = \int_{2m_{\tilde{Q}_a}}^{M_{\rm inv}} \frac{d\sigma}{dM_{\rm inv}}\, dM_{\rm inv}. \tag{6.16}$$

A common feature is that in the low invariant mass region the NLO EW contribution is positive, rather steeply decreasing as the invariant mass in-

creases, reaching the plateau at $M_{\text{inv}} \geq 2000$ GeV which corresponds to the total cross section. The left part of Fig. 6.2 shows the relative size of the individual contributions arising from the various channels. The contribution from the gluon fusion channel is always positive and dominates at lower values of M_{inv}, whereas the $q\overline{q}$ annihilation channel part is negative.

Looking at the relative contributions of the different channels in the high invariant mass region, which corresponds to the total cross section, one can understand the origin of the different behaviour of the NLO EW corrections in the case of $u^L u^{L*}$ and $c^L c^{L*}$ production. For up-squark pairs, the $\mathcal{O}(\alpha_s\alpha)$ and $\mathcal{O}(\alpha_s^2\alpha)$ terms are dominated by the the $q\bar{q}$ annihilation channels, which yield a negative contribution; for charm-squark production, however, the $\mathcal{O}(\alpha_s\alpha)$ [$\mathcal{O}(\alpha_s^2\alpha)$] corrections are dominated by the $q\gamma$ fusion [gg fusion] channel and thus positive. This shows the key role played by the partonic processes $Q\ \overline{Q}$, $Q'\ \overline{Q'} \to \tilde{Q}_a \tilde{Q}_a^*$, where Q and Q' belong to the same isospin doublet. Indeed, in the case of $u_L u_L^*$ production their contribution is negative and the largest out of the $q\bar{q}$ annihilation channels. In $c_L c_L^*$ production they are suppressed by the PDFs of the charm and strange quarks and hence the contributions from the $q\bar{q}$ annihilation channels are negligible. As a result the overall contribution to total cross section is negative at the level of 5% for the left-handed up-squarks, while for the left-handed charm-squarks it is of the same order of magnitude but positive. The contribution of the $g\gamma$ channel is independent on the squark chirality, determined only by the electric charge of the produced squarks, which makes the $g\gamma$ channel contribution for up-squark pair production four times bigger than that for down-squarks. Owing to the mass degeneracy between same-chirality and same-isospin squarks, the gg fusion channel is independent on the generation of the produced squark.

The invariant mass distribution itself is displayed in Fig. 6.3 for the various squark species, showing also the breakdown into the individual channels. For each squark species, the EW contributions are positive in the low invariant mass region and become negative for larger values of M_{inv}, reaching the level of 15% for $\tilde{u}_L$ squarks.

Fig. 6.4 contains the transverse momentum distribution of the squarks. Again, the EW effects are more pronounced for left-handed chirality yielding more than 30% negative contributions for large p_T. As new feature, the LO EW contribution can be positive for low p_T, especially for the $\tilde{d}_L$ case, originating from the PDF-enhanced parton process $u\bar{u} \to \tilde{d}_L \tilde{d}_L^*$ through t-channel chargino exchange. This positive part is practically compensated by the NLO $\mathcal{O}(\alpha_s^2\alpha)$ contributions in the $q\bar{q}$ annihilation channel.

In Fig. 6.5 we show the squark rapidity distribution and the various parts

of the EW contributions. For right-handed squarks, the EW effects are rather small; for left-handed squarks their sum is typically of the order 5%. NLO EW corrections change sign when moving from the production of the squarks of the first generation to the processes involving squarks of the second generation.

Dependence on the squark masses

To study the dependence of the EW contributions on the mass of the squarks, we vary $m_{\tilde{u},R}$, setting $m_{\tilde{d},R} = m_{\tilde{u},R}$ and $m_{\tilde{u},R} = m_{\tilde{u},L}(1+\varepsilon)$ with $\varepsilon = 0.03$, which is the value at the SPS1a′ point. The values are also taken for the other generations as well as for the sleptons. The other parameters are kept as in SPS1a′. Each parameter point was checked to satisfy the bounds on SUSY particles from LEP [53, 222] and Tevatron [214], and the bound on the mass of the light Higgs boson h^0. The mass of h^0 has been computed using `FeynHiggs 2.5.1` [56, 215, 216]. Moreover, each point fulfills the condition $|\Delta\rho| < 0.025$, where $\Delta\rho$ is the squark contribution to the electroweak ρ parameter, which is the dominant SUSY contribution to this parameter.

The relative EW contributions are shown in Fig. 6.6 for the total cross section, for each of the various squark types. The quantity ξ displayed in the right panel is the fraction of each the gg fusion and the $q\bar{q}$ annihilation channel in the total cross section, at leading order $\mathcal{O}(\alpha_s^2)$. The $q\bar{q}$ channel becomes more and more important as $m_{\tilde{u},R}$ increases. This feature, already pointed out in Ref. [11], is a consequence of the t-channel gluino exchange diagrams. The increasing importance of $q\bar{q}$ annihilation allows a better understanding of the particular role of the NLO corrections to the $q\bar{q}$ channel with increasing squark masses. Especially for left-handed up- and down-squarks, the NLO EW contributions become more important than the LO ones, with effects of more than 20%. In the charm-squark production case $q\bar{q}$ channel is sub-leading with respect to the gg and $g\gamma$ fusion channels due to the aforementioned suppression of charm and strange PDFs. The total sum of the EW contributions is shown in the right panel of Fig. 6.6. For illustration, we also give an estimate of the formal statistical uncertainty $\delta_{\text{stat}} = (L\,\sigma^{\text{NLO}})^{-1/2}$, assuming a luminosity $L = 100$ fb^{-1}.

6.3.2 Different SUSY scenarios

Here we discuss the electroweak effects in the different SUSY scenarios mentioned above. As a concrete example, we consider the production of $\tilde{u}_L$ squarks.

	SPS5	SU1	SU4
$\mathcal{O}(\alpha_s^2)$	$10.62(1) \cdot 10^{-1}$	$51.77(2) \cdot 10^{-3}$	$16.14(1) \cdot 10^{-1}$
$\mathcal{O}(\alpha_s\alpha)$	$-1.37(1) \cdot 10^{-2}$	$-7.22(1) \cdot 10^{-3}$	$-1.45(1) \cdot 10^{-1}$
$\mathcal{O}(\alpha^2)$	$9.11(1) \cdot 10^{-3}$	$4.73(1) \cdot 10^{-3}$	$10.16(1) \cdot 10^{-2}$
$\mathcal{O}(\alpha_s^2\alpha)$	$-4.83(3) \cdot 10^{-3}$	$-2.75(2) \cdot 10^{-3}$	$-2.61(1) \cdot 10^{-2}$
$\delta(\%)$	-8.9	-10.1	-4.3

Table 6.4: Same as Table 6.3 but focusing on $\tilde{u}^L\tilde{u}^{L*}$ production in different SUSY scenarios. Cross sections are expressed in pb.

In Table 6.4 we show the total cross section for the aforementioned production process. The LO contribution and the different orders entering the EW contributions are shown separately. As one can see, the absolute value of the different contributions decreases as the mass of $m_{\tilde{u},L}$ increases, while the relative yield of the EW contributions increases with the mass of the produced squarks. In the case of the SU1 scenario the EW contributions are negative and of the order of 10%. The corresponding NLO QCD corrections are estimated using the code `PROSPINO` [20]; they are positive and of the order of $45 - 50\%$. The logarithmically enhanced NNLO QCD contributions to squark hadro-production reduce the dependence on the factorization scale and are of the same size of the EW contributions, of the order of 9% of the NLO QCD corrections [21].

Fig. 6.7 contains the cumulative invariant mass distribution, again with the individual and the total EW contributions, which show a similar behaviour for all the chosen scenarios. Also the differential invariant mass distribution, displayed in Fig. 6.8, has similar qualitative features in all scenarios. At low values, the gluon fusion part dominates and renders the total EW contribution positive. At larger values, the contributions from $q\overline{q}$ annihilation turn the EW contribution to the negative region; thereby the NLO part is always of about the same size as the LO part.

In Fig. 6.9 we show the transverse momentum distribution in the various cases. Again, their shape depends only weakly on the scenario. This also applies to the rapidity distribution, which is illustrated in Fig. 6.10. The EW contributions are largest in the low rapidity region and are dominated by the negative contributions arising from the $q\overline{q}$ channel at both tree-level and NLO.

This general situation is only slightly changed when kinematical cuts are imposed, as we find from repeating our analysis for an exemplary set of cuts on the transverse momentum and on the rapidity of the two squarks,

$$p_T > 150 \text{ GeV}, \quad |y| < 2.5.$$

As can be inferred from Fig 6.10, the cut on the rapidity is not effective because the NLO EW contributions to the rapidity distribution are very small for $|y| > 2.5$. More important is the cut on the transverse momentum. It excludes the kinematical region where the largest part of the gluon channel contribution comes from. Moreover, this cut suppresses also the contribution of the $g\gamma$ channel and enhances the influence of the $q\overline{q}$ channel by excluding the region with a positive p_T distribution. As a result, the negative EW contribution to the total cross section is larger than without cuts, as one can see from Fig. 6.11.

Dependence on the gluino mass

We study the dependence of the EW contribution as a function of the mass of the gluino, $m_{\tilde{g}}$, with the other parameters kept fixed according to the SPS1a′ point. Again, the parameter range is in accordance with the phenomenological constraints described in the previous subsection 6.3.1. At LO, the gluon fusion channel does not depend on the gluino mass, while the $q\overline{q}$ annihilation channel contribution decreases with increasing $m_{\tilde{g}}$, as displayed in Fig. 6.12. In the low $m_{\tilde{g}}$ region the two channels contribute equally to the production cross section, while gluon fusion becomes dominant as the mass of the gluino increases. The relative EW contributions from the various channels are flat, adding up to a total EW contribution from -7 to -3% for gluino masses between 500 and 2000 GeV. Thereby, in $q\bar{q}$ annihilation, both the tree-level term $\mathcal{O}(\alpha_s\alpha + \alpha^2)$ and the NLO corrections $\mathcal{O}(\alpha_s^2\alpha)$, are practically of the same size.

Inclusive diagonal squark–anti-squark production

It is worth to analyse the impact of the EW contributions on the inclusive diagonal squark–anti-squark production considering the production of a squark–anti-squark pair of any flavor and chirality simultaneously. In Fig. 6.13 we show the cumulative invariant mass, the transverse momentum and the invariant mass distribution in the SPS1a′ scenario. The EW contributions to the cumulative invariant mass amounts up to 5% near threshold while the EW contributions to the total cross section, *i.e.* the cumulative invariant mass distribution in the limit $M_{\text{inv}} \to \infty$, are negative and of the

order of 1%. Indeed, in the case of the total cross section the negative contribution arising from $\tilde{u}_L\tilde{u}_L^*$ and $\tilde{d}_L\tilde{d}_L^*$ is halved in the sum with the $\tilde{u}_R\tilde{u}_R^*$ and $\tilde{d}_R\tilde{d}_R^*$ production processes. The resulting negative contribution is further reduced by the positive contribution of $\tilde{c}_L\tilde{c}_L^*$ and $\tilde{s}_L\tilde{s}_L^*$ and after the sum of $\tilde{c}_R\tilde{c}_R^*$ and $\tilde{s}_R\tilde{s}_R^*$ production processes, whose EW contributions are negligible. The impact of the aforementioned contributions on the transverse momentum (invariant mass) distribution is reduced as well and is at most of the order of 10% (6%) in the high p_T (M_{inv}) region. Notice the peculiar behaviour of the invariant mass distribution in the low invariant mass region. The EW contributions rise when the threshold for left-handed squark production is reached and the EW contributions to the production of left-handed squarks enter.

Similar considerations hold when the other scenarios are considered. In Fig. 6.14 and 6.15 we plot the cumulative invariant mass, the transverse momentum, and the invariant mass distribution in the SPS5 and SU1 scenario, respectively. The general behaviour is similar to that of the SPS1a′ point. As expected, the relative importance of the EW contributions increases when the masses of the squarks increase, since the relative importance of the EW contribution increases in each of the different squark–anti-squark production processes as the masses of the squarks increases. In the case of the SPS5 (SU1) point the EW contributions on the total cross section are negative and of the order of −1% (−2%). The relative yield of the EW contributions on the invariant mass varies from −6% (−8%) to 6% (6%). More important is the numerical impact of the EW contributions on the transverse momentum distribution; in the SPS5 (SU1) scenario it reaches −12% (−14%) in the high p_T region.

6.4 Conclusions

Chapter 6 summarizes the $\mathcal{O}(\alpha_s^2\alpha)$ NLO electroweak contributions to the production of flavor-diagonal squark–anti-squark pairs in proton–proton collisions, in combination with the electroweak LO tree-level contributions of $\mathcal{O}(\alpha_s\alpha + \alpha^2)$.

We have performed an explicit study of the electroweak contributions for $\tilde{u}_R\tilde{u}_R^*$, $\tilde{u}_L\tilde{u}_L^*$, $\tilde{d}_L\tilde{d}_L^*$, and $\tilde{c}_L\tilde{c}_L^*$ pair production. The electroweak effects can give rise to sizable modifications in cross sections and distributions, in particular for left-handed squarks. Thereby, the NLO terms are significant and have to be considered together with the tree-level contributions. They show a strong dependence on the squark masses, increasing their relative influence with the

mass of the squarks.

Moreover, we have investigated several SUSY benchmark scenarios and found that the behaviour of the electroweak contributions is only weakly dependent on the scenario. Also the gluino-mass dependence is weak. In summary, the electroweak contributions in squark-pair production can reach 20–25% in size and are thus significant; about half is carried by the NLO contributions.

When the squarks belonging to the first two generations are treated inclusively, *i.e.* when we consider the production of a squark of the first two generations of any chirality and flavor together with its own anti-particle, the numerical impact of the EW contributions is reduced. EW contributions to the total cross section are below 10%. The relative yield of the EW contributions to the differential distributions is bigger, above 10% in the high energy region.

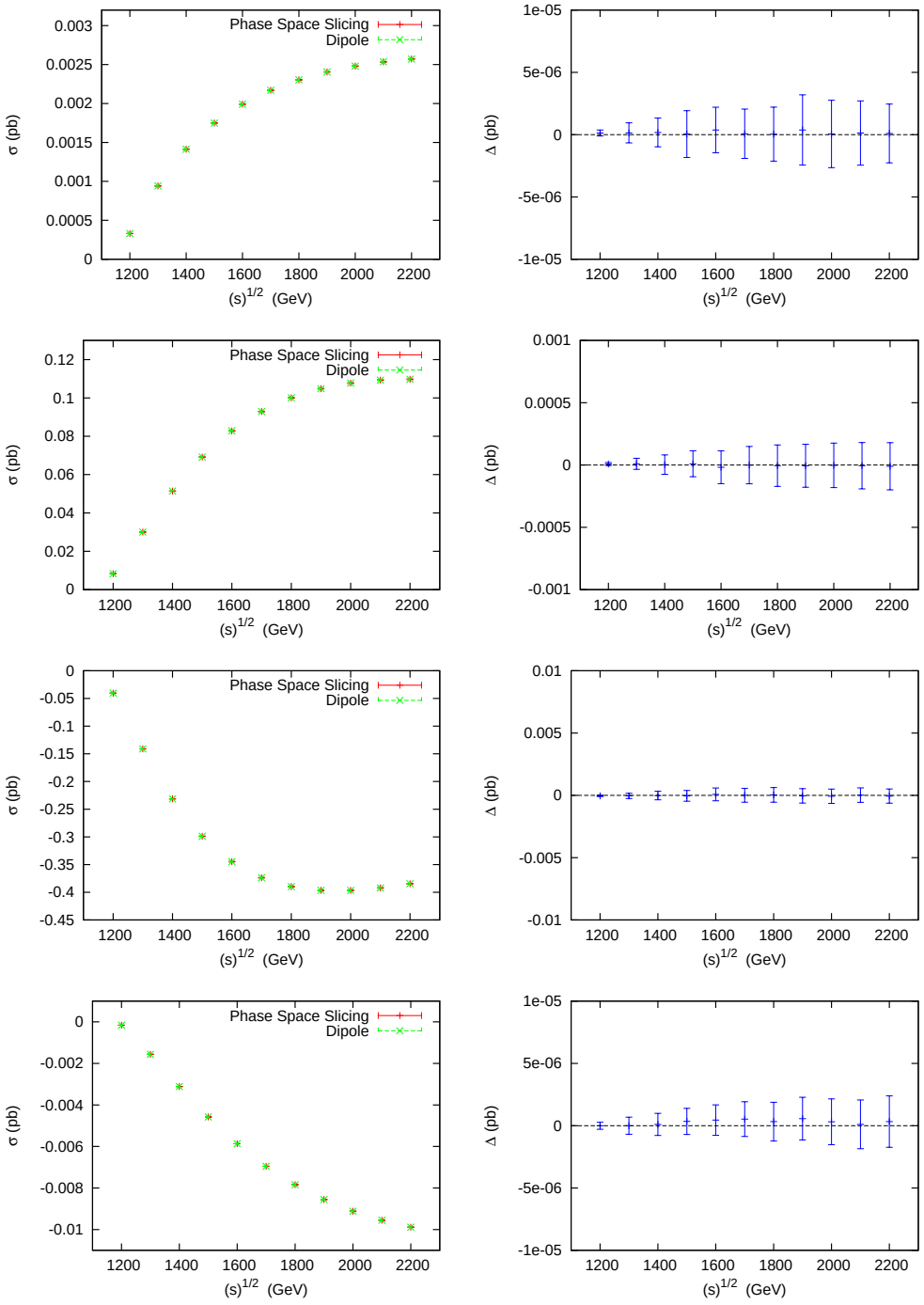

Figure 6.1: Lowest order partonic cross sections for the process $gg \to \tilde{u}_L \tilde{u}_L^* \gamma$ (first panel), $u\overline{u} \to \tilde{u}_L \tilde{u}_L^* \gamma$ (second panel), $u\overline{u} \to \tilde{u}_L \tilde{u}_L^* g$ (third panel) and $ug \to \tilde{u}_L \tilde{u}_L^* u$ (fourth panel), computed with the two different methods. Δ is defined as $\Delta = \sigma^{\text{Slicing}} - \sigma^{\text{Dipole}}$. The error bars represent the integration uncertainty. The SUSY parameters are those of the SPS1a′ point [203].

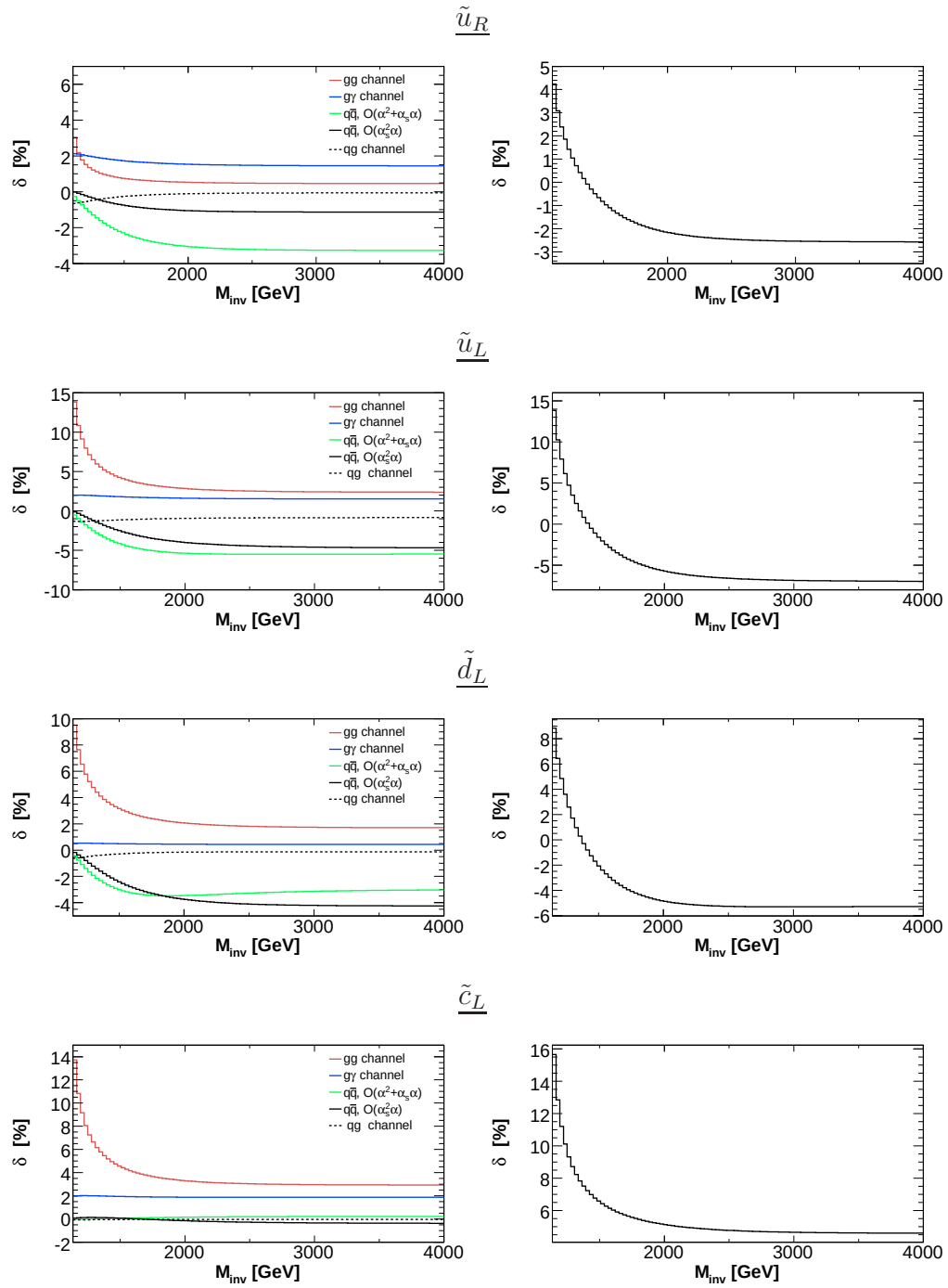

Figure 6.2: Cumulative invariant mass distribution for different species of squark pairs, defined as the cross section integrated up to M_{inv} of the invariant mass of the squark-anti-squark pair. The left panels show the relative contributions from the various channels, the right ones show the complete EW contribution. The SUSY parameter point corresponds to SPS1a′.

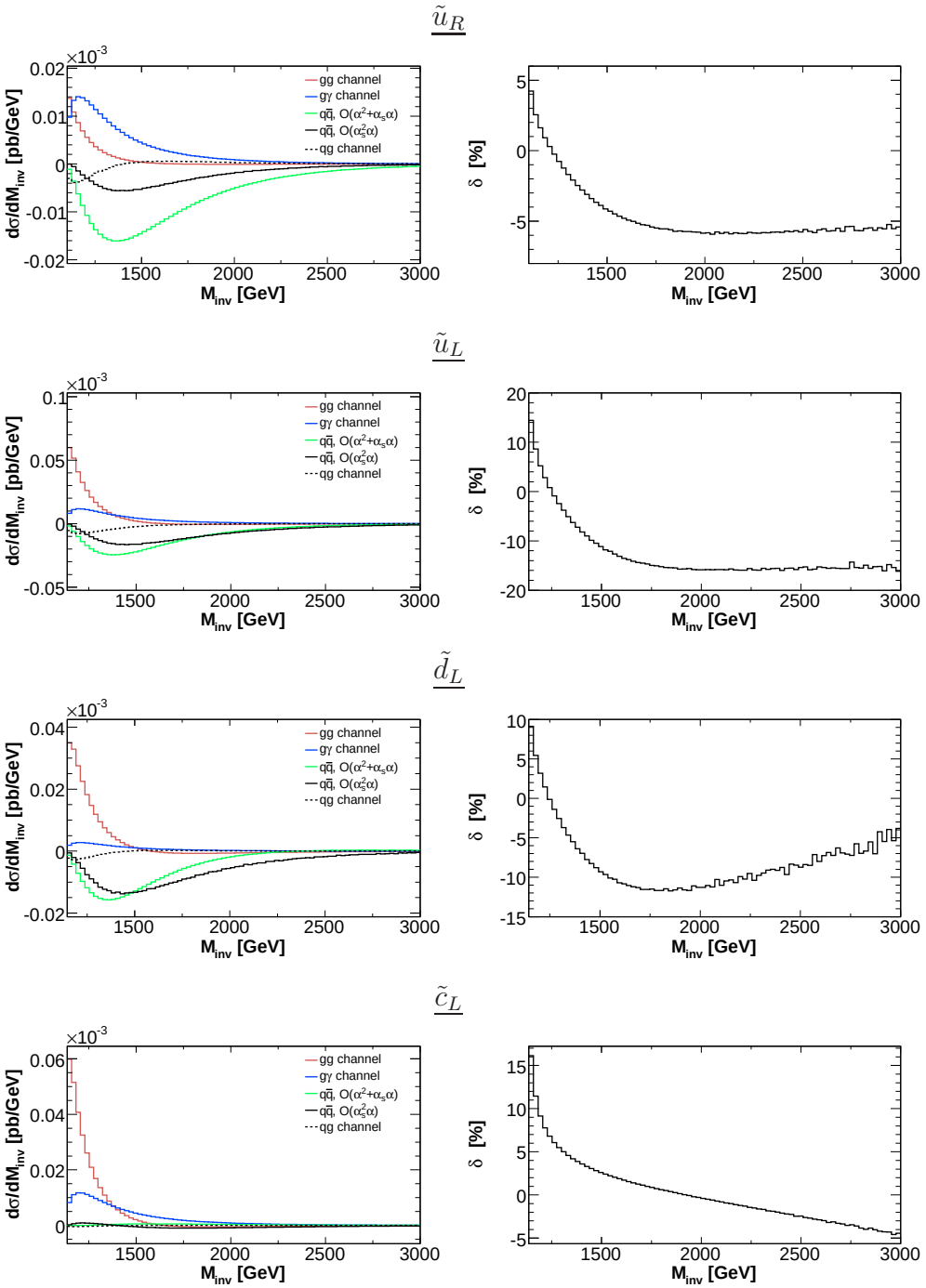

Figure 6.3: Invariant mass distribution for different species of squark pairs, for the SUSY parameter point corresponding to SPS1a′. The left panels show the contributions from the various channels, the right ones show the complete EW contribution.

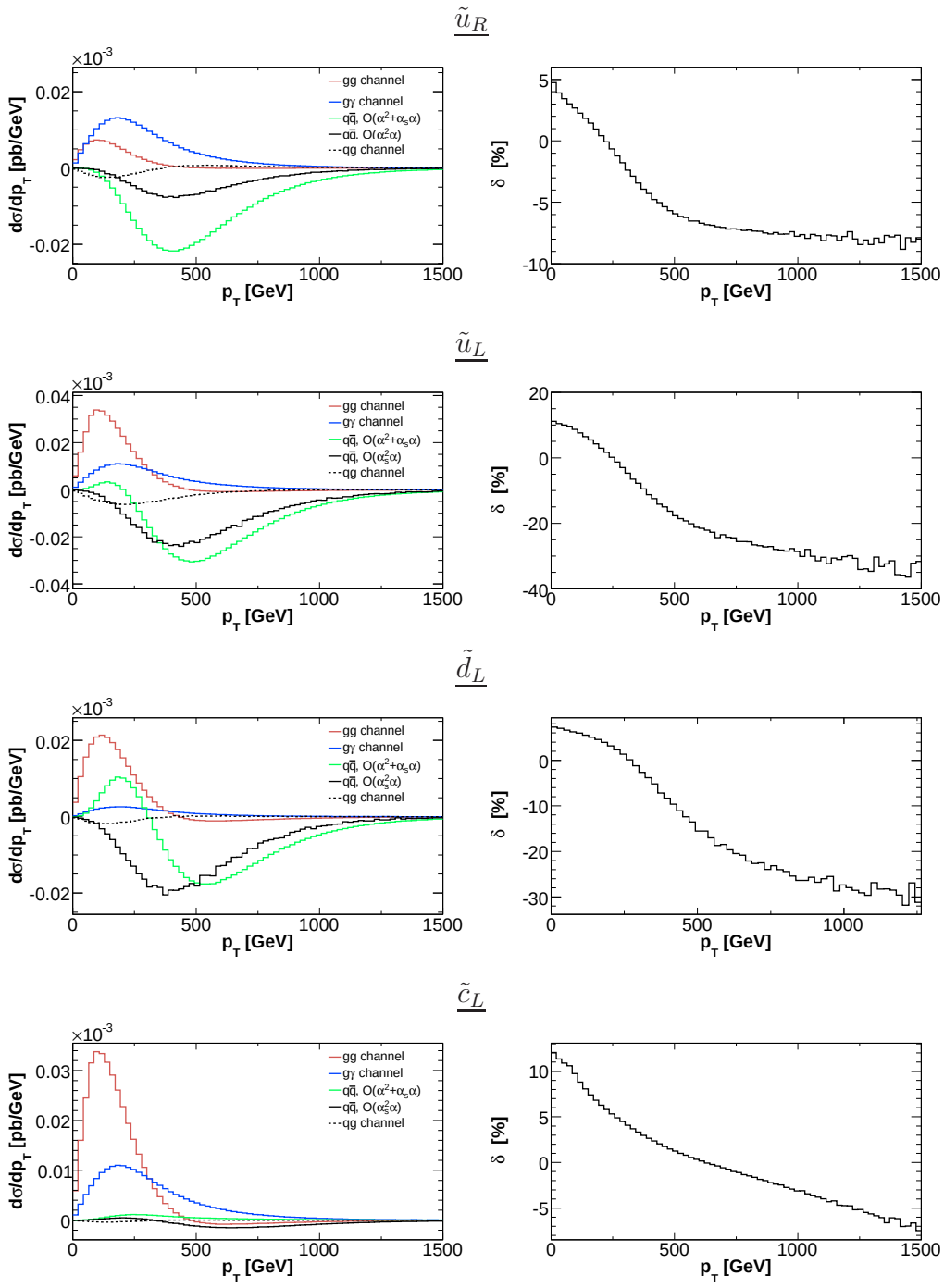

Figure 6.4: Transverse momentum distribution for different species of squark pairs. Notations and input parameters as in Fig. 6.3.

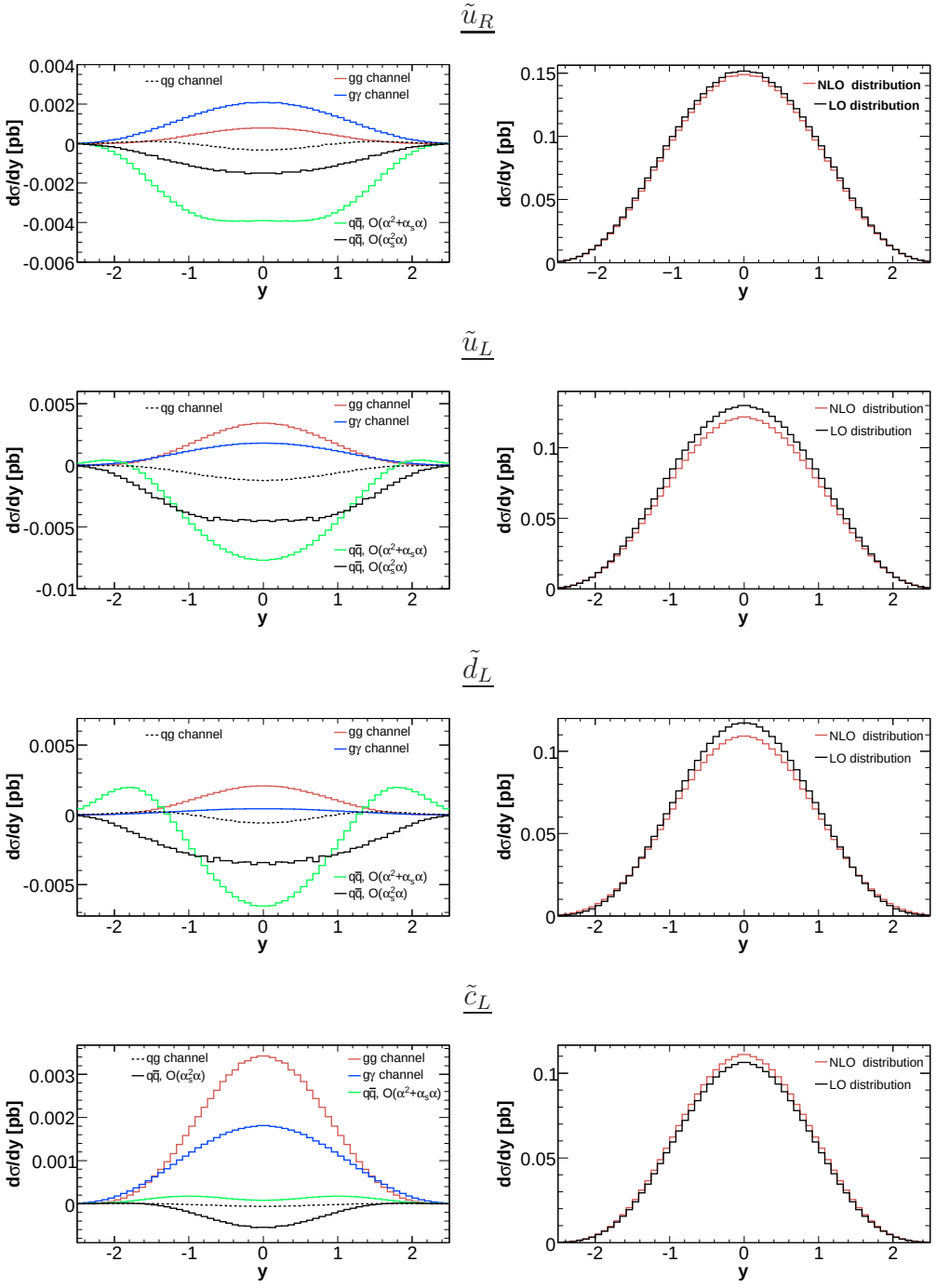

Figure 6.5: Rapidity distribution for different species of squark pairs at LO and NLO (right columns).The left panels show the EW contribution from the various channels. The SUSY parameter point corresponds to SPS1a′.

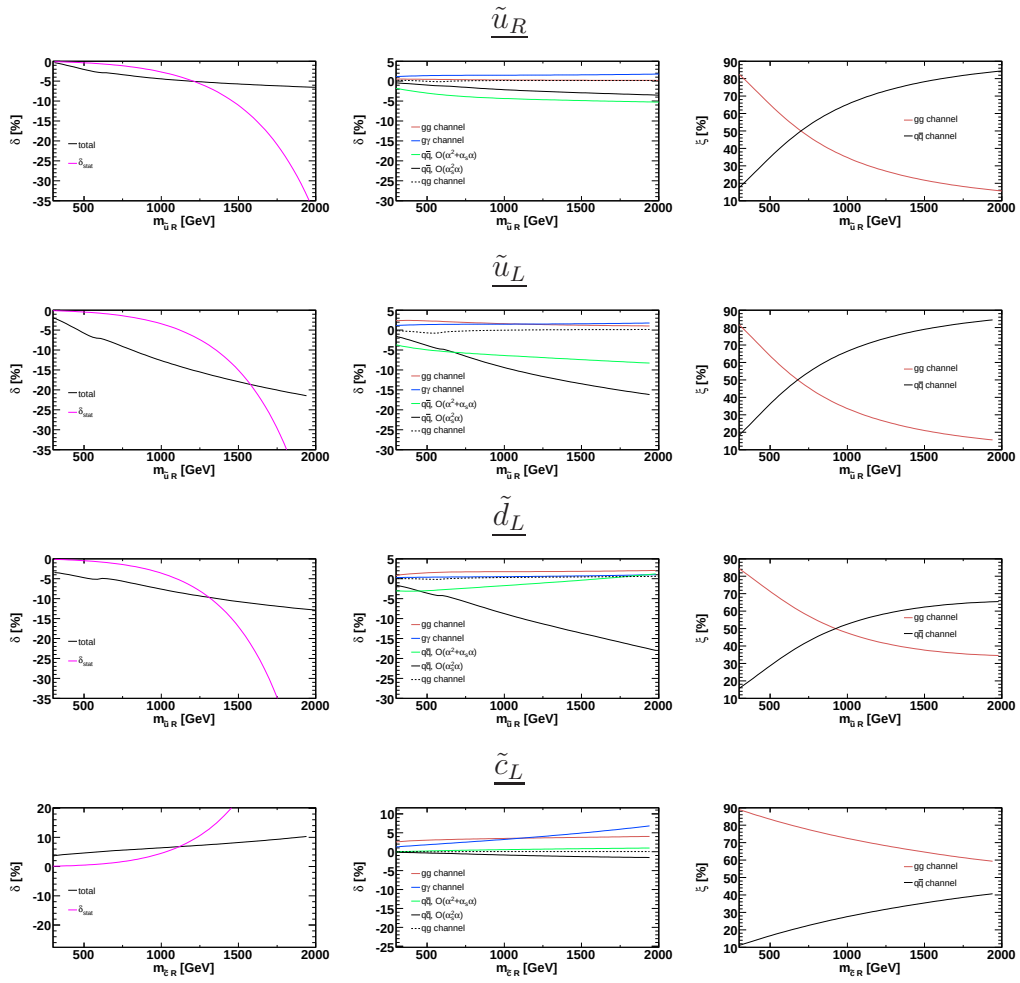

Figure 6.6: Squark-mass dependence of the EW contributions. Total EW contribution (left), individual contributions from the various channels (central). The panels in the right column show the relative yield of the two channels that contribute at LO.

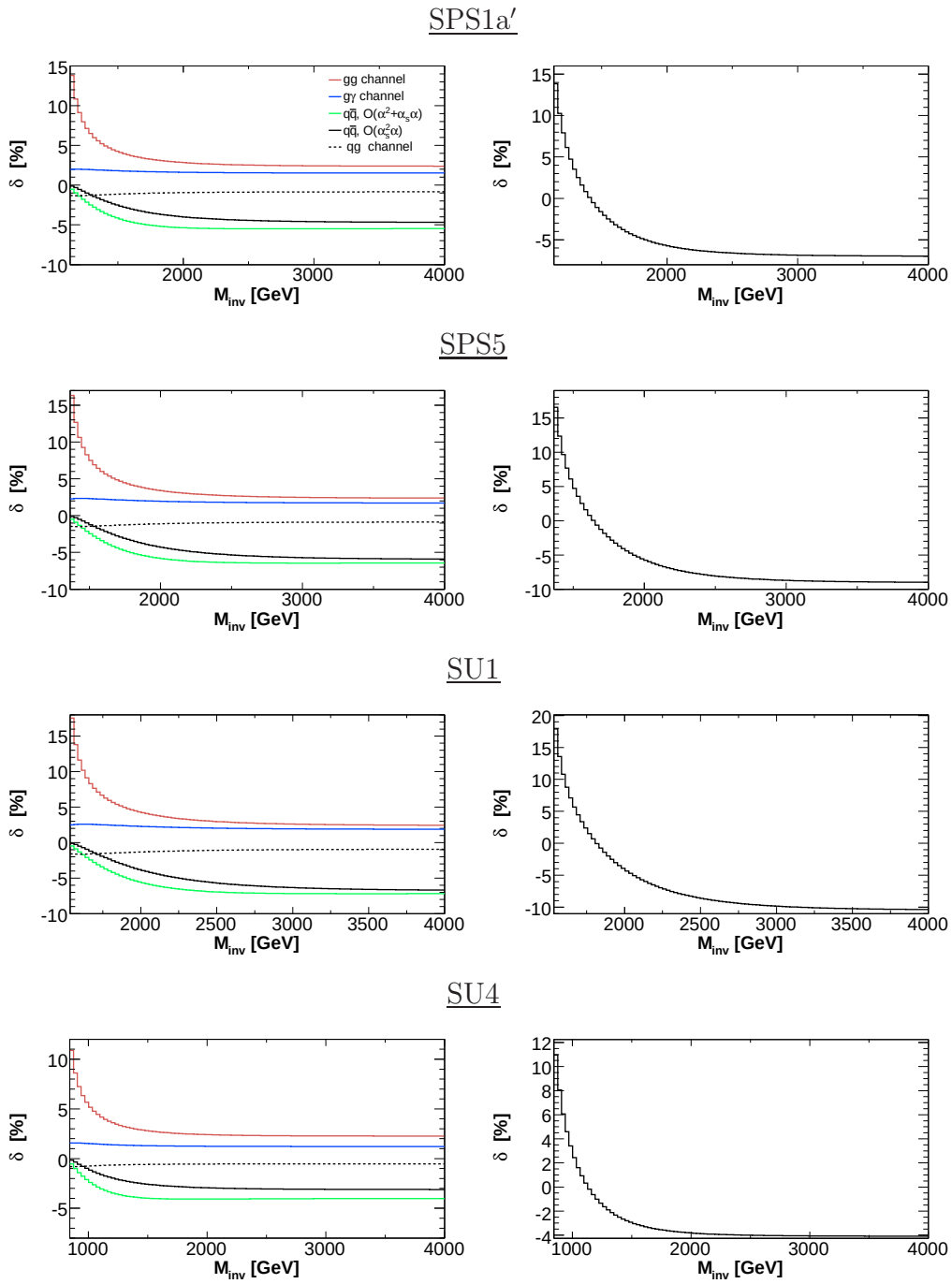

Figure 6.7: Cumulative invariant mass distribution for $PP \to \tilde{u}_L \tilde{u}_L^* X$ in different SUSY scenarios. Notations as in Fig. 6.2.

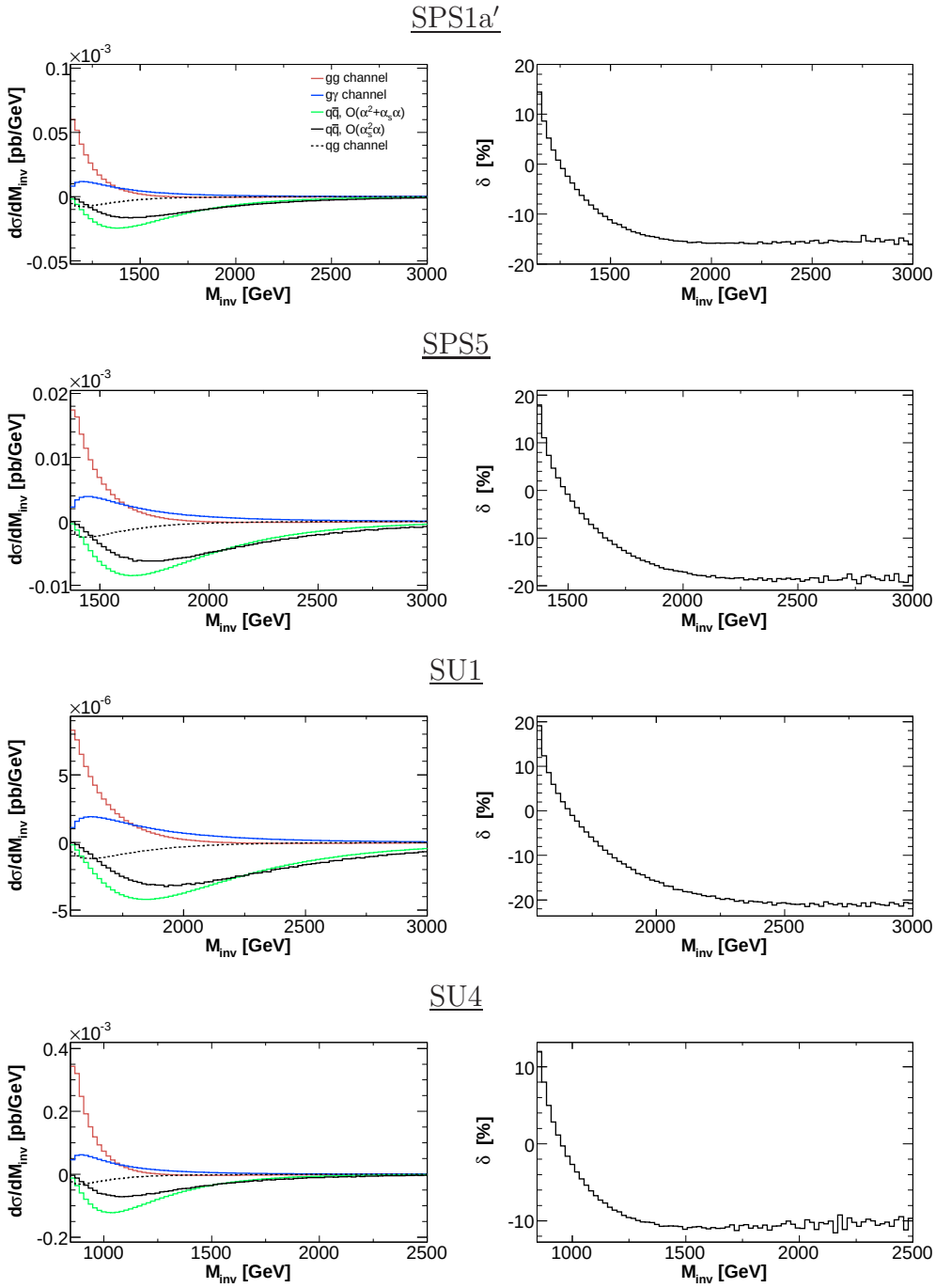

Figure 6.8: Invariant mass distribution for $PP \to \tilde{u}_L \tilde{u}_L^* X$ in different SUSY scenarios. Notations as in Fig. 6.3.

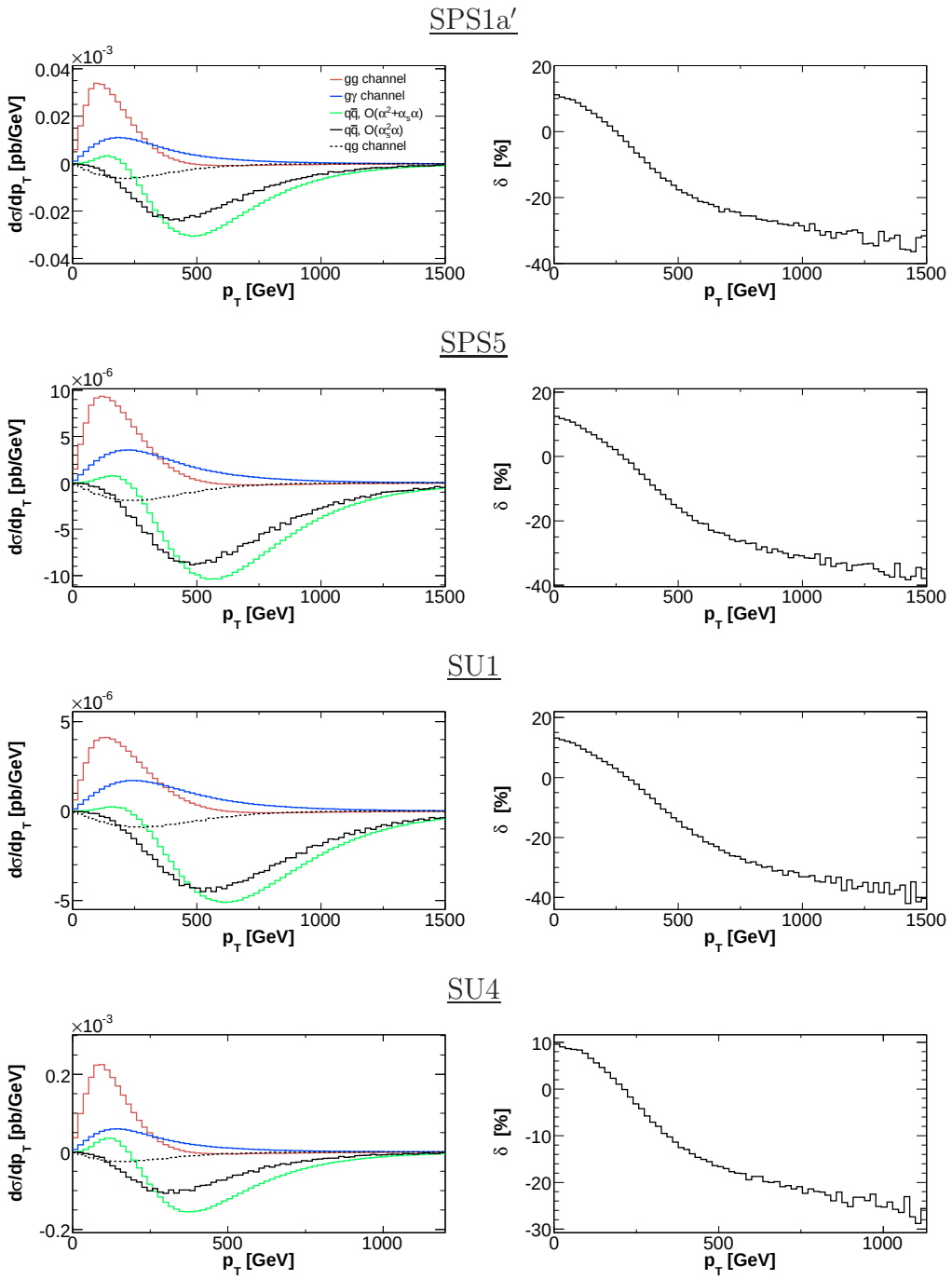

Figure 6.9: Transverse momentum distribution of the process $PP \to \tilde{u}_L \tilde{u}_L^* X$ in different SUSY scenarios. Notations as in Fig. 6.4.

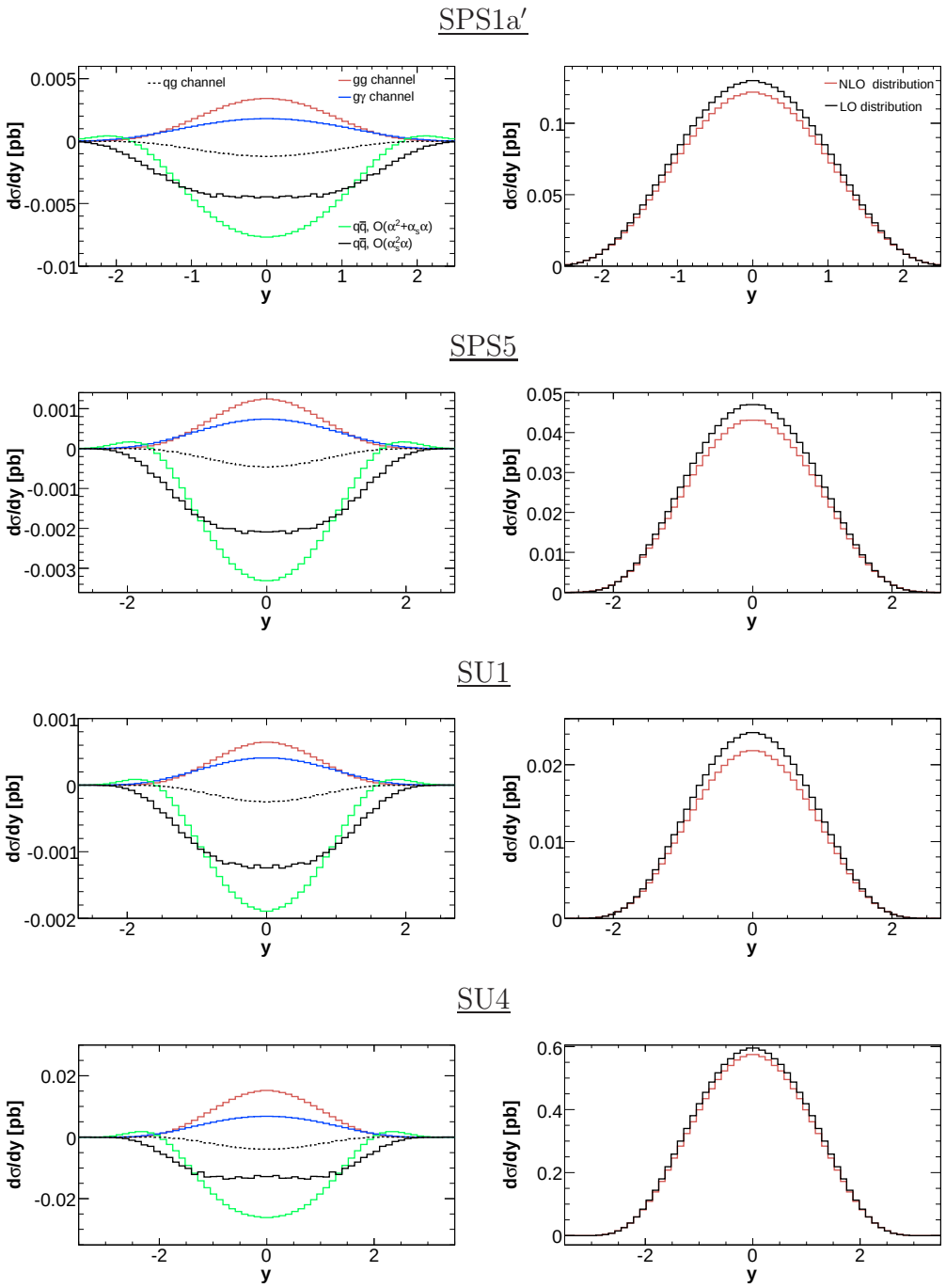

Figure 6.10: Rapidity distribution of the process $PP \to \tilde{u}_L \tilde{u}_L^* X$ in different SUSY scenarios. Notations as in Fig. 6.5.

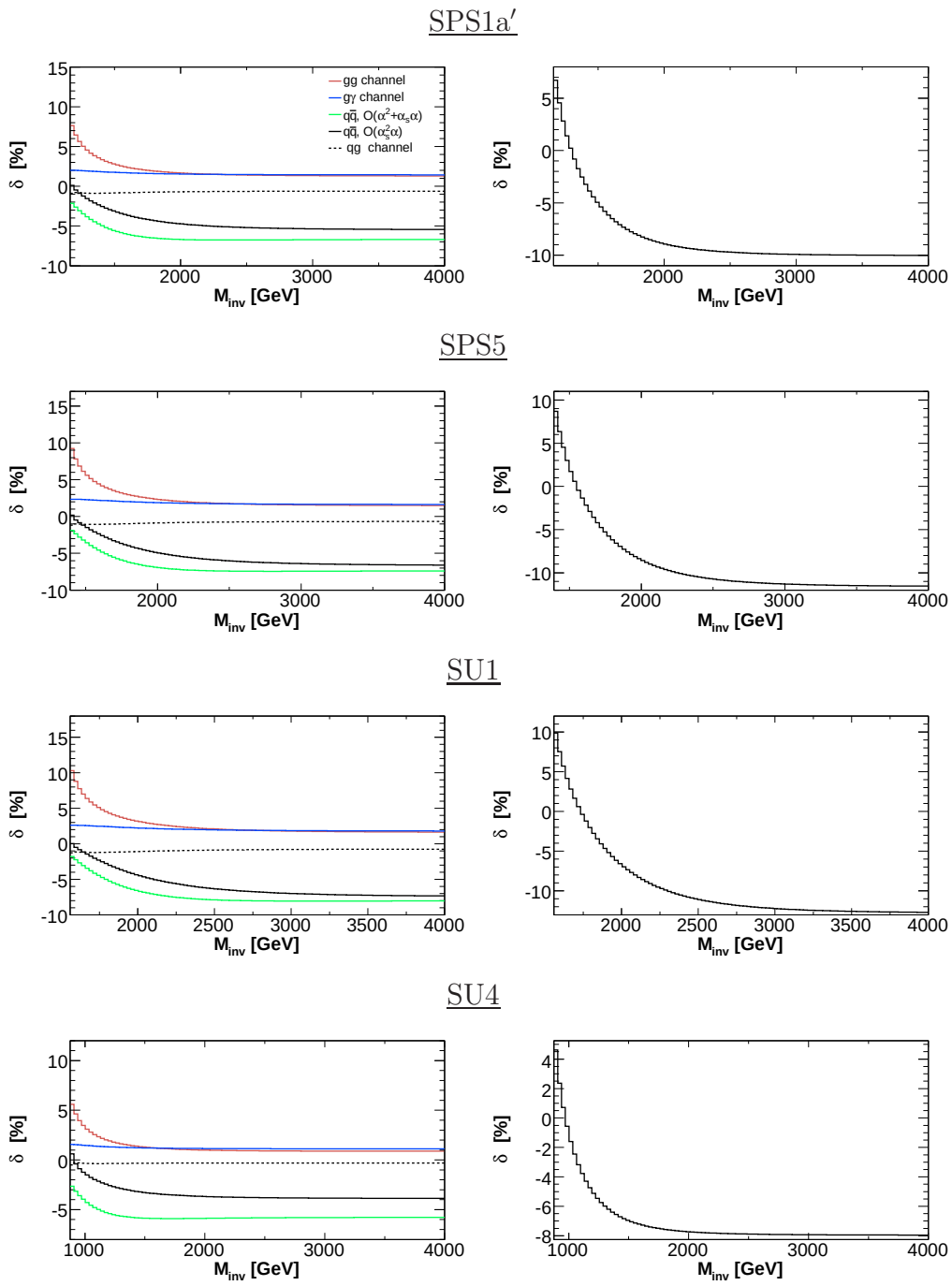

Figure 6.11: Same as Fig. 6.7, but with the kinematical cuts defined in section 6.3.2.

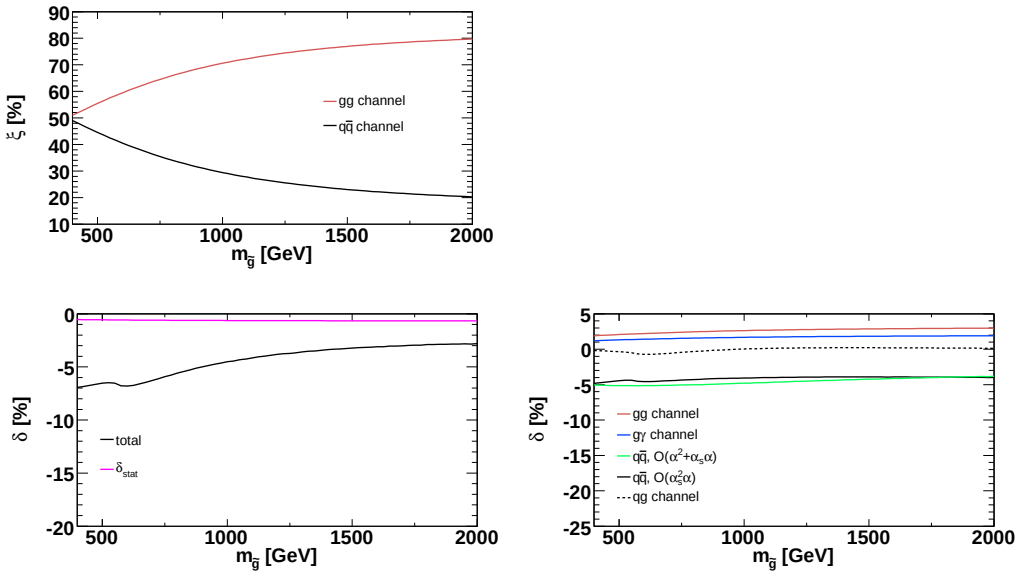

Figure 6.12: Gluino mass dependence of the total (lower left) and of the individual (lower right) EW contributions to the total cross section for $PP \to \tilde{u}_L \tilde{u}_L^* X$. The upper panel shows the relative yield of the two channels that contribute at LO.

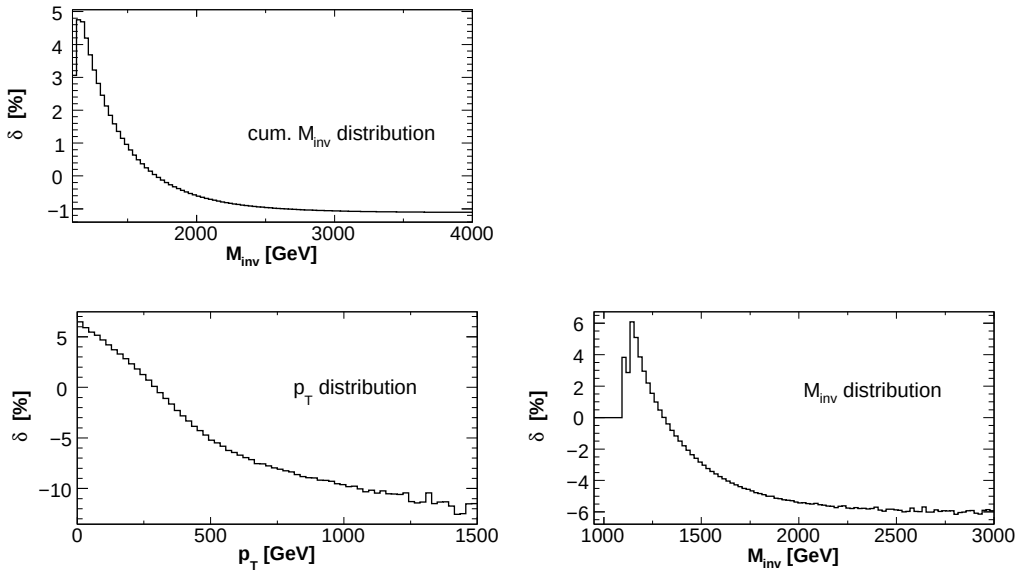

Figure 6.13: Inclusive squark-anti–squark production in the SPS1a′ scenario. The relative yield of the EW contributions to the cumulative invariant mass, transverse momentum and invariant mass distributions is shown.

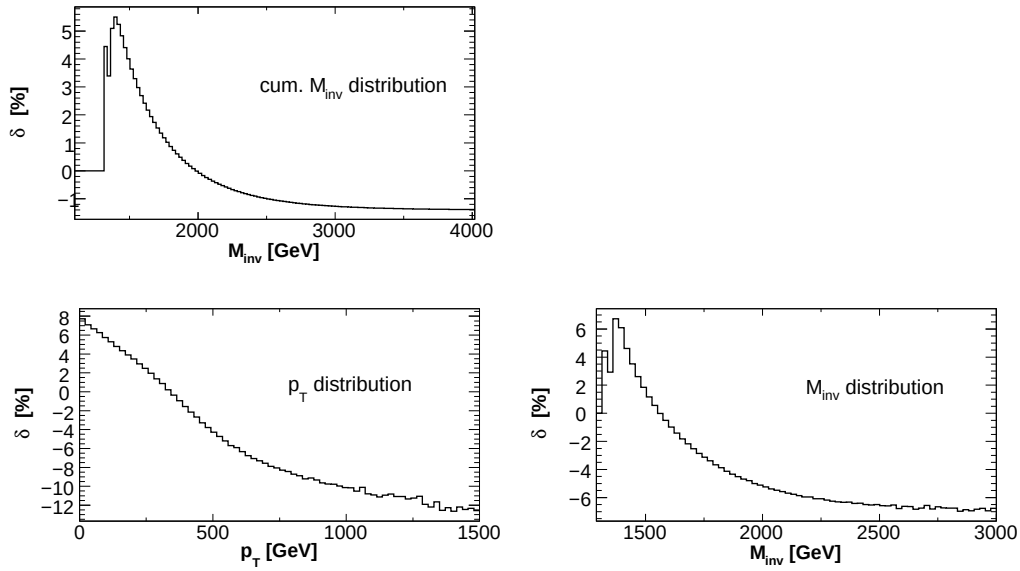

Figure 6.14: Same as Fig. 6.13, but considering the SPS5 scenario.

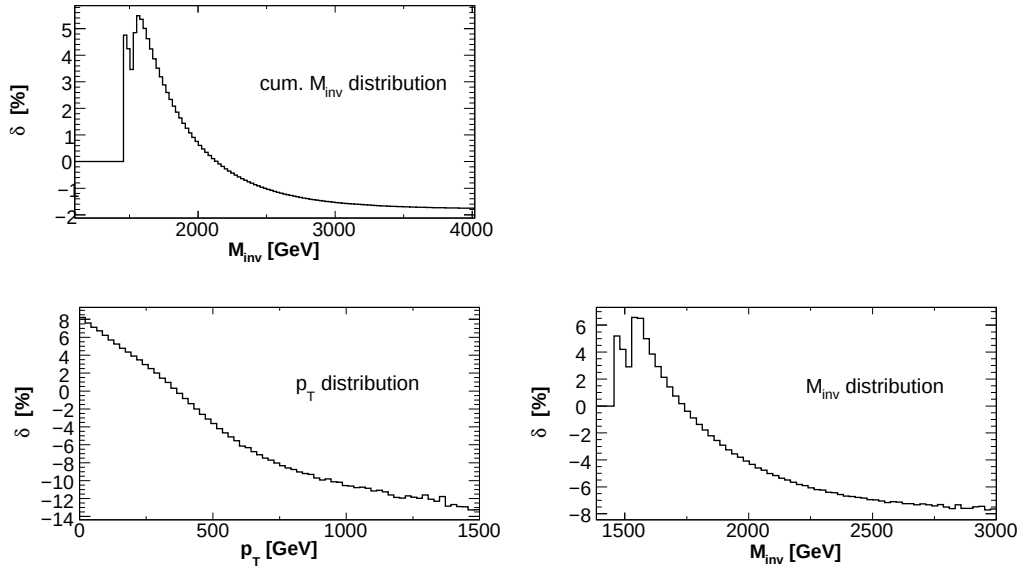

Figure 6.15: Same as Fig. 6.13, but considering the SU1 scenario.

Chapter 7

Squark-gluino production

In this chapter, we consider the associated production of squarks and gluinos and study the EW contribution. This channel is the main production mechanism of SUSY colored particles if $m_{\tilde{q}} \simeq m_{\tilde{g}} \sim 1$ TeV. As already mentioned in section 4.1, we restrict the discussion to (anti-)squarks of the first two generations,

$$PP \to \tilde{g}\tilde{Q}_a X, \quad PP \to \tilde{g}\tilde{Q}_a^* X, \qquad (Q \neq \tilde{t}, \tilde{b}). \tag{7.1}$$

The production of $\tilde{t}\,\tilde{g}$ is suppressed due to the vanishing parton density of top-quarks inside protons, while $\tilde{b}\,\tilde{g}$ production is suppressed by the bottom-quark parton distribution function. Furthermore, bottom-squarks (resp. their decay products) will be experimentally distinguishable from squarks of the first two generations [112, 114, 223]. The structure of the chapter is as follows. In section 7.1, we recall the tree-level cross sections at the partonic and the hadronic level and we introduce some basic notations. The NLO EW contributions are discussed in detail in section 7.2. In section 7.3, we present numerical results for the hadronic cross sections and distributions for squark–gluino production at the LHC.

7.1 Tree-level contributions

At hadron colliders, the tree-level contributions to the production of a gluino in association with an (anti-)squark $\tilde{Q}_a^{(*)}$ are $\mathcal{O}(\alpha_s^2)$ and $\mathcal{O}(\alpha_s\alpha)$. In the following subsections we will briefly describe such contributions introducing some basic notation.

7.1.1 Leading order contributions

The LO contribution to the processes (7.1) is QCD based and is related to the following partonic processes

$$g(p_1)\, Q(p_2) \;\rightarrow\; \tilde{g}(k_1)\, \tilde{Q}_a(k_2), \qquad g(p_1)\, \bar{Q}(p_2) \;\rightarrow\; \tilde{g}(k_1)\, \tilde{Q}_a^*(k_2), \tag{7.2}$$

via the usual convolutions

$$\begin{aligned} d\sigma^{\rm LO}_{PP\to\tilde{g}\tilde{Q}_a}(S) &= \int_{\tau_0}^1 d\tau\, \frac{dL_{gQ}}{d\tau}\, d\sigma^{2,0}_{gQ\to\tilde{g}\tilde{Q}_a}(s), \\ d\sigma^{\rm LO}_{PP\to\tilde{g}\tilde{Q}_a^*}(S) &= \int_{\tau_0}^1 d\tau\, \frac{dL_{g\bar{Q}}}{d\tau}\, d\sigma^{2,0}_{g\bar{Q}\to\tilde{g}\tilde{Q}_a^*}(s). \end{aligned} \tag{7.3}$$

S and $s = \tau S$, are the hadronic and partonic center-of-mass energy squared respectively. The production threshold is $\tau_0 = (m_{\tilde{g}} + m_{\tilde{Q}})^2/S$. The partonic luminosity is defined in Eq. (5.4). Due to CP symmetry the unpolarized cross sections $d\sigma^{2,0}_{gQ\to\tilde{g}\tilde{Q}_a}$ and $d\sigma^{2,0}_{g\overline{Q}\to\tilde{g}\tilde{Q}_a^*}$ are equal, therefore in the following we will refer to the first partonic process only.

As in the previous chapter, we will distinguish squarks with same flavor by means of their chiralities, since the quarks of the first two generations are gauge eigenstates. Furthermore, the masses of the squarks of the second generation coincide with those of the squarks in the first generation.

We parametrize the cross sections in terms of the Mandelstam variables defined in Eq. (5.9). In this case $u = m_{\tilde{g}}^2 + m_{\tilde{Q},a}^2 - s - t$. The differential partonic cross section for the process $gQ \to \tilde{g}\tilde{Q}_a$, can be obtained from the diagrams shown in Fig. H.1 of appendix H,

$$d\sigma^{2,0}_{gQ\to\tilde{g}\tilde{Q}_a}(s) = \frac{1}{96}\frac{dt}{16\pi s^2} \sum \left|\mathcal{M}^{1,0}_{gQ\to\tilde{g}\tilde{Q}_a}\right|^2 . \tag{7.4}$$

The squared spin- and color-summed lowest-order matrix element can be written as follows [15],

$$\begin{aligned} \sum \left|\mathcal{M}^{1,0}_{gQ\to\tilde{g}\tilde{Q}_a}\right|^2 = 128\alpha_s^2\pi^2 &\left[3\left(1 - 2\frac{s\,u_{\tilde{Q}_a}}{t_{\tilde{g}}^2}\right) - \frac{1}{3}\right] \\ &\times \left[-\frac{t_{\tilde{g}}}{s} + \frac{2(m_{\tilde{g}}^2 - m_{\tilde{Q}_a}^2)t_{\tilde{g}}}{s u_{\tilde{Q}_a}}\left(1 + \frac{m_{\tilde{g}}^2}{t_{\tilde{g}}} + \frac{m_{\tilde{Q}_a}^2}{u_{\tilde{Q}_a}}\right)\right]. \end{aligned} \tag{7.5}$$

7.1.2 Photon induced gluino–squark production

As an independent production channel, we also consider the photon–gluon induced subclass of gluino–(anti-)squark production, as shown in Fig. H.2 of appendix H. The contribution of this channel reads

$$\begin{aligned} d\sigma^{\text{LO EW}}_{PP\to\tilde{g}\tilde{Q}_a}(S) &= \int_{\tau_0}^1 d\tau\, \frac{dL_{\gamma Q}}{d\tau}\, d\sigma^{1,1}_{\gamma Q\to\tilde{g}\tilde{Q}_a}(s), \\ d\sigma^{\text{LO EW}}_{PP\to\tilde{g}\tilde{Q}^*_a}(S) &= \int_{\tau_0}^1 d\tau\, \frac{dL_{\gamma \overline{Q}}}{d\tau}\, d\sigma^{1,1}_{\gamma \overline{Q}\to\tilde{g}\tilde{Q}^*_a}(s). \end{aligned} \tag{7.6}$$

Photon-induced processes do not contribute at leading order at the hadronic level, owing to the non-existence of a photon distribution inside the proton. But the inclusion of NLO QED effects in the evolution of the PDFs leads to a non-zero photon density in the proton and thus to non-zero hadronic contributions. Therefore the diagrams in Fig. H.2 contribute at tree-level to the same final state and can be important.

The partonic differential cross section for the photon induced gluino–squark production reads

$$d\sigma^{1,1}_{\gamma Q\to\tilde{g}\tilde{Q}_a}(s) = \frac{1}{12}\frac{dt}{16\pi s^2}\sum\left|\mathcal{M}^{1/2,1/2}_{\gamma Q\to\tilde{g}\tilde{Q}_a}\right|^2, \tag{7.7}$$

$$\sum\left|\mathcal{M}^{1/2,1/2}_{\gamma Q\to\tilde{g}\tilde{Q}_a}\right|^2 = 256\alpha_s\alpha\pi^2\, e_Q^2\left[-\frac{t_{\tilde{g}}}{s} + \frac{2(m^2_{\tilde{g}} - m^2_{\tilde{Q}_a})t_{\tilde{g}}}{s u_{\tilde{Q}_a}}\left(1 + \frac{m^2_{\tilde{g}}}{t_{\tilde{g}}} + \frac{m^2_{\tilde{Q}_a}}{u_{\tilde{Q}_a}}\right)\right],$$

expressed in terms of the Mandelstam variables (5.9). The partonic differential cross section for the photon induced gluino–anti-squark is related to the differential cross section (7.7) via charge conjugation.

7.2 $\mathcal{O}(\alpha_s^2\alpha)$ contributions

In contrast to squark pair production, which allow for $q\bar{q}$ initial states at LO, gluino–(anti-)squark final states cannot be produced at $\mathcal{O}(\alpha^2)$. At EW NLO, gluino–squark production comprises virtual corrections and real photon radiation at $\mathcal{O}(\alpha_s^2\alpha)$. Further $\mathcal{O}(\alpha_s^2\alpha)$ contributions arise from interference of EW and QCD real quark radiation diagrams.

The complete EW contribution to the hadronic cross section for gluino–squark production is obtained from the corresponding partonic cross sections

by convolution and summation as follows,

$$d\sigma^{\text{NLO EW}}_{PP\to\tilde{g}\tilde{Q}_a X}(S) = \int_{\tau_0}^1 d\tau \left\{ \frac{dL_{gQ}}{d\tau} \left[d\sigma^{2,1}_{gQ\to\tilde{g}\tilde{Q}_a}(s) + d\sigma^{2,1}_{gQ\to\tilde{g}\tilde{Q}_a\gamma}(s) \right] \right.$$
$$+ \sum_q \left[\frac{dL_{Qq}}{d\tau}\, d\sigma^{2,1}_{Qq\to\tilde{g}\tilde{Q}_a q}(s) + \frac{dL_{Q\bar{q}}}{d\tau}\, d\sigma^{2,1}_{Q\bar{q}\to\tilde{g}\tilde{Q}_a\bar{q}}(s) \right] \quad (7.8)$$
$$\left. + \sum_{q\neq Q} \frac{dL_{q\bar{q}}}{d\tau}\, d\sigma^{2,1}_{q\bar{q}\to\tilde{g}\tilde{Q}_a\bar{Q}}(s) \right\}.$$

The respective parton luminosities refer to (5.4). Owing to charge conservation, photon-gluon induced partonic processes are possible only in combination with an additional quark in the final states,

$$g(p_1)\ \gamma(p_2)\ \to\ \tilde{g}(k_1)\ \tilde{Q}_a(k_2)\ \bar{Q}(k_3). \quad (7.9)$$

Since these processes are suppressed by the photon PDF with respect to the other bremsstrahlung processes in Eq. (7.8), we neglect them. Concerning the EW NLO contributions to gluino–anti-squark production they read

$$d\sigma^{\text{NLO EW}}_{PP\to\tilde{g}\tilde{Q}_a^* X}(S) = \int_{\tau_0}^1 d\tau \left\{ \frac{dL_{g\bar{Q}}}{d\tau} \left[d\sigma^{2,1}_{g\bar{Q}\to\tilde{g}\tilde{Q}_a^*}(s) + d\sigma^{2,1}_{g\bar{Q}\to\tilde{g}\tilde{Q}_a^*\gamma}(s) \right] \right.$$
$$+ \sum_q \left[\frac{dL_{\bar{Q}\bar{q}}}{d\tau}\, d\sigma^{2,1}_{\bar{Q}\bar{q}\to\tilde{g}\tilde{Q}_a^*\bar{q}}(s) + \frac{dL_{\bar{Q}q}}{d\tau}\, d\sigma^{2,1}_{\bar{Q}q\to\tilde{g}\tilde{Q}_a^* q}(s) \right] \quad (7.10)$$
$$\left. + \sum_{q\neq Q} \frac{dL_{q\bar{q}}}{d\tau}\, d\sigma^{2,1}_{q\bar{q}\to\tilde{g}\tilde{Q}_a^* Q}(s) \right\}.$$

In the following subsections we will discuss the partonic cross sections appearing Eq. (7.8). Indeed, the partonic cross sections in Eq. (7.10) are related the aforementioned ones by charge conjugation. `FeynArts` [195, 196], `FormCalc` and `LoopTools` [177, 178] are used for the treatment of the Feynman diagrams and of the corresponding amplitudes.

7.2.1 Virtual corrections

The first class of NLO contributions of EW origin are the virtual corrections,

$$d\sigma^{2,1}_{gQ\to\tilde{g}\tilde{Q}_a}(s) = \frac{1}{96}\frac{dt}{16\pi s^2} \sum 2\,\mathfrak{Re}\left\{ \mathcal{M}^{1,0}_{gQ\to\tilde{g}\tilde{Q}_a}\, \mathcal{M}^{1,1*}_{gQ\to\tilde{g}\tilde{Q}_a} \right\}, \quad (7.11)$$

where $\mathcal{M}^{1,1}_{gQ\to\tilde{g}\tilde{Q}_a}$ is the one-loop amplitude with EW insertions in the QCD-based gQ diagrams, leading to the diagrams shown in the appendix H, Fig. H.3 and Fig. H.4. The renormalization of the quark and squark sectors is performed in the schemes described in chapter 4. In the limit of no L–R mixing, the independent parameters for a given squark isospin doublet are the masses of the two up-type squarks $\tilde{u}_{L,R}$ and the mass of the right-handed down-type squark $\tilde{d}_R$ (see also the discussion in section 4.2.2).

7.2.2 Real photon radiation

The tree-level photon bremsstrahlung process reads, *c.f.* the diagrams in Fig. H.5 of the appendix H,

$$g(p_1)\; q(p_2) \;\to\; \tilde{g}(k_1)\; \tilde{Q}_a(k_2)\; \gamma(k_3). \tag{7.12}$$

The integral over the photon phase space is divergent in the soft region and in the collinear region. The extraction of such singularities has been performed using phase space slicing and dipole subtraction methods. The comparison between the two methods is illustrated in Fig. 7.1; the two methods are in mutual numerical agreement.

7.2.3 Real quark radiation

For each production process of a gluino in association with a squark $\tilde{Q}_a$ of a given chirality and flavor, there are eleven (quark–quark or quark–anti-quark induced) subprocesses with an additional real quark or anti-quark in the final state,

$$\begin{aligned}
Q(p_1)\; q(p_2) &\;\to\; \tilde{g}(k_1)\; \tilde{Q}_a(k_2)\; q(k_3), \\
Q(p_1)\; \bar{q}(p_2) &\;\to\; \tilde{g}(k_1)\; \tilde{Q}_a(k_2)\; \bar{q}(k_3), \qquad \text{with} \quad q \neq Q, \\
q(p_1)\; \bar{q}(p_2) &\;\to\; \tilde{g}(k_1)\; \tilde{Q}_a(k_2)\; \bar{Q}(k_3),
\end{aligned} \tag{7.13}$$

where $q = u, d, c, s$. These tree-level processes give an IR and collinear finite contribution of order $\mathcal{O}(\alpha_s^2\alpha)$ through the interference between the EW diagrams in Fig. H.6a and the QCD diagrams in Fig. H.6b and between those in Fig. H.7a and Fig. H.7b.

In specific SUSY scenarios, internal gauginos or squarks can be on-shell. The poles are regularized introducing the particle width in the corresponding propagator. If both EW and QCD diagrams provide intermediate on-shell squarks, the non-vanishing interference contribution corresponds to the production of a squark pair at order $\mathcal{O}(\alpha_s\alpha)$ with subsequent decay of one of

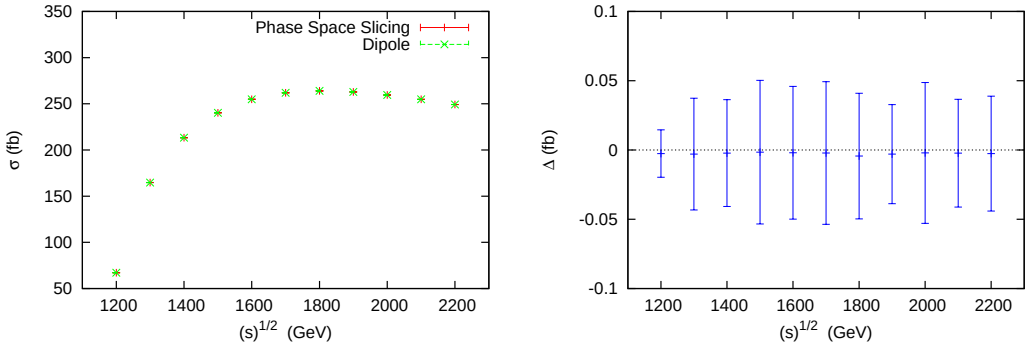

Figure 7.1: Left: Comparison of the lowest order partonic cross section for the process $gu \to \tilde{g}\,\tilde{u}_L\gamma$ using the phase space slicing or dipole subtraction method. Right: Difference $\Delta = \sigma^{\rm Dipole} - \sigma^{\rm Slicing}$ as a function of the partonic energy. The error bars represent the sum under quadrature of the integration uncertainties on $\sigma^{\rm Dipole}$ and $\sigma^{\rm Slicing}$. The SUSY parameters are those of the SPS1a′ point [203].

the two squarks,

$$\begin{aligned} Q\ q &\to \tilde{Q}_a\ \tilde{q}, \quad \tilde{q} \to \tilde{g}\ q\,, \\ q\ \bar{q} &\to \tilde{Q}_a\ \tilde{Q}_a^*, \quad \tilde{Q}_a^* \to \tilde{g}\ \bar{Q}\,. \end{aligned} \tag{7.14}$$

To avoid double counting, these resonating squark contributions have to be subtracted as explained in section 5.2.3. The pole term has thereby been isolated in the narrow width approximation.

7.2.4 Factorization of initial state singularities

In the case of squark-gluino production, the term $\mathcal{R}(x_1, x_2, s)$ in Eq. (4.8) arises from the $\mathcal{O}(\alpha)$ factorization of the quark PDF. The integral of $\mathcal{R}(x_1, x_2, s)$ over x_1 and x_2 has to be added to Eq. (7.8). Eq. (5.18) allow to trade the integral of $\mathcal{R}(x_1, x_2, s)$ with the integral over τ of the function $\overline{\mathcal{R}}(\tau, s)$ defined as

$$\overline{\mathcal{R}}(\tau, s) \;=\; -\frac{\alpha}{2\pi} e_Q^2 \frac{dL_{gQ}}{d\tau}(\tau) \int_{z_0}^1 d\tau\ [\mathcal{H}_Q^{(1)} + h^{(1)}]_+ d\sigma^{2,0}_{gQ\to\tilde{g}\tilde{Q}_a}(zs), \tag{7.15}$$

with $z_0 = (m_{\tilde{g}} + m_{\tilde{Q}_a})^2/s$. The functions $\mathcal{H}^{(1)}$ and $h^{(1)}$ are defined in Eq. (4.13). Since we are neglecting the process (7.9), terms proportional to the $g\gamma$ luminosity appearing $\overline{\mathcal{R}}$ have been neglected as well. $\mathcal{O}(\alpha)$ factorization is performed in the DIS scheme, since we use the set MRST2004qed [204]

for the parton distributions. $\overline{\mathcal{R}}$ for the process $PP \to \tilde{g}\tilde{Q}_a^*$ can be read from Eq. (7.15) substituting the gQ luminosity with the $g\bar{Q}$ one, and $d\sigma^{2,0}_{gQ\to\tilde{g}\tilde{Q}_a}$ with $d\sigma^{2,0}_{g\bar{Q}\to\tilde{g}\tilde{Q}_a^*}$. For factorization and renormalization, a common scale has been chosen, $\mu_F = \mu_R = (m_{\tilde{g}} + m_{\tilde{Q}_a})/2$.

7.3 Numerical Results

We illustrate the numerical results considering the benchmark scenarios SPS1a′, SPS5 and SU1, already introduced in the previous chapter. The corresponding input parameters are listed in Sec. 6.3. We present results both for the production of left- and right-handed, up- and down-type squarks separately and for the inclusive production.

We introduce the following conventions for the discussion of the results.

- We analyze the three different gauge invariant, IR and collinear finite subsets of the EW contributions described in the previous section. The sum of the virtual corrections and of the $\mathcal{O}(\alpha_s^2\alpha)$ contributions to real photon radiation will be labeled as "gQ channel contributions". The contributions of real quark emission processes will be referred to as "qq channel contributions", the photon induced gluino–squark production processes as "γq channel contributions".

- The sum of the three channels will be labeled as "the EW contribution".

- The relative EW contribution is defined as $\delta = (\mathcal{O}_{\text{NLO}} - \mathcal{O}_{\text{LO}})/\mathcal{O}_{\text{LO}}$, where $\mathcal{O}$ is a generic observable and $\mathcal{O}_{\text{NLO}}$ is the sum of the LO contribution (7.3) and the EW contribution.

7.3.1 Different squark species

In Table 7.1, we show the results for the hadronic cross sections for squark–gluino production at the LHC. We consider left- and right-handed, up- and down-type squark production separately. Since light quark masses are negligible, squarks of the first two generations are mass degenerate and cannot be distinguished experimentally. Therefore, the cross sections for *e.g.* $\tilde{g}\tilde{u}_a$, $\tilde{g}\tilde{c}_a$ (and by CP symmetry also for $\tilde{g}\tilde{u}_a^*$, $\tilde{g}\tilde{c}_a^*$) are always summed and are denoted by the dominant contribution, *e.g.* $\tilde{g}\tilde{u}_a$. The observables related to $\tilde{g}\tilde{d}_a$, $\tilde{g}\tilde{s}_a$, $\tilde{g}\tilde{d}_a^*$ and $\tilde{g}\tilde{s}_a^*$ are treated similarly.

	$\tilde{g}\tilde{u}_L = \tilde{g}\ (\tilde{u}_L + \tilde{u}_L^*$ $+ \tilde{c}_L + \tilde{c}_L^*\ )$	$\tilde{g}\tilde{u}_R = \tilde{g}\ (\tilde{u}_R + \tilde{u}_R^*$ $+ \tilde{c}_R + \tilde{c}_R^*\ )$	$\tilde{g}\tilde{d}_L = \tilde{g}\ (\tilde{d}_L + \tilde{d}_L^*$ $+ \tilde{d}_L + \tilde{d}_L^*\ )$	$\tilde{g}\tilde{d}_R = \tilde{g}\ (\tilde{d}_R + \tilde{d}_R^*$ $+ \tilde{s}_R + \tilde{s}_R^*\ )$
$\mathcal{O}(\alpha_s^2)$	6.427(6)	6.837(4)	3.490(2)	3.812(2)
$\mathcal{O}(\alpha_s\alpha)$	0.004179(4)	0.0044530(4)	0.0006702(5)	0.0007508(7)
$\mathcal{O}(\alpha_s^2\alpha)$	−0.1503(4)	0.00829(6)	−0.09607(6)	0.001305(8)
$\delta(\%)$	−2.26	0.13	−2.65	0.04

Table 7.1: Integrated cross sections for squark–gluino production at the LHC within the SPS1a′ scenario [203]. We show the leading order results, the EW contributions of $\mathcal{O}(\alpha_s\alpha)$ and of $\mathcal{O}(\alpha_s^2)$, and the relative corrections δ, as defined in the text. All cross sections are given in pb.

Being of QCD origin, the LO cross section of the partonic process $gQ \to \tilde{g}\tilde{Q}_a$ is independent of the chirality and of the flavor of the produced squark $\tilde{Q}$. Since all considered squark masses are of the same order (~ 550 GeV), the LO hadronic cross sections for up-type squark production are about twice as large as the cross sections for down-type squark production. In contrast, the EW contributions depend strongly on the chirality of the squarks and, to a less extent, on the squark flavors. The MSSM is a chiral theory and for the production of right-handed squarks some of the one-loop and qq channel diagrams are suppressed by the couplings. The EW contribution to all left-handed squarks, *i.e.* to $\tilde{g}\tilde{u}_L$ and $\tilde{g}\tilde{d}_L$ production, is dominated by the (negative) gQ channel contributions, and alters the LO cross section by about $-2, -3\%$. For right-handed squarks, *i.e.* for $\tilde{g}\tilde{u}_R$ and $\tilde{g}\tilde{d}_R$ production, the qq and γq channels contribute at almost the same order of magnitude than the (positive) gQ channel and the full EW contribution ranges at the permille level.

The corresponding NLO QCD corrections have been estimated using `PROSPINO` [20]. They are positive and their percentage impact is independent of the flavor and of the chirality of the produced squark. Using the PDF set MRST2004qed, the relative NLO QCD corrections at the scale $\mu_F = \mu_R = (m_{\tilde{Q}} + m_{\tilde{g}})/2$ amount to 28% of the LO contribution. The scale uncertainty of the total cross section at NLO QCD is of the order of 10%.

In order to study the behavior of the EW contribution close to the threshold we consider the distribution of the "cumulative invariant mass" distribution, obtained from the definition (6.16) performing the substitution $2m_{\tilde{Q}_a} \to m_{\tilde{g}} + m_{\tilde{Q}_a}$. In the right panels of Fig. 7.2 the relative yield of the EW contribution is depicted. The interplay of the EW contributions

of the different channels are illustrated in the left panels. For left-handed squarks, the relative EW contribution increases in absolute size as M_{inv} increases. This is a clear signal that the relative yield of the EW corrections increases in high M_{inv} region. Interestingly, the situation is reversed for right-handed squarks. In absolute numbers, the relative EW contribution to the cumulative invariant mass decreases for increasing M_{inv}. In the high invariant mass range the virtual corrections to the gQ_R channel receive negative contributions from Sudakov-like double and single logarithms and the positive, non-logarithmically enhanced part of the amplitude is suppressed.

In the left panel of Fig. 7.3, we show the interplay of the various EW contributions to the invariant mass distribution. One clearly sees that for left-handed squark production the virtual and real photon corrections to the qg channel dominate the EW contributions over the whole phase space. For right-handed squark production, the situation is more involved: the three channels are comparable and different channels lead in different energy ranges. Near threshold the positive contribution of the qg channel dominates while in the high M_{inv} region, the γq channel becomes more important and leads the EW contributions. The different behaviour of the EW contributions in the case of left-handed and right-handed squark production renders the relative yield of the EW contributions dependent on the chirality of the produced squark (right panels of Fig. 7.3). The shape of the relative corrections is similar for up- and down-type squarks of the same chirality, and also the size is comparable. For right-handed squark production, the distributions are almost flat and contribute negligibly. As expected from the cumulative invariant mass discussion, the relative yield of the EW contributions to right-handed squark production decreases as M_{inv} increases.

The impact of the EW contributions on the transverse momentum distribution of the produced squark, $p_T(\tilde{Q})$, is shown in Fig. 7.4. The general features discussed in the case of the invariant mass distribution appear here as well. The EW contributions are more important in the left-handed squark production than in the case of the processes producing a right-handed squark. The qg channel is by far the leading one in the case of the $\tilde{g}\tilde{Q}_L$ production, while in case of $\tilde{g}\tilde{Q}_R$ production, the impact of the aforementioned channel is reduced and comparable with those of the other two channels. In particular in the high p_T region the negative contribution of the qg channel cancels the positive contribution of the γq channel.

The relative yield of the EW contribution in the case of left-handed production decreases as p_T increases. Its absolute value is maximum in the high p_T region (*i.e.* $p_T > 1500$ GeV) reaching $6 - 8\%$. In the case of right-handed squarks, the EW contributions are negligible, of the order of 0.5% over the

whole p_T region considered. The distribution with respect to the transverse momentum of the gluino, $p_T(\tilde{g})$, is similar to that of $p_T(\tilde{Q})$ and therefore is not shown. At lowest order $p_T(\tilde{g})$ and $p_T(\tilde{Q})$ coincides. The (small) differences enter at NLO and they are related to the different contributions these distributions receive from real photon and real quark radiation processes. In particular the qq channels affect the p_T of the squark more, reducing (in absolute size) the EW contribution in the high p_T range. The difference is nevertheless negligible, $\mathcal{O}(1\%)$ of the LO transverse momentum distribution.

In Fig. 7.5 [7.6], we show the EW contributions to the pseudorapidity contribution of the produced squark [gluino], $\eta(\tilde{Q})$ [$\eta(\tilde{g})$]. In the left-handed case the qg-channel dominates the EW contributions to both $\eta(\tilde{Q})$ and $\eta(\tilde{g})$. This channel renders the EW contribution negative and its absolute contribution maximum in the central region, $|\eta| \leq 1$, where it reaches -3%. In the case of $\tilde{g}\tilde{Q}_R$, the situation is more involved. The different channels are comparable and mutual cancellations of these channels in the different regions in η render the relative yield of the EW contributions to $\eta(\tilde{Q})$ [$\eta(\tilde{g})$] almost flat and small, of the order of -0.5% [-0.3%]. Differences between $\eta(\tilde{g})$ and $\eta(\tilde{Q})$ are related to the real emission processes, and also to the different masses of the two final particles which affect the definition of η already at the lowest order.

Dependence on squark and gluino masses

At LO, the only SUSY parameters entering the production cross section are the masses of the final state particles. These parameters are thus crucial for the total size of the cross section and it is worth to investigate the dependence of the cross section and the EW contribution on the squark and gluino masses. To this aim, we set the independent squark masses of the first and second generation to a common value $m_{\tilde{Q}}$, which is varied for the 'squark mass variation' and fixed (to 500 GeV) for the 'gluino mass variation'. The fourth, dependent squark mass is computed at each SUSY point according to

$$(m^2_{\tilde{Q},L})_{\rm OS} = m^2_{\tilde{Q},L} + \delta m^2_{\tilde{Q},L} - \mathfrak{Re}\left\{\Sigma^{\tilde{Q}}_{L,L}(m^2_{\tilde{Q}})\right\} \quad (Q = d, s). \tag{7.16}$$

All other SUSY parameters are kept at their SPS1a′ values, while $\mu_R = \mu_F = 1$ TeV.

We give the results in Fig. 7.8 for the variation of the common squark mass $m_{\tilde{Q}}$. The variation of the gluino mass is shown in Fig. 7.7. In the left panels, the total cross sections including the EW contribution, and in the right panels, the relative EW contribution are shown.

One observes a change in the slope of the relative corrections at the point $m_{\tilde{g}} = m_{\tilde{Q}}$, since the cross section depends also on the difference of the masses. If squarks are heavier than gluinos, the resonant contributions from the qq channels have been subtracted as described in section 7.2.3 and the final contributions from these channels are tiny.

Concerning the $\tilde{g}\tilde{Q}_L$ production, the qg channels dominates the EW contributions over the whole $m_{\tilde{Q}}$ and $m_{\tilde{g}}$ range. The contribution of this channel is negative and its absolute value increases as the gluino mass and the squark mass increases. The contributions of the other channels are positive, small and weakly dependent on the mass of the produced particles. As a consequence, the overall EW contribution is mostly coincident with the qg channel contribution, the difference between the two increasing as $m_{\tilde{Q}}$ and $m_{\tilde{g}}$ increases. The EW contributions vary around -2% for light masses (< 600 GeV) and grow up to -4% for squark and gluino masses at the TeV range.

In the case of $\tilde{g}\tilde{Q}_R$ production, the qg channel is still the dominant one in the low mass region (*i.e.* ≤ 600 GeV) both in the squark mass variation and in the gluino mass variation case. The (positive) contribution of this channel decreases when the masses increase becoming comparable with those of the other two channels. In the case of gluino mass variation the qg channel become smaller than the γq channel. This interplay renders the EW contribution to $\tilde{g}\tilde{Q}_R$ production almost independent on the gluino mass and negligible; its relative yield is below 0.5% over the whole squark mass range. The dependence on the squark mass is greater but nevertheless the relative EW contribution stays below 0.5% over the whole squark mass range considered.

When the inclusive squark-gluino production is considered, Fig. 7.9, the overall EW contribution is small, of the order of -1% over the whole squark and gluino mass range. This is due to the negligible contribution from the $\tilde{g}\tilde{Q}_R$ processes that halves the relative yield of the $\tilde{g}\tilde{Q}_L$ processes and that reduces their dependence on the mass of the produced particles.

7.3.2 Dependence on the SUSY scenario

In this subsection we discuss the electroweak effect in the different benchmark SUSY scenarios mentioned above. In Table 7.2 we show the total cross section for the $\tilde{g}\tilde{u}_L$ associated production in the SPS5 and SU1 scenario. As in the diagonal squark–anti-squark case, the absolute value of the different contributions decrease as the mass of the produced particles decreases. The importance of the EW contribution relative to the LO result, instead,

	SPS5	SU1
$\mathcal{O}(\alpha_s^2)$	2.433(2)	1.182(1)
$\mathcal{O}(\alpha_s\alpha)$	0.001896(2)	0.001084(1)
$\mathcal{O}(\alpha_s^2\alpha)$	−0.0656(1)	−0.03507(7)
$\delta(\%)$	−2.61	−2.88

Table 7.2: Same as Table. 7.1 but focusing on $\tilde{g}\tilde{u}_L$ production in different SUSY scenarios.

increases with the mass of the final states. The relative yield of the electroweak contributions in the different scenarios considered is at most of the order of 3%.

The importance of the EW contributions to the different distributions of the $\tilde{g}\tilde{u}_L$ [$\tilde{g}\tilde{u}_R$] process in the SU1 and SPS5 scenarios are shown in Figs. 7.10 - 7.13 [7.14 - 7.17].

Concerning the $\tilde{g}\tilde{u}_L$ process, the general qualitative features of the cumulative invariant mass, invariant mass, transverse momentum and pseudo-rapidity, are similar in all scenarios. The qg channel is negative and dominant, while the other two channels are negligible. When the cumulative invariant mass (Fig. 7.10), the invariant mass (Fig. 7.11), the transverse momentum (Fig. 7.12), and the pseudo-rapidity (Fig. 7.13) distributions are considered, the relative yield of the EW contributions in the different scenarios is similar to that of the SPS1a′ point. In the case of the cumulative invariant mass, the EW contributions become more negative as the mass of the produced squark increases and the absolute value of the asymptotic behaviour in the limit $M_{\rm inv} \to \infty$, *i.e* the total cross section, increases as the mass of the final states increase. This feature can be inferred from Table 7.2 and it was already pointed out when the dependence on the mass of the produced particles have been discussed. Similar features appear in the $\tilde{g}\tilde{d}_L$ associated production.

The situation is different when $\tilde{g}\tilde{u}_R$ production is considered. As in the case of the SPS1a′ scenario, the qg and the γq channels are comparable. According to what observed when the dependence on squark and gluino masses was studied, the relative importance of the γq channel increases with the mass of the final states, while the relative impact of the EW corrections is small and is equal in all the scenarios considered.

In experimental analyses, usually cuts on the kinematically allowed phase

space of the final state particles are applied in order to increase the signal to background ratio. These include lower cuts on the transverse momenta, to focus on high-p_T jets, and upper cuts on the absolute value of pseudo-rapidity $|\eta|$, to restrict the scattering angles to the central region of the detector. For illustration, we give the hadronic cross sections to $\tilde{g}\tilde{u}_L$, as a function of these cuts,

$$\sigma(p_T) = \int_{p_T}^{\infty} \frac{d\sigma}{dp_T}\, dp_T, \qquad \sigma(\eta) = \int_{-\eta}^{\eta} \frac{d\sigma}{d\eta}\, d\eta. \tag{7.17}$$

We consider the SPS1a′ and the SPS5 scenario and we focus on the $\tilde{g}\tilde{u}_L$ (Fig. 7.18) and $\tilde{g}\tilde{u}_R$ (Fig. 7.19) associated production. In particular we consider the EW contribution relative to the LO as a functions of the cuts. These cuts refer to p_T and η of the produced squark. The dependence on the cuts is similar in the scenarios considered and the general qualitative behaviour is independent on the chirality of the produced squark. The relative yield of the EW contributions increases as the cut on p_T increases, the dependence being sizable. It is worth to notice that the total cross section decrease steeply as p_T increases being almost halved at $p_T \sim 400$ GeV.

In the case of $\tilde{g}\tilde{u}_L$ production, when a cut on η is set, the absolute value of the EW contributions relative to the LO increases. In the case of $\tilde{g}\tilde{u}_R$ production, the relative yield of the EW contribution decreases as the cut on η approaches zero.

Inclusive squark-gluino production

The inclusive $\tilde{g}\tilde{Q}$ production is obtained summing up all the processes. In Fig. 7.20 we show the cumulative invariant mass distribution, the distribution of the transverse momentum of the squark, and the invariant mass distribution in the SPS1a′ scenario. Considering the limit $M_{\rm inv} \to \infty$ of the cumulative invariant mass distribution the cross section is recovered. In this limit, the gq channel corrections to right-handed squarks are negligible compared to those to left-handed squarks and the size of the relative contribution is roughly halved. The qq and γq channels give both positive contributions at the permille level. The full EW contribution to the total cross section of gluino–squark production amounts -1% within the SPS1a′ scenario.

Concerning the relative corrections of the differential hadronic cross sections with respect to $M_{\rm inv}$ and $p_T(\tilde{Q})$, the relative EW contribution grows in the high-$M_{\rm inv}$ and high-p_T range, but, owing to the small corrections for right-handed squarks, it remains at the percent level only. Similar features appear in the case of $p_T(\tilde{g})$, $\eta(\tilde{g})$, and $\eta(\tilde{Q})$ distributions.

Similar results are obtained when other scenarios are considered, as can be inferred looking at Figs. 7.21 and 7.22. In particular in Fig. 7.21 [7.22], we show the cumulative invariant mass, the $p_T(\tilde{Q})$ and the invariant mass distribution for the inclusive $\tilde{g}\tilde{Q}$ production in the SU1 [SPS5] scenario.

7.4 Conclusions

In this chapter, we have computed the complete EW contribution to squark–gluino production at hadron colliders. At $\mathcal{O}(\alpha_s^2\alpha)$, the EW contributions include EW one-loop corrections together with real photon and real quark radiation processes. Furthermore, there are tree-level contributions arising from photon induced channels at $\mathcal{O}(\alpha_s\alpha)$.

We have discussed in detail the EW contribution to each case of producing a left- or right-handed, up- or down-type squark in association with a gluino. A numerical analysis is presented for squark–gluino production at the LHC within three different scenarios. The EW contribution can be sizable in distributions, in particular for left-handed squarks where the virtual $\mathcal{O}(\alpha_s^2\alpha)$ and real photon corrections dominate. We also investigated the dependence on the masses of the final state squark and gluino, which are crucial for the absolute size of the cross section. However, the relative EW contribution to inclusive squark–gluino production depends only weekly on the masses and ranges at the -1% level.

Compared to $\tilde{Q}_a\tilde{Q}_a^*$ production (*c.f.* chapter 6) and to $\tilde{t}_1\tilde{t}_1^*$ production [121], the EW contribution to squark–gluino production is small. Squark pair production profits from additional tree-level EW processes that give also non-zero interference contributions with the LO QCD diagrams. These $\mathcal{O}(\alpha_s\alpha + \alpha^2)$ channels add up to the tree-level quark radiation processes of $\mathcal{O}(\alpha_s^2\alpha)$ and enhance the EW contribution. For squarks of the third generation, L–R-mixing has to be taken into account. As a consequence, both top-squark mass eigenstates are partially left-handed and the EW contribution to the (mainly right-handed) $\tilde{t}_1$ production is less suppressed than for $\tilde{Q}_R$ production.

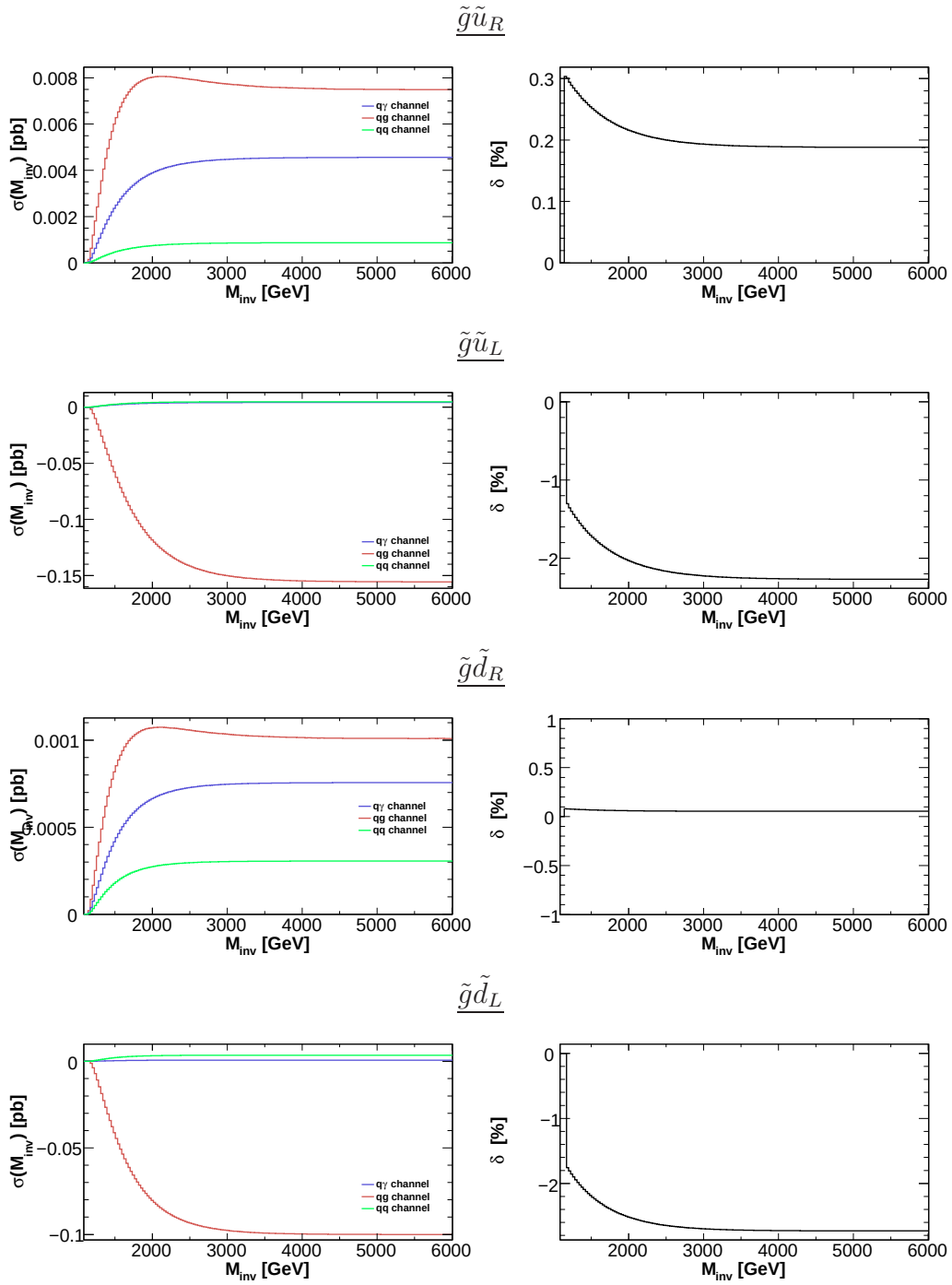

Figure 7.2: Cumulative invariant mass distribution for different species of the produced squark, defined as the cross section integrated up to M_{inv} of the invariant mass of the squark-gluino pair. The left panels show the EW contributions from the various channels, the right ones show the relative yield of the EW contribution. The SUSY parameter point corresponds to SPS1a′.

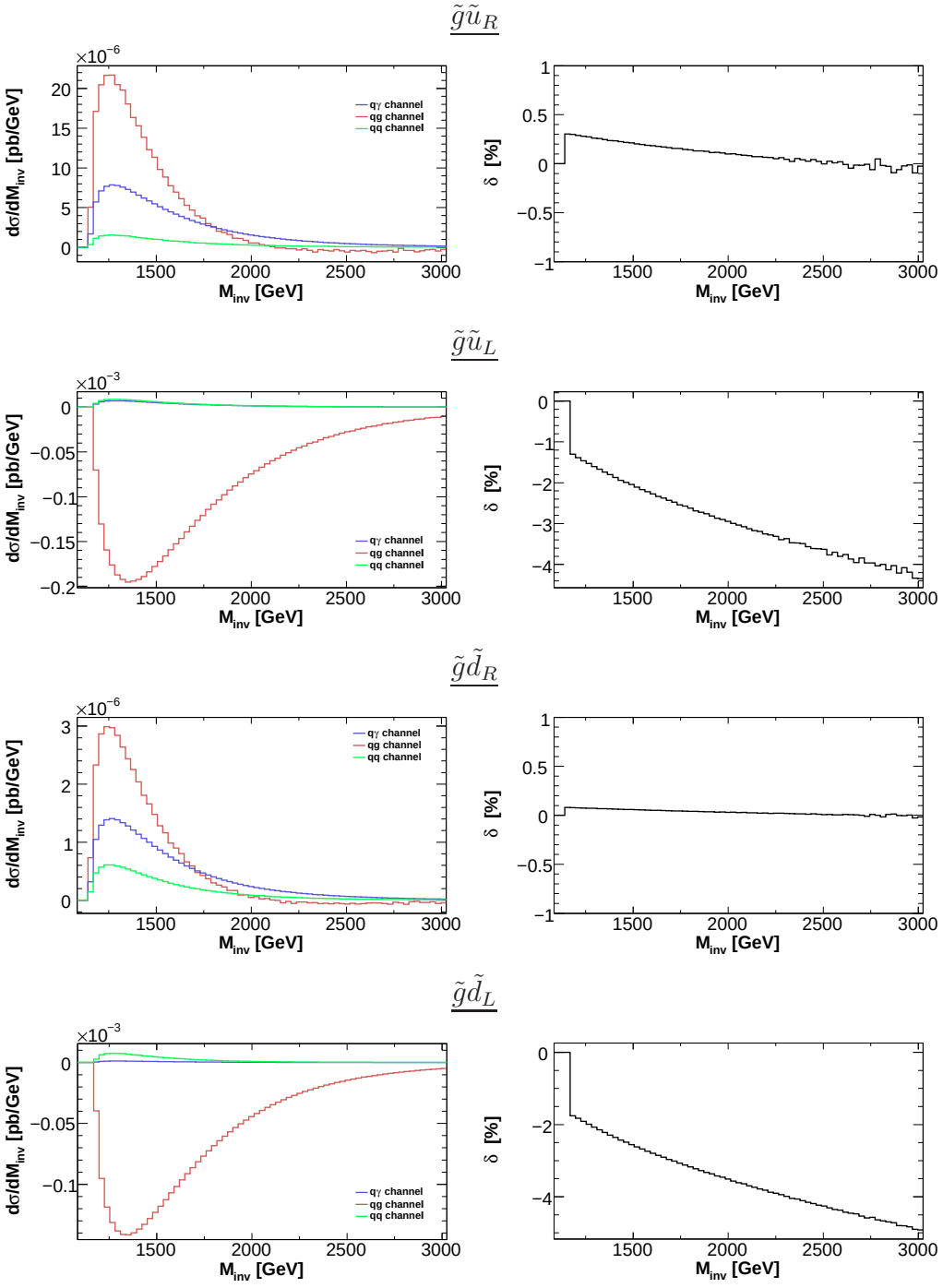

Figure 7.3: Same as Fig. 7.2, but considering the invariant mass distribution.

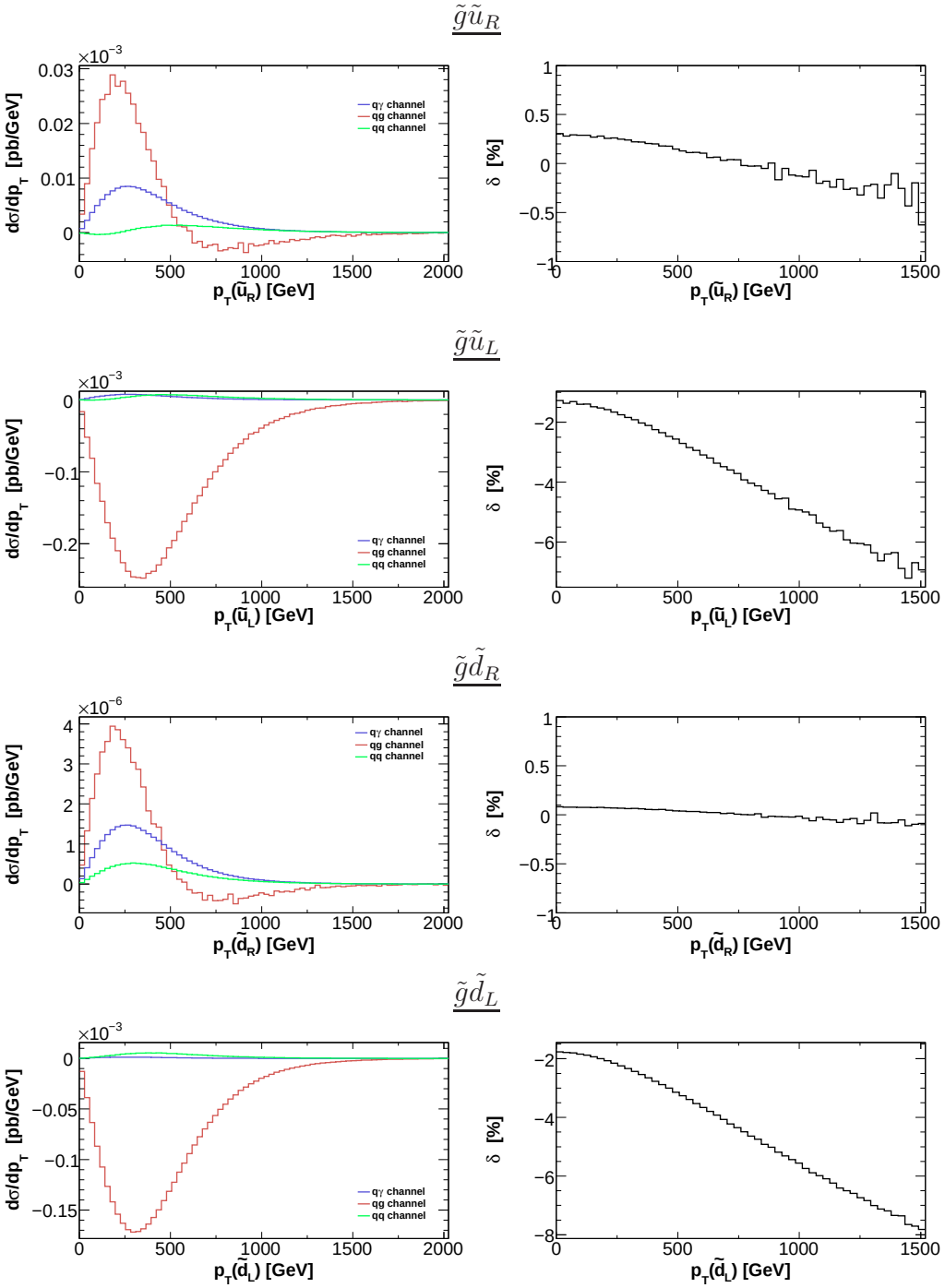

Figure 7.4: Transverse momentum distribution for the produced squark. Notations and input parameters as in Fig. 7.2.

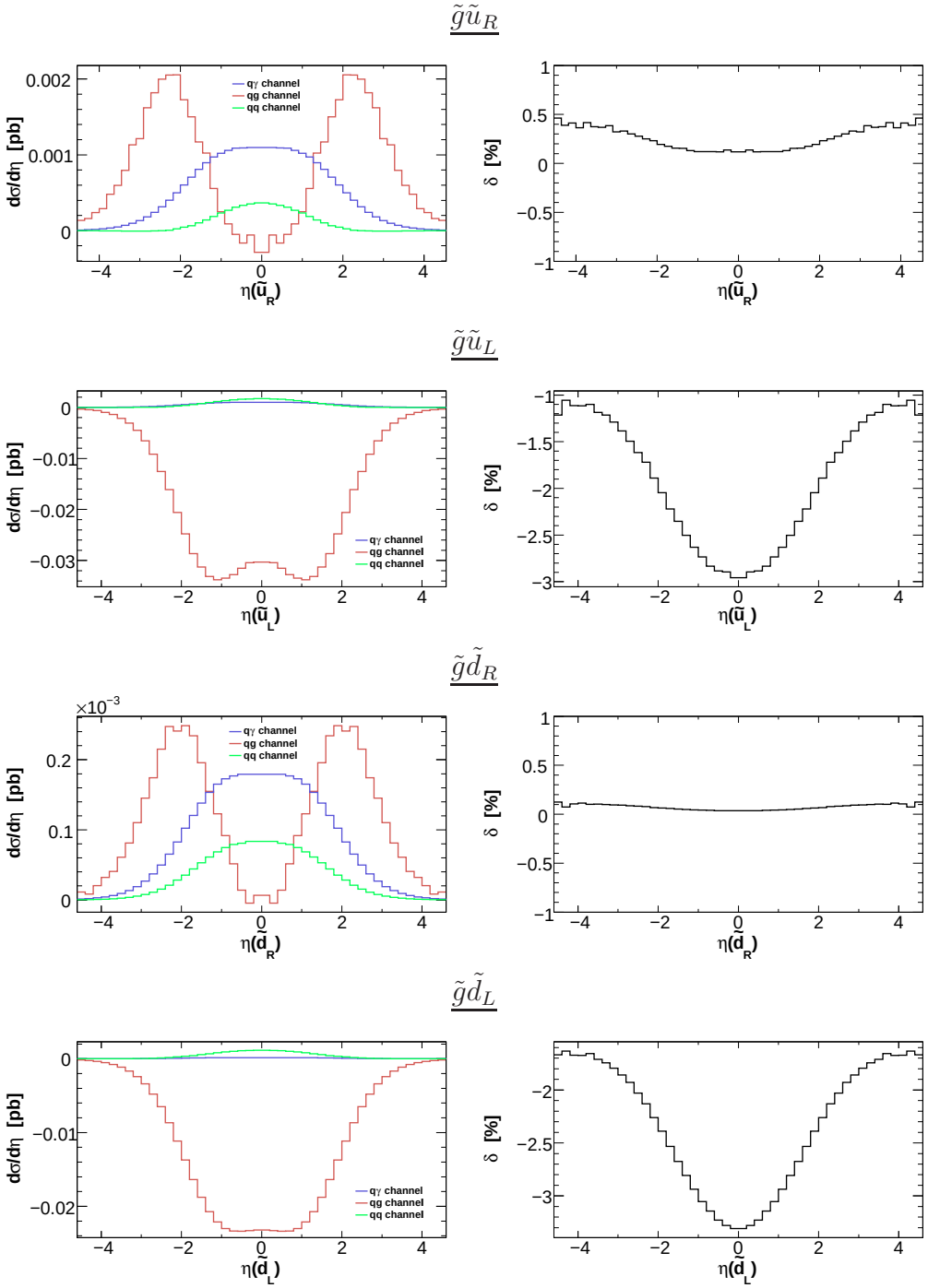

Figure 7.5: Same as Fig. 7.2 but for the pseudo-rapidity distribution of the produced squark.

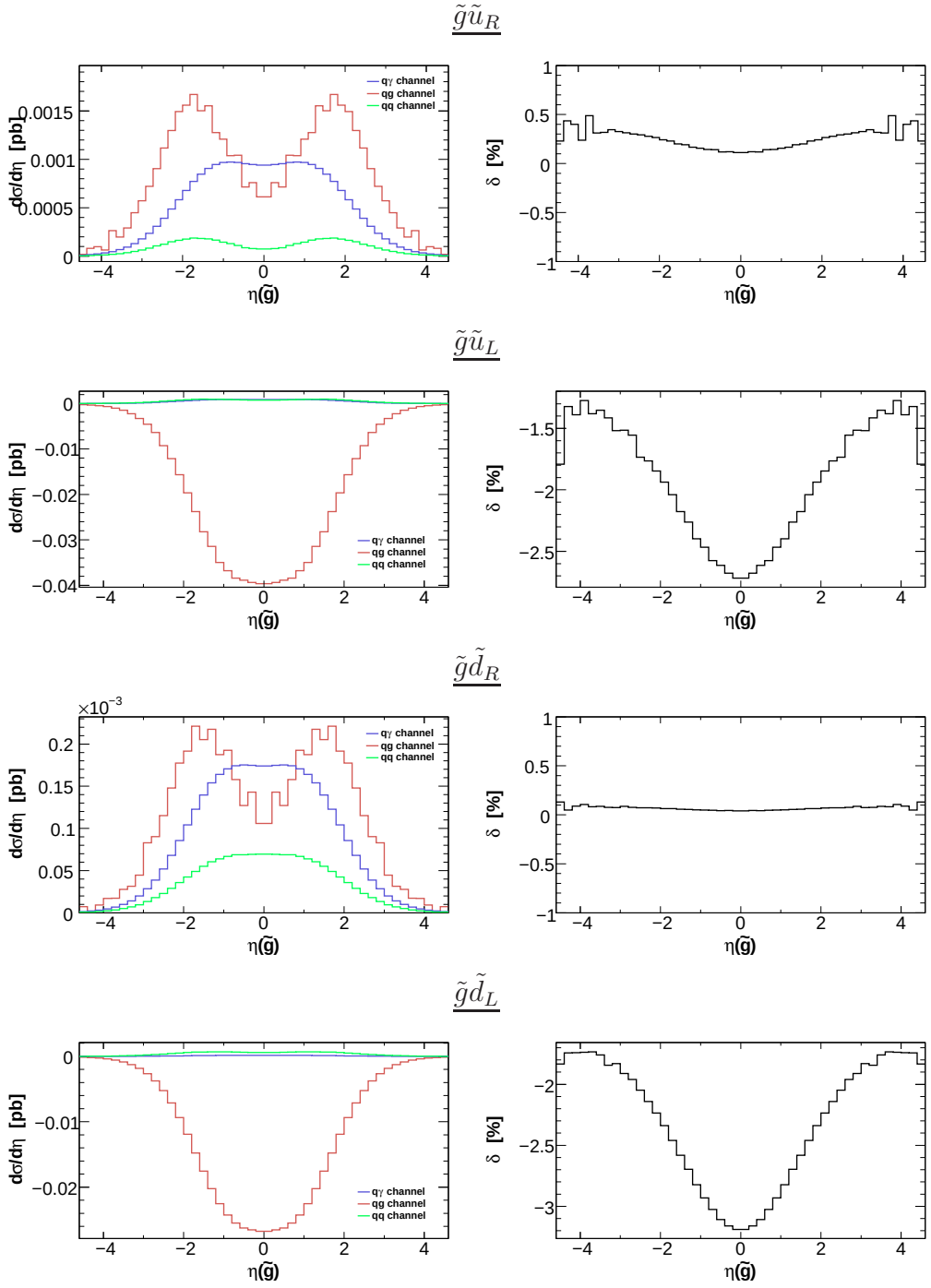

Figure 7.6: Pseudo-rapidity distribution of the produced gluino. Notations and input parameters as in Fig. 7.2.

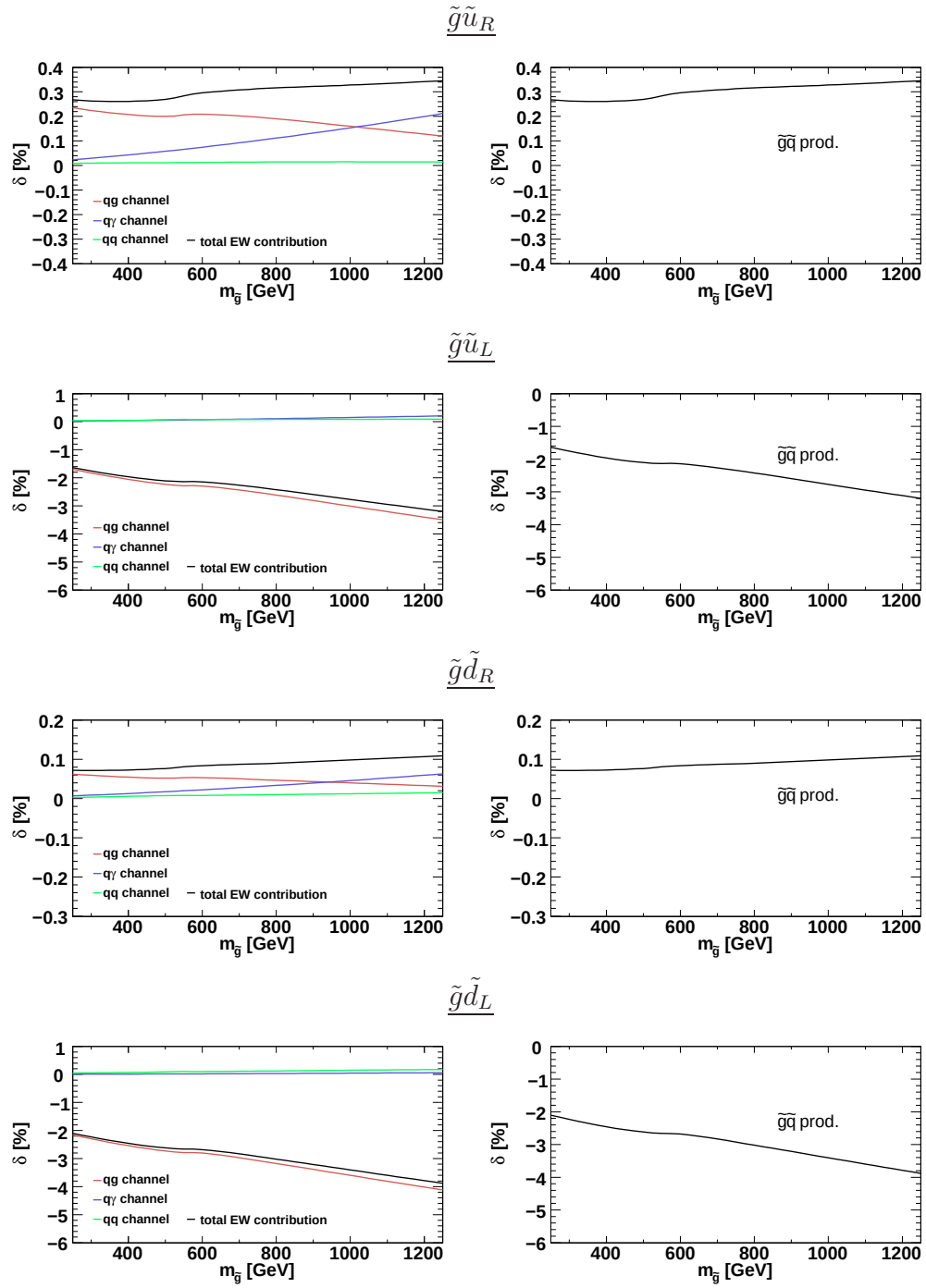

Figure 7.7: Gluino mass dependence of the EW contributions to the total cross section. Individual contributions of the different channels (left panel), and relative contributions of the EW contributions (right panel). All other parameters are fixed to their SPS1a′ values.

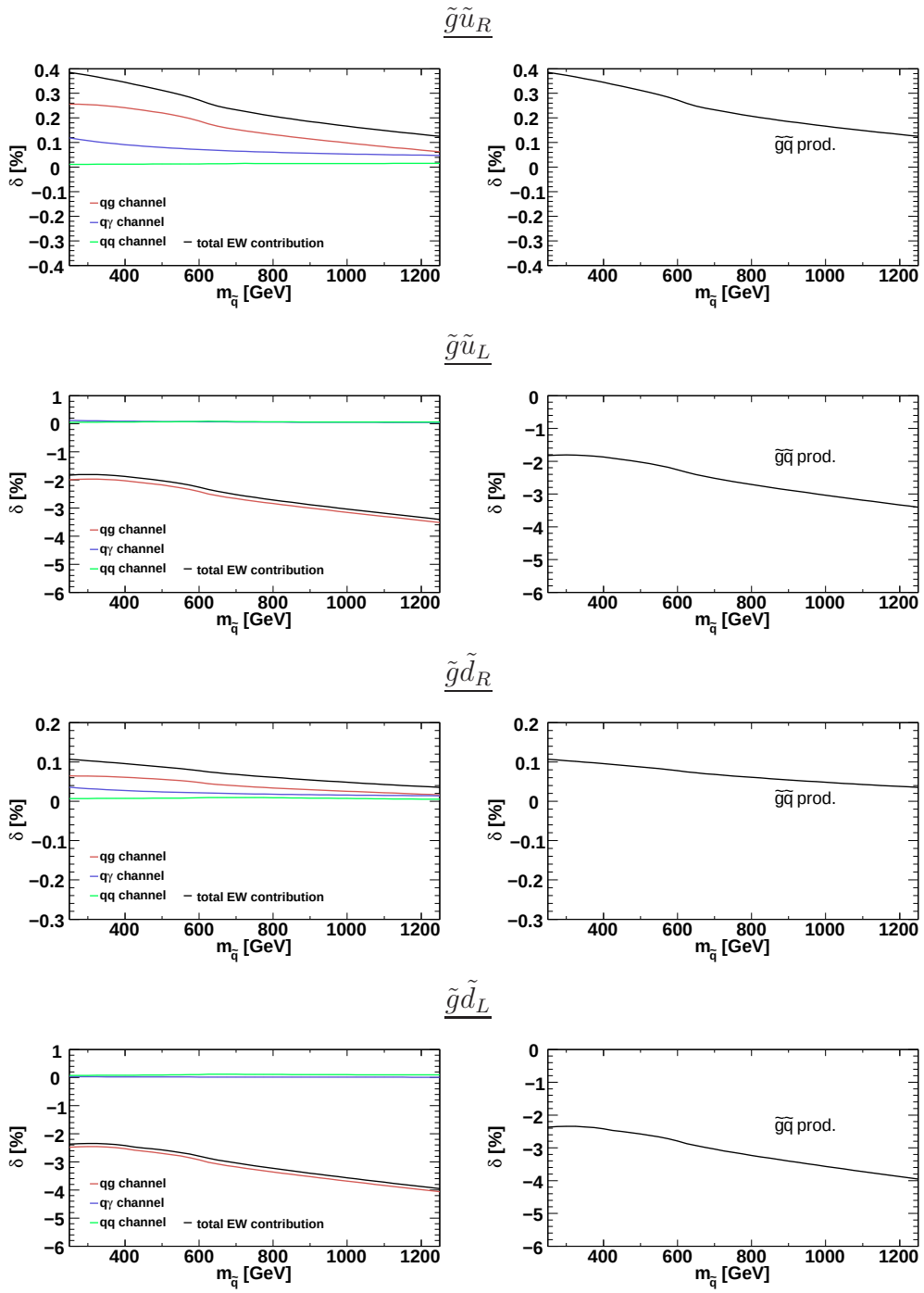

Figure 7.8: Same as Fig. 7.7, but in this case the squark mass dependence is considered.

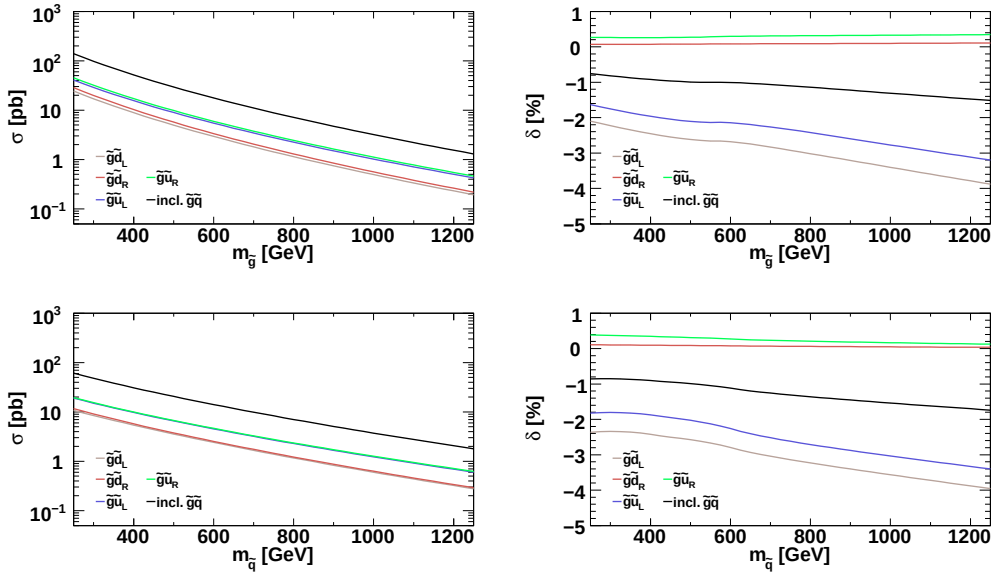

Figure 7.9: Hadronic cross sections as a function of the gluino mass (upper panels) and of a common squark mass (lower panels). Shown are the hadronic cross sections at EW NLO and the relative EW contribution for $\tilde{g}\,\tilde{u}_R$, $\tilde{g}\,\tilde{u}_L$, $\tilde{g}\,\tilde{d}_R$, $\tilde{g}\,\tilde{d}_L$ production and the $\tilde{g}\tilde{q}$ production. All other parameters are fixed to their SPS1a′ values.

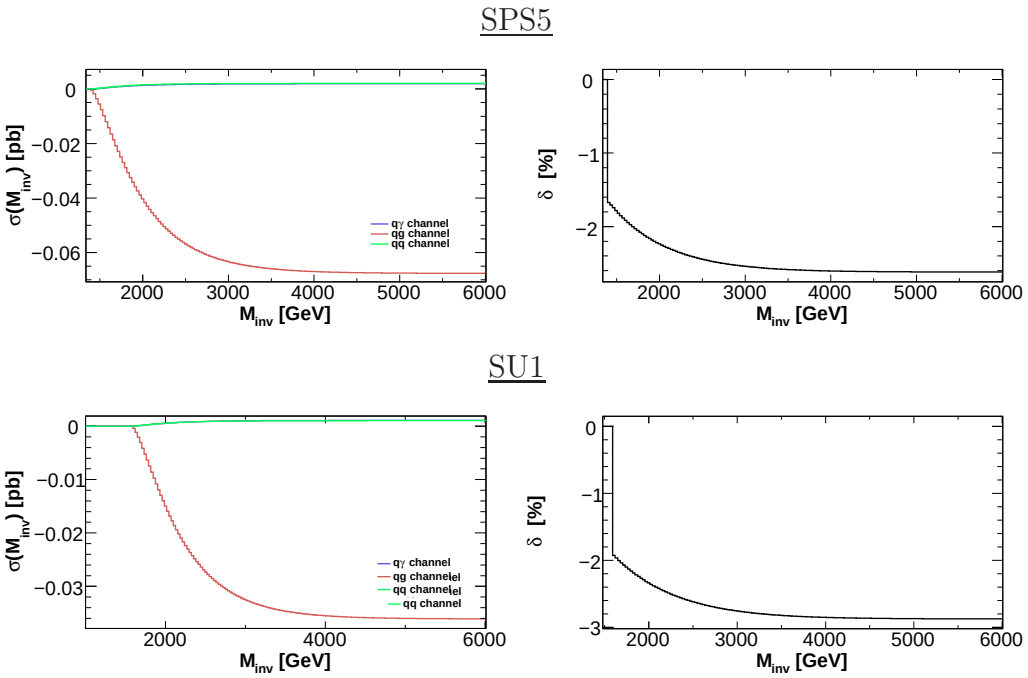

Figure 7.10: Cumulative invariant mass distribution for $PP \to \tilde{g}\tilde{u}_L X$ in different SUSY scenarios. Notation as in Fig. 7.2.

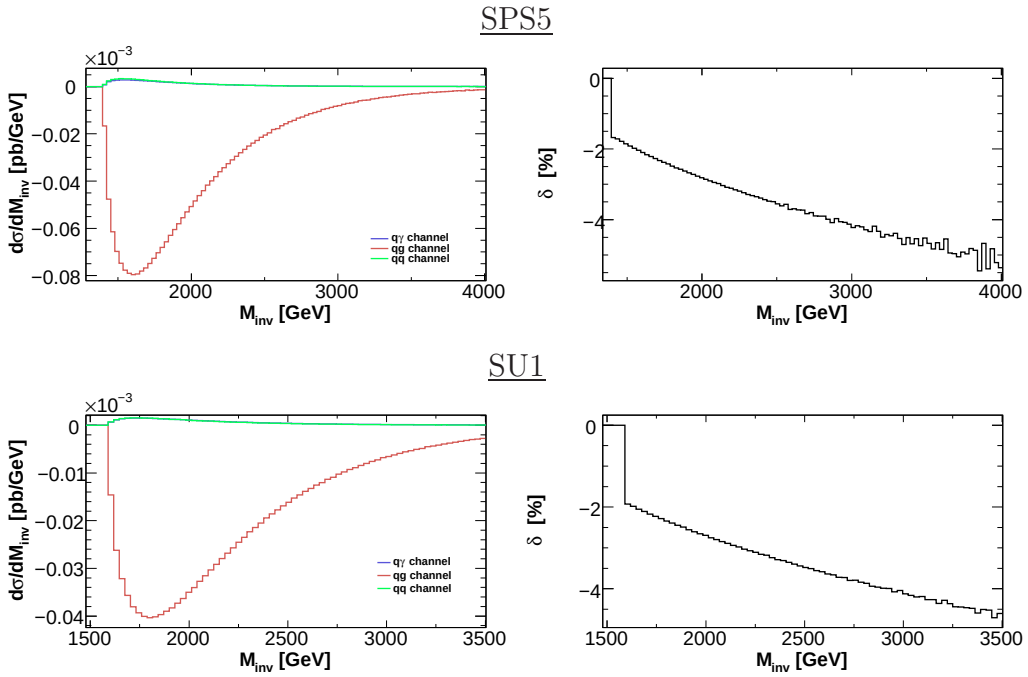

Figure 7.11: Invariant mass distribution for $PP \to \tilde{g}\tilde{u}_L X$ in different SUSY scenarios. Notation as in Fig. 7.3

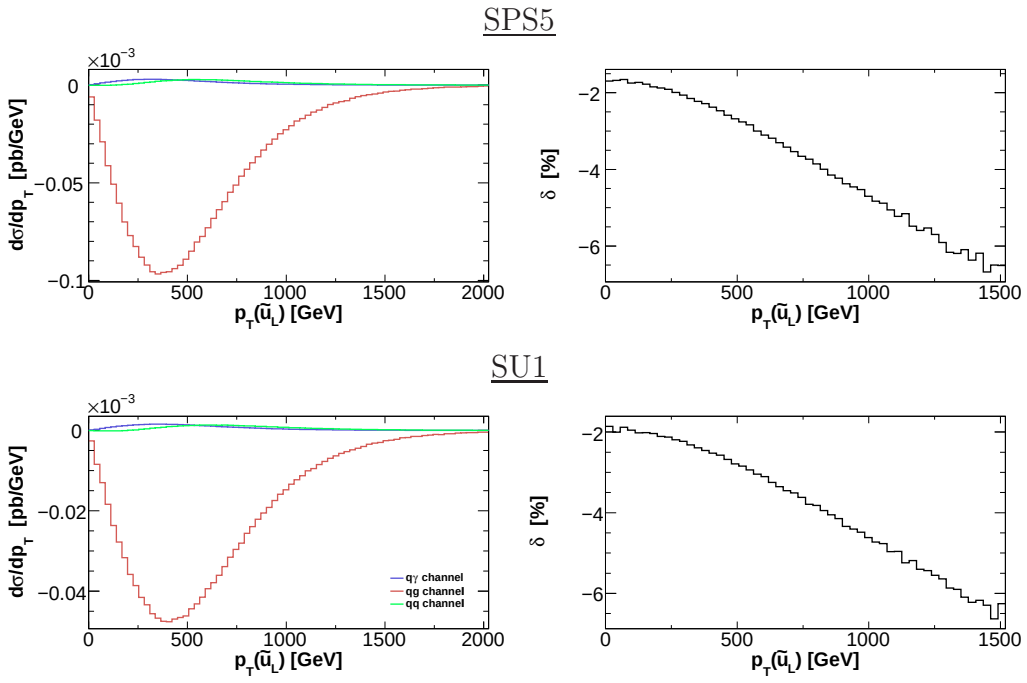

Figure 7.12: Transverse momentum distribution of $\tilde{u}_L$ for $PP \to \tilde{g}\tilde{u}_L X$ in different SUSY scenarios. Notation as in Fig. 7.4.

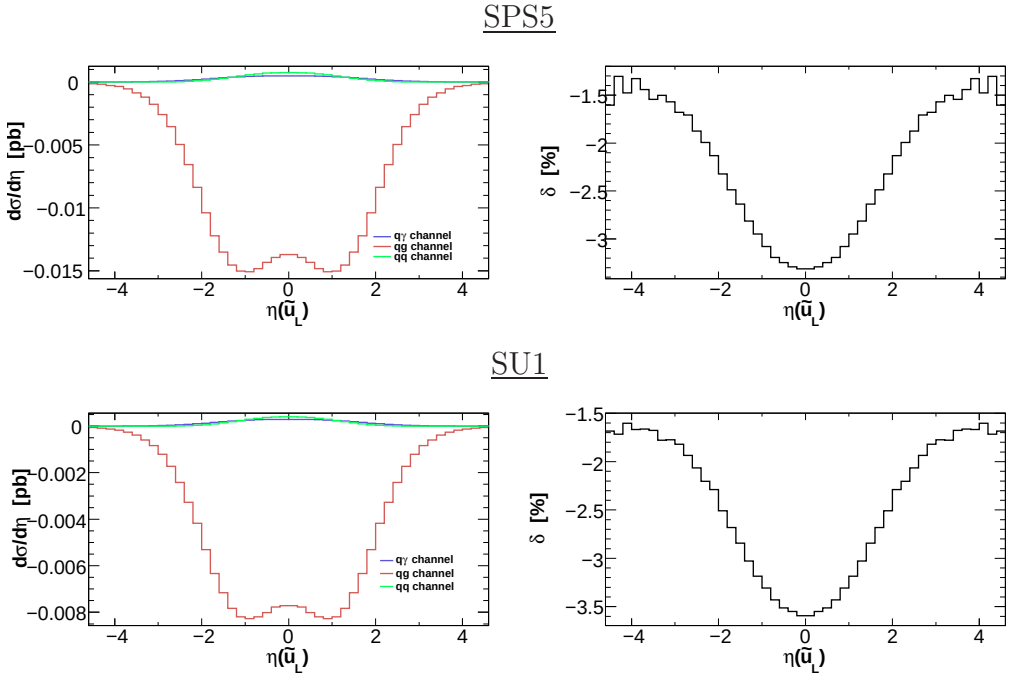

Figure 7.13: Pseudo-rapidity distribution of the produced squark for $PP \to \tilde{g}\tilde{u}_L X$ in different SUSY scenarios. Notation as in Fig. 7.5.

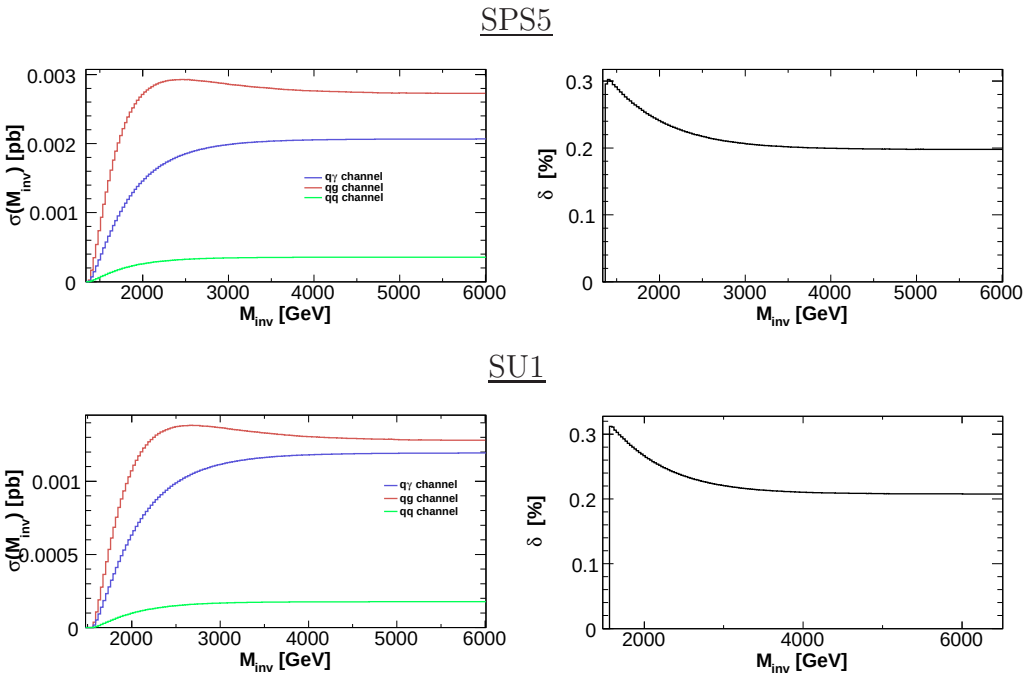

Figure 7.14: Cumulative invariant mass distribution for $PP \to \tilde{g}\tilde{u}_R X$ in different SUSY scenarios. Notation as in Fig. 7.2.

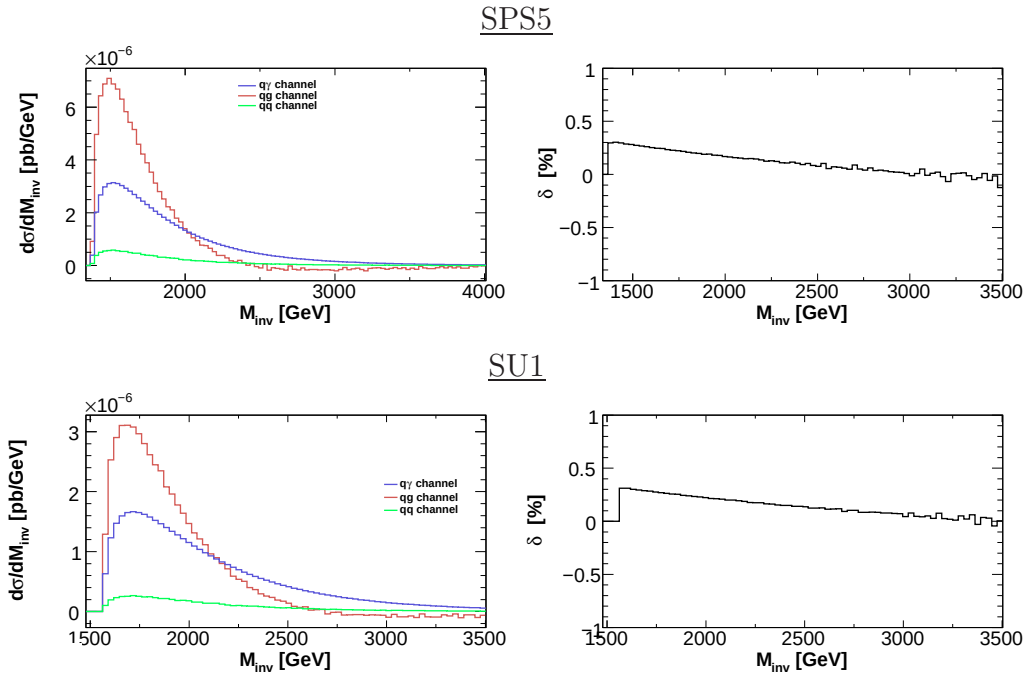

Figure 7.15: Invariant mass distribution for $PP \to \tilde{g}\tilde{u}_R X$ in different SUSY scenarios. Notation as in Fig. 7.3.

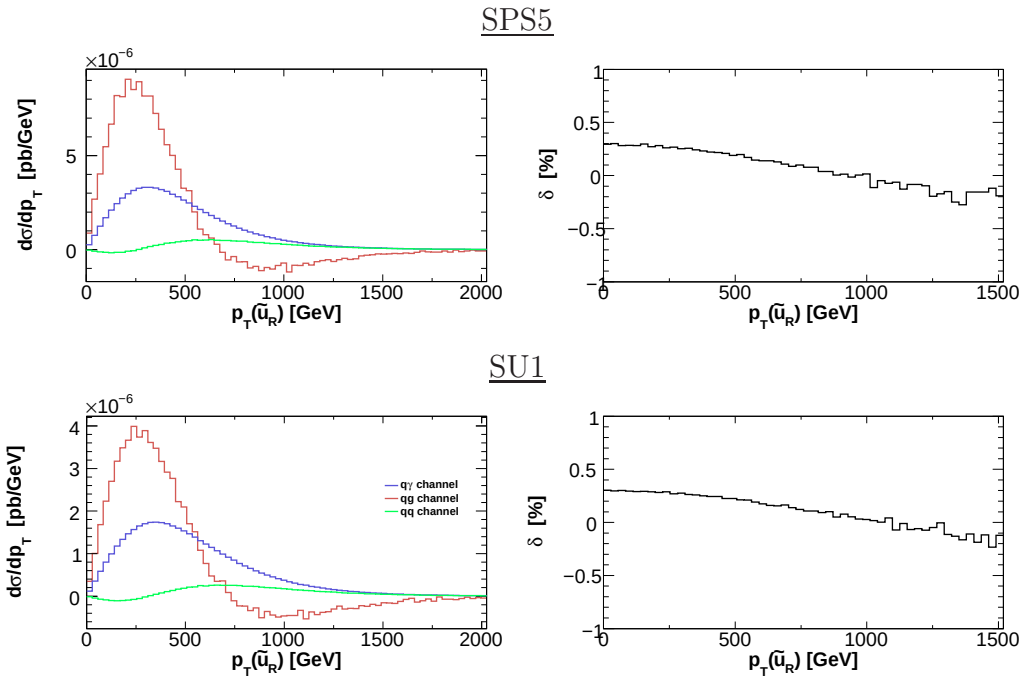

Figure 7.16: Transverse momentum distribution of the produced squark for $PP \to \tilde{g}\tilde{u}_R X$ in different SUSY scenarios. Notation as in Fig. 7.4.

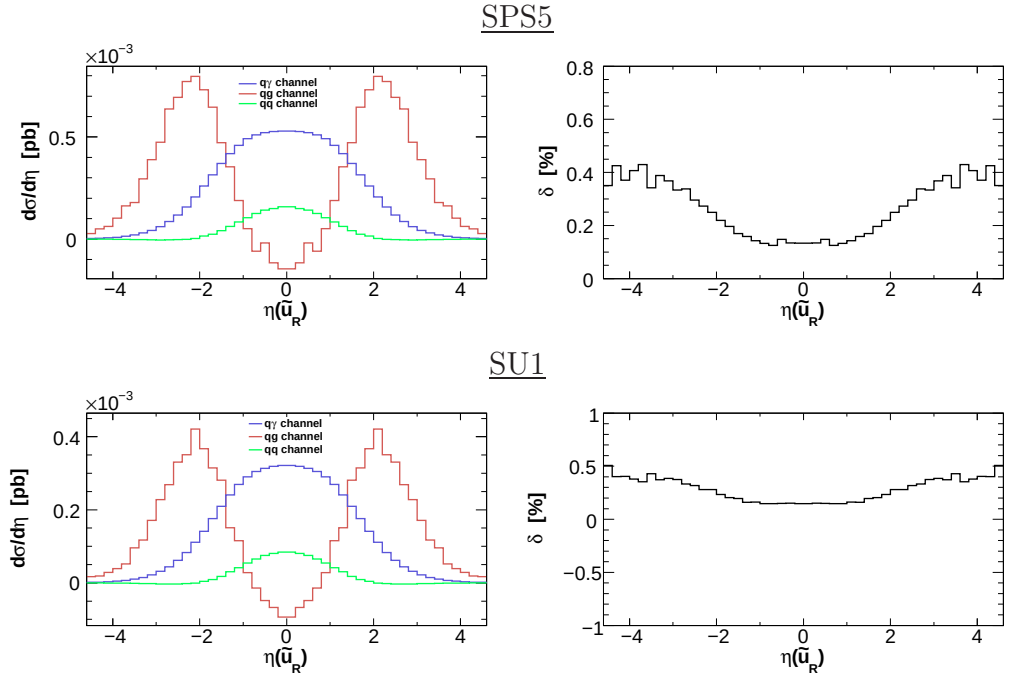

Figure 7.17: Pseudo-rapidity distribution of u_R for $PP \to \tilde{g}\tilde{u}_R X$ in different SUSY scenarios. Notation as in Fig. 7.5.

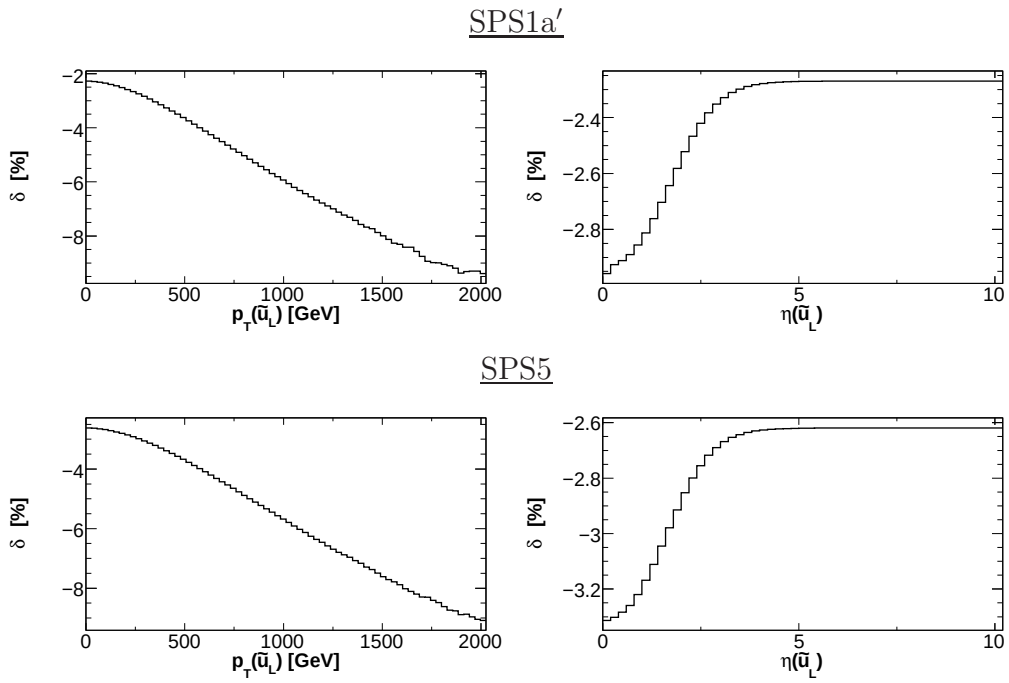

Figure 7.18: Hadronic cross sections and relative corrections as a function of a cut on p_T (left panels) and η (right panels) for left-handed up squark production in association with a gluino. The cuts refer to p_T and η of the produced squark.

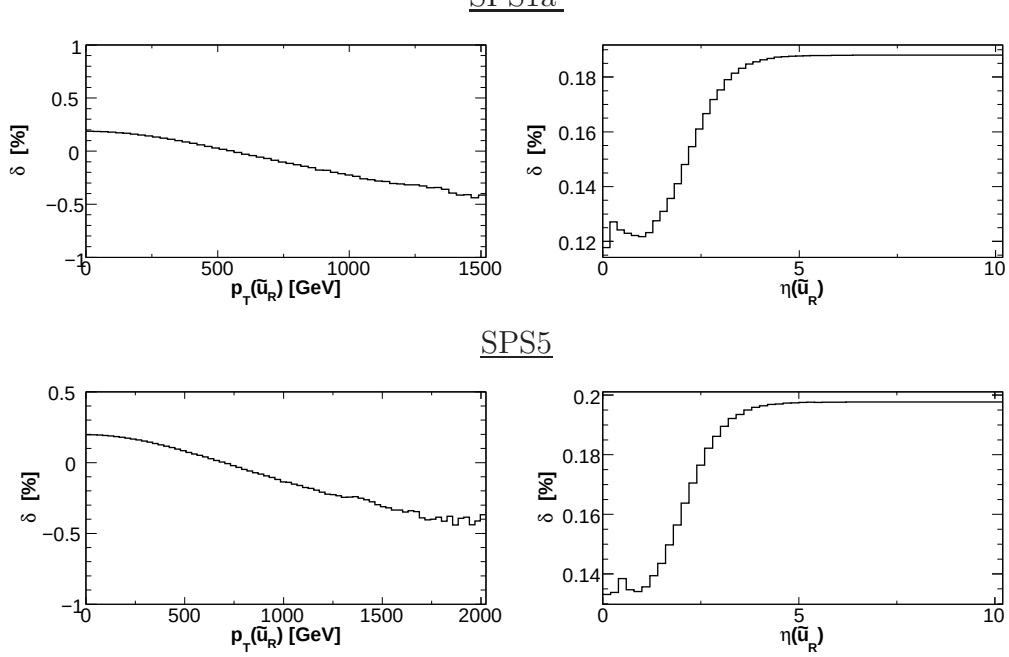

Figure 7.19: Same as Fig.7.18 but in the case of $\tilde{g}\tilde{u}_R$ production.

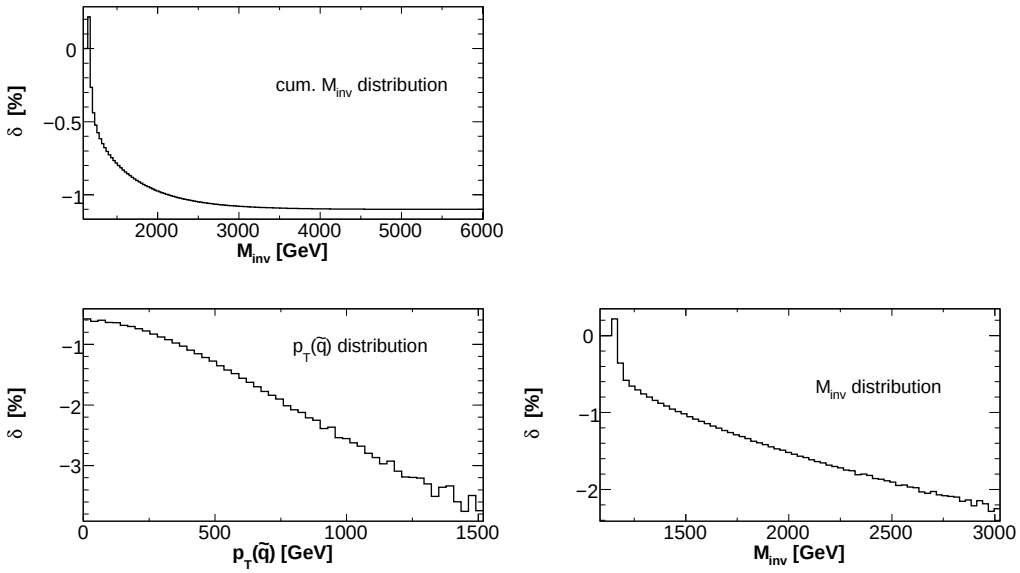

Figure 7.20: Cumulative invariant mass distribution, distribution of the transverse momentum of the produced squark and invariant mass distribution for inclusive $\tilde{g}\tilde{Q}$ production. The scenario considered is SPS1a′.

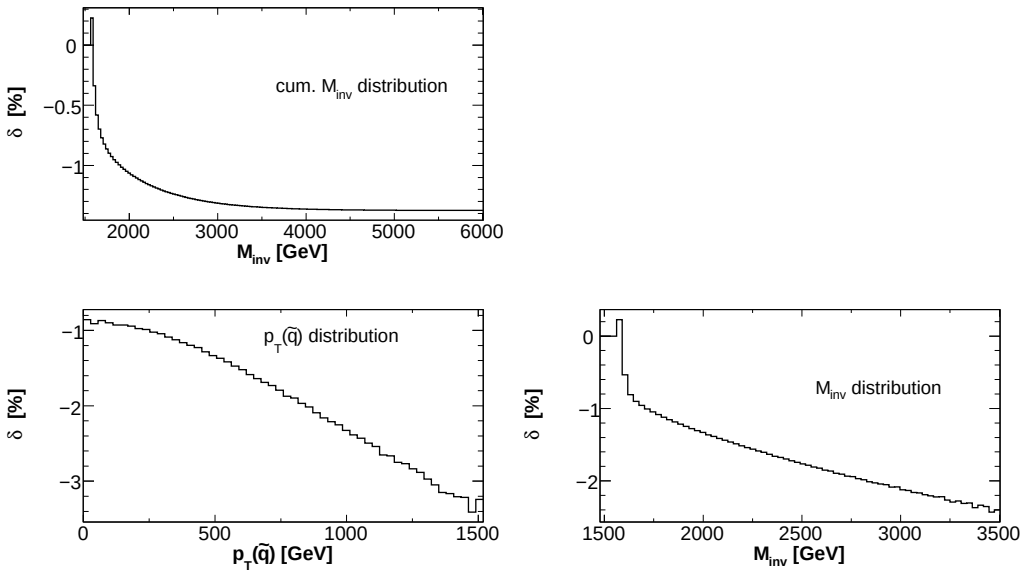

Figure 7.21: Same as Fig. 7.20, but considering the SU1 scenario.

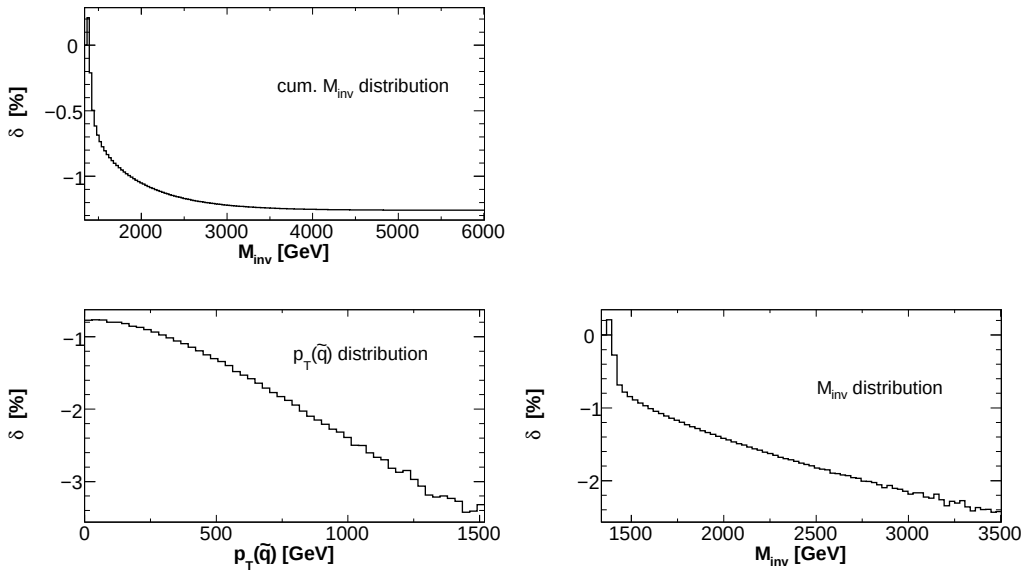

Figure 7.22: Same as Fig. 7.20, but considering the SPS5 scenario.

Chapter 8

Conclusions

In this thesis we have computed the electroweak contributions of $\mathcal{O}(\alpha_s\alpha)$, $\mathcal{O}(\alpha^2)$ and $\mathcal{O}(\alpha_s^2\alpha)$ to three different classes of processes leading to the hadronic production of the SUSY partners of quarks and gluons, *i.e.* squarks and gluinos. The theoretical framework is the Minimal Supersymmetric extension of the Standard Model, the MSSM. The three processes considered are gluino pair production, diagonal squark–anti-squark and associated squark–gluino production, which are important for SUSY searches at the LHC.

Concerning the EW contributions to gluino pair production, we have analysed their size in different scenarios and we have performed several scans on the MSSM parameter space. The EW contributions have a negligible impact on the total cross section and on the differential distributions both at the LHC and at the Tevatron. The reliability of different renormalization schemes of the squark sector have been investigated.

In the case of diagonal squark-anti–squark production, the EW contributions depend on the chirality and on the flavor of the produced squarks. For a given flavor, EW contributions are bigger in the case of left-handed squark production than in the right-handed case. The effect of such contributions is maximal in the case of $\tilde{u}_L\tilde{u}_L^*$ and $\tilde{d}_L\tilde{d}_L^*$, becoming smaller when the squarks of the second generation are produced. In the case of left-handed squark production, LO and NLO EW contributions are comparable. These general features appear in different SUSY scenarios, and the size of the EW contributions is bigger in the scenarios where the masses of the squarks are heavier. The increase of the EW contributions with increasing squark masses has been confirmed by a systematic study of the dependence of the EW corrections on the masses of the produced particles.

The peculiar dependence of the EW contributions on the chirality of the

produced squark is present in the case of associated squark–gluino production as well. We have computed these contributions in different scenarios; their impact is sizable in distributions, in particular for left-handed squarks. The dependence of the EW corrections to the mass of the final states has been investigated. In the left-handed case, the EW contributions increase as the masses of the squarks and gluino increase. In the right-handed case, the interplay between $\mathcal{O}(\alpha_s\alpha)$ and $\mathcal{O}(\alpha_s^2\alpha)$ contributions make the dependence on the masses of the produced particles mild. The importance of the EW corrections is smaller then in the squark–anti-squark production case owing to the absence of quark initiated tree-level EW contributions.

According to the current experimental studies, both ATLAS and CMS will not distinguish among squarks belonging to the first two generations. Therefore, we have considered the EW contributions to diagonal squark-anti–squark production and to squark–gluino production also for the case of treating the squarks of the first two generation inclusively. This means that we sum over the squarks of the first two generations. Owing to the small corrections for right-handed squarks, the relative yield of the EW contributions on such inclusive processes is not sizable, *i.e.* below 10%.
It should be stressed, however, that the EW contributions depend strongly on the level of inclusiveness of the experimental searches. For instance, the EW contributions are enhanced if left- and right-handed squarks can be distinguished and if charm-jets can be tagged. The distinction between squarks of different chirality is in principle possible exploiting the different decay chains of right- and left-handed squarks (*c.f.* section 3.4.1). Charm-tagging has been already performed at the Tevatron, but we are not aware of any publicly available study for the LHC.

The processes considered gave us the possibility to tackle some technical aspects of the computation of the EW contributions. These investigations will be useful for a straightforward extension of our study to the other processes producing colored SUSY particles at the LHC. Indeed, the treatment of the UV and IR divergences presented in chapter 4 is general and applies to every process leading to the production of squarks and gluinos. Moreover, the discussion on the reliability of the different schemes used to renormalize the squark sector is important when we consider processes with bottom squarks in the final state, such as $\tilde{g}\tilde{b}$ associated production and $\tilde{b}\tilde{b}^{(*)}$ production. The computation of the EW contributions of the remaining processes will therefore profit of the studies described in this thesis and is currently under investigation. At the time of writing the computation of EW contributions to squark-squark production is in a rather advanced stage. Non-diagonal squark-anti–squark production and processes producing bottom squarks are

the future projects of our collaboration.

Appendix A

Definitions and conventions

The conventions we use follow those of the book of Peskin and Schroeder [224]. The metric tensor is defined as

$$g_{\mu\nu} = g^{\mu\nu} = \begin{pmatrix} 1 & 0 & 0 & 0 \\ 0 & -1 & 0 & 0 \\ 0 & 0 & -1 & 0 \\ 0 & 0 & 0 & -1 \end{pmatrix}, \tag{A.1}$$

and is such that $g_{\mu\nu}g^{\nu\rho} = \delta^{\rho}_{\mu}$. Contravariant 4−vectors are defined as

$$x^{\mu} = (x^0, x^1, x^2, x^3) = (t, \vec{x}), \tag{A.2}$$

while the covariant ones can be obtained by means of the metric tensor,

$$x_{\mu} = g_{\mu\nu}x^{\nu} = (x^0, -x^1, -x^2, -x^3) = (t, -\vec{x}). \tag{A.3}$$

The covariant and contravariant derivatives are defined as

$$\partial_{\mu} = \frac{\partial}{\partial x^{\mu}} = \left(\frac{\partial}{\partial x^0}, \nabla\right), \quad \partial^{\mu} = g^{\mu\nu}\partial_{\mu} = \left(\frac{\partial}{\partial x^0}, -\nabla\right). \tag{A.4}$$

The Pauli matrices read

$$\sigma^1 = \begin{pmatrix} 0 & 1 \\ 1 & 0 \end{pmatrix}, \quad \sigma^2 = \begin{pmatrix} 0 & -i \\ i & 0 \end{pmatrix}, \quad \sigma^3 = \begin{pmatrix} 1 & 0 \\ 0 & -1 \end{pmatrix}. \tag{A.5}$$

These matrices can be arranged as follows,

$$\vec{\sigma} = (\sigma^1, \sigma^2, \sigma^3), \quad \sigma^{\mu} = (\mathbf{1}_2, \vec{\sigma}), \quad \overline{\sigma}^{\mu} = (\mathbf{1}_2, -\vec{\sigma}), \tag{A.6}$$

where $\mathbf{1}_n$ is the n-dimensional identity matrix.

Appendix B

Spinorial representations of the Poincaré Group

The Poincaré group is the Lie group of the isometries of the Minkowski space. The generic element of this group acts on a contravariant vector according to,

$$x^\mu \to \Lambda^\mu{}_\nu x^\nu + a^\mu, \tag{B.1}$$

where $\Lambda^\mu{}_\nu$ is an element of the Lorentz group[1]. The Poincaré group is ten dimensional, and it is the semidirect product of the Lorentz group and the Translation group. The Poincaré algebra is therefore the semidirect product of Lorentz algebra and the Translation algebra. Therefore, it exists a ten dimensional basis satisfying

$$\begin{aligned} [M_{\mu\nu}, M_{\rho\sigma}] &= i(g_{\nu\rho}M_{\mu\sigma} + g_{\mu\sigma}M_{\nu\rho} - g_{\nu\sigma}M_{\mu\rho} - g_{\mu\rho}M_{\nu\sigma}), \\ [P_\mu, P_\nu] &= 0, \\ [M_{\mu\nu}, P_\rho] &= -i(g_{\rho\mu}P_\nu - g_{\rho\nu}P_\mu). \end{aligned} \tag{B.2}$$

The generic element of the subgroup of the Poincaré group can be obtained exponentiating the Poincaré algebra. The set of the Lorentz transformations characterized by $\Lambda^0{}_0 \geq 1$ and $\det(\Lambda) = 1$, is a subgroup of the Lorentz group, the so called proper ortochronus Lorentz group. This subgroup is locally isomorphic to the group of the complex 2×2 matrix, $SL(2, C)$.

B.1 Weyl spinors

Being locally isomorphic to $SL(2, C)$, the proper ortochronus Lorentz group admits 2-dimensional representations.

[1]Therefore it satisfies $g_{\mu\nu} = g_{\sigma\rho}\Lambda^\sigma{}_\mu\Lambda^\rho{}_\nu$.

A special representation is the *left-handed spinorial representation* generated by

$$(\Sigma^L_{\mu\nu})_\alpha{}^\beta = \frac{1}{2}(\sigma_{\mu\nu})_\alpha{}^\beta, \qquad \sigma_{\mu\nu} = \frac{i}{2}(\sigma_\mu\bar{\sigma}_\nu - \bar{\sigma}_\nu\sigma_\mu)_\alpha{}^\beta,$$

where σ_μ and $\bar{\sigma}_\mu$ have been defined in appendix A. The generic elements of such representation, M, acts on a two dimensional spinor ψ_α as $\psi_\alpha \to M_\alpha{}^\beta\psi_\beta$.

The set of two-dimensional matrices defined as

$$(\Sigma^R_{\mu\nu})^{\dot\alpha}{}_{\dot\beta} = \frac{1}{2}(\bar{\sigma}_{\mu\nu})^{\dot\alpha}{}_{\dot\beta}, \qquad \bar{\sigma}_{\mu\nu} = \frac{i}{2}(\sigma_\mu\bar{\sigma}_\nu - \bar{\sigma}_\nu\sigma_\mu)^{\dot\alpha}{}_{\dot\beta},$$

generates the *right-handed spinorial representation* of the proper ortochronus Lorentz group. Let N be an element of such representation, its action on a two dimensional spinor $\bar{\chi}^{\dot\alpha}$ is $\bar{\chi}^{\dot\alpha} \to N^{\dot\alpha}{}_{\dot\beta}\bar{\chi}^{\dot\beta}$.

The *complex conjugate representation* is generated by

$$(\Sigma^c_{\mu\nu})_{\dot\alpha}{}^{\dot\beta} = \frac{1}{2}\epsilon_{\dot\alpha\dot\rho}(\bar{\sigma}_{\mu\nu})^{\dot\rho}{}_{\dot\delta}\epsilon^{\dot\delta\dot\beta},$$

where $\epsilon^{\dot\alpha\dot\beta}$ and $\epsilon_{\dot\alpha\dot\beta}$ are defined as

$$\epsilon^{\dot\alpha\dot\beta} = \begin{pmatrix} 0 & 1 \\ -1 & 0 \end{pmatrix}, \qquad \epsilon_{\dot\alpha\dot\beta} = \begin{pmatrix} 0 & -1 \\ 1 & 0 \end{pmatrix}.$$

An element of this representation, R, acts on a spinor $\bar{\xi}_{\dot\alpha}$ according to $\bar{\xi}_{\dot\alpha} \to R_{\dot\alpha}{}^{\dot\beta}\bar{\xi}_{\dot\beta}$.

The generators of the *dual representation* are

$$(\Sigma^d_{\mu\nu})^\alpha{}_\beta = \frac{1}{2}\epsilon^{\alpha\rho}(\sigma_{\mu\nu})_\rho{}^\delta\epsilon_{\delta\beta},$$

where,

$$\epsilon^{\alpha\beta} = \begin{pmatrix} 0 & 1 \\ -1 & 0 \end{pmatrix}, \qquad \epsilon_{\alpha\beta} = \begin{pmatrix} 0 & -1 \\ 1 & 0 \end{pmatrix}.$$

Given S belonging to that representation, its action on a two-dimensional spinor ϕ^α is $\phi^\alpha \to S^\alpha{}_\beta\phi^\beta$.

Notice that, given a left handed spinor ω_α, its complex conjugate $\bar{\omega}_{\dot\alpha} = (\omega_\alpha)^*$ is a right handed spinor. Moreover $\omega^\alpha = \epsilon^{\alpha\beta}\omega_\beta$ transforms according to the dual representation, while $\bar{\omega}_{\dot\alpha} = \epsilon_{\dot\alpha\dot\beta}\bar{\omega}^{\dot\beta}$ transforms under the complex conjugate representation.

Moreover, given two left handed spinor ψ and ϕ, the product $\psi\phi = \psi^\alpha\phi_\alpha$ is Lorentz invariant. Similarly, given two right handed spinors $\bar{\chi}$ and $\bar{\xi}$, $\bar{\chi}\bar{\xi} = \bar{\chi}_{\dot\alpha}\bar{\xi}^{\dot\alpha}$ is a Lorentz-invariant quantity. One can show that $(\psi\phi)^\dagger = (\bar{\psi}\bar{\phi})$.

B.2 Dirac and Majorana spinors

One can define the Clifford algebra in the Minkowski space as a four-dimensional algebra with a basis γ^μ satisfying

$$\{\gamma^\mu \gamma^\nu\} = 2g^{\mu\nu}.$$

A four dimensional representation of the Lorentz group is generated by the matrices $\Sigma^{Cl}_{\mu\nu} = i/4(\gamma_\mu\gamma_\nu - \gamma_\nu\gamma_\mu)$. A four dimensional realization of the Clifford algebra is obtained defining

$$\gamma^\mu = \begin{pmatrix} 0 & \sigma^\mu \\ \bar{\sigma}^\mu & 0 \end{pmatrix}. \tag{B.3}$$

The generators of the Lorentz group read

$$\Sigma^{Cl}_{\mu\nu} = \begin{pmatrix} \Sigma^L_{\mu\nu} & 0 \\ 0 & \Sigma^R_{\mu\nu} \end{pmatrix}. \tag{B.4}$$

A four dimensional spinor transforming according to this representation of the Lorentz group is called a Dirac spinor and is composed by a two dimensional left-handed spinor and a two dimensional right-handed one,

$$\Psi_D = \begin{pmatrix} \psi^\alpha \\ \bar{\chi}_{\dot{\alpha}} \end{pmatrix}.$$

This representation of the proper ortochronus Lorentz group is reducible. Indeed, the set of Dirac spinors characterized by

$$\bar{\psi}_{\dot{\alpha}} = \bar{\chi}_{\dot{\alpha}}, \tag{B.5}$$

is left invariant under the action of the proper ortochronus Lorentz group. Spinors fulfilling Eq. (B.5) are called Majorana spinors.

Appendix C

Grassmann variables

Grassmann variables are complex numbers θ^α satisfying

$$\{\theta^\alpha, \theta^\beta\} = \{\bar\theta^{\dot\alpha}, \bar\theta^{\dot\beta}\} = \{\theta^\alpha, \bar\theta^{\dot\beta}\} = 0. \tag{C.1}$$

As a consequence, every product involving more then two Grassmann variables vanishes:

$$\theta^\alpha\theta^\beta\theta^\gamma = 0, \qquad \bar\theta^{\dot\alpha}\bar\theta^{\dot\beta}\bar\theta^{\dot\gamma} = 0.$$

Differentiation w.r.t. Grassmann variables is defined by means of the operators

$$\partial_\alpha = \frac{\partial}{\partial\theta^\alpha}, \quad \partial^\alpha = \frac{\partial}{\partial\theta_\alpha}, \quad \bar\partial_{\dot\alpha} = \frac{\partial}{\partial\bar\theta^{\dot\alpha}}, \quad \bar\partial^{\dot\alpha} = \frac{\partial}{\partial\bar\theta_{\dot\alpha}}. \tag{C.2}$$

Their action is determined by the following definitions

$$\begin{aligned}
\partial_\alpha\theta^\beta &= \delta^\beta_\alpha, \quad \partial^\alpha\theta_\beta = \delta^\alpha_\beta, \quad \{\partial^\alpha, \bar\theta^{\dot\beta}\} = 0, \\
\bar\partial_{\dot\alpha}\bar\theta^{\dot\beta} &= \delta^{\dot\beta}_{\dot\alpha}, \quad \bar\partial^{\dot\alpha}\bar\theta_{\dot\beta} = \delta^{\dot\alpha}_{\dot\beta}, \quad \{\bar\partial^{\dot\alpha}, \theta^\beta\} = 0, \\
\partial_\alpha(\theta^\beta\theta^\gamma) &= \partial_\alpha(\theta^\beta)\theta^\gamma - \theta^\beta\partial_\alpha(\theta^\gamma), \quad \bar\partial_{\dot\alpha}(\bar\theta^{\dot\beta}\bar\theta^{\dot\gamma}) = \bar\partial_{\dot\alpha}(\bar\theta^{\dot\beta})\bar\theta^{\dot\gamma} - \bar\theta^{\dot\beta}\bar\partial_{\dot\alpha}(\bar\theta^{\dot\gamma}).
\end{aligned}$$

Directly from the definitions given above it follows that

$$\partial_\alpha = -\epsilon_{\alpha\beta}\partial^\beta, \quad \partial_\alpha\theta_\beta = \epsilon_{\beta\alpha}, \quad \bar\partial_{\dot\alpha} = -\epsilon_{\dot\alpha\dot\beta}\bar\partial^{\dot\beta}, \quad \bar\partial_{\dot\alpha}\bar\theta_{\dot\beta} = \epsilon_{\dot\beta\dot\alpha}.$$

Integration over a Grassmann variable θ is defined as follows

$$\int d\theta\ \theta = 1, \qquad \int d\theta\ = 0; \tag{C.3}$$

The integral of a given function $f(\theta)$ can be evaluated from its Taylor expansion $f(\theta) = f(0) + \theta\Delta$,

$$\int d\theta\ f(\theta) = \int d\theta(f(0) + \theta\Delta) = f(0)\int d\theta + \Delta\int d\theta\ \theta = \Delta.$$

Moreover we define

$$d^2\theta = \frac{1}{2}d\theta^1 d\theta^2 = -\frac{1}{4}d\theta^\alpha d\theta_\alpha, \quad d^2\bar{\theta} = \frac{1}{2}d\bar{\theta}^{\dot{2}} d\bar{\theta}^{\dot{1}} = -\frac{1}{4}d\bar{\theta}_{\dot{\alpha}} d\bar{\theta}^{\dot{\alpha}}, \quad d^4\theta = d^2\theta d^2\bar{\theta}.$$

The following results follow directly from the definition of integral over Grassmann variables,

$$\begin{aligned}
\int d^2\theta\ \theta^\alpha = 0, \qquad \int d^2\theta\ \theta^\alpha\theta^\beta &= -\frac{1}{2}\epsilon^{\alpha\beta}, \qquad \int d^2\theta\ (\theta\theta) = 1, \\
\int d^2\bar{\theta}\ \bar{\theta}^{\dot{\alpha}} = 0, \qquad \int d^2\bar{\theta}\ \bar{\theta}^{\dot{\alpha}}\bar{\theta}^{\dot{\beta}} &= -\frac{1}{2}\epsilon^{\dot{\alpha}\dot{\beta}}, \qquad \int d^2\bar{\theta}\ (\bar{\theta}\bar{\theta}) = 1, \\
\int d^4\theta(\theta\theta)(\bar{\theta}\bar{\theta}) &= 1.
\end{aligned}$$

Appendix D

Phase space integrations

In this appendix we give the parametrizations of the phase space for the two-particle and three-particle final state used in this thesis. The general definition of the invariant phase space element of an n-particle final state related to the process

$$1(k_1, m_1),\ 2(k_2, m_2)\ \rightarrow\ 3(k_3, m_3), \ldots, n+2(k_{r+2}, m_{r+2}), \tag{D.1}$$

can be written as

$$\begin{aligned} d\Phi_n(k_1, \ldots, k_{n+2}) &= (2\pi)^4 \left[\prod_{r=1}^{n} \frac{d^4k_{r+2}}{(2\pi)^3}\Theta(k^0_{r+2})\delta(k^2_{r+2} - m^2_{r+2})\right] \\ &\quad \times\delta^{(4)}\left(\sum_{r=1}^{n} k_{r+2} - (k_1 + k_2)\right). \end{aligned} \tag{D.2}$$

D.1 Two-particle phase space

We describe two different parametrizations of the two-particle phase space, which, after momentum conservation and the on-shell conditions are imposed, is a two-dimensional space.

The first parametrization exploits the fact that in the center-of-mass system, $\vec{k}_3$ and $\vec{k}_4$ are aligned and it uses as independent parameters the angles (φ, θ) describing the direction of $\vec{k}_3$ with respect to the beam axis. Owing to the rotational invariance the integral over the azimuthal angle φ leads to a factor 2π and the phase space measure is reduced to an integration over the polar angle θ,

$$\int d\Phi_2(s) = \frac{1}{8\pi}\frac{|\vec{k_3}|}{\sqrt{s}}\int_{-1}^{1} dc_\theta, \tag{D.3}$$

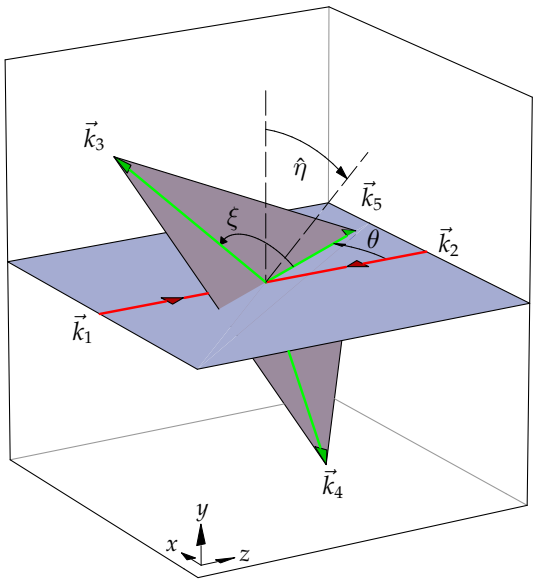

Figure D.1: Representation of the independent parameters used in the parametrization of the three particle phase space. The figure is taken from Ref. [225].

where the center-of-mass energy s is defined as $s = (k_1 + k_2)^2$. $|\vec{k_3}|$ can be written as

$$|\vec{k_3}|^2 = \frac{s^2 + m_3^3 + m_4^2 - 2(m_3^2 s + m_4^2 s + m_3^2 m_4^2)}{4s}. \tag{D.4}$$

Alternatively, the two dimensional phase space can be parametrized using the azimuthal angle φ and the Mandelstam variable $t = (k_1 - k_3)^2$. According to this parametrization the two particle phase space measure reads

$$\int d\Phi_2(s) = \frac{1}{8\pi\sqrt{\lambda(s, m_1^2, m_2^2)}} \int_{t^-}^{t^+} dt \ , \tag{D.5}$$

where the abbreviations

$$\begin{aligned} \lambda(a,b,c) &= a^2 + b^2 + c^2 - 2(ab + bc + ac), \qquad \text{(D.6)} \\ t^{\pm} &= m_1^2 + m_3^2 - \frac{1}{2s} \\ &\times \left[(s + m_1^2 - m_2^2)(s + m_3^3 - m_4^2) \mp \sqrt{\lambda(s, m_1^2, m_2^2)\lambda(s, m_3^2, m_4^2)} \right], \end{aligned}$$

have been used.

D.2 Three-particle phase space

The three-particle phase space is a five dimensional space. The independent parameters chosen for its parametrization are depicted in Fig. D.1. They are fixed in the center-of-mass system. They are chosen to be the energies of the third and the fifth particle, k_3^0 and k_5^0, the angles describing the direction of the particle 5 with respect to the beam axis, (φ, θ), and the angle $\hat{\eta}$ between the plane spanned by $(\vec{k}_1, \vec{k}_5)$ and that spanned by $(\vec{k}_3, \vec{k}_5)$. Again, the integration over φ is trivial and leads to a factor 2π. After the integration over φ, the phase space measure reads

$$\int d\Phi_3(s) = \frac{1}{128\pi^4} \int_{m_5}^{k_5^+} dk_5^0 \int_{k_3^-}^{k_3^+} dk_3^0 \int_{-1}^{1} dc_\theta \int_0^{2\pi} d\hat{\eta}. \tag{D.7}$$

The boundaries are

$$\begin{aligned} k_5^+ &= \frac{\sqrt{s}}{2} - \frac{(m_3+m_4)^2 - m_5^2}{2\sqrt{s}}, \\ k_3^\pm &= \frac{1}{2\tau}\left[\zeta(\tau + m_+ m_-) \pm |\vec{k}_5| \sqrt{(\tau - m_+^2)(\tau - m_-^2)}\right], \end{aligned} \tag{D.8}$$

where the notations $s = (k_1 + k_2)^2$, $\zeta = \sqrt{s} - k_5^0$, $\tau = \zeta^2 - |\vec{k}_5|^2$, and $m_\pm = m_3 \pm m_4$ have been used.

Appendix E

More details on the dipole formalism

E.1 Photonic divergences

As explained in section 4.3.3, in the case of the photonic soft and collinear divergences related to the process

$$1(p_1, m_1);\ 2(p_2, m_2) \to 3(p_3, m_3);\ 4(p_4, m_4);\ \gamma(p_\gamma, m_\gamma),$$

an appropriate function fulfilling the requirements of the subtraction methods is

$$|\mathcal{M}^{\rm sub}_{1,2\to3,4,\gamma}|^2 = -\frac{\alpha}{2\pi}\left\{\sum_{i\neq j;\ i,j=1}^{4} e_i\sigma_i e_j\sigma_j\ g^\gamma_{ij}\sum|\mathcal{M}^{1,0}_{1,2\to3,4}(\tilde{\Phi}^\gamma_{ij})|^2\right\}. \quad \text{(E.1)}$$

The functions g^γ_{ij} read

$$\begin{aligned}
g^\gamma_{ab} &= \frac{8\pi^2}{(p_a k_\gamma)x_{12}}\left(\frac{2}{1-x_{12}} - 1 - x_{12}\right),\\
g^\gamma_{ai} &= \frac{8\pi^2}{(p_a k_\gamma)x_{ia}}\left(\frac{2}{2-x_{ia}-z_{ia}} - 1 - x_{ia}\right),\\
g^\gamma_{ia} &= \frac{8\pi^2}{(p_i k_\gamma)x_{ia}}\left(\frac{2}{2-x_{ia}-z_{ia}} - 1 - z_{ia} - \frac{m_i^2}{(p_i k_\gamma)}\right),\\
g^\gamma_{ij} &= \frac{8\pi^2}{(p_i k_\gamma)R_j(y_i)}\left(\frac{2}{1-z_j(1-y_i)} - 1 - z_j - \frac{m_i^2}{(p_i k_\gamma)}\right), \quad \text{(E.2)}
\end{aligned}$$

where $a,b = 1,2$ and $i,j = 3,4$. The following abbreviations have been introduced

$$\begin{aligned}
x_{12} &= \frac{p_1p_2 - p_1k_\gamma - p_2k_\gamma}{p_1p_2}, \\
x_{ia} &= \frac{p_ip_a + p_ak_\gamma - p_ik_\gamma}{p_ap_i + p_ak_\gamma}, \quad z_{ia} = \frac{p_ap_i}{p_ap_i + p_ak_\gamma}, \\
y_i &= \frac{p_ik_\gamma}{p_3p_4 + p_3k_\gamma + p_4k_\gamma}, \quad z_j = \frac{p_3p_4}{p_3p_4 + p_jk_\gamma}, \\
R_j(y) &= \sqrt{\frac{[2m_j^2 + (s_{12} - m_3^2 - m_4^2)(1-y)]^2 - 4s_{12}m_j^2}{s_{12}^2 - 2s_{12}(m_3^2 + m_4^2) + (m_3^2 - m_4^2)^2}}.
\end{aligned} \tag{E.3}$$

$\tilde{\Phi}^\gamma_{ij} = (\tilde{p}_1;\tilde{p}_2;\tilde{p}_3;\tilde{p}_4)$ are the mapping from the momenta of the process $1,2 \to 3,4,\gamma$ to the momenta of the process $1,2 \to 3,4$. They read as follows

$$\begin{aligned}
\tilde{\Phi}^\gamma_{ab} &= \big(\tilde{p}_a^\mu = x_{12}p_a^\mu;\ \ \tilde{p}_b^\mu = p_b^\mu;\ \ \tilde{p}_3^\mu = \Lambda^\mu{}_\nu p_3^\nu;\ \ \tilde{p}_4^\mu = \Lambda^\mu{}_\nu p_4^\nu\big), \\
\tilde{\Phi}^\gamma_{ai} &= \big(\tilde{p}_a^\mu = x_{ia}p_a^\mu;\ \ \tilde{p}_{3-a}^\mu = p_{3-a}^\mu;\ \ \tilde{p}_i^\mu = \bar{r}_{ia}^\mu;\ \ \tilde{p}_{7-i}^\mu = p_{7-i}^\mu\big), \\
\tilde{\Phi}^\gamma_{ia} &= \big(\tilde{p}_a^\mu = x_{ia}p_a^\mu;\ \ \tilde{p}_{3-a}^\mu = p_{3-a}^\mu;\ \ \tilde{p}_i^\mu = \bar{r}_{ia}^\mu;\ \ \tilde{p}_{7-i}^\mu = p_{7-i}^\mu\big), \\
\tilde{\Phi}^\gamma_{ij} &= \big(\tilde{p}_1^\mu = p_1^\mu;\ \ \tilde{p}_2^\mu = p_2^\mu;\ \ \tilde{p}_i^\mu = p_1^\mu + p_2^\mu - r_{ij}^\mu;\ \ \tilde{p}_j^\mu = r_{ij}^\mu\big).
\end{aligned} \tag{E.4}$$

Again, $a,b = 1,2$ and $i,j = 3,4$. $\Lambda^\mu{}_\nu$, $\bar{r}_{ia}$, and r_{ij}^μ are defined as

$$\begin{aligned}
\Lambda^\mu{}_\nu &= \delta^\mu_\nu - \frac{(P_{12} + \tilde{P}_{ab})^\mu (P_{12} + \tilde{P}_{ab})_\nu}{P_{12}^2 - P_{12}\tilde{P}_{ab}} + \frac{2\tilde{P}_{ab}^\mu (P_{12})_\nu}{P_{12}^2}, \\
\bar{r}_{ia}^\mu &= p_i^\mu + k_\gamma^\mu - (1 - x_{ia})p_a^\mu, \\
r_{ij}^\mu &= \sqrt{\frac{\lambda(s_{12};m_3^2;m_4^2)}{\lambda\big((p_i+k_\gamma)^2;s_{12};m_j^2\big)}}\left(p_j^\mu - \frac{P_{34}p_j}{s_{12}}P_{34}^\mu\right) + \frac{s_{12} + m_j^2 - m_i^2}{2s_{12}}P_{34}^\mu,
\end{aligned} \tag{E.5}$$

where the abbreviations

$$\begin{aligned}
P_{12} &= p_3 + p_4, \quad \tilde{P}_{ab} = x_{12}p_a + p_b, \quad P_{34} = p_1 + p_2, \\
\lambda(x;y;z) &= x^2 + y^2 + z^2 - 2(xy + xz + yz),
\end{aligned} \tag{E.6}$$

have been used. The analytical integration of the subtracted function is available in Ref. [188, 189]. In our case the outcome is

$$\begin{aligned}
\int d\Phi_1 |\mathcal{M}^{\rm sub}_{1,2\to 3,4,\gamma}|^2 &= -\frac{\alpha}{2\pi}\Bigg\{ e_3\sigma_3 e_4\sigma_4 (G^\gamma_{34}+G^\gamma_{43}) \int_{y_{-,3}(1)}^{y_{+,3}(1)} \frac{dy}{8\pi s_{12}}\, \mathcal{A}(s_{12},y) \\
&+ e_1\sigma_1 e_2\sigma_2 \int_0^1 dx\, (\mathcal{G}_{12}(x)+\mathcal{G}_{21}(x)) \Bigg[\int_{y_{-,3}(x)}^{y_{+,3}(x)} \frac{dy}{8\pi x s_{12}} \\
&\quad \Theta(x s_{12}-th.^2) \frac{\mathcal{A}(x s_{12},y)}{x} - \int_{y_{-,3}(1)}^{y_{+,3}(1)} \frac{dy}{8\pi s_{12}} \mathcal{A}(s_{12},y) \Bigg] \\
&+ e_1\sigma_1 e_2\sigma_2 (G^\gamma_{12}+G^\gamma_{21}) \int_{y_{-,3}(1)}^{y_{+,3}(1)} \frac{dy}{8\pi s_{12}} \mathcal{A}(s_{12},y) \\
&+ \sum_{a=1}^{2}\sum_{j=3}^{4} e_a\sigma_a e_j\sigma_j \int_0^1 dx \Bigg[\int_{y_{-,j}(x)}^{y_{+,j}(x)} \frac{dy}{8\pi x s_{12}} \\
&\quad \Theta(x s_{12}-th.^2) \frac{(\mathcal{G}_{ja}(x,y)+\mathcal{G}_{aj}(x,y))}{x} \mathcal{A}(x s_{12}, t(y,x)) \\
&- \int_{y_{-,j}(1)}^{y_{+,j}(1)} \frac{dy}{8\pi s_{12}} (\mathcal{G}_{ja}(x,y)+\mathcal{G}_{aj}(x,y)) \mathcal{A}(s_{12},t(y,1)) \Bigg] \\
&+ \sum_{a=1}^{2}\sum_{j=3}^{4} e_a\sigma_a e_j\sigma_j \int_{y_{-,j}(1)}^{y_{+,j}(1)} \frac{dy}{8\pi s_{12}} (G^\gamma_{ja}(y)+G^\gamma_{aj}(y)) \\
&\quad \mathcal{A}(s_{12},t(y,1)) \Bigg\}. \qquad \text{(E.7)}
\end{aligned}$$

The functions $\mathcal{A}(s,t)$, $t(y,x)$, and $y_{\pm,j}(x)$ read

$$\begin{aligned}
\mathcal{A}(s,t) &= \sum |\mathcal{M}^{1,0}_{1,2\to 3,4}|^2, \text{ with } s=(p_1+p_2)^2, \text{ and } t=(p_1-p_3)^2, \\
t(y,x) &= \big(m_3^2+m_4^2-x s_{12}-y\big)(\delta_{a2}\delta_{j3}+\delta_{a1}\delta_{j4}) + y(\delta_{a1}\delta_{j3}+\delta_{a2}\delta_{j4}), \\
y_{\pm,j}(x) &= m_j^2 - \frac{1}{2}\left[(x s_{12}+m_j^2-m_{7-j}^2) \mp \sqrt{\lambda(x s_{12},m_3^2,m_4^2)} \right]. \qquad \text{(E.8)}
\end{aligned}$$

The functions G^γ_{ij} are defined as follows,

$$\begin{aligned}
G^\gamma_{ij} &= \ln\left(\frac{m_\gamma^2 a_3^3}{m_i^2}\right) - 2\ln\left(1-a_3^2\right) + \frac{a_3^2}{2} + \frac{3}{2} + \frac{\bar{P}^2_{ij}}{\sqrt{\lambda_{ij}}} \Bigg[\ln(a_1) \ln\left(\frac{m_\gamma^2 m_j^2}{\lambda_{ij} a_2}\right) \\
&\quad + 2\mathrm{Li}_2(a_1) + 4\mathrm{Li}_2\left(-\sqrt{\frac{a_2}{a_1}}\right) - 4\mathrm{Li}_2\left(-\sqrt{a_1 a_2}\right) + \frac{1}{2}\ln^2(a_1) - \frac{\pi^2}{3} \Bigg],
\end{aligned}$$

$$
\begin{aligned}
G^{\gamma}_{ab} &= 2-\frac{\pi^2}{3}+\left[\ln\left(\frac{m_a^2}{s_{12}}\right)\ln\left(\frac{m_\gamma^2}{s_{12}}\right)+\ln\left(\frac{m_\gamma^2}{s_{12}}\right)\right.\\
&\quad \left.-\frac{1}{2}\ln^2\left(\frac{m_a^2}{s_{12}}\right)+\frac{1}{2}\ln\left(\frac{m_a^2}{s_{12}}\right)\right],\\
G^{\gamma}_{ja}(y) &= \ln\left(\frac{m_j^2}{m_\gamma^2}\right)\ln\left(2-\frac{y}{m_j^2}\right)+2\ln\left(\frac{m_\gamma m_j}{m_j^2-y}\right)-2\mathrm{Li}_2\left(\frac{y}{y-2m_j^2}\right)\\
&+ \frac{1}{2}\ln^2\left(2-\frac{y}{m_j^2}\right)+\frac{(y-m_j^2)^2}{2y^2}\ln\left(1-\frac{y}{m_j^2}\right)-\frac{\pi^2}{6}+\frac{3}{2}+\frac{m_j^2}{2y},\\
G^{\gamma}_{aj}(y) &= \ln\left(\frac{m_\gamma^2}{m_a^2}\right)\ln\left(\frac{m_a^2(2m_j^2-y)}{(m_j^2-y)^2}\right)+\ln\left(\frac{m_\gamma^2}{m_a^2}\right)+2\mathrm{Li}_2\left(\frac{y}{2m_j^2-y}\right)\\
&\quad -2\mathrm{Li}_2\left(\frac{m_j^2}{2m_j^2-y}\right)+\frac{1}{2}\ln^2\left(\frac{m_a^2}{2m_i^2-y}\right)+\frac{3}{2}\ln\left(\frac{m_a^2}{m_j^2-y}\right)\\
&\quad 2\ln\left(\frac{m_a^2m_j^2}{(m_j^2-y)(2m_j^2-y)}\right)\ln\left(\frac{2m_j^2-y}{m_j^2-y}\right)+\frac{\pi^2}{3}-1+\frac{m_j^2}{2y}\\
&\quad +\frac{m_j^2(m_j^2-4y)}{2y^2}\ln\left(1-\frac{y}{m_j^2}\right),
\end{aligned}
\tag{E.9}
$$

using the abbreviations

$$
\lambda_{ij}=\lambda(s_{12},m_i^2,m_j^2),\qquad \bar{P}_{ij}^2=s_{12}-m_i^2-m_j^2,
\tag{E.10}
$$

$$
a_1=\frac{\bar{P}_{ij}^2+2m_i^2-\sqrt{\lambda_{ij}}}{\bar{P}_{ij}^2+2m_i^2+\sqrt{\lambda_{ij}}},\qquad a_2=\frac{\bar{P}_{ij}^2-\sqrt{\lambda_{ij}}}{\bar{P}_{ij}^2+\sqrt{\lambda_{ij}}},\quad a_3=\frac{m_i}{\sqrt{s_{12}}-m_j}.
$$

The functions $\mathcal{G}_{ij}$ read instead

$$
\begin{aligned}
\mathcal{G}_{ab}(x) &= \frac{1+x^2}{1-x}\left[\ln\left(\frac{s_{12}}{m_a^2}\right)-1\right]+(1-x),\\
\mathcal{G}_{ja}(x,y) &= \frac{1}{1-x}\left\{2\ln\left(\frac{2-x-z(x,y)}{1-x}\right)+\frac{1}{2}(z(x,y)-1)\left[3+z(x,y)\right.\right.\\
&\quad \left.\left.-\frac{4m_i^2x}{(y-m_i^2)(1-x)}\right]\right\},
\end{aligned}
$$

$$
\begin{aligned}
\mathcal{G}_{aj}(x,y) &= \frac{1+x^2}{1-x}\left\{\ln\left(\frac{m_j^2-y}{m_a^2x}\right)+\ln(1-z(x,y))-1\right\}+(1-x)\\
&\quad -\frac{2}{1-x}\ln(2-x-z(x,y))+(1+x)\ln(1-x),
\end{aligned}
\tag{E.11}
$$

defining $z(x,y)$ as

$$z(x,y) = \frac{m_i^2 x}{m_i^2 - y(1-x)}.$$

The subtraction functions matching the collinear singularities of the processes

$$\begin{aligned} \gamma(k_\gamma;m_\gamma),\ 2(p_2;m_2) &\ \to\ 3(p_3;m_3),\ 4(p_4;m_4),\ \bar{1}(p_1;m_1), \\ 1(p_1;m_1),\ \gamma(k_\gamma;m_\gamma) &\ \to\ 3(p_3;m_3),\ 4(p_4;m_4),\ \bar{2}(p_2;m_2), \end{aligned} \tag{E.12}$$

read

$$\begin{aligned} |\mathcal{M}^{\rm sub}_{\gamma,2\to3,4,\bar{1}}| &= -\frac{\alpha}{2\pi} e_1^2 h_{\gamma 2} \sum |\mathcal{M}_{1,2\to3,4}(\tilde{\Phi}^\gamma_{\gamma 2})|^2, \\ |\mathcal{M}^{\rm sub}_{1,\gamma\to3,4,\bar{2}}| &= -\frac{\alpha}{2\pi} e_2^2 h_{1\gamma} \sum |\mathcal{M}_{1,2\to3,4}(\tilde{\Phi}^\gamma_{1\gamma})|^2, \end{aligned} \tag{E.13}$$

using the functions $h_{\gamma 1}$, $h_{2\gamma}$

$$\begin{aligned} h_{\gamma 2} &= -8\pi^2 \frac{P_{gq}(x_{\gamma 2})}{x_{\gamma 2}(k_\gamma p_1)}, \qquad x_{\gamma 2} = \frac{p_2 k_\gamma - p_1 k_\gamma - p_1 p_2}{p_2 k_\gamma}, \\ h_{1\gamma} &= -8\pi^2 \frac{P_{gq}(x_{1\gamma})}{x_{1\gamma}(k_\gamma p_2)}, \qquad x_{1\gamma} = \frac{p_1 k_\gamma - p_2 k_\gamma - p_2 p_1}{p_1 k_\gamma}. \end{aligned} \tag{E.14}$$

The splitting function P_{gq} is defined in Eq. (4.14), while the mappings $\tilde{\Phi}^\gamma_{\gamma 2}$ and $\tilde{\Phi}^\gamma_{1\gamma}$ are defined as

$$\begin{aligned} \tilde{\Phi}^\gamma_{\gamma 2} &= \big(x_{\gamma 2} k_\gamma^\mu;\ p_2^\mu;\ \Lambda(1)^\mu{}_\nu p_3^\nu;\ \Lambda(1)^\mu{}_\nu p_4^\nu\big), \\ \tilde{\Phi}^\gamma_{1\gamma} &= \big(p_1^\mu;\ x_{1\gamma} k_\gamma^\mu;\ \Lambda(2)^\mu{}_\nu p_3^\nu;\ \Lambda(2)^\mu{}_\nu p_4^\nu,\big), \end{aligned} \tag{E.15}$$

where the Lorentz transformation $\Lambda(a)$ is defined according to,

$$\Lambda(a)^\mu{}_\nu = \delta^\mu_\nu - \frac{(P_a + \overline{P}_a)^\mu (P_a + \overline{P}_a)_\nu}{P_a^2 - P_a \overline{P}_a} + \frac{2\overline{P}^\mu_a (P_a)_\nu}{P_a^2}, \tag{E.16}$$

using the abbreviations

$$\begin{aligned} P_1 &= p_2 + k_\gamma - p_1, \qquad \overline{P}_1 = p_2 + x_{\gamma 2} k_\gamma, \\ P_2 &= p_1 + k_\gamma - p_2, \qquad \overline{P}_2 = p_1 + x_{1\gamma} k_\gamma. \end{aligned} \tag{E.17}$$

The integral of the subtracted function over the phase space of the final

(anti-)quark reads

$$\begin{aligned}
\int d\Phi_1 |\mathcal{M}^{\rm sub}_{\gamma,2\to 3,4,\bar{1}}|^2 &= \frac{\alpha}{2\pi} e_1^2 \int_0^1 \frac{dx}{x}\, \mathcal{H}_{\gamma 2}(x) \int_{\bar{y}_{-,3}(x)}^{\bar{y}_{+,3}(x)} \frac{dy}{8\pi s_{\gamma 2} x} \mathcal{A}(x s_{\gamma 2}, y) \\
&\quad \Theta(x s_{\gamma 2} - th^2.)(\delta_{1q} + \delta_{1\bar{q}}), \\
\int d\Phi_1 |\mathcal{M}^{\rm sub}_{1,\gamma\to 3,4,\bar{2}}|^2 &= \frac{\alpha}{2\pi} e_2^2 \int_0^1 \frac{dx}{x}\, \mathcal{H}_{1\gamma}(x) \int_{\tilde{y}_{-,3}(x)}^{\tilde{y}_{+,3}(x)} \frac{dy}{8\pi s_{1\gamma} x} \mathcal{A}(x s_{1\gamma}, y) \\
&\quad \Theta(x s_{1\gamma} - th.^2)(\delta_{2q} + \delta_{2\bar{q}}),
\end{aligned} \tag{E.18}$$

where $\mathcal{A}(s,t)$ has been defined in Eq. (E.8). $\bar{y}_{\pm,j}(x)$ [$\tilde{y}_{\pm,j}(x)$] is obtained substituting $s_{12} \to s_{\gamma 2}$ [$s_{12} \to s_{1\gamma}$] into Eq. (E.8). The functions $\mathcal{H}$ read as follows,

$$\begin{aligned}
\mathcal{H}_{\gamma 2}(x) &= P_{qg}(x) \ln\left(\frac{s_{\gamma 2}}{m_1^2}(1-x)^2\right) + 2x(1-x), \\
\mathcal{H}_{1\gamma}(x) &= P_{qg}(x) \ln\left(\frac{s_{1\gamma}}{m_2^2}(1-x)^2\right) + 2x(1-x).
\end{aligned} \tag{E.19}$$

E.2 Gluonic divergences

In the case of the gluonic mass singularities appearing in the process

$$1(p_1;m_1;c_1);\ 2(p_2;m_2;c_2) \to 3(p_3;m_3;c_3);\ 4(p_4;m_4;c_4)\ g(k_g;m_g;c), \tag{E.20}$$

the subtraction function obtained using the dipole method and performing the color algebra properly is

$$|\mathcal{M}^{\rm sub}_{1,2\to 3,4,g}|^2 = -\frac{\alpha_s}{2\pi} \left\{ \sum_{i\neq j;\ i,j=1}^{4} g_{ij}^g\ \mathcal{F}_{ij}(\tilde{\Phi}_{ij}^g) \right\}. \tag{E.21}$$

$\mathcal{F}_{ij}$ is defined in Eq. (4.71), while g_{ij}^g and $\tilde{\Phi}_{ij}^g$ can be obtained from g_{ij}^γ and $\tilde{\Phi}_{ij}^\gamma$ performing the substitution $k_\gamma \to k_g$ into Eq. (E.2) and (E.4) and in the definitions (E.3) and (E.5). The integral of the subtracted function over the

whole gluonic phase space reads

$$\begin{aligned}
\int d\Phi_1 |\mathcal{M}^{\rm sub}_{1,2\to 3,4,g}|^2 &= -\frac{\alpha_s}{2\pi}\Bigg\{(G^g_{34}+G^g_{43})\int_{y_{-,3}(1)}^{y_{+,3}(1)}\frac{dy}{8\pi s_{12}}\,\mathcal{F}_{34}(s_{12},y) \\
&+ \int_0^1 dx\,(\mathcal{G}_{12}(x)+\mathcal{G}_{21}(x))\Bigg[\int_{y_{-,3}(x)}^{y_{+,3}(x)}\frac{dy}{8\pi x s_{12}} \\
&\quad \Theta(xs_{12}-th.^2)\frac{\mathcal{F}_{12}(xs_{12},y)}{x}-\int_{y_{-,3}(1)}^{y_{+,3}(1)}\frac{dy}{8\pi s_{12}} \\
&\quad \mathcal{F}_{12}(s_{12},y)\Bigg]+(G^g_{12}+G^g_{21})\int_{y_{-,3}(1)}^{y_{+,3}(1)}\frac{dy}{8\pi s_{12}}\mathcal{F}_{12}(s_{12},y) \\
&+ \sum_{a=1}^{2}\sum_{j=3}^{4}\int_0^1 dx\Bigg[\int_{y_{-,j}(x)}^{y_{+,j}(x)}\frac{dy}{8\pi x s_{12}}\Theta(xs_{12}-th.^2) \\
&\quad \frac{(\mathcal{G}_{ja}(x,y)+\mathcal{G}_{aj}(x,y))}{x}\mathcal{F}_{ja}(xs_{12},t(y,x)) \\
&- \int_{y_{-,j}(1)}^{y_{+,j}(1)}\frac{dy}{8\pi s_{12}}(\mathcal{G}_{ja}(x,y)+\mathcal{G}_{aj}(x,y))\mathcal{F}_{ja}(s_{12},t(y,1))\Bigg] \\
&+ \sum_{a=1}^{2}\sum_{j=3}^{4}\int_{y_{-,j}(1)}^{y_{+,j}(1)}\frac{dy}{8\pi s_{12}}\,(G^g_{ja}+G^g_{aj}) \\
&\quad \mathcal{F}_{ja}(s_{12},t(y,1))\Bigg\}. \qquad \text{(E.22)}
\end{aligned}$$

The functions G^g_{ij} can be obtained from the functions G^γ_{ij} after substituting $m_\gamma \to m_g$ into Eq. (E.9).

The collinear singularities of the processes:

$$\begin{aligned}
&g(k_g;m_g;c),\ 2(p_2;m_2;c_2) \ \to\ 3(p_3;m_3;c_3),\ 4(p_4;m_4;c_4),\ \bar{1}(p_1;m_1;c_1), \\
&1(p_1;m_1;c_1),\ g(k_g;m_g;c) \ \to\ 3(p_3;m_3;c_3),\ 4(p_4;m_4;c_4),\ \bar{2}(p_2;m_2;c_2),
\end{aligned}$$

are cancelled by means of the following subtraction functions,

$$\begin{aligned}
|\mathcal{M}^{\rm sub}_{g,2\to 3,4,\bar{1}}| &= -\frac{\alpha_s}{2\pi}T_R h_{g2}\,\mathcal{F}(\tilde{\Phi}^g_{g2}), \\
|\mathcal{M}^{\rm sub}_{1,g\to 3,4,\bar{2}}| &= -\frac{\alpha_s}{2\pi}T_R h_{1g}\,\mathcal{F}(\tilde{\Phi}^g_{1g}), \qquad \text{(E.23)}
\end{aligned}$$

where $\mathcal{F}$ is defined in Eq. (4.73). The functions h_{g2}, h_{1g}, $\tilde{\Phi}^g_{g2}$, $\tilde{\Phi}^g_{1g}$ can be obtained from $h_{\gamma 2}$, $h_{1\gamma}$, $\tilde{\Phi}^\gamma_{\gamma 2}$, $\tilde{\Phi}^\gamma_{1\gamma}$ substituting k_γ with k_g into Eqs. (E.14 –

E.17). The integral of the subtracted function over the phase space of the final (anti-)quark reads [189, 190]

$$\begin{aligned}
\int d\Phi_1 |\mathcal{M}^{\rm sub}_{g,2\to 3,4,\bar{1}}|^2 &= \frac{\alpha_s}{2\pi} T_R \int_0^1 \frac{dx}{x}\, \mathcal{H}_{g2}(x) \int_{\bar{y}_{-,3}(x)}^{\bar{y}_{+,3}(x)} \frac{dy}{8\pi x s_{g2}} \mathcal{F}(x s_{g2}, y) \\
&\quad \Theta(x s_{g2} - th.^2)(\delta_{1q} + \delta_{1\bar{q}}), \\
\int d\Phi_1 |\mathcal{M}^{\rm sub}_{1,g\to 3,4,\bar{2}}|^2 &= \frac{\alpha_s}{2\pi} T_R \int_0^1 \frac{dx}{x}\, \mathcal{H}_{1g}(x) \int_{\tilde{y}_{-,3}(x)}^{\tilde{y}_{+,3}(x)} \frac{dy}{8\pi x s_{1g}} \mathcal{F}(x s_{1g}, y) \\
&\quad \Theta(x s_{1g} - th.^2)(\delta_{2q} + \delta_{2\bar{q}}),
\end{aligned} \tag{E.24}$$

where $\mathcal{H}_{g2} = \mathcal{H}_{\gamma 2}$ and $\mathcal{H}_{1g} = \mathcal{H}_{1\gamma}$. $\bar{y}_{\pm,j}(x)$ [$\tilde{y}_{\pm,j}(x)$] is obtained substituting $s_{12} \to s_{g2}$ [$s_{12} \to s_{1g}$] into Eq. (E.8)

Appendix F

Feynman diagrams entering $PP \to \tilde{g}\tilde{g}X$

In this appendix we collect the Feynman diagrams responsible for the $\mathcal{O}(\alpha_s^2)$ and $\mathcal{O}(\alpha_s^2\alpha)$ contributions to gluino pair production. In the following the label S^0 is used to denote the neutral Higgs bosons h^0, H^0, A^0, G^0 while the label S denotes the charged Higgs bosons $H^\pm$, $G^\pm$. $V^0 = \gamma, Z$ and $V = Z, \gamma, W$.

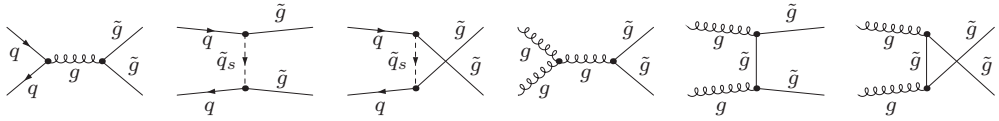

Figure F.1: Tree level diagrams for the processes $q\overline{q} \to \tilde{g}\tilde{g}$ and $gg \to \tilde{g}\tilde{g}$; $s = 1, 2$.

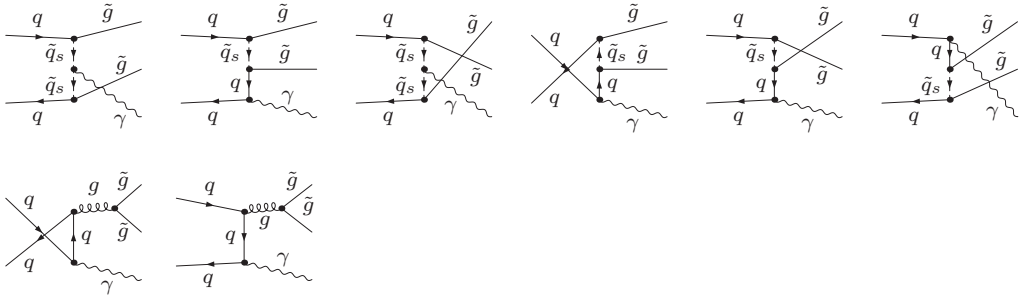

Figure F.2: Tree level diagrams for real photon emission in $q\overline{q} \to \tilde{g}\tilde{g}\gamma$.

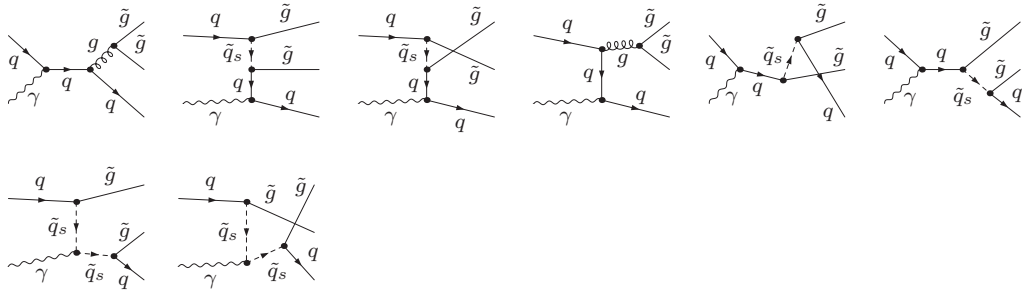

Figure F.3: Tree level diagrams for the process $q\gamma \to \tilde{g}\tilde{g}q$. The diagrams for the process $\gamma\overline{q} \to \tilde{g}\tilde{g}\overline{q}$ can be obtained inverting the arrows.

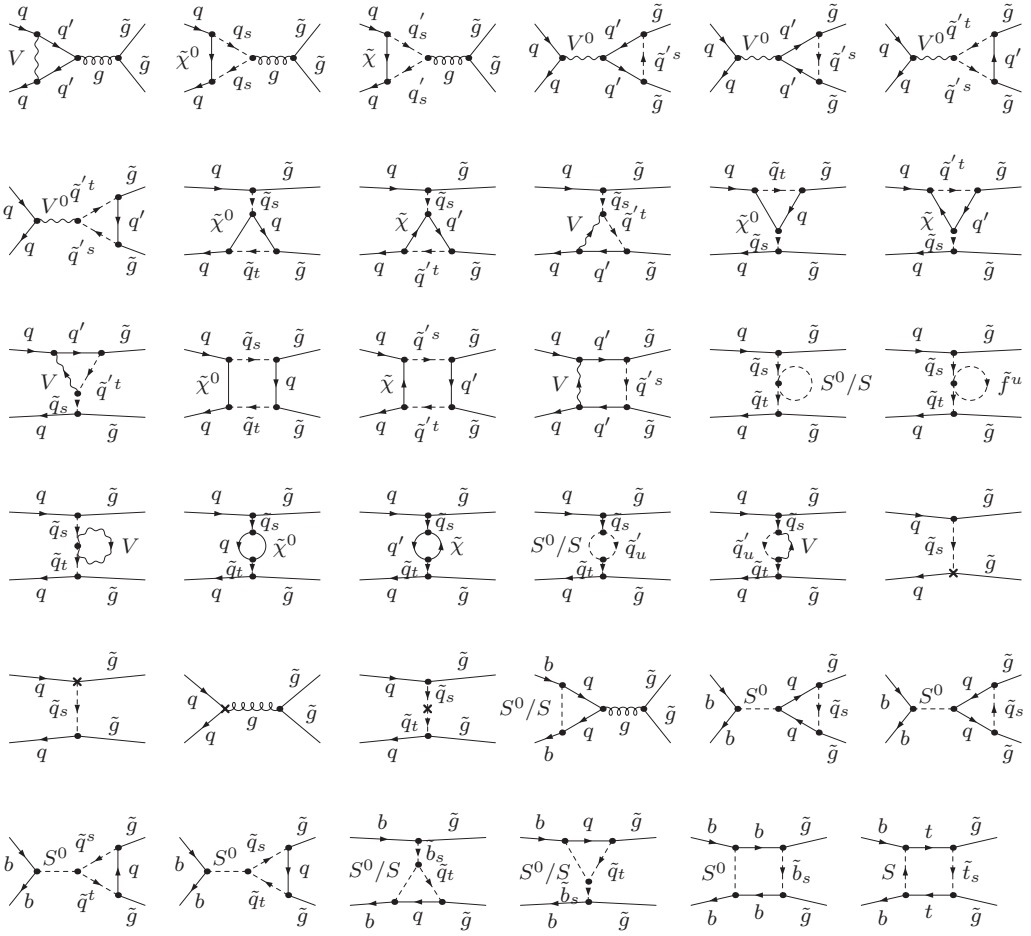

Figure F.4: One-loop EW diagrams for the process $q\overline{q} \to \tilde{g}\tilde{g}$. Diagrams with crossed final states are not shown.

Appendix G

Feynman diagrams entering $PP \to \tilde{Q}_a \tilde{Q}_a^* X$

In this appendix generic diagrams for the various contributions to the different channels are shown. We choose the up-squark case as a specific example. In the following we will use the label S^0 (S) to denote all the neutral (charged) Higgs bosons. $V^0 = \gamma, Z$, while V denotes the gauge bosons Z, γ, W.

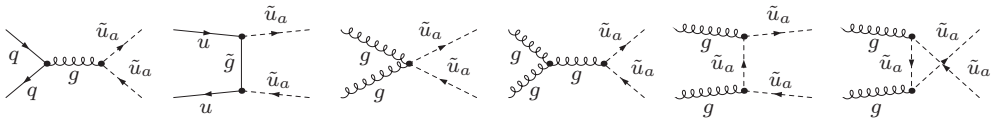

Figure G.1: Tree-level QCD diagrams for $q\overline{q} \to \tilde{u}_a \tilde{u}_a^*$ and for $gg \to \tilde{u}_a \tilde{u}_a^*$.

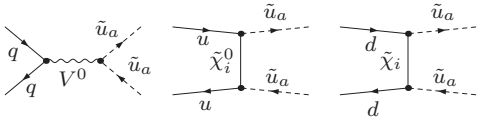

Figure G.2: Tree-level EW diagrams for $q\overline{q} \to \tilde{u}_a \tilde{u}_a^*$.

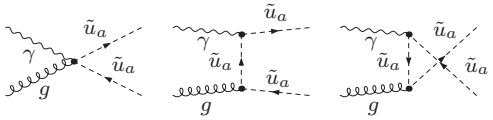

Figure G.3: Lowest-order diagrams for photon–gluon fusion $\gamma g \to \tilde{u}_a \tilde{u}_a^*$.

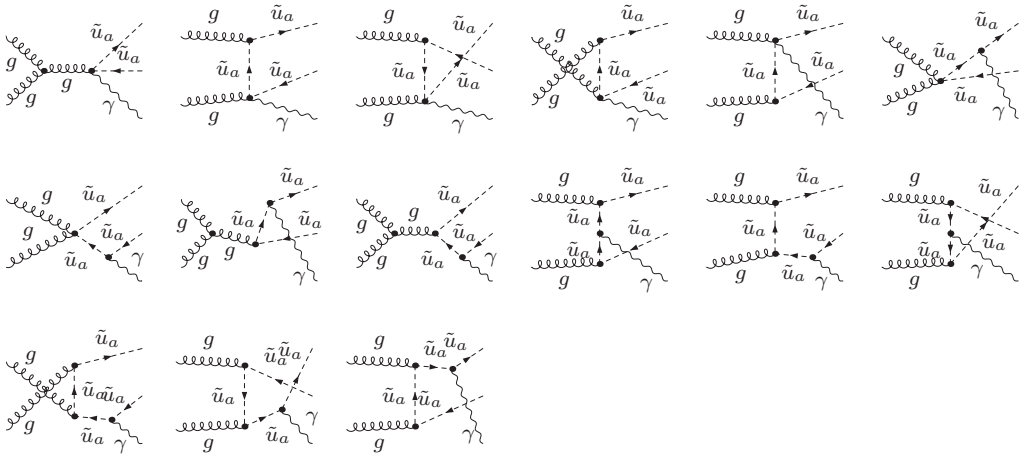

Figure G.4: Tree-level diagrams for real photon emission in $gg \to \tilde{u}_a \tilde{u}_a^* \gamma$.

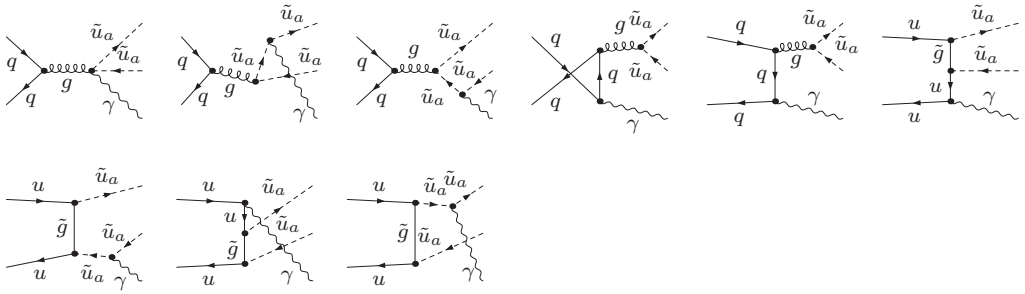

Figure G.5: $\mathcal{O}(\alpha_s^2 \alpha)$ real photon emission in $q\overline{q} \to \tilde{u}_a \tilde{u}_a^* \gamma$. The last four diagrams contribute only if $q = u$.

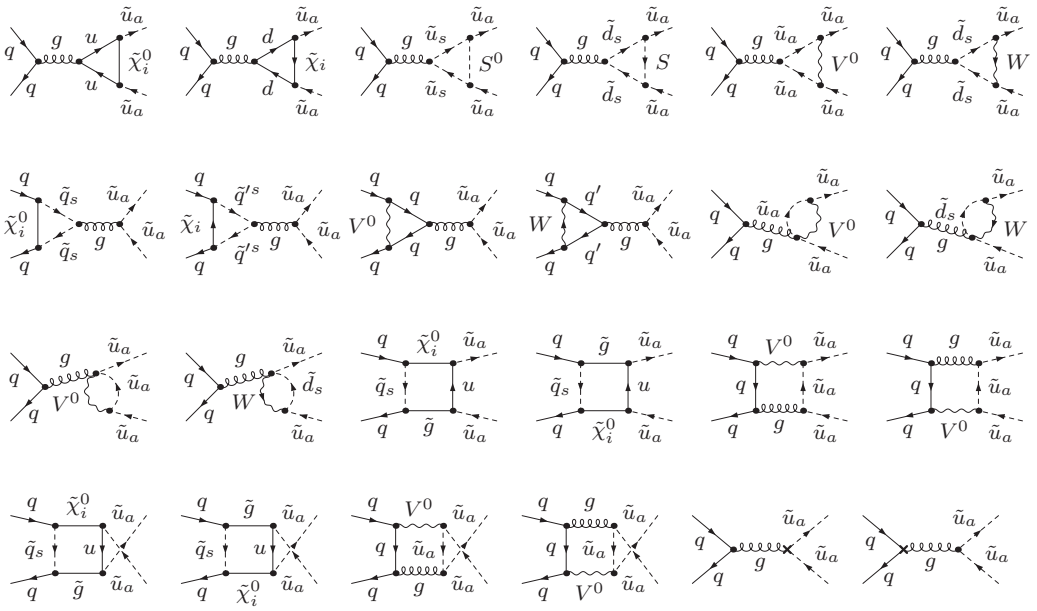

Figure G.6: One-loop EW diagrams for $q\overline{q} \to \tilde{u}_a\tilde{u}_a^*$. The renormalization constants in the counter terms have to be evaluated at $\mathcal{O}(\alpha)$.

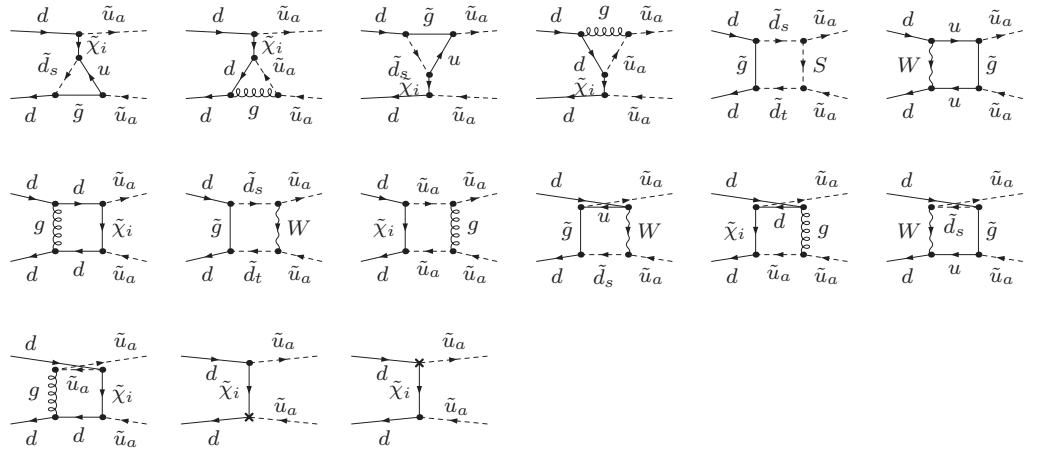

Figure G.7: One-loop EW diagrams that enter only in the case of the process $d\overline{d} \to \tilde{u}_a\tilde{u}_a^*$. The renormalization constants in the counter terms have to be evaluated at $\mathcal{O}(\alpha_s)$.

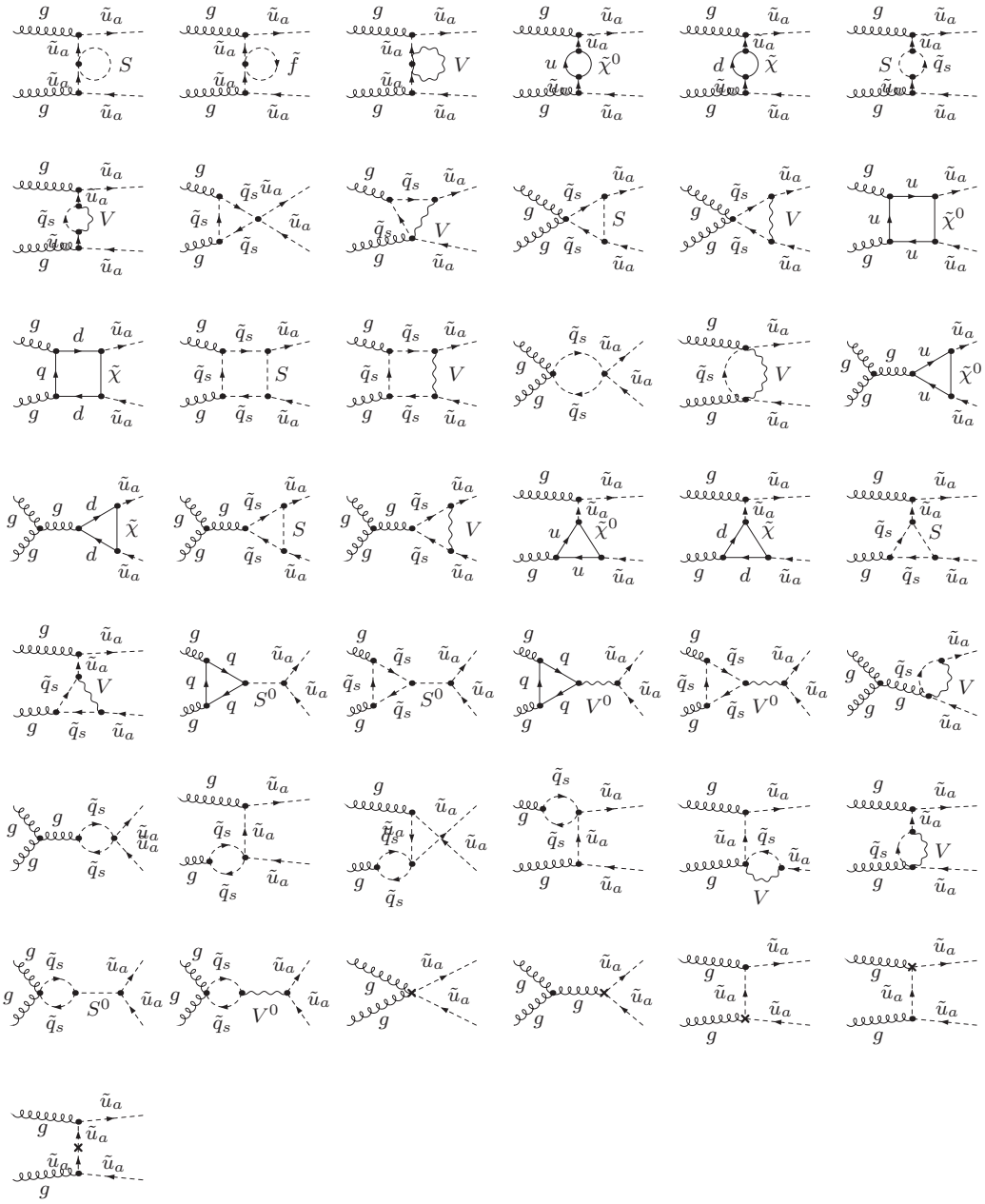

Figure G.8: One-loop EW diagrams for $gg \to \tilde{u}_a \tilde{u}_a^*$. The renormalization constants in the counter terms have to be evaluated at $\mathcal{O}(\alpha)$.

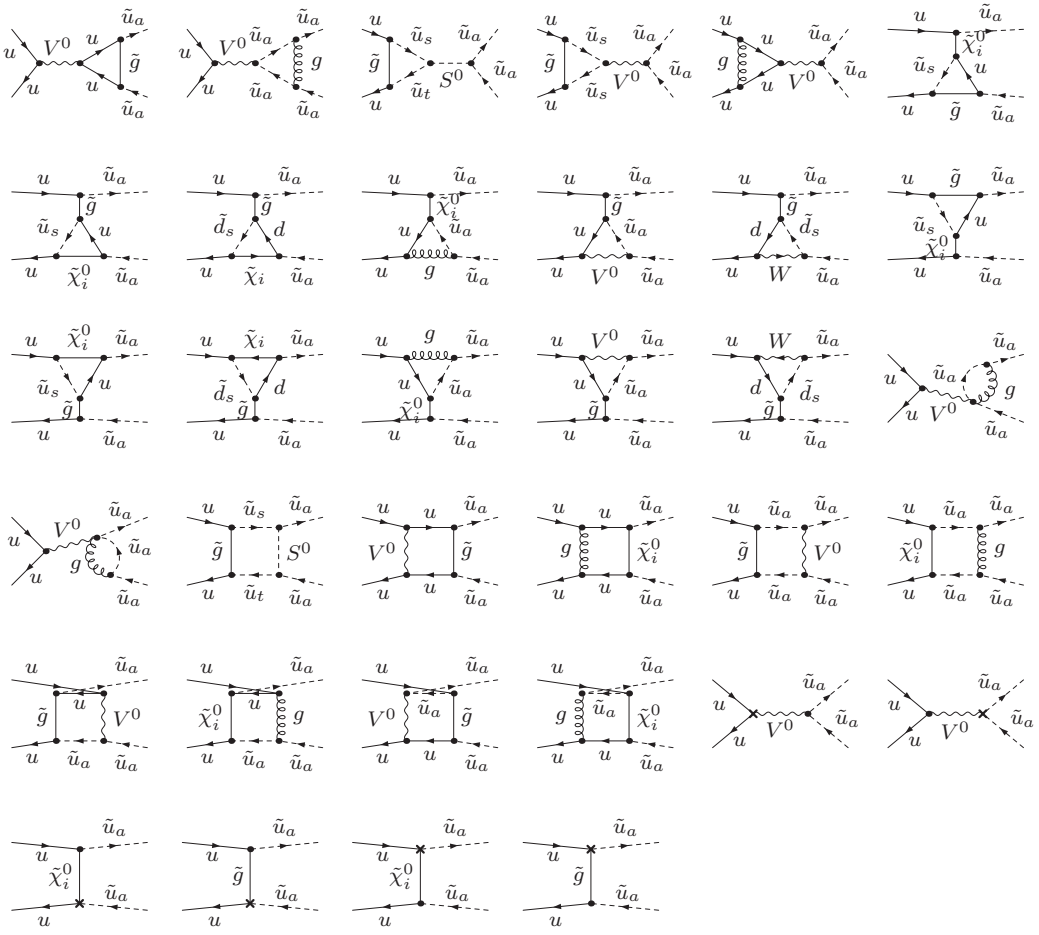

Figure G.9: One-loop EW diagrams that enter only in the case of the process $u\overline{u} \to \tilde{u}_a \tilde{u}_a^*$. The renormalization constants in the quark–squark–gluino counter term have to be evaluated at $\mathcal{O}(\alpha)$, the other ones at $\mathcal{O}(\alpha_s)$.

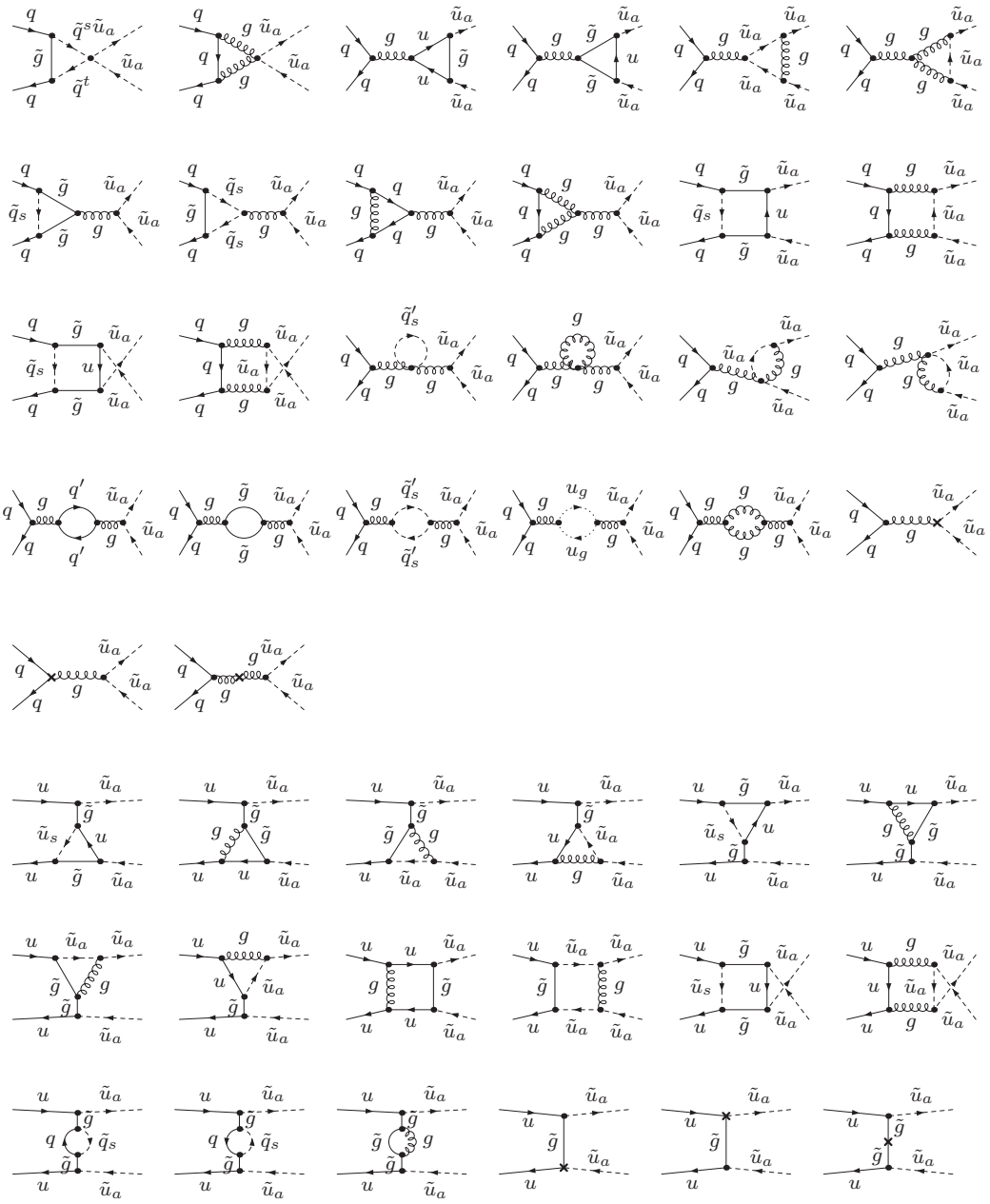

Figure G.10: One-loop QCD diagrams for the process $q\overline{q} \to \tilde{u}_a \tilde{u}_a^*$. These diagrams interfere with those of Fig. G.2 yielding $\mathcal{O}(\alpha_s^2 \alpha)$ contributions. The renormalization constants appearing in the counter terms have to be evaluated at $\mathcal{O}(\alpha_s)$.

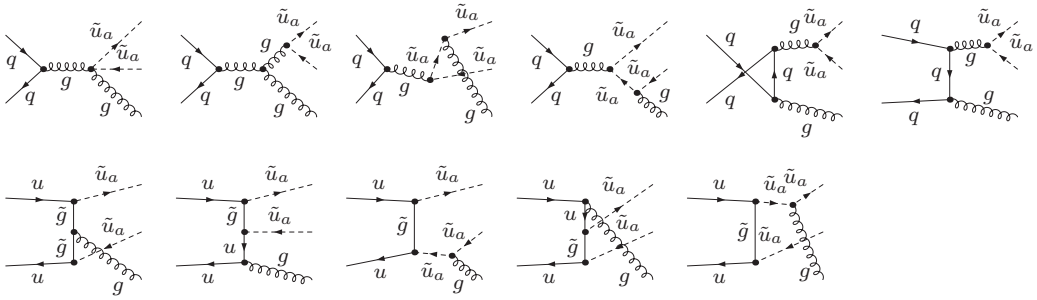

(a)

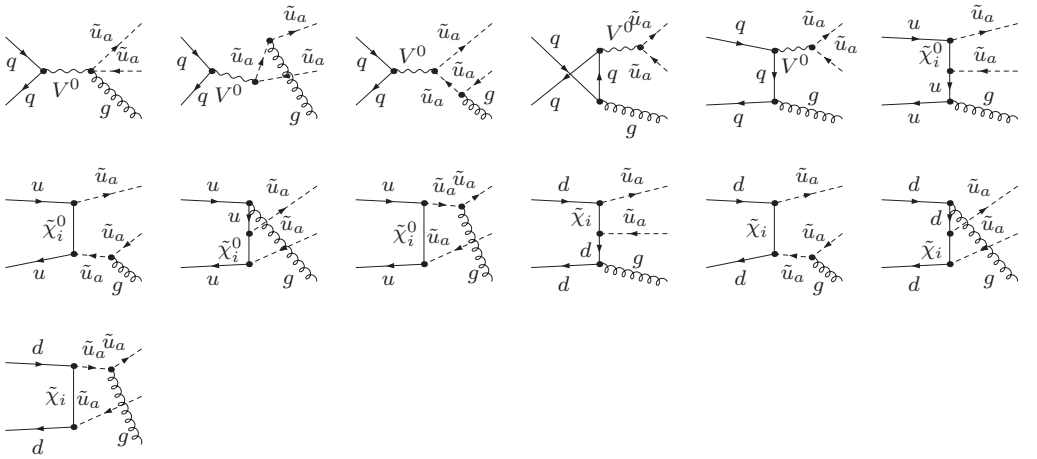

(b)

Figure G.11: Diagrams for gluon bremsstrahlung from QCD (a) and EW (b) Born diagrams. They contribute at $\mathcal{O}(\alpha_s^2\alpha)$ through QCD–EW interference

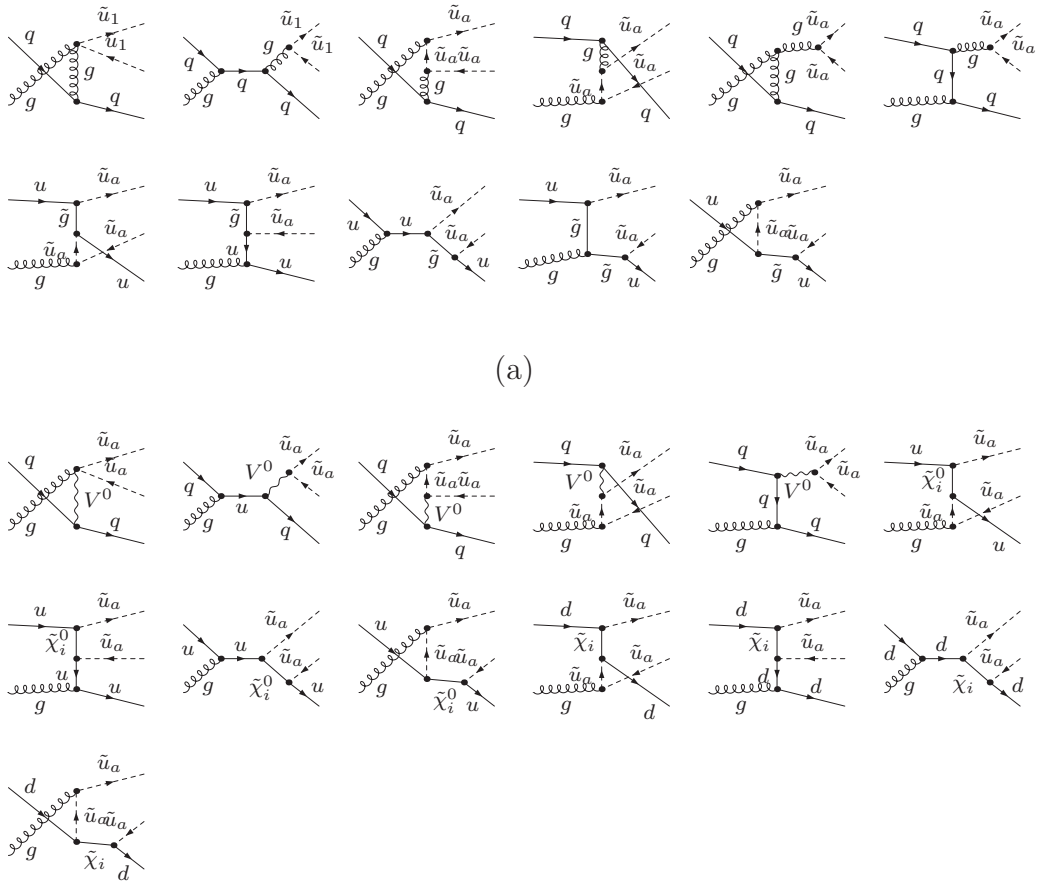

(a)

(b)

Figure G.12: QCD (a) and EW (b) Born diagrams for quark gluon fusion channels. Their interference contributes at $\mathcal{O}(\alpha_s^2 \alpha)$.

Appendix H

Feynman diagrams entering $PP \to \tilde{g}\tilde{Q}_a X$

We show all Feynman diagrams at the parton level for the example process $g\,u \to \tilde{g}\,\tilde{u}_a$. We use a common label V to denote the three gauge bosons γ, Z, and W. The label S^0 refers to the neutral (charged) Higgs bosons.

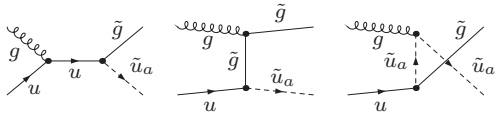

Figure H.1: LO Feynman diagrams for the process $g\,u \to \tilde{g}\,\tilde{u}_a$.

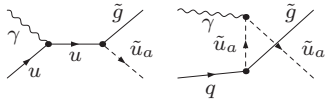

Figure H.2: Feynman diagrams for photon–quark fusion at lowest order.

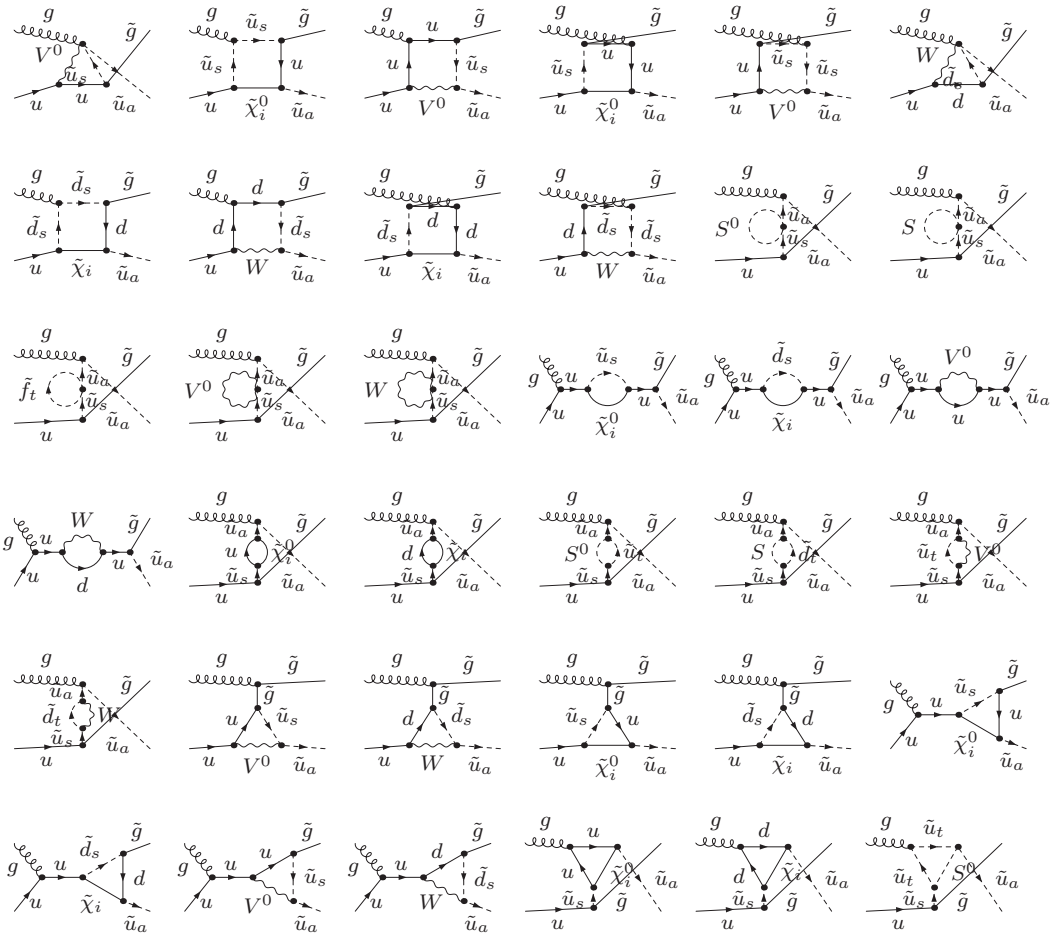

Figure H.3: Feynman diagrams entering the $\mathcal{O}(\alpha_s^2\alpha)$ to the process $ug \to \tilde{g}\tilde{u}_a$. The renormalization constants appearing in the counter terms have to be evaluated at $\mathcal{O}(\alpha_s)$.

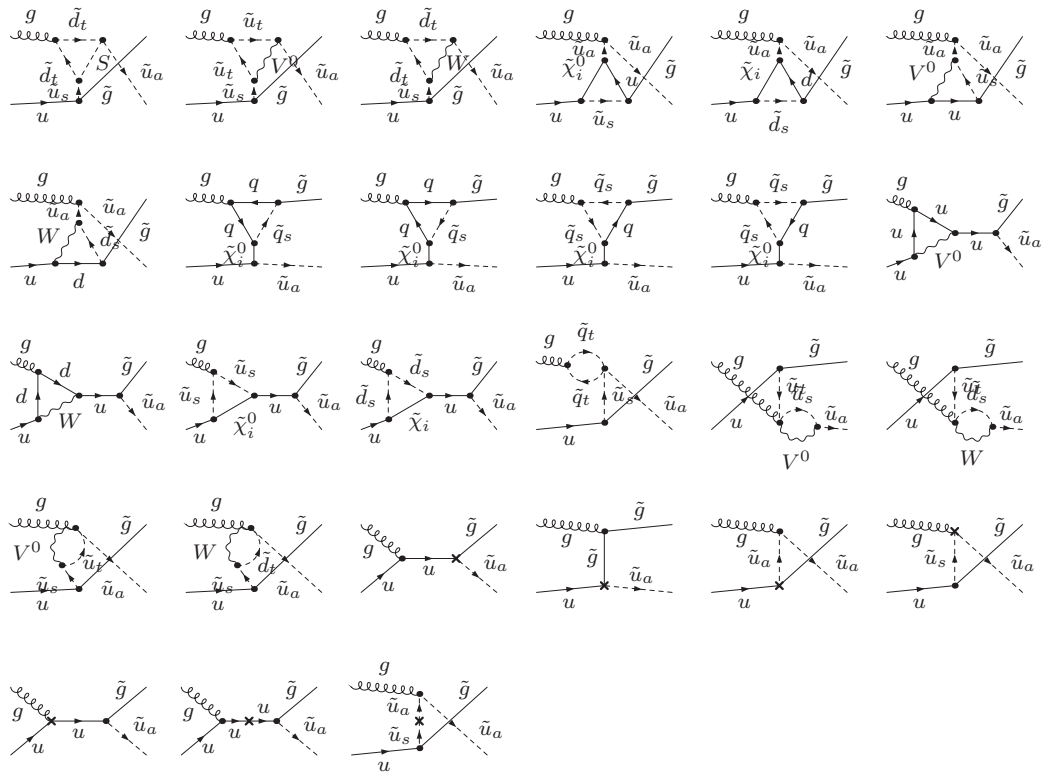

Figure H.4: Fig. H.3, continued.

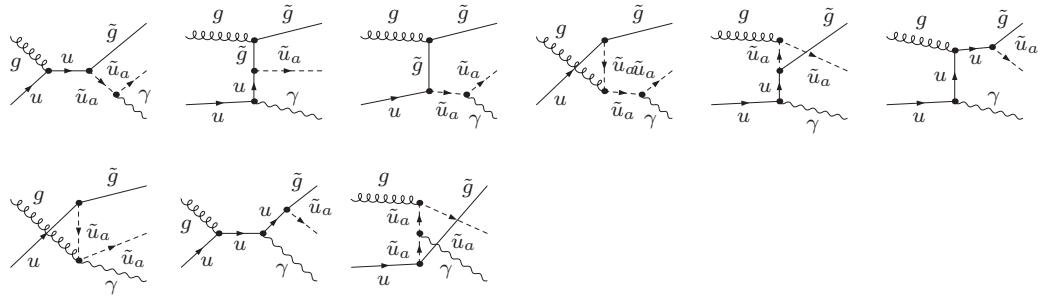

Figure H.5: Feynman diagrams for real photon radiation. The first six diagrams are IR divergent, the last three are IR finite.

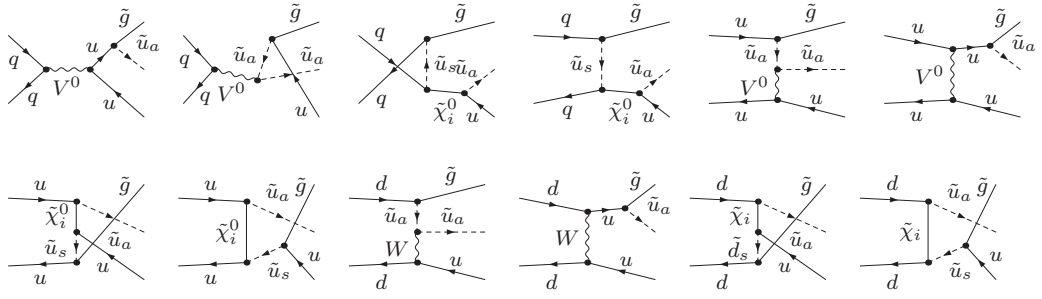

(a)

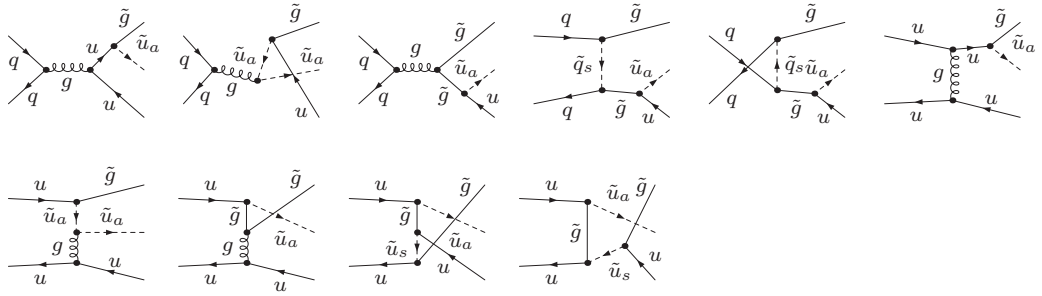

(b)

Figure H.6: Feynman diagrams for quark radiation via $q\bar{q} \to \tilde{g}\tilde{u}_a\bar{u}$, with $q = u$, d, c, s. Only interference terms from EW (a) and QCD (b) diagrams contribute at $\mathcal{O}(\alpha_s^2\alpha)$. In panel (a), the last eight diagrams contribute only for $q = u, d$. In panel (b), the last five diagrams contribute only for $q = u$.

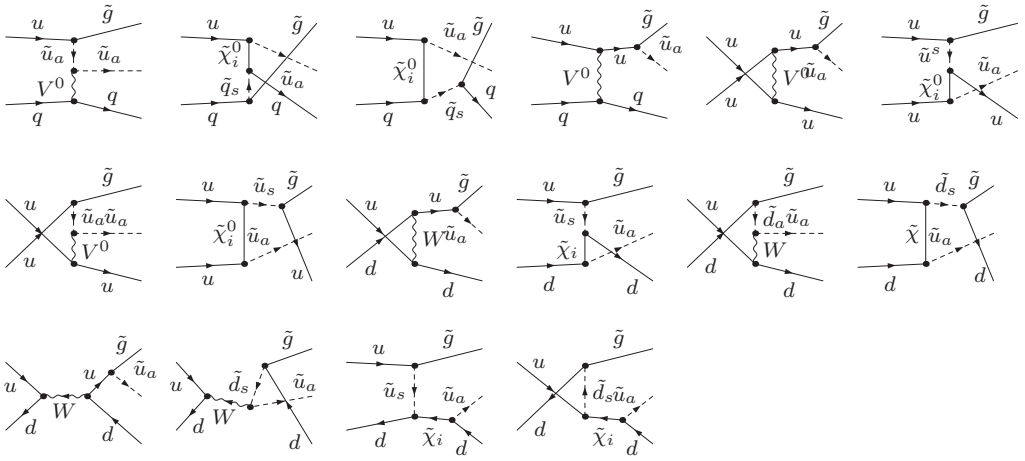

(a)

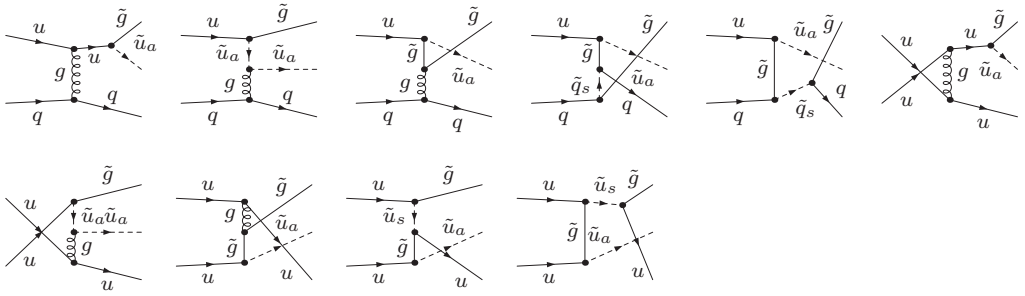

(b)

Figure H.7: Feynman diagrams for quark radiation via $uq \to \tilde{g}\tilde{u}_a q$, with $q = u,\, d,\, c,\, s,\, \bar{d},\, \bar{c},\, \bar{s}$. Only interference terms from EW (a) and QCD (b) diagrams contribute at $\mathcal{O}(\alpha_s^2\alpha)$.

Bibliography

[1] S. Weinberg, *A Model of Leptons*, *Phys. Rev. Lett.* **19** (1967) 1264–1266.

A. Salam, *Weak and Electromagnetic Interactions*, . Originally printed in *Svartholm: Elementary Particle Theory, Proceedings Of The Nobel Symposium Held 1968 At Lerum, Sweden*, Stockholm 1968, 367-377.

S. L. Glashow, *Partial Symmetries of Weak Interactions*, *Nucl. Phys.* **22** (1961) 579–588.

S. L. Glashow, J. Iliopoulos, and L. Maiani, *Weak Interactions with Lepton-Hadron Symmetry*, *Phys. Rev.* **D2** (1970) 1285–1292.

[2] D. J. Gross and F. Wilczek, *Asymptotically Free Gauge Theories. 1*, *Phys. Rev.* **D8** (1973) 3633–3652.

D. J. Gross and F. Wilczek, *Ultraviolet behavior of non-Abelian gauge theories*, *Phys. Rev. Lett.* **30** (1973) 1343–1346.

D. J. Gross and F. Wilczek, *Asymptotically free gauge theories. 2*, *Phys. Rev.* **D9** (1974) 980–993.

O. W. Greenberg, *Spin and Unitary Spin Independence in a Paraquark Model of Baryons and Mesons*, *Phys. Rev. Lett.* **13** (1964) 598–602.

H. D. Politzer, *Reliable perturbative results for strong interactions?*, *Phys. Rev. Lett.* **30** (1973) 1346–1349.

H. Fritzsch, M. Gell-Mann, and H. Leutwyler, *Advantages of the Color Octet Gluon Picture*, *Phys. Lett.* **B47** (1973) 365–368.

[3] J. Wess and B. Zumino, *Supergauge Transformations in Four-Dimensions*, *Nucl. Phys.* **B70** (1974) 39–50.

D. V. Volkov and V. P. Akulov, *Is the Neutrino a Goldstone Particle?*, *Phys. Lett.* **B46** (1973) 109–110.

[4] H. P. Nilles, *Supersymmetry, Supergravity and Particle Physics*, *Phys. Rept.* **110** (1984) 1–162.

H. E. Haber and G. L. Kane, *The Search for Supersymmetry: Probing Physics Beyond the Standard Model*, *Phys. Rept.* **117** (1985) 75–263.

R. Barbieri, *Looking Beyond the Standard Model: The Supersymmetric Option*, *Riv. Nuovo Cim.* **11N4** (1988) 1–45.

[5] S. Heinemeyer, W. Hollik, and G. Weiglein, *Electroweak precision observables in the minimal supersymmetric standard model*, *Phys. Rept.* **425** (2006) 265–368, [hep-ph/0412214].

[6] J. R. Ellis, S. Heinemeyer, K. A. Olive, A. M. Weber, and G. Weiglein, *The Supersymmetric Parameter Space in Light of B^- physics Observables and Electroweak Precision Data*, *JHEP* **08** (2007) 083, [arXiv:0706.0652].

[7] O. Buchmueller *et. al.*, *Prediction for the Lightest Higgs Boson Mass in the CMSSM using Indirect Experimental Constraints*, *Phys. Lett.* **B657** (2007) 87–94, [arXiv:0707.3447].

[8] **Muon g-2** Collaboration, G. W. Bennett *et. al.*, *Measurement of the Positive Muon Anomalous Magnetic Moment to 0.7 ppm*, *Phys. Rev. Lett.* **89** (2002) 101804, [hep-ex/0208001].

[9] **Muon g-2** Collaboration, G. W. Bennett *et. al.*, *Measurement of the negative muon anomalous magnetic moment to 0.7-ppm*, *Phys. Rev. Lett.* **92** (2004) 161802, [hep-ex/0401008].

[10] G. L. Kane and J. P. Leveille, *Experimental Constraints on Gluino Masses and Supersymmetric Theories*, *Phys. Lett.* **B112** (1982) 227.

[11] P. R. Harrison and C. H. Llewellyn Smith, *Hadroproduction of Supersymmetric Particles*, *Nucl. Phys.* **B213** (1983) 223.

[12] E. Reya and D. P. Roy, *Supersymmetric particle production at $p\,\bar{p}$ collider energies*, *Phys. Rev.* **D32** (1985) 645.

[13] S. Dawson, E. Eichten, and C. Quigg, *Search for Supersymmetric Particles in Hadron - Hadron Collisions*, *Phys. Rev.* **D31** (1985) 1581.

[14] H. Baer and X. Tata, *Component formulae for hadroproduction of left-handed and right-handed squarks*, *Phys. Lett.* **B160** (1985) 159.

[15] W. Beenakker, R. Hopker, M. Spira, and P. M. Zerwas, *Squark and gluino production at hadron colliders*, *Nucl. Phys.* **B492** (1997) 51–103, [hep-ph/9610490].

[16] W. Beenakker, R. Hopker, M. Spira, and P. M. Zerwas, *Gluino pair production at the Tevatron*, *Z. Phys.* **C69** (1995) 163–166, [hep-ph/9505416].

[17] W. Beenakker, R. Hopker, M. Spira, and P. M. Zerwas, *Squark production at the Tevatron*, *Phys. Rev. Lett.* **74** (1995) 2905–2908, [hep-ph/9412272].

[18] W. Beenakker, M. Kramer, T. Plehn, and M. Spira, *SUSY particle production at the Tevatron*, hep-ph/9810290.

[19] W. Beenakker, M. Kramer, T. Plehn, M. Spira, and P. M. Zerwas, *Stop production at hadron colliders*, *Nucl. Phys.* **B515** (1998) 3–14, [hep-ph/9710451].

[20] W. Beenakker, R. Hopker, and M. Spira, *PROSPINO: A program for the PROduction of Supersymmetric Particles In Next-to-leading Order QCD*, hep-ph/9611232.

[21] U. Langenfeld and S.-O. Moch, *Higher-order soft corrections to squark hadro- production*, arXiv:0901.0802.

[22] A. Kulesza and L. Motyka, *Threshold resummation for squark-antisquark and gluino- pair production at the LHC*, *Phys. Rev. Lett.* **102** (2009) 111802, [arXiv:0807.2405].

[23] A. Kulesza and L. Motyka, *Soft gluon resummation for the production of gluino-gluino and squark-antisquark pairs at the LHC*, arXiv:0905.4749.

[24] S. Bornhauser, M. Drees, H. K. Dreiner, and J. S. Kim, *Electroweak Contributions to Squark Pair Production at the LHC*, *Phys. Rev.* **D76** (2007) 095020, [arXiv:0709.2544].

[25] S. Bornhauser, M. Drees, H. K. Dreiner, and J. S. Kim, *Electroweak Contributions to Squark Pair Production*, arXiv:0710.2035.

[26] S. R. Coleman and J. Mandula, *All possible symmetries of the S-matrix*, *Phys. Rev.* **159** (1967) 1251–1256.

[27] **Particle Data Group** Collaboration, C. Amsler *et. al.*, *Review of particle physics*, *Phys. Lett.* **B667** (2008) 1.

[28] P. W. Higgs, *Broken symmetries, massless particles and gauge fields*, *Phys. Lett.* **12** (1964) 132–133.

P. W. Higgs, *Broken symmetries and the masses of gauge bosons*, *Phys. Rev. Lett.* **13** (1964) 508–509.

P. W. Higgs, *Spontaneous Symmetry Breakdown Without Massless Bosons*, *Phys. Rev.* **145** (1966) 1156–1163.

F. Englert and R. Brout, *Broken symmetry and the mass of gauge vector mesons*, *Phys. Rev. Lett.* **13** (1964) 321–322.

T. W. B. Kibble, *Symmetry breaking in non-Abelian gauge theories*, *Phys. Rev.* **155** (1967) 1554–1561.

[29] A. Schellekens, *Beyond the Standard Model*, . Lectures given at the 1995 AIO/OIO school of theoretical high energy physics, Dalfsen January 1995.

R. Barbieri, *Ten Lectures on the ElectroWeak Interactions*, `arXiv:0706.0684`.

[30] N. Cabibbo, *Unitary Symmetry and Leptonic Decays*, *Phys. Rev. Lett.* **10** (1963) 531–533.

M. Kobayashi and T. Maskawa, *CP Violation in the Renormalizable Theory of Weak Interaction*, *Prog. Theor. Phys.* **49** (1973) 652–657.

[31] **WMAP** Collaboration, C. L. Bennett *et. al.*, *First Year Wilkinson Microwave Anisotropy Probe (WMAP) Observations: Preliminary Maps and Basic Results*, *Astrophys. J. Suppl.* **148** (2003) 1, [`astro-ph/0302207`].

WMAP Collaboration, D. N. Spergel *et. al.*, *First Year Wilkinson Microwave Anisotropy Probe (WMAP) Observations: Determination of Cosmological Parameters*, *Astrophys. J. Suppl.* **148** (2003) 175, [`astro-ph/0302209`].

[32] **WMAP** Collaboration, D. N. Spergel *et. al.*, *Wilkinson Microwave Anisotropy Probe (WMAP) three year results: Implications for cosmology*, *Astrophys. J. Suppl.* **170** (2007) 377, [`astro-ph/0603449`].

[33] A. D. Sakharov, *Violation of CP Invariance, c Asymmetry, and Baryon Asymmetry of the Universe*, *Pisma Zh. Eksp. Teor. Fiz.* **5** (1967) 32–35.

[34] S. Weinberg, *Implications of Dynamical Symmetry Breaking*, *Phys. Rev.* **D13** (1976) 974–996.

S. Weinberg, *Implications of Dynamical Symmetry Breaking: An Addendum*, *Phys. Rev.* **D19** (1979) 1277–1280.

L. Susskind, *Dynamics of Spontaneous Symmetry Breaking in the Weinberg- Salam Theory*, *Phys. Rev.* **D20** (1979) 2619–2625.

[35] E. Farhi and L. Susskind, *Technicolor*, *Phys. Rept.* **74** (1981) 277.

[36] N. Arkani-Hamed, S. Dimopoulos, and G. R. Dvali, *The hierarchy problem and new dimensions at a millimeter*, *Phys. Lett.* **B429** (1998) 263–272, [hep-ph/9803315].

I. Antoniadis, N. Arkani-Hamed, S. Dimopoulos, and G. R. Dvali, *New dimensions at a millimeter to a Fermi and superstrings at a TeV*, *Phys. Lett.* **B436** (1998) 257–263, [hep-ph/9804398].

L. Randall and R. Sundrum, *A large mass hierarchy from a small extra dimension*, *Phys. Rev. Lett.* **83** (1999) 3370–3373, [hep-ph/9905221].

[37] M. Drees, *An introduction to supersymmetry*, hep-ph/9611409.

[38] P. G. O. Freund, *Introduction to Supersymmetry*, . Cambridge, Uk: Univ. Pr. (1986) 152 P. (Cambridge Monographs On Mathematical Physics).

[39] R. Haag, J. T. Lopuszanski, and M. Sohnius, *All Possible Generators of Supersymmetries of the s Matrix*, *Nucl. Phys.* **B88** (1975) 257.

[40] A. Salam and J. A. Strathdee, *Supergauge Transformations*, *Nucl. Phys.* **B76** (1974) 477–482.

[41] J. Wess and B. Zumino, *A Lagrangian Model Invariant Under Supergauge Transformations*, *Phys. Lett.* **B49** (1974) 52.

[42] J. Wess and B. Zumino, *Supergauge Invariant Extension of Quantum Electrodynamics*, *Nucl. Phys.* **B78** (1974) 1.

S. Ferrara and B. Zumino, *Supergauge Invariant Yang-Mills Theories*, *Nucl. Phys.* **B79** (1974) 413.

[43] L. M. Krauss and F. Wilczek, *Discrete Gauge Symmetry in Continuum Theories*, *Phys. Rev. Lett.* **62** (1989) 1221.

L. E. Ibanez and G. G. Ross, *Discrete gauge symmetry anomalies*, *Phys. Lett.* **B260** (1991) 291–295.

T. Banks and M. Dine, *Note on discrete gauge anomalies*, *Phys. Rev.* **D45** (1992) 1424–1427, [hep-th/9109045].

L. E. Ibanez, *More about discrete gauge anomalies*, *Nucl. Phys.* **B398** (1993) 301–318, [hep-ph/9210211].

[44] L. O'Raifeartaigh, *Spontaneous Symmetry Breaking for Chiral Scalar Superfields*, *Nucl. Phys.* **B96** (1975) 331.

[45] P. Fayet and J. Iliopoulos, *Spontaneously Broken Supergauge Symmetries and Goldstone Spinors*, *Phys. Lett.* **B51** (1974) 461–464.

[46] L. Girardello and M. T. Grisaru, *Soft Breaking of Supersymmetry*, *Nucl. Phys.* **B194** (1982) 65.

[47] J. Rosiek, *Complete Set of Feynman Rules for the Minimal Supersymmetric Extension of the Standard Model*, *Phys. Rev.* **D41** (1990) 3464.

J. Rosiek, *Complete set of Feynman rules for the MSSM – ERRATUM*, hep-ph/9511250.

T. Fritzsche, *Berechnung von Observablen zur supersymmetrischen Teilchenerzeugung an Hochenergie-Collidern unter Einschluss hoeherer Ordnungen*, . Cuvillier Verlag Goettingen, 2005.

[48] F. Gabbiani, E. Gabrielli, A. Masiero, and L. Silvestrini, *A complete analysis of FCNC and CP constraints in general SUSY extensions of the standard model*, *Nucl. Phys.* **B477** (1996) 321–352, [hep-ph/9604387].

[49] **MSSM Working Group** Collaboration, A. Djouadi *et. al.*, *The Minimal supersymmetric standard model: Group summary report*, hep-ph/9901246.

[50] S. P. Martin, *A Supersymmetry Primer*, hep-ph/9709356.

[51] M. A. Luty, *2004 TASI lectures on supersymmetry breaking*, hep-th/0509029.

[52] D. J. H. Chung *et. al.*, *The soft supersymmetry-breaking Lagrangian: Theory and applications*, *Phys. Rept.* **407** (2005) 1–203, [hep-ph/0312378].

[53] **ALEPH** Collaboration, S. Schael *et. al.*, *Search for neutral MSSM Higgs bosons at LEP*, *Eur. Phys. J.* **C47** (2006) 547–587, [hep-ex/0602042].

[54] **CDF** Collaboration, A. Abulencia *et. al.*, *Search for neutral MSSM Higgs bosons decaying to tau pairs in $p\bar{p}$ collisions at $\sqrt{s} = 1.96$ TeV*, *Phys. Rev. Lett.* **96** (2006) 011802, [hep-ex/0508051].

D0 Collaboration, M. Owen, *Search for Neutral Higgs Boson Production in the Decay $h \to \tau_\mu \tau$ with the D0 Detector*, arXiv:0705.2329.

[55] S. Heinemeyer, *MSSM Higgs physics at higher orders*, *Int. J. Mod. Phys.* **A21** (2006) 2659–2772, [hep-ph/0407244].

[56] G. Degrassi, S. Heinemeyer, W. Hollik, P. Slavich, and G. Weiglein, *Towards high-precision predictions for the MSSM Higgs sector*, *Eur. Phys. J.* **C28** (2003) 133–143, [hep-ph/0212020].

[57] **ALEPH** Collaboration, D. Decamp *et. al.*, *ALEPH: a detector for electron-positron annihilations at LEP*, *Nucl. Instrum. Meth.* **A294** (1990) 121–178.

ALEPH Collaboration, D. Buskulic *et. al.*, *Performance of the ALEPH detector at LEP*, *Nucl. Instrum. Meth.* **A360** (1995) 481–506.

[58] **DELPHI** Collaboration, P. A. Aarnio *et. al.*, *The DELPHI detector at LEP*, *Nucl. Instrum. Meth.* **A303** (1991) 233–276.

DELPHI Collaboration, P. Abreu *et. al.*, *Performance of the DELPHI detector*, *Nucl. Instrum. Meth.* **A378** (1996) 57–100.

[59] **L3** Collaboration, *The construction of the L3 experiment*, *Nucl. Instrum. Meth.* **A289** (1990) 35–102.

[60] **OPAL** Collaboration, K. Ahmet *et. al.*, *The OPAL detector at LEP*, *Nucl. Instrum. Meth.* **A305** (1991) 275–319.

[61] **OPAL** Collaboration, G. Abbiendi *et. al.*, *Search for neutral Higgs boson in CP-conserving and CP- violating MSSM scenarios*, *Eur. Phys. J.* **C37** (2004) 49–78, [hep-ex/0406057].

DELPHI Collaboration, J. Abdallah *et. al.*, *Final results from DELPHI on the searches for SM and MSSM neutral Higgs bosons*, *Eur. Phys. J.* **C32** (2004) 145–183, [hep-ex/0303013].

L3 Collaboration, P. Achard *et. al.*, *Search for neutral Higgs bosons of the minimal supersymmetric standard model in e^+e^- interactions at $\sqrt{s}$ = 209-GeV*, *Phys. Lett.* **B545** (2002) 30–42, [hep-ex/0208042].

ALEPH Collaboration, A. Heister *et. al.*, *Final results of the searches for neutral higgs bosons in e^+ e^- collisions at up to 209 gev*, *Physics Letters B* **526** (2002), no. 3-4 191 – 205.

[62] **LEP Higgs Working for Higgs boson searches** Collaboration, *Searches for invisible Higgs bosons: Preliminary combined results using LEP data collected at energies up to 209- GeV*, hep-ex/0107032.

[63] **DELPHI** Collaboration, J. Abdallah *et. al.*, *Search for charged Higgs bosons at LEP in general two Higgs doublet models*, *Eur. Phys. J.* **C34** (2004) 399–418, [hep-ex/0404012].

OPAL Collaboration, G. Abbiendi *et. al.*, *Search for Charged Higgs Bosons in e^+ e^- Collisions at $\sqrt{s}$ = 189-209 GeV*, arXiv:0812.0267.

ALEPH Collaboration, A. Heister *et. al.*, *Search for charged Higgs bosons in e^+e^- collisions at energies up to $\sqrt{s}$ = 209-GeV*, *Phys. Lett.* **B543** (2002) 1–13, [hep-ex/0207054].

L3 Collaboration, *Search for charged higgs bosons at lep*, *Physics Letters B* **575** (2003), no. 3-4 208 – 220.

[64] **LEP Higgs Working Group for Higgs boson searches** Collaboration, *Search for charged Higgs bosons: Preliminary combined results using LEP data collected at energies up to 209- GeV*, hep-ex/0107031.

[65] LEPSUSYWG, ALEPH, DELPHI, L3 and OPAL experiments, note LEPSUSYWG/01-03.01.

[66] LEPSUSYWG, ALEPH, DELPHI, L3 and OPAL experiments, note LEPSUSYWG/02-04.01.

[67] LEPSUSYWG, ALEPH, DELPHI, L3 and OPAL experiments, note LEPSUSYWG/04-07.01.

[68] LEPSUSYWG, ALEPH, DELPHI, L3 and OPAL experiments, note LEPSUSYWG/02-06.02.

[69] LEPSUSYWG, ALEPH, DELPHI, L3 and OPAL experiments, note LEPSUSYWG/04-01.01.

[70] **ALEPH** Collaboration, A. Heister *et. al.*, *Absolute lower limits on the masses of selectrons and sneutrinos in the MSSM*, *Phys. Lett.* **B544** (2002) 73–88, [hep-ex/0207056].

L3 Collaboration, *Search for scalar leptons and scalar quarks at lep*, *Physics Letters B* **580** (2004), no. 1-2 37 – 49.

[71] *Precision electroweak measurements on the z resonance*, *Physics Reports* **427** (2006), no. 5-6 257 – 454.

[72] LEPSUSYWG, ALEPH, DELPHI, L3 and OPAL experiments, note LEPSUSYWG/04-02.01.

[73] **D0** Collaboration, V. M. Abazov *et. al.*, *A search for the scalar top quark in $p\bar{p}$ collisions at $\sqrt{s} = 1.8$ TeV*, *Phys. Rev. Lett.* **88** (2002) 171802, [hep-ex/0108018].

[74] **CDF** Collaboration, A. A. Affolder *et. al.*, *Search for scalar top and scalar bottom quarks in $p\bar{p}$ collisions at $\sqrt{s} = 1.8$ TeV*, *Phys. Rev. Lett.* **84** (2000) 5704–5709, [hep-ex/9910049].

[75] **ALEPH** Collaboration, A. Heister *et. al.*, *Search for scalar quarks in e^+e^- collisions at $\sqrt{s}$ up to 209-GeV*, *Phys. Lett.* **B537** (2002) 5–20, [hep-ex/0204036].

[76] **CDF** Collaboration, F. Abe *et. al.*, *The CDF detector: an overview*, *Nucl. Instr. Meth.* **A271** (1988) 387–403.

[77] **D0** Collaboration, V. M. Abazov *et. al.*, *The Upgraded D0 Detector*, *Nucl. Instrum. Meth.* **A565** (2006) 463–537, [physics/0507191].

[78] **CDF** Collaboration, *Search for neutral MSSM Higgs bosons decaying to tau pairs with 1.8 fb^{-1} of data*, . CDF note 9071 (October 2007).

[79] **D0** Collaboration, *Search for neutral MSSM Higgs boson production in di-tau final states with $\mathcal{L} = 2.2$ fb^{-1} at the D0 detector*, . D0 note 5740-CONF (July 2008).

[80] **D0** Collaboration, *Search for neutral Higgs bosons in multi-b-jets events in $p\bar{p}$ collisions at $\sqrt{s} = 1.96$ TeV*, . D0 note 5726-CONF (July 2008).

[81] **CDF** Collaboration, *Search for Higgs bosons produced in association with b quarks*, . CDF note 9284 (April 2008).

[82] **D0** Collaboration, *A search for neutral Higgs bosons at high* $\tan\beta$ *in the mode* $\phi b \to \tau_\mu \tau_h b$ *in Run IIb data*, . D0 note 5727-CONF (August 2008).

[83] **CDF** Collaboration, A. Abulencia *et. al.*, *Search for charged Higgs bosons from top quark decays in* $p\bar{p}$ *collisions at* $\sqrt{s} = 1.96$*-TeV*, *Phys. Rev. Lett.* **96** (2006) 042003, [hep-ex/0510065].

[84] **D0** Collaboration, *A search for charged Higgs bosons at in tbart events*, . D0 note 5715-CONF (July 2008).

[85] **D0** Collaboration, V. M. Abazov *et. al.*, *Search for charged Higgs bosons decaying to top and bottom quarks in* $p\bar{p}$ *collisions*, arXiv:0807.0859.

[86] **D0** Collaboration, V. M. Abazov *et. al.*, *Search for associated production of charginos and neutralinos in the trilepton final state using 2.3* fb^{-1} *of data*, arXiv:0901.0646.

[87] **CDF** Collaboration, T. Aaltonen *et. al.*, *Search for Supersymmetry in* $p\bar{p}$ *Collisions at* $\sqrt{s} = 1.96$*-TeV Using the Trilepton Signature of Chargino-Neutralino Production*, *Phys. Rev. Lett.* **101** (2008) 251801, [arXiv:0808.2446].

[88] **D0** Collaboration, V. M. Abazov *et. al.*, *Search for neutral supersymmetric Higgs bosons in multijet events at* $\sqrt{s} = 1.96$*-TeV*, *Phys. Rev. Lett.* **95** (2005) 151801, [hep-ex/0504018].

[89] *Search for squarks and gluinos in events with jets and missing transverse energy using 2.1* fb^{-1} *of collision data at*, *Physics Letters B* **660** (2008), no. 5 449 – 457.

[90] **CDF** Collaboration, T. Aaltonen *et. al.*, *Inclusive Search for Squark and Gluino Production in* $p\bar{p}$ *Collisions at* $\sqrt{s} = 1.96$*-TeV*, arXiv:0811.2512.

[91] **CDF** Collaboration, *Search for Pair Production of Stop Quarks Mimicking Top Event Signatures*, . CDF note 9439 (July 2008).

[92] **D0** Collaboration, V. M. Abazov *et. al.*, *Search for the lightest scalar top quark in events with two leptons in* $p\bar{p}$ *collisions at* $\sqrt{s} = 1.96$*-TeV*, arXiv:0811.0459.

[93] **D0** Collaboration, V. M. Abazov *et. al.*, *Search for scalar top quarks in the acoplanar charm jets and missing transverse energy final state in $p\bar{p}$ collisions at $\sqrt{s}$ = 1.96-TeV*, *Phys. Lett.* **B665** (2008) 1–8, [arXiv:0803.2263].

[94] **CDF** Collaboration, T. Aaltonen *et. al.*, *Search for Direct Pair Production of Supersymmetric Top and Supersymmetric Bottom Quarks in $p\bar{p}$ Collisions at $\sqrt{s}$ = 1.96-TeV*, *Phys. Rev.* **D76** (2007) 072010, [arXiv:0707.2567].

[95] **D0** Collaboration, V. M. Abazov *et. al.*, *Search for pair production of scalar bottom quarks in $p\bar{p}$ collisions at $\sqrt{s}$ = 1.96-TeV*, *Phys. Rev. Lett.* **97** (2006) 171806, [hep-ex/0608013].

[96] **CDF** Collaboration, T. Aaltonen *et. al.*, *Search for Gluino-Mediated Sbottom Production in $p\bar{p}$ Collisions at $\sqrt{(s)} = 1.96$ TeV*, arXiv:0903.2618.

[97] **H1** Collaboration, A. Aktas *et. al.*, *Search for squark production in R parity violating supersymmetry at HERA*, *Eur. Phys. J.* **C36** (2004) 425–440, [hep-ex/0403027].

[98] **H1** Collaboration, *The h1 detector at hera*, *Nuclear Instruments and Methods in Physics Research Section A: Accelerators, Spectrometers, Detectors and Associated Equipment* **386** (1997), no. 2-3 310 – 347.

H1 Collaboration, *The tracking, calorimeter and muon detectors of the h1 experiment at hera*, *Nuclear Instruments and Methods in Physics Research Section A: Accelerators, Spectrometers, Detectors and Associated Equipment* **386** (1997), no. 2-3 348 – 396.

[99] E. Hartouni *et. al.*, *HERA-B: An experiment to study CP violation in the B system using an internal target at the HERA proton ring. Design report*, . DESY-PRC-95-01.

[100] **HERMES** Collaboration, K. Ackerstaff *et. al.*, *HERMES spectrometer*, *Nucl. Instrum. Meth.* **A417** (1998) 230–265, [hep-ex/9806008].

[101] **ZEUS** Collaboration, *The zeus detector*, . Status report (unpublished), DESY (1993).

[102] **ZEUS** Collaboration, *Search for stop production in R-parity-violating supersymmetry at HERA*, *Eur. Phys. J.* **C50** (2007) 269–281, [hep-ex/0611018].

[103] **H1** Collaboration, A. Aktas *et. al.*, *Search for bosonic stop decays in R-parity violating supersymmetry in e+ p collisions at HERA*, *Phys. Lett.* **B599** (2004) 159–172, [hep-ex/0405070].

[104] **ATLAS** Collaboration, G. Aad *et. al.*, *The ATLAS Experiment at the CERN Large Hadron Collider*, *JINST* **3** (2008) S08003.

[105] T. C. Collaboration, *Cms physics technical design report, volume ii: Physics performance*, *Journal of Physics G: Nuclear and Particle Physics* **34** (2007), no. 6 995–1579.

[106] **ALICE** Collaboration, e. . Carminati, F. *et. al.*, *ALICE: Physics performance report, volume I*, *J. Phys.* **G30** (2004) 1517–1763.

ALICE Collaboration, e. . Alessandro, B. *et. al.*, *ALICE: Physics performance report, volume II*, *J. Phys.* **G32** (2006) 1295–2040.

[107] **LHCb** Collaboration, A. A. Alves *et. al.*, *The LHCb Detector at the LHC*, *JINST* **3** (2008) S08005.

[108] **The ATLAS** Collaboration, G. Aad *et. al.*, *Expected Performance of the ATLAS Experiment - Detector, Trigger and Physics*, arXiv:0901.0512.

[109] C. G. Lester and D. J. Summers, *Measuring masses of semiinvisibly decaying particles pair produced at hadron colliders*, *Phys. Lett.* **B463** (1999) 99–103, [hep-ph/9906349].

C. G. Lester, *Model independent sparticle mass measurements at ATLAS*, . CERN-THESIS-2004-003.

A. J. Barr, C. G. Lester, M. A. Parker, B. C. Allanach, and P. Richardson, *Discovering anomaly-mediated supersymmetry at the LHC*, *JHEP* **03** (2003) 045, [hep-ph/0208214].

[110] O. Buchmueller *et. al.*, *Predictions for Supersymmetric Particle Masses in the CMSSM using Indirect Experimental and Cosmological Constraints*, *JHEP* **09** (2008) 117, [arXiv:0808.4128].

[111] J. M. Campbell *et. al.*, *Higgs boson production in association with bottom quarks*, hep-ph/0405302.

[112] F. E. Paige, *SUSY signatures in ATLAS at LHC*, hep-ph/0307342.

[113] M. Chiorboli and A. Tricomi, *Squark and gluino reconstruction in CMS*, . CMS-NOTE-2004-029.

[114] K. Kawagoe, M. M. Nojiri, and G. Polesello, *A new SUSY mass reconstruction method at the CERN LHC*, *Phys. Rev.* **D71** (2005) 035008, [hep-ph/0410160].

[115] S. Kraml and A. R. Raklev, *Same-sign top quarks as signature of light stops at the LHC*, *Phys. Rev.* **D73** (2006) 075002, [hep-ph/0512284].

[116] S. P. Martin, *Exploring compressed supersymmetry with same-sign top quarks at the Large Hadron Collider*, *Phys. Rev.* **D78** (2008) 055019, [arXiv:0807.2820].

[117] M. Carena, A. Freitas, and C. E. M. Wagner, *Light Stop Searches at the LHC in Events with One Hard Photon or Jet and Missing Energy*, *JHEP* **10** (2008) 109, [arXiv:0808.2298].

[118] E. Reya and D. P. Roy, *Gluino and squarks search at Tevatron collider energies*, *Z. Phys.* **C32** (1986) 615.

[119] J. Pumplin *et. al.*, *New generation of parton distributions with uncertainties from global QCD analysis*, *JHEP* **07** (2002) 012, [hep-ph/0201195].

[120] W. Hollik, M. Kollar, and M. K. Trenkel, *EW NLO corrections to pair production of top-squarks at the LHC*, arXiv:0710.2472.

[121] W. Hollik, M. Kollar, and M. K. Trenkel, *Hadronic production of top-squark pairs with electroweak NLO contributions*, *JHEP* **02** (2008) 018, [arXiv:0712.0287].

[122] W. Hollik, E. Mirabella, and M. K. Trenkel, *Electroweak contributions to squark–gluino production at the LHC*, *JHEP* **02** (2009) 002, [arXiv:0810.1044].

[123] W. Hollik *et. al.*, *Renormalization of the minimal supersymmetric standard model*, *Nucl. Phys. Proc. Suppl.* **116** (2003) 397–401, [hep-ph/0210016].

[124] W. Hollik *et. al.*, *Renormalization of the minimal supersymmetric standard model*, *Nucl. Phys.* **B639** (2002) 3–65, [hep-ph/0204350].

[125] W. Pauli and F. Villars, *On the Invariant regularization in relativistic quantum theory*, *Rev. Mod. Phys.* **21** (1949) 434–444.

[126] C. G. Bollini and J. J. Giambiagi, *Dimensional Renormalization: The Number of Dimensions as a Regularizing Parameter*, *Nuovo Cim.* **B12** (1972) 20–25.

[127] J. F. Ashmore, *A Method of Gauge Invariant Regularization*, *Lett. Nuovo Cim.* **4** (1972) 289–290.

[128] G. 't Hooft and M. J. G. Veltman, *Regularization and Renormalization of Gauge Fields*, *Nucl. Phys.* **B44** (1972) 189–213.

[129] W. Siegel, *Supersymmetric Dimensional Regularization via Dimensional Reduction*, *Phys. Lett.* **B84** (1979) 193.

[130] D. M. Capper, D. R. T. Jones, and P. van Nieuwenhuizen, *Regularization by Dimensional Reduction of Supersymmetric and Nonsupersymmetric Gauge Theories*, *Nucl. Phys.* **B167** (1980) 479.

[131] F. del Aguila, A. Culatti, R. M. Tapia, and M. Perez-Victoria, *Supersymmetric calculations with component fields in differential renormalization*, `hep-ph/9711474`.

[132] F. del Aguila, A. Culatti, R. Munoz-Tapia, and M. Perez-Victoria, *Constraining differential renormalization in abelian gauge theories*, *Phys. Lett.* **B419** (1998) 263–271, [`hep-th/9709067`].

[133] F. del Aguila, A. Culatti, R. Munoz Tapia, and M. Perez-Victoria, *Techniques for one-loop calculations in constrained differential renormalization*, *Nucl. Phys.* **B537** (1999) 561–585, [`hep-ph/9806451`].

[134] J. C. Collins, *Renormalization. An introduction to renormalization, the renormalization group and the operator product expansion*, . Cambridge, Uk: Univ. Pr. (1984) 380p.

[135] P. Breitenlohner and D. Maison, *Dimensional Renormalization and the Action Principle*, *Commun. Math. Phys.* **52** (1977) 11–38.

[136] P. Breitenlohner and D. Maison, *Dimensionally Renormalized Green's Functions for Theories with Massless Particles. 2*, *Commun. Math. Phys.* **52** (1977) 55.

[137] J. G. Korner, D. Kreimer, and K. Schilcher, *A Practicable γ_5 scheme in dimensional regularization*, *Z. Phys.* **C54** (1992) 503–512.

[138] W. A. Bardeen, *Regularization of gauge field theories*, *eConf* **C720906V2** (1972) 295–298.

[139] M. S. Chanowitz, M. Furman, and I. Hinchliffe, *The Axial Current in Dimensional Regularization*, *Nucl. Phys.* **B159** (1979) 225.

[140] F. Jegerlehner, *Facts of life with γ_5*, *Eur. Phys. J.* **C18** (2001) 673–679, [hep-th/0005255].

[141] G. Passarino and M. J. G. Veltman, *One Loop Corrections for e^+ e^- Annihilation into μ^+ μ^- in the Weinberg Model*, *Nucl. Phys.* **B160** (1979) 151.

[142] A. Denner, *Techniques for calculation of electroweak radiative corrections at the one loop level and results for W physics at LEP-200*, *Fortschr. Phys.* **41** (1993) 307–420, [arXiv:0709.1075].

[143] G. J. van Oldenborgh and J. A. M. Vermaseren, *New Algorithms for One Loop Integrals*, *Z. Phys.* **C46** (1990) 425–438.

[144] A. Denner and S. Dittmaier, *Reduction schemes for one-loop tensor integrals*, *Nucl. Phys.* **B734** (2006) 62–115, [hep-ph/0509141].

[145] A. Denner and S. Dittmaier, *Reduction of one-loop tensor 5-point integrals*, *Nucl. Phys.* **B658** (2003) 175–202, [hep-ph/0212259].

[146] T. Binoth, J. P. Guillet, G. Heinrich, E. Pilon, and C. Schubert, *An algebraic / numerical formalism for one-loop multi-leg amplitudes*, *JHEP* **10** (2005) 015, [hep-ph/0504267].

[147] P. Majumdar, E. C. Poggio, and H. J. Schnitzer, *The Supersymmetry Ward identity for the Supersymmetric non-Abelian gauge theory*, *Phys. Rev.* **D21** (1980) 2203.

[148] I. Jack and D. R. T. Jones, *Regularisation of supersymmetric theories*, hep-ph/9707278.

[149] W. Hollik, E. Kraus, and D. Stockinger, *Renormalization and symmetry conditions in supersymmetric QED*, *Eur. Phys. J.* **C11** (1999) 365–381, [hep-ph/9907393].

[150] W. Hollik and D. Stockinger, *Regularization and supersymmetry-restoring counterterms in supersymmetric QCD*, *Eur. Phys. J.* **C20** (2001) 105–119, [hep-ph/0103009].

[151] I. Fischer, W. Hollik, M. Roth, and D. Stockinger, *Restoration of supersymmetric Slavnov-Taylor and Ward identities in presence of soft and spontaneous symmetry breaking*, *Phys. Rev.* **D69** (2004) 015004, [hep-ph/0310191].

[152] S. J. Gates, M. T. Grisaru, M. Rocek, and W. Siegel, *Superspace, or one thousand and one lessons in supersymmetry*, *Front. Phys.* **58** (1983) 1–548, [hep-th/0108200].

[153] D. Stockinger, *Regularization by dimensional reduction: Consistency, quantum action principle, and supersymmetry*, *JHEP* **03** (2005) 076, [hep-ph/0503129].

[154] W. Siegel, *Inconsistency of Supersymmetric Dimensional Regularization*, *Phys. Lett.* **B94** (1980) 37.

[155] L. V. Avdeev, G. A. Chochia, and A. A. Vladimirov, *On the scope of supersymmetric dimensional regularization*, *Phys. Lett.* **B105** (1981) 272.

[156] L. V. Avdeev and A. A. Vladimirov, *Dimensional regularization and Supersymmetry*, *Nucl. Phys.* **B219** (1983) 262.

[157] A. Signer and D. Stockinger, *Using Dimensional Reduction for Hadronic Collisions*, *Nucl. Phys.* **B808** (2009) 88–120, [arXiv:0807.4424].

[158] S. P. Martin and M. T. Vaughn, *Regularization dependence of running couplings in softly broken supersymmetry*, *Phys. Lett.* **B318** (1993) 331–337, [hep-ph/9308222].

[159] I. Jack, D. R. T. Jones, and C. G. North, *$N = 1$ supersymmetry and the three loop anomalous dimension for the chiral superfield*, *Nucl. Phys.* **B473** (1996) 308–322, [hep-ph/9603386].

[160] I. Jack, D. R. T. Jones, and C. G. North, *$N = 1$ supersymmetry and the three loop gauge beta function*, *Phys. Lett.* **B386** (1996) 138–140, [hep-ph/9606323].

[161] I. Jack, D. R. T. Jones, and C. G. North, *Scheme dependence and the NSVZ beta-function*, *Nucl. Phys.* **B486** (1997) 479–499, [hep-ph/9609325].

[162] W. Hollik and H. Rzehak, *The sfermion mass spectrum of the MSSM at the one-loop level*, *Eur. Phys. J.* **C32** (2003) 127–133, [hep-ph/0305328].

[163] Y. Yamada, *Gauge dependence of the on-shell renormalized mixing matrices*, *Phys. Rev.* **D64** (2001) 036008, [hep-ph/0103046].

[164] A. Dabelstein, *The One loop renormalization of the MSSM Higgs sector and its application to the neutral scalar Higgs masses*, *Z. Phys.* **C67** (1995) 495–512, [hep-ph/9409375].

[165] M. Frank, S. Heinemeyer, W. Hollik, and G. Weiglein, *FeynHiggs1.2: Hybrid MS-bar / on-shell renormalization for the CP-even Higgs boson sector in the MSSM*, hep-ph/0202166.

[166] A. Freitas and D. Stockinger, *Gauge dependence and renormalization of* $\tan(\beta)$ *in the MSSM*, *Phys. Rev.* **D66** (2002) 095014, [hep-ph/0205281].

[167] S. Heinemeyer, W. Hollik, H. Rzehak, and G. Weiglein, *High-precision predictions for the MSSM Higgs sector at* $\mathcal{O}(\alpha_b alpha_s)$, *Eur. Phys. J.* **C39** (2005) 465–481, [hep-ph/0411114].

[168] T. Fritzsche and W. Hollik, *Complete one-loop corrections to the mass spectrum of charginos and neutralinos in the MSSM*, *Eur. Phys. J.* **C24** (2002) 619–629, [hep-ph/0203159].

[169] A. Freitas, A. von Manteuffel, and P. M. Zerwas, *Slepton production at* $e^+\ e^-$ *and* $e^-\ e^-$ *linear colliders*, *Eur. Phys. J.* **C34** (2004) 487–512, [hep-ph/0310182].

[170] S. Berge, W. Hollik, W. M. Mosle, and D. Wackeroth, *SUSY QCD one-loop effects in (un)polarized top-pair production at hadron colliders*, *Phys. Rev.* **D76** (2007) 034016, [hep-ph/0703016].

[171] W. Beenakker, R. Hopker, T. Plehn, and P. M. Zerwas, *Stop decays in SUSY-QCD*, *Z. Phys.* **C75** (1997) 349–356, [hep-ph/9610313].

[172] T. Kinoshita, *Mass singularities of Feynman amplitudes*, *J. Math. Phys.* **3** (1962) 650–677.

[173] T. D. Lee and M. Nauenberg, *Degenerate Systems and Mass Singularities*, *Phys. Rev.* **133** (1964) B1549–B1562.

[174] F. Bloch and A. Nordsieck, *Note on the Radiation Field of the electron*, *Phys. Rev.* **52** (1937) 54–59.

[175] B. Lautrup, *Renormalization Constants and Asymptotic Behavior in Quantum Electrodynamics*, *Nucl. Phys.* **B105** (1976) 23.

[176] S. Catani, S. Dittmaier, and Z. Trocsanyi, *One-loop singular behaviour of QCD and SUSY QCD amplitudes with massive partons*, *Phys. Lett.* **B500** (2001) 149–160, [hep-ph/0011222].

[177] T. Hahn and M. Perez-Victoria, *Automatized one-loop calculations in four and D dimensions*, *Comput. Phys. Commun.* **118** (1999) 153–165, [hep-ph/9807565].

[178] T. Hahn and M. Rauch, *News from FormCalc and LoopTools*, *Nucl. Phys. Proc. Suppl.* **157** (2006) 236–240, [hep-ph/0601248].

[179] D. R. Yennie, S. C. Frautschi, and H. Suura, *The infrared divergence phenomena and high-energy processes*, *Ann. Phys.* **13** (1961) 379–452.

[180] S. Weinberg, *Infrared photons and gravitons*, *Phys. Rev.* **140** (1965) B516–B524.

[181] V. N. Baier, V. S. Fadin, and V. A. Khoze, *Quasireal electron method in high-energy quantum electrodynamics*, *Nucl. Phys.* **B65** (1973) 381–396.

[182] S. Catani and M. H. Seymour, *The Dipole Formalism for the Calculation of QCD Jet Cross Sections at Next-to-Leading Order*, *Phys. Lett.* **B378** (1996) 287–301, [hep-ph/9602277].

[183] S. Catani and M. H. Seymour, *A general algorithm for calculating jet cross sections in NLO QCD*, *Nucl. Phys.* **B485** (1997) 291–419, [hep-ph/9605323].

[184] R. K. Ellis, D. A. Ross, and A. E. Terrano, *The Perturbative Calculation of Jet Structure in e^+ e^- Annihilation*, *Nucl. Phys.* **B178** (1981) 421.

S. D. Ellis, Z. Kunszt, and D. E. Soper, *The One Jet Inclusive Cross-Section at Order α_s^3. 1. Gluons Only*, *Phys. Rev.* **D40** (1989) 2188.

M. L. Mangano, P. Nason, and G. Ridolfi, *Heavy quark correlations in hadron collisions at next-to- leading order*, *Nucl. Phys.* **B373** (1992) 295–345.

Z. Kunszt and D. E. Soper, *Calculation of jet cross-sections in hadron collisions at order α_s^3*, *Phys. Rev.* **D46** (1992) 192–221.

S. Frixione, Z. Kunszt, and A. Signer, *Three-jet cross sections to next-to-leading order*, *Nucl. Phys.* **B467** (1996) 399–442, [hep-ph/9512328].

Z. Nagy and Z. Trocsanyi, *Calculation of QCD jet cross sections at next-to-leading order*, *Nucl. Phys.* **B486** (1997) 189–226, [hep-ph/9610498].

J. M. Campbell, M. A. Cullen, and E. W. N. Glover, *Four jet event shapes in electron positron annihilation*, *Eur. Phys. J.* **C9** (1999) 245–265, [hep-ph/9809429].

[185] L. Phaf and S. Weinzierl, *Dipole formalism with heavy fermions*, *JHEP* **04** (2001) 006, [hep-ph/0102207].

[186] S. Catani, S. Dittmaier, M. H. Seymour, and Z. Trocsanyi, *The dipole formalism for next-to-leading order QCD calculations with massive partons*, *Nucl. Phys.* **B627** (2002) 189–265, [hep-ph/0201036].

[187] S. Weinzierl, *Subtraction terms at NNLO*, *JHEP* **03** (2003) 062, [hep-ph/0302180].

S. Weinzierl, *Subtraction terms for one-loop amplitudes with one unresolved parton*, *JHEP* **07** (2003) 052, [hep-ph/0306248].

A. Gehrmann-De Ridder, T. Gehrmann, and G. Heinrich, *Four-particle phase space integrals in massless QCD*, *Nucl. Phys.* **B682** (2004) 265–288, [hep-ph/0311276].

C. Anastasiou, K. Melnikov, and F. Petriello, *A new method for real radiation at NNLO*, *Phys. Rev.* **D69** (2004) 076010, [hep-ph/0311311].

C. Anastasiou, K. Melnikov, and F. Petriello, *Fully differential Higgs boson production and the di- photon signal through next-to-next-to-leading order*, *Nucl. Phys.* **B724** (2005) 197–246, [hep-ph/0501130].

T. Binoth and G. Heinrich, *Numerical evaluation of phase space integrals by sector decomposition*, *Nucl. Phys.* **B693** (2004) 134–148, [hep-ph/0402265].

A. Gehrmann-De Ridder, T. Gehrmann, and E. W. N. Glover, *Infrared Structure of $e^+e^- \to 2$ jets at NNLO*, *Nucl. Phys.* **B691** (2004) 195–222, [hep-ph/0403057].

A. Gehrmann-De Ridder, T. Gehrmann, and E. W. N. Glover, *Quark-Gluon Antenna Functions from Neutralino Decay*, *Phys. Lett.* **B612** (2005) 36–48, [hep-ph/0501291].

A. Gehrmann-De Ridder, T. Gehrmann, and E. W. N. Glover, *Gluon-Gluon Antenna Functions from Higgs Boson Decay*, *Phys. Lett.* **B612** (2005) 49–60, [hep-ph/0502110].

A. Gehrmann-De Ridder, T. Gehrmann, and E. W. N. Glover, *Antenna Subtraction at NNLO*, *JHEP* **09** (2005) 056, [hep-ph/0505111].

W. B. Kilgore, *Subtraction terms for hadronic production processes at next-to-next-to-leading order*, *Phys. Rev.* **D70** (2004) 031501, [hep-ph/0403128].

S. Frixione and M. Grazzini, *Subtraction at NNLO*, *JHEP* **06** (2005) 010, [hep-ph/0411399].

G. Somogyi, Z. Trocsanyi, and V. Del Duca, *Matching of singly- and doubly-unresolved limits of tree- level QCD squared matrix elements*, *JHEP* **06** (2005) 024, [hep-ph/0502226].

S. Catani and M. Grazzini, *An NNLO subtraction formalism in hadron collisions and its application to Higgs boson production at the LHC*, *Phys. Rev. Lett.* **98** (2007) 222002, [hep-ph/0703012].

[188] S. Dittmaier, *A general approach to photon radiation off fermions*, *Nucl. Phys.* **B565** (2000) 69–122, [hep-ph/9904440].

[189] S. Dittmaier, A. Kabelschacht, and T. Kasprzik, *Polarized QED splittings of massive fermions and dipole subtraction for non-collinear-safe observables*, *Nucl. Phys.* **B800** (2008) 146–189, [arXiv:0802.1405].

[190] K. P. O. Diener, S. Dittmaier, and W. Hollik, *Electroweak higher-order effects and theoretical uncertainties in deep-inelastic neutrino scattering*, *Phys. Rev.* **D72** (2005) 093002, [hep-ph/0509084].

T. Plehn, *Production of supersymmetric particles at high-energy colliders*, hep-ph/9809319.

[191] A. Alves, O. Eboli, and T. Plehn, *It's a gluino*, *Phys. Rev.* **D74** (2006) 095010, [hep-ph/0605067].

[192] R. M. Barnett, J. F. Gunion, and H. E. Haber, *Discovering supersymmetry with like sign dileptons*, *Phys. Lett.* **B315** (1993) 349–354, [hep-ph/9306204].

[193] S. Y. Choi, M. Drees, A. Freitas, and P. M. Zerwas, *Testing the Majorana Nature of Gluinos and Neutralinos*, *Phys. Rev.* **D78** (2008) 095007, [arXiv:0808.2410].

[194] M. M. Nojiri *et. al.*, *Physics Beyond the Standard Model: Supersymmetry*, arXiv:0802.3672.

[195] T. Hahn, *Generating Feynman diagrams and amplitudes with FeynArts 3*, *Comput. Phys. Commun.* **140** (2001) 418–431, [hep-ph/0012260].

[196] T. Hahn and C. Schappacher, *The implementation of the minimal supersymmetric standard model in FeynArts and FormCalc*, *Comput. Phys. Commun.* **143** (2002) 54–68, [hep-ph/0105349].

[197] T. Banks, *Supersymmetry and the Quark Mass Matrix*, *Nucl. Phys.* **B303** (1988) 172.

[198] L. J. Hall, R. Rattazzi, and U. Sarid, *The Top quark mass in supersymmetric SO(10) unification*, *Phys. Rev.* **D50** (1994) 7048–7065, [hep-ph/9306309].

[199] R. Hempfling, *Yukawa coupling unification with supersymmetric threshold corrections*, *Phys. Rev.* **D49** (1994) 6168–6172.

[200] M. S. Carena, M. Olechowski, S. Pokorski, and C. E. M. Wagner, *Electroweak symmetry breaking and bottom - top Yukawa unification*, *Nucl. Phys.* **B426** (1994) 269–300, [hep-ph/9402253].

[201] M. S. Carena, D. Garcia, U. Nierste, and C. E. M. Wagner, *Effective Lagrangian for the $\bar{t}bH^+$ interaction in the MSSM and charged Higgs phenomenology*, *Nucl. Phys.* **B577** (2000) 88–120, [hep-ph/9912516].

[202] H. Eberl, K. Hidaka, S. Kraml, W. Majerotto, and Y. Yamada, *Improved SUSY QCD corrections to Higgs boson decays into quarks and squarks*, *Phys. Rev.* **D62** (2000) 055006, [hep-ph/9912463].

[203] J. A. Aguilar-Saavedra *et. al.*, *Supersymmetry parameter analysis: SPA convention and project*, *Eur. Phys. J.* **C46** (2006) 43–60, [hep-ph/0511344].

[204] A. D. Martin, R. G. Roberts, W. J. Stirling, and R. S. Thorne, *Parton distributions incorporating QED contributions*, *Eur. Phys. J.* **C39** (2005) 155–161, [hep-ph/0411040].

[205] R. S. Thorne and R. G. Roberts, *An ordered analysis of heavy flavour production in deep inelastic scattering*, *Phys. Rev.* **D57** (1998) 6871–6898, [hep-ph/9709442].

[206] R. S. Thorne and R. G. Roberts, *A practical procedure for evolving heavy flavour structure functions*, *Phys. Lett.* **B421** (1998) 303–311, [hep-ph/9711223].

[207] R. S. Thorne and R. G. Roberts, *A variable number flavour scheme for charged current heavy flavour structure functions*, *Eur. Phys. J.* **C19** (2001) 339–349, [hep-ph/0010344].

[208] **Particle Data Group** Collaboration, W. M. Yao *et. al.*, *Review of particle physics*, *J. Phys.* **G33** (2006) 1–1232.

[209] B. C. Allanach *et. al.*, *The Snowmass points and slopes: Benchmarks for SUSY searches*, *Eur. Phys. J.* **C25** (2002) 113–123, [hep-ph/0202233].

[210] W. Porod, *SPheno, a program for calculating supersymmetric spectra, SUSY particle decays and SUSY particle production at e+ e- colliders*, *Comput. Phys. Commun.* **153** (2003) 275–315, [hep-ph/0301101].

[211] A. Djouadi, J.-L. Kneur, and G. Moultaka, *SuSpect: A Fortran code for the supersymmetric and Higgs particle spectrum in the MSSM*, *Comput. Phys. Commun.* **176** (2007) 426–455, [hep-ph/0211331].

[212] B. C. Allanach, *SOFTSUSY: A C++ program for calculating supersymmetric spectra*, *Comput. Phys. Commun.* **143** (2002) 305–331, [hep-ph/0104145].

[213] E. Accomando, A. Denner, and C. Meier, *Electroweak corrections to $W\gamma$ and $Z\gamma$ production at the LHC*, *Eur. Phys. J.* **C47** (2006) 125–146, [hep-ph/0509234].

[214] **D0** Collaboration, V. M. Abazov *et. al.*, *Search for squarks and gluinos in events with jets and missing transverse energy in $p\bar{p}$ collisions at $\sqrt{s} = 1.96$-TeV*, *Phys. Lett.* **B638** (2006) 119–127, [hep-ex/0604029].

[215] S. Heinemeyer, W. Hollik, and G. Weiglein, *FeynHiggs: a program for the calculation of the masses of the neutral CP-even Higgs bosons in the MSSM*, *Comput. Phys. Commun.* **124** (2000) 76–89, [hep-ph/9812320].

[216] M. Frank *et. al.*, *The Higgs boson masses and mixings of the complex MSSM in the Feynman-diagrammatic approach*, *JHEP* **02** (2007) 047, [hep-ph/0611326].

[217] **D0** Collaboration, B. Abbott *et. al.*, *Search for squarks and gluinos in events containing jets and a large imbalance in transverse energy*, *Phys. Rev. Lett.* **83** (1999) 4937–4942, [hep-ex/9902013].

[218] **CDF** Collaboration, A. A. Affolder *et. al.*, *Search for gluinos and scalar quarks in $p\bar{p}$ collisions at $\sqrt{s} = 1.8$ TeV using the missing energy plus multijets signature*, *Phys. Rev. Lett.* **88** (2002) 041801, [hep-ex/0106001].

[219] M. Beccaria, G. Macorini, L. Panizzi, F. M. Renard, and C. Verzegnassi, *Stop-antistop and sbottom-antisbottom production at LHC: a one-loop search for model parameters dependence*, *Int. J. Mod. Phys.* **A23** (2008) 4779–4810, [arXiv:0804.1252].

[220] Y. Kurihara, D. Perret-Gallix, and Y. Shimizu, *$e^+e^- \to e^-\bar{\nu}_e u\bar{d}$ from LEP to linear collider energies*, *Phys. Lett.* **B349** (1995) 367–374, [hep-ph/9412215].

[221] ATLAS Data Challenge 2 DC2 points. http://paige.home.cern.ch/paige/fullsusy/romeindex.html.

[222] **ALEPH** Collaboration, R. Barate *et. al.*, *Search for supersymmetric particles in e^+ e^- collisions at $\sqrt{s}$ up to 202-GeV and mass limit for the lightest neutralino*, *Phys. Lett.* **B499** (2001) 67–84, [hep-ex/0011047].

[223] M. Chiorboli and A. Tricomi, *Squark and gluino reconstruction in CMS*, . CMS-NOTE-2004-029.

[224] M. E. Peskin and D. V. Schroeder, *An Introduction to quantum field theory*, . Reading, USA: Addison-Wesley (1995) 842 p.

[225] T. Hahn, *FormCalc 4 User's Guide*, .

Acknowledgements

Hic sunt leones... Hard, if possible at all, to write a rhetoric-free acknowledgement. Let me try.

I would like to thank Prof. Wolfgang Hollik, my supervisor. I am indebted to him for all the discussions we had, both on my PhD. project and on my other projects. He was always open to my questions and objections arguing me on his point of view, without imposing it.

I am indebted to my office mates Jianhui and Maxi (l'avvocato...) for the warm atmosphere they creates in the office. It was a lot of fun to share with them big part of the day (afternoon/night in the case of Maxi...). More than colleagues, friends.

Many thanks go to the people I worked with during these years. I would like to start mentioning Maike Trenkel and Jan Germer. Part of this thesis is based on the work we did together, and the entire thesis profits from the discussions I had with them. I acknowledge Matteo Beccaria, Carlo Carloni Calame, Guido Macorini, Luca Panizzi, Fulvio Piccinini, Fernard Renard and Claudio Verzagnassi for the pleasant collaborations we had in several occasions. Special thanks to Tilman Plehn. I am grateful to him for countless suggestions and for a the wonderful time I had in Edinburgh. I hope to have the occasion to work together in the future.

It was a pleasure to have the possibility to join the theory group of the Max Planck Institut für Physik, and I thank all of my colleagues. In particular I am indebted with Stefan Dittmaier, Thomas Hahn, and Stefano Pozzorini for the suggestions they gave to me. Many thanks to the other IMPRS students, in particular to Steve Blanchet, Florian Hahn-Wörnle, Sophio Pataraia, Josef Pradler, and Thi Nhung Dao.

Ringrazio mia madre, mio padre, Francesca, Giuseppe ed i miei nipoti Daniele e Matilde. Troppe le cose per cui li voglio ringraziare, in primis per l'amore incondizionato che mi danno. A proposito di famiglia, non posso dimenticare De Prezzo (fratuma, come si dice dalle nostre parti), Lucia e la loro ospitalitá durante i miei soggiorni a Rimini. Un grazie di cuore va anche a Roby e Terlizzi per avermi onorato della loro amicizia in tutti questi anni.

Il mio ultimo pensiero va a Paola. Grazie perché "... fra i tanti, bella, che hai colpito ti sei gettata addosso proprio a me ... "